Investigating the molecular mechanism underlying CMT1c disease

A thesis submitted to the University of Manchester

for the degree of

Doctor of *Philosophy* in the Faculty of Biology, Medicine and Health

2021

Rebecca Yarwood

School of Biological Sciences

Division of Molecular and Cellular Function

List of Contents

Word count: 48,403

List of Figures

List of Tables

List of abbreviations

ABM-2	ALG-2-binding motif 2
ACN	Acetonitrile
ADP	Adenosine diphosphate
AIP4	Atrophin-1-interacting protein 4
ALG-2	Apoptosis-linked gene 2
ANOVA	Analysis of variance
AP-2	Adaptor protein complex 2
APS	Ammonium persulphate
Arf6	ADP-ribosylation factor 6
Arp2/3	Actin related protein 2/3
ATP	Adenosine triphosphate
BAP31	B cell receptor associated protein 31
BAR	Bin/amphiphysin/Rvs
BCA	Bicinchoninic acid
BioID	Proximity dependent biotin identification
BirA	Biotin--[acetyl-CoA-carboxylase] ligase
BLAST	Basic local alignment search tool
Cas9	CRISPR associated protein 9
Cavα1c	Voltage-dependent L-type calcium channel subunit alpha-1C
Cbl	Casitas B-lineage lymphoma
CCC	CCDC93, CCDC22 and COMMD
CCDC	Coiled-coil domain containing protein
CD98	Cluster of differentiation 98
CDIP1	Cell death inducing protein 1
cDNA	complementary DNA
CHEVI	class C homologues in endosome-vesicle interaction
CHMP	Charged multivesicular body protein
CIE	Clathrin independent endocytosis
CI-MPR	Cation-independent mannose phosphate receptor
CIP	Calf intestinal phosphatase
CME	Clathin mediated endocytosis
CMT1c	Charcot Marie Tooth disease type 1c
CNS	Central nervous system
COMMD1	Copped metabolism domain containing 1
CORVET	Class C core vacuole/endosome tethering
CRISPR	Clustered regularly interspaced short palindromic repeats
Crm1	Chromosome region maintenance 1 protein homolog
CUL3	Cullin-3
DAPI	4′,6-diamidino-2-phenylindole
DMEM	Dulbecco's minimum essential media
DMSO	Dimethyl sulfoxide
DNA	Deoxyribonucleic acid

dpf	days post fertilisation
DSCR3	Down syndrome critical region 3
DTT	Dithiothreitol
DUIM	Double sided UIM
EAP	ELL-associated protein
EARP	Endosome-associated recycling protein
EDTA	Ethylenediamine tetraacetic acid
EEA1	Early endosome antigen 1
EET-1	Estrogen-enhanced transcript 1
EGFR	Epidermal growth factor receptor
EGTA	Ethylene glycol tetraacetic acid
EHD1	Epsin homology domain 1
EIF1A	Elongation initiation factor 1A
ELL	Eleven-nineteen lysine-rich leukaemia protein
EMEM	Eagle's minimum essential media
EMPD	Extramammary Paget's disease
ENTH	Epsin N-terminal homology
Eps15	Epsin homology protein 15
ER	Endoplasmic reticulum
ErbB	Erythroblastic oncogene B
ERC	Endosomal recycling compartment
Erk1/2	Extracellular signal-regulated kinase 1/2
ESCPE-1	Endosomal SNX-BAR sorting complex for promoting exit
ESCRT	Endosomal sorting complexes required for transport
FAM21	Family with sequence similarity 21
FBS	Fetal bovine serum
FDR	False discovery rate
FERARI	Factors for endosome recycling and Rab interaction
FGD4	FYVE, RhoGEF and PH domain-containing protein 4
FIG4	Factor-induced gene 4
FV3	Frog virus 3
FYVE	Fab1, YOTB, Vac1, EEA1
GAP	GTPase-activating protein
GDAP1	Ganglioside-induced differentiation-associated protein 1
GEF	Guanine nucleotide exchange factor
GFP	Green fluorescent protein
GILP	Glutathione-induced LITAF domain protein
GLUE	GRAM-like ubiquitin in EAP45
GO	Gene ontology
GRAM	Glucosyltransferase/Rab-like GTPase activator/myotubularin domain
GTP	Guanosine triphosphate
GWAS	Genome wide association screen
HD-PTP	His domain-containing protein tyrosine phosphatase

HECT	Homologous to E6-AP carboxyl terminus
HEK	Human embryonic kidney
HEPES	N-2-Hydroxyethylpiperazine-N'-2-Ethanesulfonic Acid
HOIL-1	Heme-oxidized IRP2 ubiquitin ligase 1
HOPS	homotypic fusion and protein sorting
hpf	Hours post fertilisation
HR	Hydrophobic region
Hrs	Hepatocyte growth factor-regulated tyrosine kinase substrate
Hsp	Heat shock protein
h-TERT	Human telomerase reverse transcriptase
IAA	iodoacetamide
ILV	Intraluminal vesicle
IRP2	Iron regulatory protein 2
ISTI	Increased sodium tolerance protein 1
ITCH	Itchy homologue
KEGG	Kyoto Encyclopedia of Gene and Genomes
Kif5a	Kinesin heavy chain isoform 5A
KLHL12	Kelch-like protein 12
KO	Knock-out
LAMP	lysosome-associated membrane protein
LB	Luria-Bertani
LC-MS	Liquid chromatography mass spectrometry
LFQ	Label free quantification
LITAF	Lipopolysacharide-induced tumour necrosis factor alpha factor
LPS	Lipopolysacharide
MBP	Myelin basic protein
MHCI	Major histocompatibility complex class 1
MICAL L1	Molecules interacting with with CasL-Like1
MPZ	Myelin protein zero
MRC-5	Medical research council 5
mRNA	messenger RNA
MS222	tricaine methanesulfonate
MTMR	Myotubularin related
MTOC	Microtubule organising centre
MVB	Multivesicular body
MVB12	Multivesicular body subunit 12
N4WBP3	Nedd4 WW domain binding protein 3
NDFIP2	Nedd4-family interacting protein 2
NDRG1	N-myc downstream-regulated gene 1 protein
NEB	New England biosciences
Nedd4	Neural precursor cell expressed developmentally down-regulated protein 4
NEFL	Neurofilament light polypeptide
NFκB	Nuclear factor kappa-light-chain-enhancer of activated B cells

NHE-RF1	Na(+)/H(+) exchange regulatory cofactor
NMR	Nuclear magnetic resonance
OTU	ovarian tumour
Pacsin2	Protein kinase C and casein kinase substrate in neurons 2
PAMP	Pathogen-associated molecular pattern
PBS	Phosphate buffered saline
PCA	Principal component analysis
PCDHGA11	Protocadherin gamma-A11
PCR	Polymerase chain reaction
PE	Phosphatidylethanolamine
PEI	Polyethylenimine
PETAL	Proteome epitope tag antibody library
PFA	Paraformaldehyde
PI	Phosphatidylinositol
PI(3,4)P²	Phosphatidylinositol-3,4-phosphate
PI3K	Phosphatidylinositol-3 kinase
PI3P	Phosphotidylinositol-3-phosphate
PI4P	Phosphotidylinositol-4-phosphate
PIG-7	p53 induced gene 7
PLP	Proteolipid protein
PMP22	Peripheral myelin protein 22
PMSF	phenylmethylsulfonyl fluoride
PNS	Peripheral nervous system
PTK7	Protein tyrosine kinase 7
PTM	Post translational modification
PVDF	polyvinylidene difluoride
PX	Phox
qPCR	Quantitative PCR
Rab	Ras-related in brain
Rab11FIP	Rab 11 family-interacting protein
RBR	RING between RING
RFFL	RING finger and FYVE-like domain-containing protein 1
RILP	Rab-interacting lysosomal protein
RING	Really interesting new gene
RIPA	Radioimmunoprecipitation assay buffer
RME-8	Receptor-mediated endocytosis 8
RNA	Ribonucleic acid
RNF207	RING finger protein 207
RPE-1	Retinal pigment epithelial-1
RT-PCR	Reverse transcriptase polymerase chain reaction
SD	Standard deviation
SDS-PAGE	Sodium dodecyl sulphate polyacrylamide gel electrophoresis
SE	Sorting endosome
Sec31A	Secretory protein 31A

sgRNA	Single guide RNA
SH3TC2	SH3 domain and tetratricopeptide repeat-containing protein 2
SIMPLE	Small integral membrane protein of the late endosome/lysosome
siRNA	Silencing RNA
SLC	Solute carrier
SLD	SIMPLE-like domain
SNARE	Soluble N-ethylmaleimide-sensitive factor attachment protein receptor
SNX	Sorting nexin
STAM1/2	Signal transducing adaptor molecule 1/2
STAT6	Signal transducer and activation of transcription
STRING	Search tool for the retrieval of interacting genes/proteins
TAE	Tris acetate EDTA buffer
TBC1D5	Tre-2/Bub2/Cdc16 domain family member 5
TBST	Tris buffered saline with Tween
TCEP	Tris(2-carboxyethyl)phosphine
TEMED	Tetramethylethylenediamine
TfR	Transferrin receptor
TFV	Tiger frog virus
Tgfbrap1	Transforming growth factor-beta receptor-associated protein 1
TGN	*trans*-Golgi network
TJP2	Tight junction protein 2
TNFα	Tumour necrosis factor alpha
TPD54	Tumour protein D54
TRE	Tubular recycling endosome
Tsg101	Tumour susceptibility gene 101
UBA	Ubiquitin binding associated
UBAP1	Ubiquitin associated protein 1
Ubc13	Ubiquitin conjugating enyzme 13
UBD	Ubiquitin binding domain
UBPY	Ubiquitin isopeptidase Y
UEV	Ubiquitin E2 variant
UIM	Ubiquitin interacting motif
VAP	Vesicle associated protein
VHS	Vps27, Hrs, STAM
VIPAS39	VPS33B Interacting Protein, Apical-Basolateral Polarity Regulator, Spe-39 Homolog
Vps	Vacuolar protein sorting
WASH	Wiskott-Aldrich syndrome protein and SCAR homolog
WT	Wild type
WWOX	WW domain-containing oxidoreductase

Abstract

Endocytosis involves the incorporation of surface proteins into intracellular vesicles and downstream compartments from where they are sorted to different destinations. This highly regulated process is essential for information exchange between the extracellular environment and the cell, and is required for uptake of nutrients, regulation of signalling and transport of proteins within the cell. Dysregulated endocytic trafficking is implicated in a wide range of diseases including cancer, infectious disease and neurological disorders.

Charcot-Marie-Tooth (CMT) disease is the most common inherited peripheral neuropathy, estimated to affect 1:2500 people, with at least 80 genes identified as causative. Missense mutations in lipopolysaccharide-induced tumour necrosis factor α factor (LITAF) result in CMT type 1c, which is an autosomal dominant demyelinating disease. It is likely that LITAF functions in endocytic trafficking. However, its precise mechanism of action is still not clear and hence the molecular cause of CMT1c is not well understood.

Here, we show that CMT1c mutations in LITAF impaired localisation to recycling endosomes. These mutations rendered LITAF unable to regulate the tubular recycling compartment, and disrupted trafficking of an endocytic recycling cargo, CD98. We performed a proximity labelling BioID screen to identify potential interactors of LITAF and LITAF containing two CMT1c mutations. A large number of potential interacting partners were identified, and novel protein associations with LITAF have begun to be uncovered. Links with integrin trafficking were revealed as well as other adhesion proteins which are likely to have relevance to the disease. Additionally, we generated transgenic zebrafish lacking LITAF or a similar protein, cell death inducing p53-target protein 1 (CDIP1) and double LITAF and CDIP1 knock-out zebrafish. The zebrafish are viable and have no overt phenotype, and they may provide a useful model in which to further explore the function of these proteins in a physiological context.

Overall this study indicates that CMT1c disease may result from dysregulation of the endocytic recycling pathway and provides additional insights into the possible links between LITAF and demyelination. Further understanding of the function of LITAF and the molecular cause of this disease is required to develop therapeutic targets for this group of demyelinating disorders.

Declaration

No portion of the work referred to in the thesis has been submitted in support of an application for another degree or qualification of this or any other university or other institute of learning.

Copyright

Acknowledgements

First and foremost, I would like to thank my supervisors Philip Woodman and Martin Lowe for giving me the opportunity to join their research groups. Your gentle encouragement and knowledgeable guidance throughout the past four years has been invaluable and I really appreciate all the support you have given me and everything you have taught me.

I am also very grateful to the Woodman and Lowe lab groups who have all contributed to a welcoming and collaborative working environment and provided excellent technical scientific expertise. I would like to express a big thank you to all members of the Woodman, Lowe, Allan and High research groups on B wing especially Cynthia Li, Gab Parkinson, Roisin Cassidy, Lydia Wunderley, Wei-Hsiang Lin, Dan Newman, Alaa Droubi, Joe Morgan, Guanhua Yan, Emmanuel Lemarie, Kirsten Garner, Hannah Perkins, Dan Han, Katie Downes and Quentin Roebuck. Their understanding and support throughout the ups and downs has meant a lot and they've injected so much fun into my PhD. Additionally, a big thank you goes to the biological services facility staff, in particular Vicky Taylor and Zach Bowden.

I would also like to extend my gratitude to all the people who have been there for me during this time for quick coffee breaks and celebrations. I don't think I could have got through this PhD without my cohort: Llilians Calvo, Emma Linney, Sabrina Ghadaouia, Chris Bates and Sam Ogden. Also, thanks go to Caitlin and Caro for getting me out and active, especially during this last year. I would like to thank Nikki, Louisa and Izzy for all your emotional support and laughter and so many fun-filled weekends away. Dale, thank you for everything in the last 6 months, you have motivated me and made this last part so much more fun than I thought was possible.

A special thanks go to my family; to my parents Charles and Nicky, and my older siblings Richard and Vanessa as well as Jamie, Ziggy and Marmite. Thank you for always being there and the unwavering support you give me every day. Last, but by no means least, my thanks go to my twin, Lizzy. We have shared so much laughter and growing up together has made me who I am and your friendship has meant the most to me. Thank you for always believing in me and being my biggest supporter.

Chapter 1: Introduction

1.1 Endocytosis

There are a huge number of integral membrane proteins encoded in the human genome, and they are transported throughout the cell by membrane trafficking. The plasma membrane composition results from a balance of the endocytic pathway and the secretory pathway and is affected by physiological inputs. This allows the cell to sense the environment, signal in response to changes, adhere to and migrate through matrix and achieve cellular polarity.

Many different types of membrane proteins and membrane components are present at the plasma membrane and internalised into cells in a complex process called endocytosis. This process can be constitutive or stimulated by events at the cell surface, such as ligand binding to receptors. Membrane proteins function at the plasma membrane and some are also active whilst in endocytic compartments. These internalised membrane proteins (cargo) enter the cell through clathrin-mediated endocytosis (CME) and clathrin-independent endocytosis (CIE) mechanisms. The plasma membrane invaginates, while coat proteins such as clathrin and associated adaptor proteins induce membrane curvature, and scission proteins pinch off the endocytic pit to form an intracellular vesicle. These endocytic vesicles fuse with early endosomes. The fast recycling process transports some cargo back to the plasma membrane whilst others are trafficked along microtubules to fuse with the sorting endosome. Once cargoes reach the sorting endosome, different complexes recognise and direct them to a range of compartments within the cell (Figure 1.1).

1.1.1 Ubiquitination, and its role in endocytosis

Ubiquitination regulates both internalisation and endosomal sorting. Ubiquitination is a post-translational modification (PTM) involving covalent attachment of the 76 amino acid protein ubiquitin to lysine residues (or in specialised cases the amino terminus) of target proteins. E1 enzymes activate ubiquitin so it covalently attaches to E2 ubiquitin conjugating enzymes. E3 ubiquitin ligases directly or indirectly attach ubiquitin to the specific target protein (Leon and Haguenauer-Tsapis, 2009). E3 ubiquitin ligases recognise target proteins by the presence of a signal such as phosphorylation, protein interaction domain, or can be recruited by an adaptor protein. E3 ubiquitin ligase adaptors bind specific E3 ubiquitin ligases and target proteins, thereby bringing them

into proximity to promote ubiquitination of the target protein. Such adaptors may contribute to spatial regulation of ubiquitination as they can recruit these components to a specific location (Shearwin-Whyatt et al., 2006).

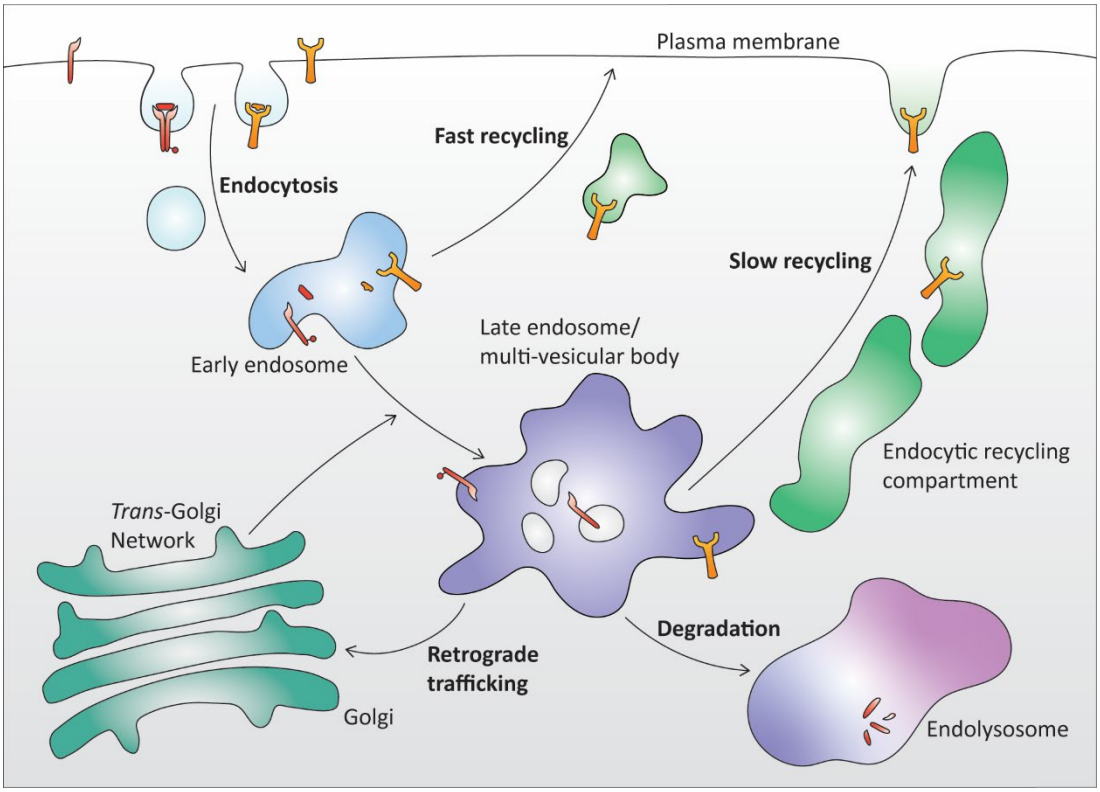

Figure 1.1. Overview of membrane trafficking in endocytosis.
Cargo such as receptors, transporters, ion channels and adhesion proteins are internalised by various clathrin-dependent and clathrin-independent mechanisms into endocytic vesicles, which fuse with the early endosome. Cargo that is returned to the plasma membrane (orange) is sorted into membrane subdomains by retrieval complexes. The membrane buds off to form tubular recycling endosomes which are transported back to the plasma membrane. Cargo destined for lysosomal degradation (red) is sorted into membrane subdomains which undergo membrane remodelling to form ILVs by the action of ESCRTs. This endosome matures to form a MVB containing ILVs. The late endosome fuses with an endolysosome containing hydrolytic enzymes which degrade proteins present.

E3 ubiquitin ligases confer the substrate specificity, as well as the spatial and temporal regulation, with around 600 E3 ubiquitin ligases encoded in the mammalian genome (Metzger et al., 2012, Li et al., 2008). Homologous E6 C-terminus (HECT) domain E3 ubiquitin ligases and really interesting new gene (RING) finger E3 ubiquitin ligases ubiquitinate endocytic cargo, targeting them for ubiquitin-dependent sorting into early endosomes. HECT domain family members have a variable N-terminal region which interacts with substrates. A flexible hinge region links the C-terminal region, in which an active site cysteine residue receives ubiquitin that is transferred from the E2 conjugating enzyme. The ubiquitin moiety is subsequently transferred to the target substrate protein. Alternatively, RING finger E3 ubiquitin ligases catalyse the transfer of ubiquitin directly from the E2 onto the substrate. RING finger ligases co-ordinate zinc by cysteine and histidine residues and interact with both the E2 ubiquitin conjugating enzyme and the target substrate. Casitas c-linkage lymphoma (Cbl) is a well-studied example of a RING finger E3 ligase which is recruited to activated receptor tyrosine kinases at the plasma membrane and catalyses their ubiquitination.

There are also non-canonical E3 ubiquitin ligase families such as RING in-between RING (RBR). Haem oxidised IRP2 ubiquitin ligase-1 (HOIL-1) is an example of an RBR ubiquitin ligase which generates linear ubiquitin chains. It contains a RING domain which interacts with ubiquitin-conjugated E2, an intervening RBR domain and a second RING2 domain which contains the active site cysteine residue which receives the ubiquitin, which is then transferred to the substrate, similar to HECT domain E3s (Dove and Klevit, 2017, Kelsall et al., 2019). Additionally, the A20 ubiquitin ligase contains an N-terminal ovarian tumour (OTU) domain which has deubiquitylase activity whilst the C-terminal region contains seven zinc fingers, the fourth of which is necessary for ubiquitination of substrates (Wertz et al., 2004).

Ubiquitination enhances, but is not obligatory, for internalisation of some proteins such as epidermal growth factor receptor (EGFR) (Hicke and Riezman, 1996), as this post translational modification (PTM) recruits machinery required for endocytosis to occur (Piper et al., 2014). However, other cargo uptake signals include peptides such as YXXΦ (where Φ represents a bulky residue), di-leucine recognition motifs, whilst phosphorylation may also be an important signal (Acconcia et al., 2009, Sorkin, 2004, Bonifacino and Traub, 2003). Ubiquitination is required for endosomal sorting of

many proteins, and ubiquitinated cargo proteins are recognised by various endocytic adaptor proteins containing ubiquitin binding domains (UBDs), which generally link this signal to degradation at the endosome, though there are some examples of ubiquitination promoting recycling (Piper et al., 2014). Over 20 UBDs are present in more than 150 proteins (Dikic et al., 2009), with many of them involved in the endocytic pathway (Haglund and Dikic, 2012).

1.1.2 ESCRT-dependent sorting

Ubiquitination is recognised by endosomal sorting complexes required for transport (ESCRTs), many subunits of which contain various UBDs (Raiborg and Stenmark, 2009, Dikic et al., 2009). These multi-protein complexes sequentially recognise ubiquitinated cargo present on endosomal membranes and sort it into membrane domains, and then remodel the membrane to form intraluminal vesicles (ILVs) containing these cargoes (Figure 1.2). The efficiency of protein sorting is enhanced by the presence of multiple UBDs in ESCRTs and ESCRT accessory and adaptor proteins, which bind multiple ubiquitin moieties on cargo proteins and increase binding avidity (Dikic et al., 2009, Piper et al., 2014, Raiborg and Stenmark, 2009).

Formation of a multivesicular body (MVB) containing ILVs is dependent on the sequential action of ESCRTs. Hepatocyte growth factor-regulated tyrosine kinase substrate (Hrs) and signal transducing adaptor molecule 1/2 (STAM1/2) interact to form ESCRT-0 (Asao et al., 1997). ESCRT-0 recognises ubiquitinated cargo proteins which are targeted for lysosomal degradation via UBDs in both Hrs and STAM. Specifically, both Hrs and STAM contain vacuolar protein sorting 27 (Vps27), Hrs and STAM (VHS) domains. Hrs also contains a DUIM domain. ESCRT-0 also interacts with Epsin homology protein 15 (Eps15), another ubiquitin binding protein (Bache et al., 2004). Hrs binds to clathrin (Raiborg et al., 2001a) and also contains a Fab1, YOTB, Vac1, EEA1 (FYVE) domain that binds to phosphatidylinositol-3-phosphate (PI3P), which is enriched on the early endosome membrane (Raiborg et al., 2001b) (Figure 1.2). Therefore, ESCRT-0 facilitates recruitment of ubiquitinated cargo to a clathrin-coated subdomain of the early endosome.

ESCRT-I is formed by tumour susceptibility gene 101 (Tsg101) (Babst et al., 2000), Vps28 (Bishop and Woodman, 2001), Vps37A, B or C (Bache et al., 2004, Eastman et al., 2005, Stuchell et al., 2004) and multivesicular body 12 (MVB12) A, B (Morita et al., 2007) or ubiquitin-associated protein 1 (UBAP1) (Stefani et al., 2011, Agromayor et al., 2012). Tsg101 contains a ubiquitin-conjugated enzyme E2 variant (UEV) domain which weakly binds to ubiquitinated cargo. Additionally, Tsg101 binds to ESCRT-0 (Babst et al., 2000) and Vps28 binds to ELL-associated protein of 45kDa (Eap45), a component of ESCRT-II (Kostelansky et al., 2006) and CHMP6, a component of ESCRT-III (Pineda-Molina et al., 2006). Accordingly, ESCRT-I may contribute to sequestering ubiquitinated cargo and also functions as a link between ESCRT-0 and ESCRT-II and/or ESCRT-III (Figure 1.2).

ESCRT-II is composed of Eap30, Eap45 and two Eap20 proteins (Katzmann et al., 2001, Babst et al., 2002b). Eap45 contains a GRAM-like ubiquitin binding in Eap45 (GLUE) domain that binds to ubiquitin and also binds to phospholipids including PI3P on the endosomal membrane (Slagsvold et al., 2005, Teo et al., 2006). Eap20 interacts with charged multivesicular body protein (CHMP) 6 in the ESCRT-III complex (Teo et al., 2006, Yorikawa et al., 2005) (Figure 1.2). It is not yet evident how these early acting ESCRT-0, -I and -II complexes are released from the membrane, but clearly they contribute to sorting and clustering ubiquitinated cargo into subdomains on the endosomal membrane and link to the next complex, ESCRT-III.

ESCRT-III is assembled sequentially on the endosome membrane and is composed of CHMP6, which seeds the assembly of many subunits of CHMP4A/B/C, followed by CHMP3 and CHMP2A/B, which bind to the end of the CHMP4 polymer (Figure 1.2) (Babst et al., 2002a, Saksena et al., 2009, Henne et al., 2012). CHMP1 and CHMP5 may have accessory roles associated with the function of the core complex (Babst et al., 2002a). ESCRT-III does not interact with ubiquitin, but functions to drive membrane deformation instead. CHMP6 anchors to the membrane by an N-myristoylation PTM (Yorikawa et al., 2005) and CHMP4 contains an N-terminal amphipathic helix which inserts into the membrane (Buchkovich et al., 2013), while CHMP3 selectively binds to $PI(3,5)P_2$ and $PI(3,4)P_2$ in the membrane (Whitley et al., 2003). CHMP4 polymerises and forms an array of spiral filaments on the surface of the endosome membrane which supports budding of the ILV into the endosome

(Figure 1.2) (Hanson et al., 2008, Henne et al., 2012). These spirals may limit diffusion of cargo away from this subdomain so that specific cargo is included in the budding ILV (Frankel and Audhya, 2018). CHMP2B binds to Vps4, and CHMP4 stabilises this interaction (Adell et al., 2014). Vps4A/B functions to disassemble and recycle ESCRT-III components in an ATP hydrolysis-dependent process and may have a role in scission of the ILV (Babst et al., 1998, Saksena et al., 2009, Adell et al., 2014).

Histidine domain phospho-tyrosine phosphatase (HD-PTP) binds multiple ESCRT components, including CHMP4B, Tsg101 (Ichioka et al., 2007) and STAM2 (Ali et al., 2013), and is essential for sorting ubiquitinated EGFR to the MVB (Ali et al., 2013). It functions alongside ubiquitin-specific protease Y (UBPY) so that cargo such as EGFR is released from early acting ESCRTs and deubiquitinated before being handed over to ESCRT-III (Ali et al., 2013). This occurs before the ILV membrane is severed to recycle free ubiquitin.

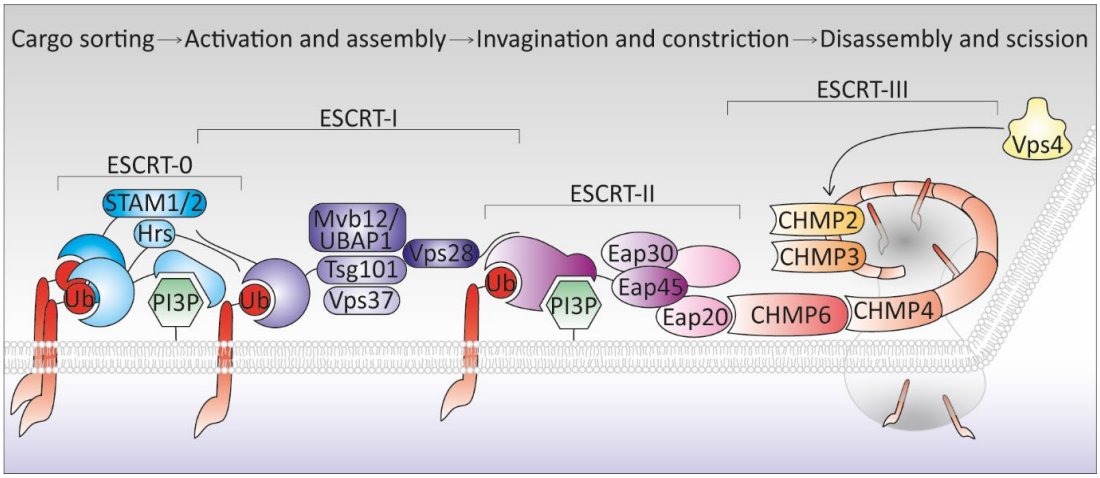

Figure 1.2. Assembly of ESCRT complexes in ubiquitin-mediated endosomal trafficking.
Sorting of ubiquitinated cargo is initiated by ESCRT-0 (blue) which binds PI3P and ubiquitinated cargo. ESCRT-I (purple) binds both ESCRT-0 and ESCRT-II and binds ubiquitinated cargo. ESCRT-II (pink) is recruited to the endosomal membrane and binds both ubiquitin and phospholipids. ESCRT-III subunits (orange) assemble on the membrane and polymerise to form filaments which line the neck of the ILV budding into the endosome. Vps4 disassembles these complexes and catalyses scission of the ILV. Adapted from (Schmidt and Teis, 2012).

The endosomal limiting membrane buds into the endosome lumen, a process that differs from other membrane budding events, which occur towards the cytoplasm. Specialised protein machinery comprised of ESCRTs and accessory proteins are required to achieve this. The exact mechanism of this reverse membrane topology budding and scission is still not exactly clear (Schoneberg et al., 2017). ESCRTs play a vital role in cytokinesis, viral budding, nuclear envelope repair and autophagy, which all involve reverse topology membrane scission and so have similar requirements of the molecular machinery (Hurley and Hanson, 2010).

The sequential action of ESCRTs results in formation of many ILVs in the MVB. The fully-formed, mature MVB is termed a late endosome. The late endosome fuses with the lysosome to form an endolysosome, where cargo proteins undergo hydrolytic degradation by lysosomal proteases (Figure 1.1). This pathway targets selected proteins for degradation and thereby functions to attenuate receptor signalling and alter cellular behaviour. Alternatively, some MVBs may be trafficked to the plasma membrane where the ILV contents are released as exosomes (Huotari and Helenius, 2011).

1.1.3 Recycling pathways

Following internalisation of cell surface proteins, proteins which are not sorted into ILVs remain on the endosomal limiting membrane and may be recycled to the plasma membrane or the *trans*-Golgi network (TGN) (Burd and Cullen, 2014). The recycling pathway allows for the continued function of membrane proteins at the plasma membrane, and can contribute to cellular processes such as integrin recycling for cell migration and invasion (Caswell and Norman, 2008).

Internalised cargoes may not require specific signal-dependent sorting to the recycling pathway, as the majority of the sorting endosome membrane is pinched off to form tubules such that efficient recycling may occur by bulk-flow (Maxfield and McGraw, 2004). However, increasing evidence points to the signal-mediated recycling of a vast range of cargoes. Retrieval machinery recognise sorting motifs in the cytoplasmic tails of cargoes, target them to membrane subdomains and couple this with membrane remodelling machinery to form tubules (Cullen and Steinberg, 2018, Chen et al., 2019). The retromer, retriever and endosomal SNX-BAR sorting complex for promoting exit (ESCPE-1) complexes function in an alternative pathway to ubiquitin-

mediated ESCRT-mediated endocytic trafficking by concentrating specific cargo into distinct membrane subdomains and sorting these cargo to recycling tubules (Burd and Cullen, 2014, McNally et al., 2017, Simonetti et al., 2019).

Retromer is involved in selective trafficking of cargo from endosomes. Previous work has shown a role for retromer in retrograde transport of CI-MPR from endosomes to the TGN (Seaman, 2004, Arighi et al., 2004) but other studies have shown that retrograde transport of CI-MPR occurs independently of retromer (Kvainickas et al., 2017, Evans et al., 2020) and indicate a role for retromer in recycling of cargoes from endosomes to the plasma membrane (Temkin et al., 2011, Steinberg et al., 2013, Evans et al., 2020). The retromer complex is composed of a core heterotrimer of Vps26, Vps29 and Vps35 (Figure 1.3A) (Seaman et al., 1997, Bonifacino and Hurley, 2008). Vps26A/B contains an arrestin domain and binds Vps35 (Shi et al., 2006, Collins et al., 2008). Vps29 contains a phosphodiesterase domain and also binds Vps35 (Hierro et al., 2007), whilst Vps35 contains an α-solenoid domain (Hierro et al., 2007, Bonifacino and Hurley, 2008). Rab7 interacts with retromer and recruits this complex to endosomes (Rojas et al., 2008, Seaman et al., 2009). Rab5 interacts with VPS34 (Christoforidis et al., 1999), a PI3 kinase which produces PI3P on endosomal membranes and so may contribute to recruitment of sorting nexin (SNX) proteins on endosomes and thus subsequent recruitment of retromer (Rojas et al., 2008). SNX3 may have a role in targeting retromer to endosomal membranes as it contains a phox homology (PX) domain, which mediates binding to phosphoinositides, including PI3P, on endosomal membranes (Carlton et al., 2005, Harterink et al., 2011, Chandra et al., 2019). SNX3 also acts as a cargo adaptor (Harterink et al., 2011, Kovtun et al., 2018), as does SNX27 (Lauffer et al., 2010, Temkin et al., 2011, Steinberg et al., 2013) (Figure 1.3A). These bind specific cargo and target them to the retrieval subdomains on endosomes (van Weering et al., 2012).

Retriever is composed of DSCR3, C16orf62 and Vps29, and is likely to have structural homology to retromer (McNally et al., 2017). This heterotrimer binds to the coiled-coil domain containing 93 (CCDC93), CCDC22 and copper metabolism domain containing 1 (COMMD1) (CCC) complex to form the COMMander complex and associates with SNX17, which acts as the cargo adaptor (Figure 1.3A). Retriever is

required for the recycling of various membrane proteins to the plasma membrane including α5β1 integrin (McNally et al., 2017).

Another complex which has a role in sorting cargo is the ESCPE-1 complex, which is formed of SNX1/2-SNX5/6 heterodimers (Simonetti et al., 2019). SNX1, 2, 5 and 6 contain a PX domain (Carlton et al., 2005). Phosphoinositide binding by SNX1 and 2 has relatively low affinity, so dimerisation may facilitate efficient targeting of SNX1/2 to PI3P-positive membranes (Carlton et al., 2005, Chandra et al., 2019). SNX5/6 are likely to facilitate cargo selectivity (Kvainickas et al., 2017, Simonetti et al., 2017).

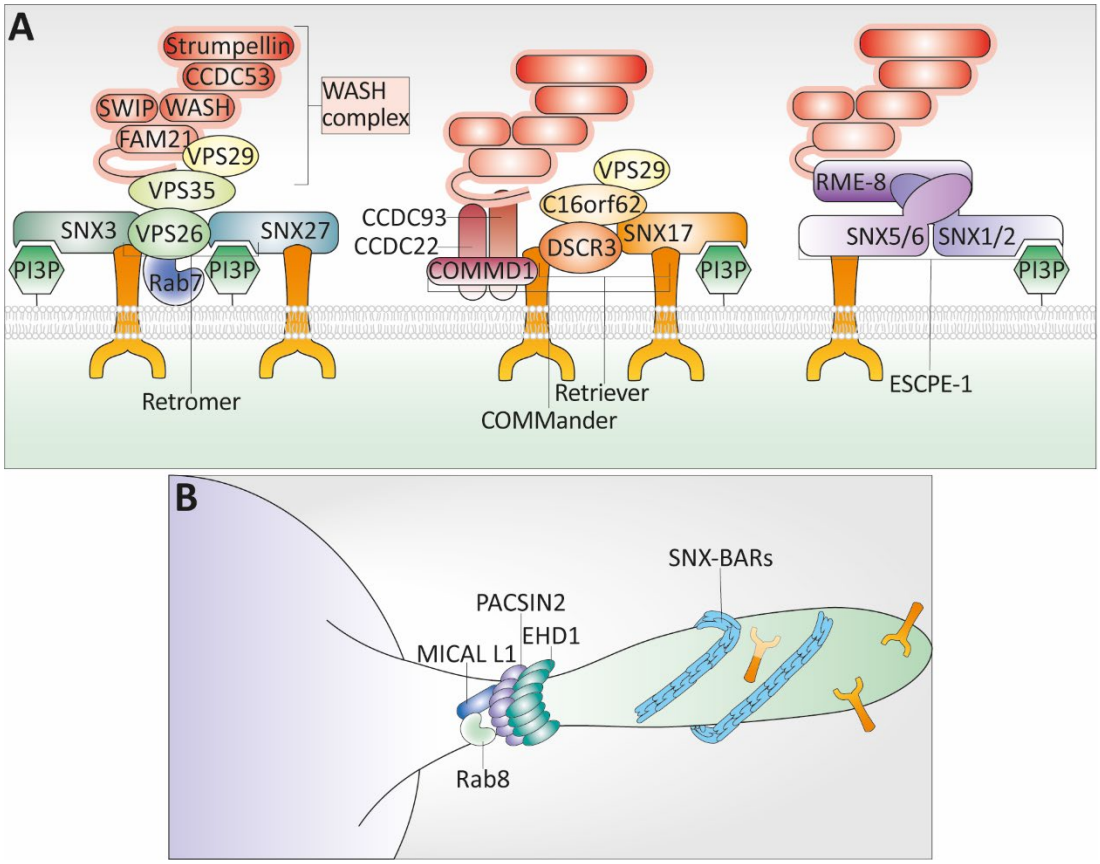

Figure 1.3. Assembly of retrieval complexes for recycling in the endosomal pathway.
A. Multiprotein complexes assemble on the cytoplasmic side of sorting endosomes as they bind to PIP present in the membrane. They have a role in retrieving recycling cargo into retrieval domains in a signal sequence-dependent manner. B. Tubules extend from the retrieval subdomain of the sorting endosome. SNX-BAR proteins assemble onto the membrane through electrostatic interactions, binding to PI3P and scaffolding membrane curvature. SNX-BAR dimers oligomerise and induce and/or stabilise membrane tubulation. Various molecular machinery including Pacsin2, Rab8 and EHD1 are recruited onto the membrane by interactions with MICAL L1. The final scission step may be carried out by EHD1. Adapted from (Cullen and Steinberg, 2018, Simonetti and Cullen, 2019).

ESCPE-1 sorts cargo such as CI-MPR from endosomes to the TGN independently from other complexes and is distinct from retromer (Evans et al., 2020), but is able to associate transiently with retromer (Simonetti et al., 2019, Kvainickas et al., 2017, Simonetti et al., 2017).

The Wiskott-Aldrich syndrome proteins and SCAR homologue (WASH) complex links the different retrieval complexes to the actin cytoskeleton. Family with sequence similarity 21 (FAM21) is a subunit of WASH that has an extended tail region which mediates binding to specific components of these sorting complexes. FAM21 interacts with VPS35 in retromer (Harbour et al., 2012), the CCC complex which binds retriever (Phillips-Krawczak et al., 2015) and receptor mediated endocytosis 8 (RME-8), which also associates with ESCPE-1 (Freeman et al., 2014) (Figure 1.3A). The WASH complex localises to endosomes and activates Arp2/3, which results in actin polymerisation that is necessary for recycling of cargo. The local actin cytoskeleton stabilises endosomal tubules (Puthenveedu et al., 2010) and also contributes to sorting by anchoring sorting complexes (Simonetti and Cullen, 2019). Actin contributes to membrane remodelling, as it drives formation of tubules from recycling cargo-enriched subdomains (Simonetti and Cullen, 2019) as well as possibly providing the force to sever these tubules (MacDonald et al., 2018). Actin binding is a sorting signal for the recycling pathway in itself (Puthenveedu et al., 2010, MacDonald et al., 2018).

Efficient sorting of cargo to the appropriate destination compartment is required for cellular homeostasis (Weeratunga et al., 2020). The retrieval complexes function in distinct pathways, as the complexes directly or indirectly (through associated adaptor proteins) recognise different signals in recycling cargo and may direct them to different acceptor compartments. Various cargo motifs which bind to retrieval machinery in a wide range of membrane receptors have been identified (Weeratunga et al., 2020): retromer-SNX3 is able to recognise the sorting motif ΩΦ[LMV] (Tabuchi et al., 2010), retromer-SNX27 recognises the sorting motif [-][-]x[-][ST]xϕ (Steinberg et al., 2013, Clairfeuille et al., 2016), commander-SNX17 recognises ΦxNxx[YF] (McNally et al., 2017) and ESCPE-1 recognises $\Phi x\Omega^{0}x\Phi[x_{n}]\Phi$ (Simonetti et al., 2019) (where Φ is a bulky/hydrophobic residue, Ω is an aromatic residue and - is a negatively charged residue).

Whilst the retrieval complexes sort specific cargo to tubular extensions of the sorting endosome, separate machinery is required to generate these tubules alongside the actin/WASH machinery. This generation of high membrane curvature requires the physical deformation or bending of the lipid bilayer. Induction of membrane curvature is a morphological change required for tubulation and is a key step in tubule formation in the recycling pathway (van Weering et al., 2012). Induction of membrane curvature is an active process that requires specific proteins that bind to the membrane as well as specific phospholipids. Local curvature can be induced by changes in lipid composition (Kooijman et al., 2003), assembly of scaffolding proteins or insertion of an amphipathic helix between the polar headgroups of membrane lipids (McMahon and Gallop, 2005). Various components of the machinery involved in membrane tubulation are able to sense and/or generate membrane curvature.

Bin/Amphiphysin/Rvs (BAR) domain-containing proteins are required for membrane tubulation from endosomes (Zimmerberg and Kozlov, 2006). Protein kinase C and casein kinase II interacting protein (Pacsin2) is an F-BAR domain-containing protein and SNX1, 2, 4, 5 and 6 are SNX-BAR proteins. These BAR domains dimerise and form a curved scaffold that binds to the membrane to deform the membrane and thus induce local membrane curvature (McMahon and Gallop, 2005, van Weering et al., 2012, Carlton et al., 2005). These proteins, as well as Epsin-homology domain-containing protein 1 (EHD1) (see below), also contain short amphipathic helices that insert into the membrane and form a wedge which contributes to membrane deformation (van Weering et al., 2012).

EHD1 is involved in membrane reorganisation events on the early endosome as well as recycling tubules. EHD1 can tubulate membranes *in vitro* (Daumke et al., 2007) and was found to have a specific role in vesiculating recycling tubules (Cai et al., 2013). EHD proteins contain a dynamin-like domain and have ATPase activity and so may also have a role in the remodelling and scission of these tubules from the endosome, similar to dynamin (Deo et al., 2018). EHD1 binds to PI4P (which is enriched on recycling tubules (Jovic et al., 2009)) and to retromer subunits, and stabilises SNX1-positive tubules (Gokool et al., 2007). EHD1 can also recruit Pacsin2 to membranes and this interaction is required for recycling to occur (Braun et al., 2005). Pacsin2 and Molecules interacting with casl-like 1 (MICAL-L1) bind to phosphatidic acid which is

also present on recycling endosomes, and the action of these proteins together leads to membrane tubulation (Figure 1.3B) (Giridharan et al., 2013). MICAL-L1 is an important regulatory protein which also localises to the tubular retrieval domain and binds various proteins which have important roles on recycling endosomes. MICAL-L1 binds to Rab8, Rab35 and ADP-ribosylation factor 6 (Arf6), which are key regulators of the tubular recycling endosome (TRE) (Rahajeng et al., 2012). Arfs are a family of small GTPases which regulate membrane trafficking (Donaldson and Jackson, 2011). Arf6 is involved in regulating recycling of specific cargo (Eyster et al., 2009); activation of Arf6 is required for recycling of cargo to the plasma membrane while inactivation of Arf6 results in protein sorting into late endosomes (Radhakrishna and Donaldson, 1997). MICAL-L1 also links Rab8 and EHD1 on these tubules (Sharma et al., 2009, Kieken et al., 2010). These data show that various interacting proteins on the TRE are important in generating membrane tubules and regulating receptor recycling (Sharma et al., 2009, Braun et al., 2005, Rahajeng et al., 2012, Giridharan et al., 2013).

1.1.4 Regulation of endosomal compartments

Endosomal maturation from an early endosome to the late endosome occurs as the endosome migrates into the cell. Maturing of the endosome is associated with various molecular alterations such as changes in the Rabs that are present on the membrane. Rabs are considered master regulators of membrane trafficking and function to regulate events such as vesicle formation, movement, tethering and fusion, by recruiting transport machinery and regulatory components (Pfeffer, 2017). As endosomes are transported through the cell they get progressively more acidic due to the action of the vacuolar proton pump V-ATPase (Podinovskaia and Spang, 2018). Furthermore, as the endosome matures there is conversion of phosphoinositides, notably from PI3P to PI3,5P_2. Phosphoinositides also have a role in conferring the identity of endosomal compartments, and their generation and interconversion is tightly regulated (Wallroth and Haucke, 2018). These small GTPases and phosphoinositides target proteins to membranes by mediating interactions and contribute to the directionality of transport (Huotari and Helenius, 2011, Podinovskaia and Spang, 2018).

Early endosomes are present throughout the cell and accept cargo from the plasma membrane. Early endosome antigen 1 (EEA1) is found exclusively on early endosomes and binds the PI3P-enriched membrane via its FYVE domain, and is also recruited to the membrane by Rab5 (Simonsen et al., 1998, Gillooly et al., 2000). EEA1 is a membrane tether required for early endosome fusion, where it binds to the soluble N-ethylmaleimide-sensitive factor attachment protein receptor (SNARE) syntaxin-6 (Simonsen et al., 1999) and syntaxin-13 (McBride et al., 1999). Rab5 also associates with the class C core vacuole/endosome tethering (CORVET) complex, which tethers early endosomes together before homotypic fusion occurs (Perini et al., 2014). CORVET is composed of the core class C complex Vps11, Vps16, Vps18 and Vps33A (Huizing et al., 2001) as well as Vps8 and Tgfbrap1, which bind Rab5 (Peplowska et al., 2007, Perini et al., 2014). Vps33A is likely to mediate interactions with specific SNAREs which drive membrane fusion (Saleeb et al., 2019) but other CORVET subunits may directly contribute to fusion (Kim et al., 2001). Combinations of specific tethers as well as SNAREs provides specificity as to which membranes fuse (Spang, 2016). Early endosomes contain another tethering complex containing Vps33B and VIPAS39 (which has homology to Vps16) that may act as a dimer (van der Kant et al., 2015) or may recruit other proteins in the class C homologues in endosome-vesicle interaction (CHEVI) complex which receives vesicles from the TGN (Spang, 2016).

Maturation from an early to a late endosome is associated with translocation to the perinuclear area, increased ILV contentnd the acquisition from the Golgi of highly glycosylated proteins such as LAMP1, LAMP2 and the tetraspanin CD63 (Janvier and Bonifacino, 2005). Late endosomes also contain lysobisphosphatidic acid (LBPA), which may contribute to ILV formation (Matsuo et al., 2004). Preceding fusion with the lysosome is an enrichment of PI(3,5)P2 in the membrane (Li et al., 2013). Additionally, there is a switch from a Rab5-positive to a Rab7-positive membrane (Rink et al., 2005, Poteryaev et al., 2010). The homotypic fusion and protein sorting (HOPS) tethering complex is recruited and mediates fusion between late endosomes and the late endosome with the lysosome (Pols et al., 2013). HOPS shares the core class C heterotetramer with CORVET but also contains Vps41 and Vps39 (Richardson et al., 2004, Pols et al., 2013) in the place of Vps8 and Tgfbrap1. Vps41 and Vps18 mediate interaction with Rab-interacting lysosomal protein (RILP), which is a Rab7

effector (van der Kant et al., 2015). Displacement of the Rab5-binding subunits of CORVET means that the late endosome can no longer fuse with early endosomes (Spang, 2016).

Associated with endosomal maturation is the removal of recycling cargo into recycling endosomes. Regions of the sorting endosome that will form recycling endosomes are organised into tubular domains. Tubular domains of late endosomes are PI3,5P deficient and this may contribute to subdomain segregation (Takatori et al., 2016). PI4P, and possibly PI(4,5)P_2, is generated on recycling endosomes, and is required for eventual fusion of recycling intermediates with the plasma membrane (Jovic et al., 2009). Recycling endosomes also contain phosphatidic acid, and this may enhance membrane tubulation activity (Giridharan et al., 2013).

Recycling compartments can also be distinguished spatially and morphologically, as the endosomal recycling compartment (ERC) typically localises close to the microtubule organising centre (MTOC) in the perinuclear area (Grant and Donaldson, 2009, Maxfield and McGraw, 2004) whilst the TRE is tubulovesicular and extends into the cytoplasm towards the plasma membrane from endosomes. There is evidence to suggest that the Rab11-positive ERC is composed of clustered single vesicles and is involved in recycling CME cargo whilst the TRE, labelled with MICAL-L1, is involved in recycling CIE cargo (Xie et al., 2016). TREs may also transport cargo from the SE to the ERC (Xie et al., 2016). The TRE transports cargo back to the plasma membrane along microtubules and actin (Grant and Donaldson, 2009). It is not yet clear if the ERC and the TRE are distinct or overlapping compartments.

There are kinetically distinct recycling pathways that can be distinguished from each other; Rab4-dependent fast recycling of cargo back to the plasma membrane occurs in a short loop, direct from the early endosome, whilst slow recycling of cargo in a long loop recycling pathway involves an intermediate compartment (the ERC and/or the TRE) and is dependent on Rab11 (Sonnichsen et al., 2000) and/or Rab8 (Goldenring, 2015). (Figure 1.1). Rab4 and Rab11 are separated from the sorting endosome at an early stage in endosomal maturation, which may indicate that these pathways are restricted from this point. Rab11 also has a role in tethering of recycling endosomes to the plasma membrane, where the contents are eventually released by the action of the exocyst complex (Takahashi et al., 2012).

The factors for endosome recycling and Rab interaction (FERARI) is a tethering complex which is involved in Rab11-dependent recycling from sorting endosomes to the plasma membrane, and may tether Rab11-recycling endosomes to SNX1-tubules for cargo sorting to occur before pinching off (Spang, 2016). FERARI consists of rabenosyn-5, which binds to Rab5 on sorting endosomes, and Rab11 family interacting partner 5 (Rab11FIP5), which binds to Rab11. Rab11FIP5 also binds to the Vps45 and VIPAS39 module that in turn interacts with syntaxin 6, which mediates fusion with the plasma membrane, and syntaxin 7, which mediates endosomal trafficking (Solinger et al., 2020). EHD1 is another FERARI component, binding to Rab11FIP5. As described above, EHD1 mediates membrane scission (Solinger et al., 2020). Another complex involved in forming recycling intermediates is endosome-associated recycling protein (EARP) which consists of Vps51/Ang2, Vps52, Vps53 and syndetin (Schindler et al., 2015). Vps52 may bind to Rab4 (Spang, 2016) and EARP is present mainly on Rab4-positive fast recycling endosomes but also localises to slow recycling endosomes. EARP may act as a tethering factor on fast recycling endosomes which associates with SNAREs on endosomes, as this complex associates with syntaxin-6 (Schindler et al., 2015).

1.1.5 Co-ordination of degradation and retrieval

Maturing endosomes contain both ESCRT and retrieval machinery, but they are separated into spatially distinct subdomains (Cullen and Steinberg, 2018). Precise co-ordination between the degradation and retrieval subdomains is required to control the maturation of the late endosome and fusion with the lysosome and also release of recycling tubules. The degradative subdomain contains ESCRT machinery and ubiquitinated receptors and is a flat, clathrin coated surface (Raiborg et al., 2002), whilst the retrieval domain contains retrieval machinery and has a tubular morphology which is stabilised by actin (Simonetti and Cullen, 2019). Rab4, Rab5 and Rab11 are also localised to distinct areas on the same endosomal membrane (Sonnichsen et al., 2000). Furthermore, phosphoinositides are also localised to microdomains on endosomes, such as PI3P-rich domains (Gillooly et al., 2000) and there is separation of PI4P and PI4,5P domains (Yoshida et al., 2017). These domains are likely to have functional importance and their segregation is necessary to prevent inappropriate targeting of cargos. Recent work has provided insights into the regulatory interactions between the two domains (Podinovskaia and Spang, 2018).

Whilst Hrs has a defined role in the initiation of the ESCRT assembly, it also recruits the WASH complex to endosomes (MacDonald et al., 2018). The WASH complex may have a role in segregating these domains by generating an actin network that restricts lateral movement of cargos recognised by retrieval machinery (Derivery et al., 2012, Simonetti and Cullen, 2019). Hrs binds endosomal clathrin, which may contribute to its organisation into a flat membrane subdomain separate from retromer components (Raiborg et al., 2001a, Raiborg et al., 2002). Furthermore, SNX1 and RME-8 interaction on endosomes negatively regulates local clathrin accumulation and allows retrograde trafficking to occur (Shi et al., 2009). SNX1 and 2 have further roles in separating the retromer subdomain containing RME-8 (Norris et al., 2017) from the ESCRT domain. Cargo binding to actin directly or via accessory proteins directs them to the recycling pathway (Puthenveedu et al., 2010, MacDonald et al., 2018).

Rab7 interacts with machinery targeting cargo to both degradative and retrieval pathways and so could have a regulatory role. Rab7 recruits retromer to endosomes but the Rab-GAP TBC1D5 negatively regulates this interaction (Seaman et al., 2009). It was shown in yeast that Rab7 binds retromer and is subsequently displaced as SNX-BAR proteins associate and localise to tubular domains. This displacement ensures that Rab7 is available for binding to other tethering complexes, allowing the endosome to fuse with lysosomes (Purushothaman et al., 2017). RILP is a Rab7 effector that also interacts with ESCRT-II, though the significance of this interaction is still not clear. RILP is a microtubule adaptor and so may couple endosomal maturation with movement towards the MTOC (Progida et al., 2006, Wang and Hong, 2006).

The ESCRT machinery is also associated with microtubule severing that is required for recycling. ESCRT-III interacts with increased sodium tolerance 1 (IST1). IST1 is dispensable for degradation of cargo (Agromayor et al., 2009), but required for correct sorting of recycling cargo. Spastin interacts with CHMP1B (associated with ESCRT-III) (Reid et al., 2005) and is recruited to endosomes by ISTI (Allison et al., 2013). Spastin is a ATP-dependent microtubule severing protein which is required for scission of recycling tubules from the endosome (Allison et al., 2013).

Ubc13 is a ubiquitin ligase which ubiquitinates cargo destined for lysosomal degradation. However, recently it was found to be required for retromer-mediated recycling of cargo in *C. elegans*. This indicates that there is cross talk between

degradative and recycling components, and various proteins such as Ubc-13 are required to regulate their segregation (Zhang et al., 2018). Additionally, ubiquitination of recycling machinery is required to maintain separation between recycling and degradative subdomains, as loss of RFFL E3 ubiquitin ligase affects the recycling compartment (Sakai et al., 2019).

In summary, the dynamic localisation of proteins at the plasma membrane and in endosomal compartments is dependent on the balance between endocytosis and subsequent targeting to degradation or recycling pathways. Functions of cargo proteins may be dependent upon their trafficking and therefore, regulation of endocytosis is required for correct protein trafficking, signalling and cellular organisation. This is highlighted by the range of diseases which are caused by dysregulation of endocytosis, including cancer (Mellman and Yarden, 2013), infectious disease and neurodegenerative diseases (Stuffers et al., 2009). As described above, numerous accessory proteins contribute to the organisation of this complex process but their roles have not been fully characterised.

1.2 LITAF

Lipopolysaccharide-induced tumour necrosis factor-α factor (LITAF), also known as small integral membrane protein of the late endosome (SIMPLE) (Moriwaki et al., 2001) and p53-induced gene 7 (PIG-7) (Polyak et al., 1997), is a protein associated with endosomal membranes and may have a role in regulating protein sorting. Mutations in LITAF result in disease, indicating that it has an important function.

1.2.1 Expression

LITAF is ubiquitous and abundantly expressed (Myokai et al., 1999, Polyak et al., 1997, Everett et al., 1997, Jolliffe et al., 2000, Lee et al., 2011). LITAF expression is induced by p53 (Polyak et al., 1997, Zhu et al., 1999), by LPS during a TNFα-regulated transcriptional response (Myokai et al., 1999), and by pathogen-associated molecular patterns (PAMPs) in monocytes (Moriwaki et al., 2001). Similarly, the rat orthologue, estrogen-enhanced transcript-1 (EET-1), now identified as LITAF, is induced by oestrogen (Everett et al., 1997). High LITAF mRNA expression was detected in human placenta, peripheral blood leukocytes, lymph nodes and spleen (Myokai et al., 1999). LITAF is expressed in human sciatic nerve cell types, including Schwann cells

(Bennett et al., 2004). LITAF protein is widely expressed in mouse tissues including Schwann cells and peripheral nerves (Lee et al., 2011). LITAF protein is specifically expressed in the myelinating Schwann cell body but not in neuronal axons in mice and rat (Lee et al., 2013). Therefore, LITAF is expressed in multiple cell types, where it may have a similar fundamental basic function.

1.2.2 Localisation

There are varying reports of LITAF's subcellular localisation, and this may depend on the cell type and expression system used. LITAF was predicted to localise to the nucleus but this was not confirmed experimentally (Moriwaki et al., 2001). A later study indicated that LITAF may translocate to the nucleus when in complex with STAT6 (Tang et al., 2006). However, many studies have concluded that LITAF mainly localises to perinuclear late endosomes and lysosomes (Moriwaki et al., 2001, Ludes-Meyers et al., 2004, Eaton et al., 2011, Zhu et al., 2013, Lacerda et al., 2014, Qin et al., 2016). LITAF was localised inside ILVs in MVBs and inside exosomes by immunoelectron microscopy (Zhu et al., 2013). LITAF has also been reported to be localised partially to the Golgi (Ludes-Meyers et al., 2004, Shirk et al., 2005, Moriwaki et al., 2018), plasma membrane (Shirk et al., 2005, Qin et al., 2016) and early endosomes (Lee et al., 2011, Qin et al., 2016). Recent studies have determined that LITAF localises to recycling endosomes (Moriwaki et al., 2018) and that LITAF knock down in cells results in expansion of the TRE (Wunderley et al., 2021). Endogenous LITAF was also localised to the aggresome, but the functional significance of this is unknown (Eaton et al., 2012). The endocytic system is dynamic, and LITAF may exist transiently in many of these endocytic compartments and at the cell surface.

1.2.3 Structure

LITAF has an interesting structure that is likely to be relevant to its function. It is a 17kDa protein which is unglycosylated (Moriwaki et al., 2001) and is phosphorylated on tyrosine residues in response to stimulation of cells by EGF (Lee et al., 2012). LITAF was predicted to insert into, but not cross, the membrane to form a zinc-finger (Ponting et al., 2001) but also predicted to be a transmembrane protein due to the presence of a hydrophobic region in the C-terminus (Lee et al., 2011). Structural and biochemical data have now shown that LITAF is a monotopic membrane protein which inserts into the membrane so both N and C termini are cytoplasmic (Figure 1.4A) (Qin

et al., 2016, Ho et al., 2016). The structure of full length LITAF could not be solved but the structure of LITAF Δ114-139 (lacking the membrane associated hydrophobic region) (Figure 1.4, purple) was solved by NMR. The N-terminus is flexible and likely to be unstructured. The C-terminal LITAF domain contains 5 β strands, the first of which is the most flexible. The first three β strands are before the hydrophobic region, and the two β strands at the C-terminus after the hydrophobic region form a β hairpin (Ho et al., 2016). LITAF could not be crystallised and it is too small for current cryoelectron microscopy methods, so the structure of full length wild-type (WT) LITAF has not been elucidated (Ho et al., 2016).

1.2.3.1 N-Terminal domain

The N-terminal domain of LITAF is proline-rich (Moriwaki et al., 2001) and contains several motifs which are important for its interactions with other proteins. The NMR structure showed that the N-terminal domain is relatively flexible and exposed to the cytoplasm while the region from amino acid 22-34 containing proline protein interaction motifs is slightly more rigid, which could facilitate protein interactions in this region (Ho et al., 2016). Interactions with other proteins mediated by this domain are likely to be important for LITAF function and may also affect its subcellular localisation (Ho et al., 2016).

LITAF contains two PPXY motifs near its N-terminus (Figure 1.4B). PPXY motifs bind to WW domains on other proteins (Macias et al., 2002). In the case of LITAF, the first PPXY may mediate an interaction with WW domain oxioreductase (WWOX) (Ludes-Meyers et al., 2004). Meanwhile, both PPXY motifs in LITAF are required for its interaction with ITCH, also known as atrophin-1-interacting protein 4 (AIP4). Murine LITAF (N4WBP3) also interacts with neuronal precursor cell expressed developmentally downregulated 4 (Nedd4) via its first PPXY motif (Jolliffe et al., 2000). This was confirmed in a human cell line using endogenous proteins (Shirk et al., 2005). Nedd4 and ITCH are Nedd4 family ligases which are HECT domain E3 ubiquitin ligases. Their N-terminal region contains a C2 domain that may target them to membranes and 4 WW domains, which interact with PPXY motifs on target substrates as well as adaptor proteins. ITCH has a role in endosomal sorting of proteins, as it ubiquitinates membrane receptors as well as Hrs, a component of ESCRT-0 (Marchese et al., 2003). LITAF also interacts with the ESCRT-I component

TSG101 through its PSAP motif (Figure 1.4B) (Shirk et al., 2005), an interaction which may involve the UEV domain of TSG101, similar to the interaction of TSG101 with Hrs (Lu et al., 2003). LITAF also directly interacts with STAM1, and forms a ternary complex with STAM1 and Hrs (Lee et al., 2012). TSG101, STAM1 and Hrs are ESCRT proteins which bind mono-ubiquitinated proteins and have a role in protein sorting (see above) (Katzmann et al., 2001).

LITAF subcellular localisation is likely to be affected by its protein interactions. Disruption of PPXY motifs in LITAF resulted in greater plasma membrane localisation (Ho et al., 2016) or increased early endosome localisation (Eaton et al., 2013). Additionally, LITAF localises to early and late endosomes, where ESCRT components are also located. The influence of other proteins may therefore explain the

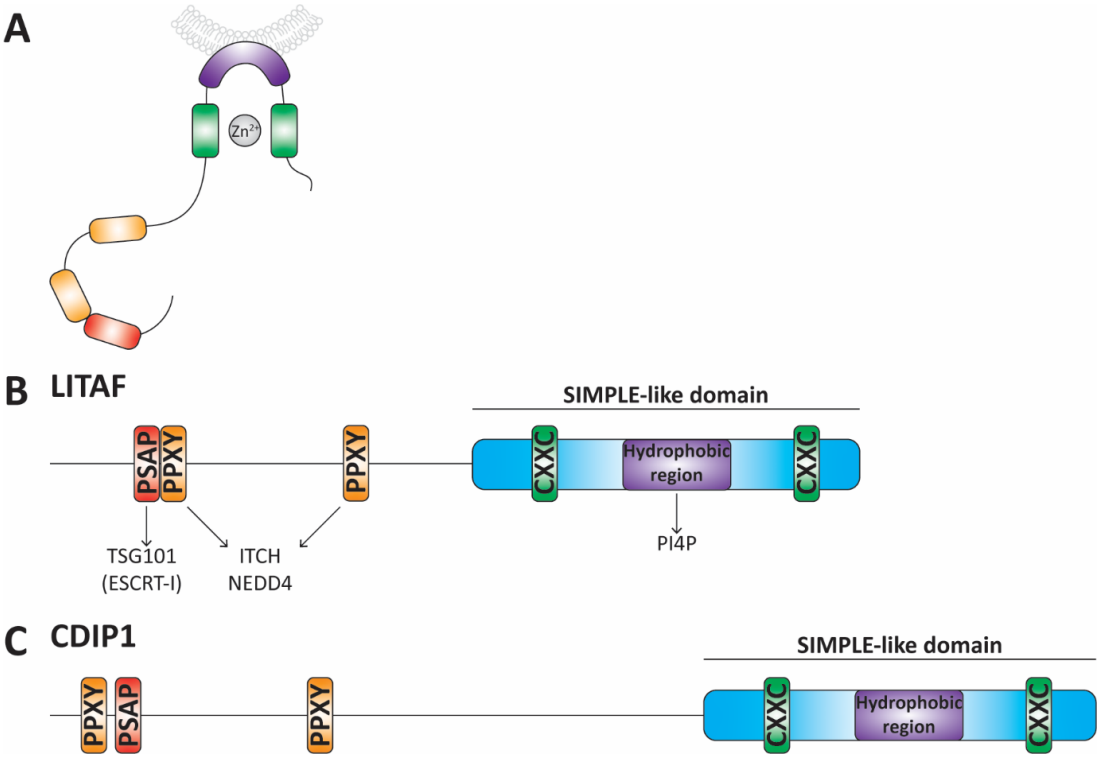

Figure 1.4. Schematic of LITAF and CDIP1 structure and domains.
A. LITAF is a monotopic membrane protein. The hydrophobic region (HR) of the LITAF domain inserts into the membrane so both C and N termini are cytoplasmic. This membrane topology is conserved in CDIP1. B. LITAF binds TSG101, and ITCH/Nedd4 through proline interaction motifs near its N-terminus. The C-terminal domain of LITAF contains two CXXC motifs which co-ordinate zinc, separated by a hydrophobic region (HR), termed the LITAF domain or small integral membrane protein of the lysosome/late endosome (SIMPLE)-like domain. LITAF contains di-leucine and YXXΦ endocytic motifs at its C-terminus. C. CDIP1 has a similar domain organisation to LITAF. It contains a PPXY and PTAP motifs in the N-terminus and the conserved C-terminal SIMPLE-like domain. Adapted from (Qin et al., 2016).

differences in LITAF subcellular localisation observed in different cell types (Ho et al., 2016).

The PSAP motif and the first PPXY motif in LITAF overlap, sharing a proline residue (Figure 1.4B). Therefore, it seems unlikely that both TSG101 and WW domain-containing proteins can bind to LITAF simultaneously, due to steric hindrance. Therefore it may be that these proteins bind at different stages of the lysosomal degradation pathway (Shirk et al., 2005). Alternatively, these proteins may be recruited to different LITAF proteins, which then homo-oligomerise. LITAF can form homo-oligomers (Lee et al., 2012) and LITAF-domain containing proteins are able to hetero-oligomerise (Eaton et al., 2013, Chen et al., 2016), such that complex formation could facilitate multiple interactions.

1.2.3.2 C-Terminal LITAF domain

The C-terminal region of LITAF is cysteine-rich and contains a highly conserved domain called the SIMPLE-like domain or LITAF domain (Figure 1.4B, Figure 1.5) (Moriwaki et al., 2001, Ho et al., 2016, Qin et al., 2016). This domain contains two CXXC motifs which co-ordinate zinc (Figure 1.4A, B) (Ho et al., 2016, Qin et al., 2016). The zinc finger may stabilise the membrane interaction. HXCXXC is the second motif and the histidine is conserved (Figure 1.5) (Qin et al., 2016). These CXXC motifs are required for integration into endosomal membranes (Qin et al., 2016) and mutation of cysteine residues results in insoluble protein (Ho et al., 2016). There is a hydrophobic region in the centre of the C-terminal LITAF domain that is predicted to anchor to the membrane, but the NMR structure of this region was not solved. Specific residues within the LITAF domain interact with phosphatidylethanolamine (PE) head groups. Deletion or mutation of this domain abolishes membrane

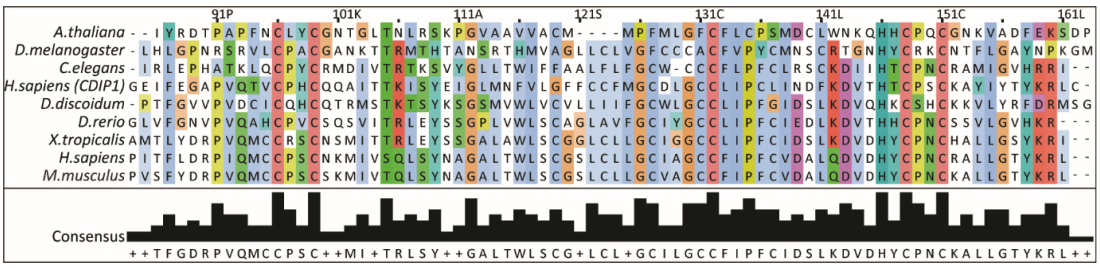

Figure 1.5. Alignment of eukaryotic LITAF domain.
The LITAF domain from various eukaryotic LITAF homologs and human CDIP1 was aligned. There is a high level of identity in this region and critical residues are conserved, indicated in the consensus histogram sequence. Adapted from (Qin et al., 2016).

association. (Ho et al., 2016). In another study, LITAF (115-141) was shown to bind specifically to PI4P but not PE (Moriwaki et al., 2018). Therefore, although the precise nature of the membrane interaction is not clear, co-ordination of zinc and hydrophobic interactions are required for LITAF's membrane association.

LITAF contains a di-leucine motif followed by a YKRL motif at its C-terminus (Figure 1.5) (Moriwaki et al., 2001). The YXXΦ consensus sequence, where Y is a tyrosine residue, X is any amino acid and Φ is a bulky amino acid, mediates binding to AP-2, which is an adaptor protein associated with clathrin. This motif is a sorting signal for internalisation via clathrin-dependent endocytosis and also for protein sorting. It is present in many endocytic proteins including membrane receptors and lysosomal proteins (Bonifacino and Traub, 2003). The di-leucine motif is also involved in targeting to the late endosome/lysosome and also has a role mediating binding to AP-2 (Bonifacino and Traub, 2003). These motifs are functionally important for formation of exosomes containing LITAF (Zhu et al., 2013). However, it is yet to be established whether these motifs do act as AP-2 binding motifs or perform other function(s).

The LITAF domain is a conserved modular domain which is found in other proteins (Ponting et al., 2001). A closely related protein found in humans is cell death-inducing p53-target protein 1 (CDIP1), which has similarity to LITAF in both its N-terminal domain and LITAF domain (Figure 1.4C, 1.5). These are the only known proteins containing the conserved LITAF domain in humans. The LITAF domain is also found in proteins from other species, and critical amino acids that are likely essential for function are conserved (Figure 1.5). Information on the function of these conserved proteins may be relevant to the properties and function of human LITAF as it could be common between species.

1.3 LITAF domain containing proteins

1.3.1 CDIP1

LITAF has homology to CDIP1 (Brown et al., 2007) but their functional relationship is unknown. CDIP1 is highly expressed in the brain, expressed in the heart, skeletal muscle, kidney, pancreas and liver but is weakly expressed in the placenta and lung (Bhalla et al., 1999). CDIP1 expression is induced by p53 but not by LPS, and is also associated with induction of TNF-α (Brown et al., 2007). CDIP1 expression is

upregulated in mouse livers in response to endoplasmic reticulum (ER) stress (Namba et al., 2013).

The function of CDIP1 is unknown, but ectopic expression promoted apoptosis with increased caspase-8 activity (Brown et al., 2007) and increased caspase 3/7-mediated cell death (Inukai et al., 2021). The N-terminus of CDIP1 interacts with BAP31 at the ER membrane under stress conditions, and this complex regulates mitochondrial apoptosis (Namba et al., 2013). CDIP1 knockout mice have reduced apoptosis in the liver in response to stress, confirming that CDIP1 is a pro-apoptotic factor (Namba et al., 2013). CDIP1 was predicted to be localised to the nucleus (Bhalla et al., 1999), but was shown to localise to late endosomes and lysosomes similar to LITAF. LITAF and CDIP1 co-localise in these compartments (Qin et al., 2016) but it is not known whether they hetero-oligomerise. Whilst CDIP1 localises to the endocytic pathway, it could have other functions at the ER.

Recent evidence has pointed to CDIP1 function on endosomes as CDIP1 can interact with apoptosis-linked gene 2 (ALG-2) via a PQPGF sequence, and TSG101 in a calcium ion-dependent manner and vesicle associated membrane protein-associated protein A (VAPA) and VAPB independently of calcium (Inukai et al., 2021). Overexpression of CDIP1 resulted in increased cell death, and expression of ALG-2 potentiated this effect (Inukai et al., 2021). In contrast, LITAF did not co-immunoprecipitate with ALG-2, does not contain the PQPDGF sequence, pulled down much lower amounts of VAPA and B, and doesn't have one of the key conserved residues of the FFAT-like motif (Inukai et al., 2021). This indicates that whilst LITAF and CDIP1 may share some interaction partners, they also have unique interactions and so may have non redundant functions.

CDIP1 also has a proline-rich N-terminus that contains a PPXY motif and a PSAP motif but the functional importance of these has not been investigated. The C-terminus is cysteine-rich and also contains the YKRL motif (but not the di-leucine motif) which is typical of endocytic proteins (Bonifacino and Traub, 2003). CDIP1 contains the conserved LITAF domain and is also a monotopic membrane protein with similar topology to LITAF (Figure 1.4A, C). This mode of membrane insertion of the C-terminal LITAF domain is likely to be common to other LITAF domain-containing proteins (Qin et al., 2016).

1.3.2 The LITAF domain in other proteins

There is a high degree of conservation of the LITAF domain in viruses (Chen et al., 2016, Eaton et al., 2013), plants (He et al., 2011) and metazoa (Ponting et al., 2001) but there is no orthologue in *Saccharomyces cerevisiae*. There are 19 proteins in *Drosophila melanogaster* and 14 proteins in *Caenorhabditis elegans* which contain the LITAF domain, whereas in mammals there are only two (El-Gebali et al., 2019). In particular, critical residues in the zinc-binding CXXC and HXCXXC motifs are well conserved (Figure 1.5) (Ponting et al., 2001, Qin et al., 2016, Ho et al., 2016). Glutathione-induced LITAF domain protein (GILP) is found in *Arabidopsis thaliana*, and contains the conserved LITAF domain, but not the N-terminal proline-rich domain. It is localised to the plasma membrane and regulates hypersensitive cell death (He et al., 2011). GILP may act as an membrane anchor and recruit other components of the cell death pathway to the plasma membrane (He et al., 2011). Frog virus 3 (FV3) 75L and Tiger frog virus (TFV) ORF080L are viral proteins which contain LITAF domains but also do not have the N-terminal domain. FV375L and TFV ORF080L co-localise with human LITAF at late endosomes and lysosomes and at the plasma membrane respectively (Eaton et al., 2013, Chen et al., 2016). FV375L is normally localised to early endosomes, but translocates to late endosomes and lysosomes when co-expressed with human LITAF (Eaton et al., 2013). FV375L interacts with human LITAF, and LITAF PPXY motifs do not mediate this interaction (Eaton et al., 2013). TFV ORF080L interacts with human and zebrafish LITAF (Chen et al., 2016). TFV ORF080L expression resulted in EGFR trafficking defects in human cell lines, and this may be due to sequestration of functional human LITAF so that it cannot regulate normal endosomal trafficking (Chen et al., 2016).

1.4 Functions of LITAF

LITAF was originally described as a transcription factor with a role in the TNF-α transcriptional response (Myokai et al., 1999), and LITAF may have a role in regulating transcription of inflammatory cytokines in conjunction with STAT6 (Tang et al., 2005, Tang et al., 2006). LITAF was predicted to be a E3 ubiquitin ligase as its C-terminal domains is similar to a RING finger domain (Moriwaki et al., 2001, Saifi et al., 2005). However, LITAF had no ubiquitin ligase activity and does not interact with several E2 ubiquitin conjugating enzymes (Lee et al., 2012). LITAF has been

shown to localise to endosomal membranes and is likely to have a role in endosomal protein sorting due to its interactions with sorting complexes and ubiquitin ligases.

1.4.1 LITAF as an adaptor protein

LITAF may act as an adaptor for E3 ubiquitin ligases that brings E3 ligases to ESCRT proteins, and recruit these to other target proteins and membrane subdomains (Figure 1.6). E3 ubiquitin ligase adaptor proteins function to recognise target proteins and recruit E3 ubiquitin ligases, hence bringing these proteins into proximity, so that the ligase can specifically ubiquitinate the target protein. LITAF interacts with ITCH and Nedd4 E3 ubiquitin ligases (Shirk et al., 2005, Eaton et al., 2011). LITAF may recruit specific interactors such as ITCH to specific locations within the cell. Expression of LITAF has been shown to translocate ITCH, though not Nedd4, to lysosomal compartments (Eaton et al., 2011). LITAF may have a similar role to Nedd family interacting protein 1 (NDFIP1) and NDFIP2, which activate ITCH and Nedd4 by binding to multiple WW domains via their PPXY motifs (Mund and Pelham, 2009). They recruit Nedd4 to endocytic compartments and may act as adaptors for these E3 ubiquitin ligases (Shearwin-Whyatt et al., 2004, Shearwin-Whyatt et al., 2006). LITAF has a role in ubiquitination and degradation of L-type calcium channel alpha-1c subunit (Cavα1c) and this is likely to occur through its interaction with NEDD4 (Moshal et al., 2019) as well as directly regulating ubiquitination and degradation of Nedd4-2 itself (Turan et al., 2020).

Furthermore, CDIP1 interacts with ALG-2 (Inukai et al., 2021), which associates with Peflin, and this heterodimer functions as an adaptor for the ubiquitin ligase adaptor CUL3-KLHL12 which ubiquitinates Sec31A (McGourty et al., 2016). Another LITAF domain-containing protein, GILP, acts as a membrane anchor to recruit components of a molecular pathway (He et al., 2011). These data indicate that an adaptor function, such as recruiting ubiquitin ligases to sites of action, could be a common feature of LITAF domain proteins.

LITAF may also contribute to the recruitment of ESCRT-I to endosomes and thus have a direct role in endocytic traffic (Shirk et al., 2005, Lee et al., 2012) (Figure 1.6). Loss of LITAF results in larger endosomes and altered endosome morphology (Lee et al., 2012). Loss of LITAF does not affect EGFR endocytosis, but results in decreased lysosomal degradation of EGFR. The PSAP motif in LITAF is required for trafficking of EGFR for degradation. Additionally, loss of LITAF in mouse Schwann cells results in increased neuregulin-activated ErbB2 and ErbB3 signalling and Erk1/2 phosphorylation, due to reduced lysosomal degradation of these receptors (Lee et al., 2012). This indicates that the LITAF interaction with ESCRT-I is required for correct endosomal sorting of proteins (Lee et al., 2012). LITAF is required for correct protein sorting, and it may mediate this through formation of MVBs.

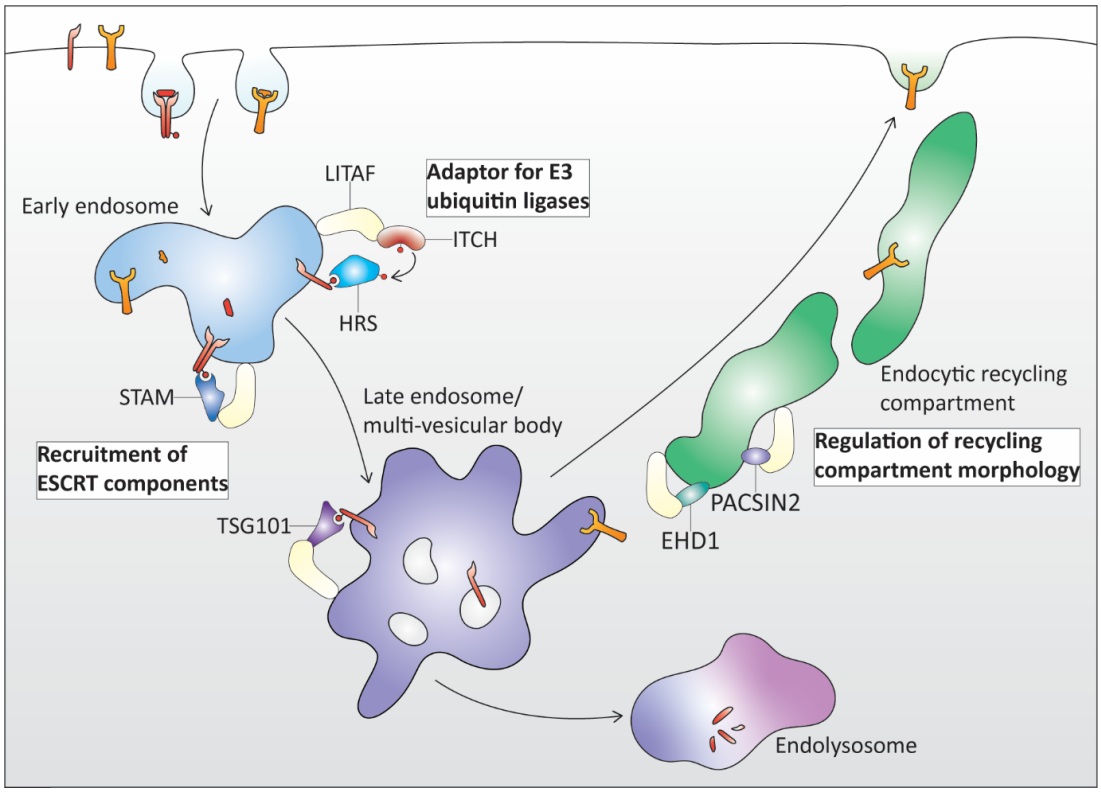

Figure 1.6. Overview of the possible cellular functions of LITAF in endocytosis. There are various suggested roles of LITAF in endocytosis. It may act as an adaptor for ubiquitin ligases by recruiting the ligase and the target protein into proximity on the membrane. LITAF may also recruit ESCRT components to endosomal membranes. LITAF may also have a role in the regulating the recycling compartment. Further work is required to define the cellular role of LITAF.

1.4.2 LITAF and the regulation of recycling

LITAF localises to recycling endosomes (Moriwaki et al., 2018) (Wunderley et al., 2021) (Figure 1.6). siRNA-mediated depletion of LITAF results in expansion of this compartment (Wunderley et al., 2021). Loss of LITAF does not appear to affect internalisation of the recycling cargo, Transferrin receptor (TfR), but the recycling of TfR was shown to be delayed (Moriwaki et al., 2018). However, this result was not replicated (Wunderley et al., 2021). LITAF interacts with various known components of recycling endosomes such as PI4P (Moriwaki et al., 2018), Pacsin2 and EHD1 (Wunderley et al., 2021). Clearly LITAF has a function in the regulation of the recycling compartment morphology, but further study is required to elucidate the exact function of LITAF in this pathway.

1.4.3 MVB biogenesis and exosome formation

LITAF has been functionally linked to events in the endocytic pathway, specifically the formation of MVBs (see above) and exosomes, that are carried out by ESCRTs and associated proteins, including TSG101 (Baietti et al., 2012). Exogenous expression of LITAF results in increased exosome formation (Zhu et al., 2013). Conversely, loss of LITAF reduces MVB formation in mouse embryonic fibroblasts (MEFs). LITAF associates with ESCRT machinery and so could be an important component in formation of ILVs and MVBs. Membrane remodelling is essential for the formation of these structures and there is some evidence to suggest that LITAF is involved in this process.

1.4.4 Membrane curvature

It has been suggested that LITAF may have a role in sensing and generating membrane curvature and in membrane structure integrity due to its membrane insertion (Qin et al., 2016) and interaction with phosphatidylethanolamine head groups (Ho et al., 2016). The hydrophobic region of LITAF is a putative amphipathic helix which inserts into the membrane (Ho et al., 2016). Insertion of an amphipathic helix into the membrane is a common mechanism to sense or generate membrane curvature. Addition of LITAF to liposomes results in formation of smaller diameter liposomes, which further supports this hypothesis (Wunderley et al., 2021).

In summary, LITAF may have several functions within the endocytic pathway, which is consistent with its presence in various endocytic compartments, but more work is required to investigate the precise molecular function of LITAF. Correct regulation of endocytosis is necessary for the cell to function properly, as defects in this process are associated with a wide range of diseases. Investigation into how mutations affect the function of LITAF is necessary to understand why mutations are deleterious.

1.5 LITAF-associated diseases

Mutations in LITAF are associated with several diseases, including Charcot-Marie-Tooth (CMT) disease (see below), whereas there are currently no known diseases caused by mutations in CDIP1. However, there may be genomic alterations in CDIP1 linked to cancer (Namba et al., 2013), and CDIP1 was proposed as a possible biomarker for sensitivity of cancers to TNFα-induced apoptosis (Brown-Endres et al., 2012). LITAF gene mutation and overexpression was detected in extramammary Paget's disease (EMPD), which is a malignant skin cancer (Matsumura et al., 2004). LITAF has also been linked to inflammatory signalling in cancer (Li et al., 2015) and is upregulated in inflammatory diseases, including Crohn's disease and ulcerative colitis (Huang and Bennett, 2007).

Genome wide association study (GWAS) loci associated with prolonged QT interval which predisposes for sudden cardiac death were found close to LITAF and two E3 ubiquitin ligases, RING finger protein 207 (RNF207) and RING finger and FYVE-like domain containing E3 ubiquitin ligase (RFFL) (Newton-Cheh et al., 2009, Pfeufer et al., 2009). LITAF has been linked to regulation of cardiac excitation as morpholino treatment-mediated knockdown of LITAF in zebrafish embryos resulted in increased amplitudes of calcium ion transients, and overexpression of LITAF in adult rabbit cardiomyocytes resulted in decreased amplitudes of calcium ion transients and decreased abundance of Cavα1c (Moshal et al., 2019). Specifically, increased expression of LITAF and NEDD4-1 resulted in increased ubiquitination and subsequent lysosomal degradation of a calcium ion channel in tsA201 cells. Furthermore, LITAF has been shown to also regulate sodium ion channels in rabbit cardiomyocytes. Overexpression of LITAF resulted in increased Nav1.5 sodium ion channel expression and increased the ubiquitination and degradation of NEDD4-2

(Turan et al., 2020). This indicates LITAF can modulate ubiquitin ligase activity and that this is functionally important (Moshal et al., 2019, Turan et al., 2020).

1.5.1 Charcot-Marie-Tooth disease

CMT is a peripheral neuropathy which affects 1:2500 people (Skre, 1974), and is the most common inherited neuromuscular disorder, although its prevalence depends on subtype and geographic location (Barreto et al., 2016). CMT is a slowly progressive neuropathy that causes distal muscle weakness, reduced nerve conduction velocity (less than 38m/sec) and sensory loss (Berger et al., 2002b, Street et al., 2003). Age of onset of CMT disease is broad, from 5-69 years, with 3 maxima at 12, 35 and 53 years (Skre, 1974). There is a diverse range of disease phenotypes which is consistent with the large diversity in the genetic causes, as more than 70 genes have been found to be associated with the different types of CMT (Baets et al., 2014). CMT type 1 is the autosomal dominant demyelinating type and accounts for two thirds of CMT. It can be subdivided into several subtypes that are caused by mutations in different proteins, including myelin proteins and endocytic regulators (Table 1.1). Point mutations in LITAF cause Charcot-Marie-Tooth disease type 1C (Figure 1.7).

It is important to highlight that other types of CMT are linked to mutations in membrane trafficking proteins (Pereira et al., 2012) (Table 1.2). Intriguingly, these mutations are autosomal recessive whilst LITAF mutations are autosomal dominant (Table 1.2). The autosomal recessive mutations are likely to cause loss of function, whilst the effect of mutations on LITAF function is not clear. In particular, disease mutations in SH3 domain and tetratricopeptide repeat containing protein 2 (SH3TC2) cause loss of association with Rab11-positive recycling endosomes, which is proposed to be the molecular cause of CMT4C (Roberts et al., 2010, Stendel et al., 2010). Additionally, N-myc downstream-regulated gene 1 (NDRG1) is an effector for Rab4 and regulates recycling of E-cadherin (Kachhap et al., 2007), endosomal trafficking of LDL receptor, and formation of MVBs (Pietiainen et al., 2013).

Furthermore, mutations in phosphatidylinositol phosphatases factor-induced gene 4 (FIG4) (Lenk et al., 2011), myotubularin related (MTMR) 2 (Bolino et al., 2000), MTMR13 (Azzedine et al., 2003, Senderek et al., 2003) and MTMR5 (Nakhro et al., 2013) are also implicated in this disease (Table 1.2). FIG4 hydrolyses $PI(3,5)P_2$ to PI3P on late endosomes and it is required to regulate endosomal compartments

Type	Proportion	Cause	Protein function	References
CMT1A	70-80%	Duplication of peripheral myelin protein 22 (PMP22)	Myelin component	(Valentijn et al., 1992)
CMT1B	6-10%	Point mutations in myelin protein 0 (MPZ)	Structural component of peripheral myelin	(Hayasaka et al., 1993)
CMT1C	1-2%	Point mutations in LITAF	Endosomal trafficking/sorting	(Street et al., 2003)
CMT1D	<2%	Point mutations in early growth response 2 (EGR2) (Krox20)	E3 sumo ligase/ transcription regulatory factor	(Warner et al., 1998)
CMT1E	<5%	Point mutations in PMP22	Myelin component	(Kovach et al., 1999)
CMT1F/2E	<5%	Mutations in neurofilament light polypeptide (NEFL)	Cytoskeleton component	(Jordanova et al., 2003)
CMT1G		Mutations in peripheral myelin protein 2	Myelin component, binds fatty acids	(Hong et al., 2016)
CMT1X	16%	Mutations in connexin-32 (GJB1)	Gap junctions	(Bergoffen et al., 1993)

Table 1. 1. CMT type 1 dominant peripheral demyelinating diseases are caused by autosomal mutations in various proteins.
Mutations in various proteins with different functions have been detected in CMT1 patients. Mutations in PMP22, a structural component of myelin, account for the largest proportion of CMT1 disease (CMT1A and CMT1E). Other mutations, including LITAF mutations, are less common and account for the remaining CMT1 disease.

(Sbrissa et al., 2007, Bharadwaj et al., 2016). Myotubularins hydrolyse PI3P to produce PI. CMT-associated mutations in MTMR2 result in loss of this hydrolytic activity (Berger et al., 2002a). Interestingly, MTMR2 may have a role in regulating RME-8 localisation to endosomes and this links MTMR2 to endosomal recycling (Xhabija et al., 2011). MTMR13 and MTMR5 are pseudophosphatases that interact with MTMR2 and may regulate its function (Kim et al., 2003, Robinson and Dixon, 2005). Additionally they may have Rab-GEF activity for Rab28 (Yoshimura et al., 2010), a Rab whose function is not well studied, but which may regulate retromer and ESCRT-dependent pathways (Lumb et al., 2011). Correct regulation of phosphoinositides is required for endosome compartmentalisation and function (Wallroth and Haucke, 2018). Taken together, these data indicate that dysregulation of

endosomal pathways, in particular the recycling pathway, may be common to several subtypes of this disease.

Type	Mutations	Function
1 Autosomal Dominant Demyelinating	PMP22	Myelin protein
	MPZ	Myelin protein
	LITAF	Endocytic regulator
	EGR2	E3 sumo ligase/transcription factor
	NEFL	Cytoskeleton
	PMP2	Myelin protein
	Connexin-32	Myelin protein
2 Autosomal Dominant Axonal	Mitofusin 2	Mitochondrial fusion
	Rab7	Lysosomal trafficking
	Dynamin 2	Membrane scission
	Kif5a	Axonal vesicular transport
	TrpV4	Calcium ion channel
	Hsp27	Molecular chaperone
	Hsp22	Molecular chaperone
4 Autosomal Recessive Demyelinating	GDAP1	Mitochondrial fission
	MTMR13/2/5	Phosphoinositol phosphatase
	SH3TC2	Rab11 effector
	NDRG1	Protein trafficking
	FIG4	Polyphosphoinositide phosphatase
	Periaxin	Scaffolding protein
	FGD4	Activates CDC42

Table 1.2. Mutations in various proteins cause different types of CMT disease. Some mutations are in myelin proteins, and several CMT-causing mutations are found in proteins involved in endocytic trafficking.

1.5.2 Schwann cells

In the peripheral nervous system (PNS) Schwann cells wrap around peripheral neuron axons and form the myelin sheath in a process called myelination (Pereira et al., 2012). Schwann cells are the glial cells of the PNS and function to provide structure and support to the neuron, and have an important role in responding to nerve injury. The ErbB receptor on Schwann cells is activated by neuregulin1 and stimulates signalling pathways that lead to activation of Schwann cell differentiation and myelination. The fatty myelin sheath insulates the nerve axon and facilitates saltatory conduction of electrical signals, which allows for fast nerve signal conduction velocity.

Myelinating Schwann cells generate up to $20mm^2$ of membrane that wraps around large axons, which is 2000 times more surface membrane than a typical epithelial cell

(Kidd et al., 2013). These membranes are highly specialised and contain distinct domains that have a specific composition. Approximately 70% of the membrane is made up of lipids, including galactosphingolipids, saturated long chain fatty acids and cholesterol. Additionally, myelination requires the polarised delivery of a few myelin proteins, including protein 0 (P0) (70%), myelin basic protein (MBP) (5%), the tetraspanin peripheral myelin protein 22 (PMP22) (5%) and peripheral myelin protein 2 (PMP2) (15%) to the surface of the Schwann cells (Salzer, 2015, Kidd et al., 2013). It is likely that the endosomal pathway is involved in this delivery, as has been demonstrated in oligodendrocytes but is not as well studied in Schwann cells (Simons and Trotter, 2007).

It was shown in oligodendrocytes of the central nervous system (CNS) that the myelin protein proteolipid protein (PLP) is endocytosed into endosomes, and then transported to the plasma membrane when the cell is stimulated (Trajkovic et al., 2006). PMP22 localises to late endosomes and was also localised to vacuoles in Schwann cells, indicating that it may traffic through the endosomal compartment (Chies et al., 2003). More recently, it was shown that P0 is localised to endosomes and lysosomes in Schwann cells, and is also delivered to the plasma membrane in response to stimuli. This is dependent on the function of Rab27a (Chen et al., 2012). Expression of dominant negative Rab11 disrupts the recycling pathway and results in aberrant myelination (Stendel et al., 2010). Furthermore, regulation of phosphoinositides is necessary for myelination. Firstly, phosphatidylinositol 3-kinase (PI3K) was shown to be activated by neuregulin, and pharmacological inhibition of PI3K blocked initial myelination in Schwann cells (Maurel and Salzer, 2000). Meanwhile, activation of Akt, a protein kinase that acts in signalling downstream of PI3K, resulted in increased myelination (Ogata et al., 2004). Additionally, the phosphoinositide kinase VPS34, whose function in PI3P production at the endosome opposes MTMR2, is necessary for correct endosomal trafficking and myelination in Schwann cells (Logan et al., 2017). These studies indicate the importance of endosomal trafficking in myelination, which is common in both the CNS and the PNS. However, although the overall organisation is similar and many myelin proteins are shared (Patzig et al., 2011), myelination in the CNS and the PNS are different and myelin diseases are usually restricted to the PNS (such as CMT) or the CNS (Salzer, 2015).

1.5.3 LITAF mutations in CMT1c

Various point mutations in LITAF associated with CMT1c have been identified, but information on the onset of disease and resulting phenotype is lacking due to insufficient patient numbers, and there may therefore be variable clinical onset and phenotype (Table 1.3). CMT1c patient mutations in LITAF occur mainly in the C-terminal domain (Figure 1.7) and cause Charcot-Marie-Tooth disease 1c (CMT1c) (Somandin et al., 2012, Street et al., 2003, Saifi et al., 2005, Li et al., 2015, Bennett et al., 2004, Guimaraes-Costa et al., 2017, Gerding et al., 2009, Latour et al., 2006). The mechanism linking LITAF mutations to CMT1c is unknown. The effect of LITAF patient mutations on various properties of LITAF has been studied to investigate this further, but a range of studies have come to differing conclusions on the effects of CMT1c-causing mutations.

1.5.3.1 Effect of mutations on LITAF localisation

Given the location of the amino acid substitutions proximal to the hydrophobic region, which is required for membrane association (Figure 1.7) (Ho et al., 2016), it is plausible that mutations may affect membrane insertion. A series of studies have drawn different conclusions about the effect of CMT1c mutations on subcellular localisation; some have shown that mutations do not affect localisation (Shirk et al., 2005, Zhu et al., 2013, Ho et al., 2016), whilst others have indicated that mutations result in LITAF mislocalisation (Lee et al., 2011, Lacerda et al., 2014). Different disease-associated mutations may have different effects on LITAF localisation, but differences may also be due to cell type, expression system used, as seen for the observed localisation of WT LITAF.

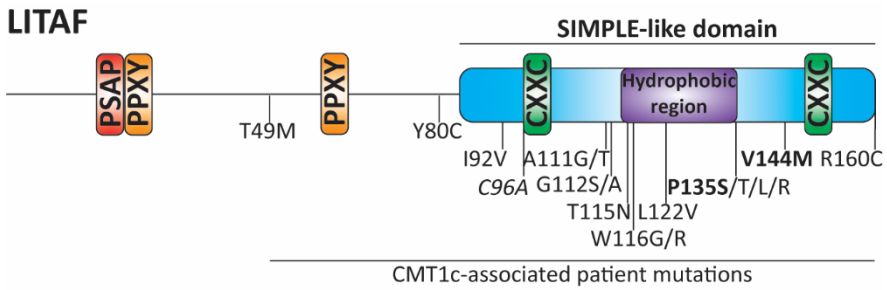

Figure 1.7. CMT1c disease-associated mutations.
Schematic indicating locations of missense mutations in LITAF detected in patients with CMT1c disease. They are mainly clustered around the hydrophobic region (HR) in the C-terminal LITAF domain. Mutations in bold indicate patient mutations studied further here. The mutation in italics indicate a mutation which disrupts the structure and renders the protein cytosolic.

Mutation	Age of Onset	Phenotype	References
T49M	Childhood (compound with R160C)	Rare variant Possibly benign	(Guimaraes-Costa et al., 2017) (Saifi et al., 2005) (Zhu et al., 2013)
Y80C	18 years (compound with R160C)	Possibly benign	(Guimaraes-Costa et al., 2017)
I92V	Early onset of CMT1a (compound with G112S)	Also occurs in 16.2% unrelated control chromosomes	(Sinkiewicz-Darol et al., 2015) (Meggouh et al., 2005)
A111G			(Latour et al., 2006)
A111T	Late onset		(Guimaraes-Costa et al., 2017)
G112S	80% childhood onset (variable) Early onset of CMT1a (compound with I92V)	Mild disease similar to CMT1A	(Street et al., 2003) (Meggouh et al., 2005) (Jerath and Shy, 2017) (Bennett et al., 2004) (Klein et al., 2014)
G112A	27 years		(Guimaraes-Costa et al., 2017)
T115N		Increased tumour susceptibility Paralysis in old age in mice	(Li et al., 2015) (Street et al., 2003) (Zhu et al., 2013)
W116G	Broad age of onset in humans (6-41 years) Late onset in mice (1 year)		(Lee et al., 2013) (Bennett et al., 2004) (Street et al., 2003)
W116R	33 years, 13 years		(Guimaraes-Costa et al., 2017)
L122V		Rare polymorphism	(Saifi et al., 2005) (Zhu et al., 2013)
A129T	Late onset	Possibly pathogenic	(Luigetti et al., 2014)
P135T			(Latour et al., 2006)
P135S			(Latour et al., 2006)
P135L	10 years		(Guimaraes-Costa et al., 2017)
P135R	10-31 years		(Ciotti et al., 2014)
V144M	Variable age of onset		(Gerding et al., 2009) (Ho et al., 2016)
R160C	15 years	Possibly pathogenic	(Guimaraes-Costa et al., 2017)

Table 1.3. Point mutations in LITAF that are implicated in CMT1c.
Some studies provided information on the age of onset of disease in patients containing these mutations. Some mutations may be benign polymorphisms but several are likely to be pathogenic. Not all of these mutations have been verified experimentally and their pathogenicity is uncertain.

1.5.3.2 Effect of mutations on LITAF stability

Mutations in LITAF may affect its structure so that it is unstable or misfolded. The V144M mutation results in dispersed chemical perturbations observed in NMR spectroscopy compared to WT LITAF, which indicates that although the mutation may cause biophysical changes, the overall secondary structure of LITAF remains the same. The biggest changes in structure were observed in residues that interact with phosphatidylethanolamine (PE), indicating that the V144M mutation may alter this interaction, perhaps resulting in instability or misfolding (Ho et al., 2016). LITAF W116G and P135T (Lee et al., 2011) and V144M (Ho et al., 2016) were degraded more rapidly than WT LITAF in cells, which may be consistent with some degree of misfolding. In patient fibroblasts the level LITAF L125P was reduced, whilst the level of LITAF T115N was unchanged compared to WT (Edgar et al., 2020).

Additionally LITAF W116G and P135T accumulated in aggresomes, indicating that they may be aggregated and misfolded (Lee et al., 2011). LITAF W116G structure simulation indicated that the mutant protein may have reduced stability and misfold (Kumar et al., 2015). However, LITAF T115N (Street et al., 2003, Zhu et al., 2013) and W116G (Street et al., 2003) mutations did not affect LITAF protein expression levels. Clearly there is some discrepancy between studies.

1.5.3.3 Effect of mutations on endosomal sorting

Expression of LITAF containing CMT1c patient mutations can affect endocytic trafficking. Thus, several LITAF mutants show reduced secretion in exosomes, and LITAF T115N expression results in fewer and smaller exosomes (Zhu et al., 2013). In CMT1c patient B cells and mouse Schwann cells containing LITAF mutations, MVBs are vacuolated, indicating reduced formation of ILVs. This supports the conclusion that mutation of LITAF affects biogenesis of MVBs and exosomes (Zhu et al., 2013). In agreement with this data, patient-derived fibroblasts containing LITAF T115N had large vacuolated late endosome/lysosome compartments (Edgar et al., 2020). CMT4J mutations in FIG4 result in similar vacuolated endosomes (Bharadwaj et al., 2016), indicating that they are derived via a common mechanism (Edgar et al., 2020). LITAF W116G and P135T mutant overexpression in a LITAF knockdown background results in reduced degradation of EGFR, indicating a defect in protein trafficking (Lee et al., 2012). This finding was confirmed in mouse Schwann cells, as expression of these

mutants resulted in prolonged Erk1/2 activation, which may be due to reduced lysosomal trafficking of ErbB2 and ErbB3 receptors, similar to the effect of loss of LITAF (Lee et al., 2012).

1.5.3.4 Effect of mutations on myelination

CMT1c disease involves progressive loss of myelin surrounding peripheral neurons, which is produced by Schwann cells. Therefore, LITAF may have a role in myelination. LITAF is not required for peripheral nerve myelination during development in mice (Somandin et al., 2012), which is consistent with moderate LITAF mRNA expression levels during sciatic nerve development in rats (Street et al., 2003), and LITAF knockout mice did not have a peripheral nerve phenotype (Somandin et al., 2012, Zhu et al., 2013). Transgenic mice expressing LITAF W116G mutation did have a peripheral nerve phenotype, and myelin infolding which resulted in altered morphology of axons. This may be relevant to the demyelinating phenotype of CMT1c patients, as LITAF W116G mice had late onset (from 1 year) neuropathy and impaired motor and sensory function (Lee et al., 2013). This indicates that mutations are dominant and may be gain-of-function.

In summary, there is not a clear consensus on the effect of mutations on LITAF's subcellular localisation, protein stability or protein interactions. Certainly, these discrepancies could be due to differences in experimental conditions between studies. LITAF mutations are reported to cause defective MVB and exosome formation (Zhu et al., 2013), dysregulation of endocytic sorting, prolonged ErbB signalling (Lee et al., 2012) and altered myelin morphology (Lee et al., 2013). However, it is not clear how LITAF mutations affect its function so as to result in altered Schwann cell behaviour and how this leads to the pathology.

1.5.4 How do mutations result in pathogenesis?

CMT1c mutations result in peripheral demyelinating disease, indicating that Schwann cells are particularly susceptible to defects in LITAF. LITAF is ubiquitously expressed (Lee et al., 2011) so deleterious effects may be specific to Schwann cells due to sensitivity of this specialised cell type or to a particularly critical role of endocytosis in myelination. Schwann cells may express unique interaction partners that may drive the cell type specificity. Alternatively, a potential functional redundancy with CDIP1 may ameliorate defects in other cell types. Mutations in LITAF may cause CMT1c due

to defects in endocytosis, which may affect myelin protein trafficking, altered signalling of endocytosed receptors or accumulation of misfolded and aggregated protein. It is not yet clear whether LITAF loss or gain of function affects myelin sheath formation in development, or whether LITAF mutations may be result in an inability to maintain the myelin, which would be a homeostatic defect.

Defects in endocytosis could negatively affect myelin homeostasis and maintenance in Schwann cells as endocytosis is important for myelination and delivery of myelin proteins to the plasma membrane to form the myelin sheath (Simons and Trotter, 2007). Localisation of PMP22 to MHCI-positive vacuoles is dependent on Arf6, suggesting a role of recycling endosomes in the trafficking of myelin proteins (Chies et al., 2003). Mislocalisation or altered protein dynamics of LITAF could affect interactions with E3 ubiquitin ligases, ESCRTs and recycling proteins which are required for protein sorting and membrane remodelling in endocytosis. Studies of other proteins mutated in CMT have indicated the importance of correct regulation of endocytic pathways in the maintenance of myelin (Verhoeven et al., 2003, Roberts et al., 2010, Stendel et al., 2010, Sidiropoulos et al., 2012, Pietiainen et al., 2013).

Defects in endosomal trafficking may dysregulate functions of cargo proteins present in the endocytic network. Duration and localisation of signalling by EGFR is regulated by endocytosis. LITAF mutations may affect EGFR signalling by disrupting its trafficking (Lee et al., 2012, Lee et al., 2017). This may have downstream consequences for Schwann cell myelination, as correct signalling of EGFR is required for myelination and Schwann cell migration in different animal models (Freeman and Doherty, 2006) including zebrafish (Lyons et al., 2005). Prolonged Erk1/2 signalling has been linked to demyelination in mice (Ishii et al., 2016).

Accumulation of proteins may be damaging in neuronal cell types, so endocytosis and lysosomal delivery of proteins has a neuroprotective role (Stuffers et al., 2009). LITAF mutants may affect the function of interacting E3 ubiquitin ligases. This may lead to the accumulation of aggregated proteins or defects in normal protein degradation, with toxic cellular effects. A LITAF mutant has been detected in aggresomes in cells (Eaton et al., 2012). Misfolding proteins and aggregate formation may be common to several subtypes of CMT1 (Bennett et al., 2004). Schwann cells undergoing myelination may have a high rate of protein turnover, as there are proteins such as PMP22 that are prone

to misfolding, and so any dysregulation of the lysosomal degradation pathway may have deleterious effects, and this could lead to peripheral nerve demyelination.

Interestingly, one study linked LITAF to Wallerian degeneration (Somandin et al., 2012). PNS Wallerian degeneration occurs when Schwann cells proximal to the site of injury die and cells distal regenerate and replace cells at the site of injury. Initially Schwann cells scavenge myelin from dead/injured cells and degrade it by myelinophagy, followed by phagocytosis of myelin by activated macrophages (Jessen and Mirsky, 2016). Loss of LITAF results in increased macrophage activity after injury, which also take up dead Schwann cells and myelin (Somandin et al., 2012). This is consistent with increased LITAF expression over 58 days after nerve crush, especially proximal to the site of injury (Street et al., 2003). There may be partial redundancy between myelinophagy and phagocytosis of myelin by macrophages during Wallerian degeneration. Hence, Schwann cells with endocytosis defects due to loss of LITAF may not be able to carry out their normal function, so macrophages compensate with an alternative pathway for clearing debris (Somandin et al., 2012). It is unclear whether Wallerian degeneration is implicated in CMT1c disease, but this finding indicates that LITAF may have a specific role in Schwann cells.

In summary, it is not yet clear how LITAF mutations result in peripheral neuropathy. The mechanisms that have been suggested may account for this, or there may be a mechanism that has not been considered or investigated yet. There are several possibilities, but further study is required. Previous studies in cell culture models do not recapitulate the complex organisation and specialisation of Schwann cells and of myelination. Schwann cells may be uniquely susceptible to mutations in LITAF and this may be due to the enhanced role of endocytosis and membrane trafficking in myelination. For example, LITAF may have a function in the recycling pathway in endocytosis, and this has been linked to various neurological disorders including CMT (Li and DiFiglia, 2012). Strikingly, other types of CMT are linked to mutations in endocytic proteins, highlighted in Table 1.2. Clearly regulation of membrane trafficking is implicated in this disease. Without correct functioning of this pathway, cellular homeostasis is disrupted which could eventually result in demyelination and CMT1c symptoms.

1.6 LITAF in animal models

Various LITAF knock-out and CMT1c mutation knock-in animal models have been generated to look at different roles of LITAF *in vivo*. Studies examining the *in vivo* function of LITAF in myelination and the effect of mutations are most relevant here (Somandin et al., 2012, Lee et al., 2013, Zhu et al., 2013). The development and maintenance of peripheral nerves was not affected in a LITAF knockout mouse (Somandin et al., 2012). However, there was a delay in the onset of remyelination and increased macrophage recruitment to sites of nerve injury in the LITAF knock out mice compared to WT (Somandin et al., 2012). Transgenic mice overexpressing exogenous LITAF W116G in a LITAF WT background had motor and sensory nerve defects and abnormal myelin organisation (Lee et al., 2013). These mice had reduced nerve conduction velocity, which recapitulates the human CMT1c phenotype, and had a mild motor phenotype, exhibited by increased limb flexing. Mutant mice had increased myelin infoldings at 8 months which was specific to the PNS (Lee et al., 2013). Endogenous LITAF T115N knock in mice were generated to examine the effect of loss of LITAF and CMT1c mutation on exosome production. Expression of LITAF results in increased exosomes, while expression of LITAF T115N in MEFs, primary mouse Schwann cells and patient B cells resulted in reduced exosomes (Zhu et al., 2013). Some mice expressing LITAF T115N in one or both alleles had increased limb clasping during the first year, but nerve conduction velocity was not affected. Additionally, at 1.5 years, 15% of these mice had paralysis, but none of the WT or LITAF knock out mice exhibited this phenotype (Zhu et al., 2013). These studies indicate that CMT1c mutations affect myelination in mice and are likely to be toxic gain of function, as their effect is not recapitulated by LITAF knockout.

Additionally, further work has examined the role of LITAF in other physiological processes including inflammation and cardiac excitation. LITAF knockout mice were used to study the role of LITAF in inflammatory responses. Global loss of LITAF resulted in reduced endotoxic shock and reduced inflammatory arthritis (Merrill et al., 2011) whilst macrophage-specific loss of LITAF did not have such a marked effect but resulted in delayed secretion of cytokines (Srinivasan et al., 2010). LITAF+/T115N MEFs had altered interleukin-1 and TGF-β signalling and NF-κB activation compared to LITAF WT. LITAF+/T115N mice were more susceptible to

tumours in a syngeneic xenograft mouse models and had increased levels of chemokines and cytokines. The authors suggested that the altered inflammatory signalling may contribute to increased tumour growth (Li et al., 2015). Zebrafish injected with LITAF morpholinos were used to study cardiac excitation (Moshal et al., 2019). These morphants had increased calcium transients. Adenoviral overexpression of LITAF in rabbit cardiomyocytes resulted in reduced calcium transients and had reduced expression of Cavα1c (Moshal et al., 2019).

The role of CDIP1 in ER stress-induced apoptosis has been studied in WT and CDIP1 knock out mice. CDIP1 expression was induced in the liver upon ER stress and CDIP1 knock out mice were protected from cell death in the liver after exposure to ER stress (Namba et al., 2013). Overall these studies show that LITAF and CDIP1 are functionally important proteins in vivo. However, the exact role they have in Schwann cells is not yet clear. Additionally, the mechanism by which the mutations result in peripheral neuropathy is also not evident.

1.7 Summary and project aims

Endocytosis is a highly regulated process that selectively sorts proteins to recycling or degradative pathways. Sorting of proteins into MVBs and recycling tubules requires specialised molecular machinery, with different multi-protein complexes regulating different steps in this process. Characterisation of the function of accessory proteins such as LITAF is required to understand how recycling endosomes and MVBs are formed, and how dysregulation may lead to diseases such as CMT1c.

LITAF is an endosomal membrane protein that is likely to function in endocytic trafficking of proteins. It is expected to have an important function, particularly in Schwann cells, as mutations lead to demyelinating CMT1c. Previous work has shown that LITAF and CDIP1 are present in the endocytic pathway (Qin et al., 2016). However, the precise function of LITAF is not well characterised and this information is required to elucidate the molecular mechanism underlying CMT1c disease. Mutations in LITAF may affect its association with the membrane (Ho et al., 2016). Disease-associated mutations cause dysregulation of endocytic trafficking including altered morphology of endocytic compartments (Zhu et al., 2013) and aberrant

signalling (Lee et al., 2013). However, it is not known how mutations result in the demyelination of peripheral neurones that is associated with CMT1c neuropathy.

Therefore, the aims of this project are to better define the cellular functions of LITAF and understand how mutations affect its cellular functions and protein interactions. In order to further investigate the function of LITAF it is important to examine the organismal consequences of loss of LITAF and CDIP1, and this may be achieved by characterising the phenotype of zebrafish lacking LITAF and CDIP1.

Chapter 2: Materials and Methods

All reagents were from Sigma or Fisher Scientific unless otherwise stated.

2.1 Molecular biology

2.1.1 cDNA plasmids

Construct	Method	Source
pEGFP-C1	-	Clontech
pEGFP-C1-LITAF	LITAF cDNA was subcloned into pEGFP-C1	Elaine Small
pEGFP-C1-LITAF C96A	Standard site-directed mutagenesis	Dr Lydia Wunderley
pEGFP-C1-LITAF P135S	Standard site-directed mutagenesis	Dr Lydia Wunderley
pEGFP-C1-LITAF V144M	Standard site-directed mutagenesis	Dr Lydia Wunderley
pEGFP-C1-LITAF SLD	LITAF SLD cDNA was subcloned into pEGFP-C1	Dr Wendy Qin
pEGFP-C1-LITAF SLD I92V	Standard site-directed mutagenesis	Dr Wendy Qin
pEGFP-C1-LITAF SLD A111G	Standard site-directed mutagenesis	Dr Wendy Qin
pEGFP-C1-LITAF SLD G112S	Standard site-directed mutagenesis	Dr Wendy Qin
pEGFP-C1-LITAF SLD T115N	Standard site-directed mutagenesis	Dr Wendy Qin
pEGFP-C1-LITAF SLD W116G	Standard site-directed mutagenesis	Dr Wendy Qin
pEGFP-C1-LITAF SLD L122V	Standard site-directed mutagenesis	Dr Wendy Qin
pEGFP-C1-LITAF SLD P135S	Standard site-directed mutagenesis	Dr Wendy Qin
pEGFP-C1-LITAF SLD V144M	Standard site-directed mutagenesis	Dr Wendy Qin
pXLG3	-	Prof Peter Cullen, University of Bristol
psPAX2	-	Prof Peter Cullen, University of Bristol
pMG.2	-	Prof Peter Cullen, University of Bristol
pXLG3-LITAF	LITAF cDNA was subcloned into pXLG3 using BamHI site	This study
pXLG3-LITAF P135S	Standard site-directed mutagenesis	This study
pXLG3-LITAF V144M	Standard site-directed mutagenesis	This study
pXLG3-BioID2-V5-LITAF	BioID2-V5-LITAF cDNA was subcloned into pXLG3 using SpeI and BamHI sites	This study
pXLG3-BioID2-V5-LITAF C96A	Standard site-directed mutagenesis	This study
pXLG3-BioID2-V5-LITAF P135S	Standard site-directed mutagenesis	This study
pXLG3-BioID2-V5-LITAF V144M	Standard site-directed mutagenesis	This study
pT3TS-nCas9n	-	Wenbiao Chen (Addgene plasmid # 46757) (Jao et al., 2013)
HA-Arf6	-	Prof Elizabeth Sztul, University of Alabama
HA-Arf6 T44N	-	Prof Elizabeth Sztul, University of Alabama
pcDNA3-mCherry	-	Stratagene
myc-SPG20	-	Prof Evan Reid, Cambridge Institute for Medical Research
mCherry-TPD54	-	Prof Stephen Royle, University of Warwick

Table 2.1. Mammalian expression plasmids used in this study.

2.1.2 Bacterial transformation

Purified plasmid DNA constructs were transformed into chemically competent Top10 *E. coli* cells (Life Technologies). 1 µl plasmid DNA was added to 50 µl Top10 cells and incubated for 30 minutes on ice. The cells and plasmid DNA were heat shocked at 42°C for 45 seconds and placed back onto ice for 2 minutes. 200 µl Luria-Bertani (LB) broth was added and this was incubated into a shaking incubator for up to 1 hour at 37°C and 225 rpm. Cells were spread across pre-warmed 10cm plates containing LB agar (Melford) (1.5% w/v) containing either 100 µg/ml ampicillin or 50 µg/ml kanamycin antibiotic for positive selection. Plates were incubated at 37°C overnight.

2.1.3 Plasmid DNA extraction

A single isolated bacterial colony was picked using a pipette tip and used to inoculate 6 ml or 200 ml LB broth containing the appropriate antibiotic for miniprep and midipreps respectively, and incubated in a shaking incubator at 37°C and 225 rpm overnight. The bacterial cell suspension was then centrifuged at 5000rpm for 15 minutes at 4°C. The supernatant was discarded and the cell pellet was used use for plasmid DNA extraction using the Isolate II plasmid Mini Kit (Bioline) or the NucleoBond Xtra Midi Plus kit (Macherey Nagel) using the manufacturer's instructions. Purified plasmid was eluted in either 30 µl (miniprep) or 500 µl (midiprep) elution buffer, and the concentration was quantified using the NanoDrop spectrophotometer (Thermo Scientific).

2.1.4 Agarose gel and visualisation

Agarose gels were made by boiling the appropriate amount of agarose (SeaKem) in TAE buffer (Lonza) and then adding 0.001% ethidium bromide and left to set at room temperature for 30 minutes. DNA or RNA samples were loaded in loading buffer (Bioline) alongside 100bp or 1000bp markers (Bioline) as a reference for lengths of DNA and gels were run at 100V for up to 40 minutes in TAE buffer. The gel was visualized on a Gel Doc transilluminator, and images were analysed using ImageJ, Adobe Photoshop and Illustrator.

2.1.5 Polymerase chain reaction

All cDNA amplification and mutagenesis reactions of mammalian cell expression vectors were performed using KOD HotStart DNA polymerase (Merck Millipore) according the manufacturer's instructions. PCR products used for cDNA cloning were then purified using the NucleoSpin Gel and PCR clean up kit (Macherey-Nagel) and eluted in 30 µl nuclease-free water.

2.1.6 Site-directed mutagenesis

Nucleotide substitutions were introduced by incorporating the desired nucleotide change into the centre of the forward and reverse primer flanked by 15 complementary nucleotides on both sides of the mutation (Table 2.2).

Primer name	Sequence
LITAF C96A fwd	CCCATCCCAATGTGTGCTCCTTCCTGCAACAA
LITAF C96A rev	TTGTTGCAGGAAGGAGCACACATTTGGATGGG
LITAF P135S fwd	GGCTGCTGCTTCATCTCCTTCTGCGTGGATG
LITAF P135S rev	CATCCACGGAGAAGGAGATGAAGCAGCAGCC
LITAF V144M fwd	GATGCCCTGCAGGACATGGACCATTACTGTC
LITAF V144M rev	GACAGTAATGGTCCATGTCCTGCAGGGCATC

Table 2.2. Primers used for mutagenesis.
Substitutions are underlined.

Number of cycles	Temperature (°C)	Time	Step
1	94	2 minutes	Initial denaturation
12	94	30 seconds	Denaturation
	55	1 minute	Annealing
	72	1 minute/kb	Extension
1	72	10 minutes	Final extension

Table 2.3. KOD HotStart DNA PCR parameters for mutagenesis.

PCR reactions containing the mutagenesis primers and 200ng template plasmid were prepared in 50 µl nuclease-free water. These PCRs were carried out according to the parameters in Table 2.3. The original methylated template DNA plasmid was then digested using 1 µl Dpn1 (NEB) overnight at 37°C.

2.1.7 cDNA cloning

Primers with an overhanging sequence containing the restriction enzyme recognition site were used to amplify cDNA encoding the appropriate construct containing restriction enzyme recognition sites which can be digested to generate sticky ends. Sequences of primers used for cloning are shown in Table 2.4. The PCRs were carried out according to the parameters in Table 2.5. The original methylated template DNA plasmid was then digested using 1 µl Dpn1 (NEB) overnight at 37°C.

Primer name	Sequence
XLG3-miniBioID-V5-LITAF SpeI Fwd	GCGGCGACTAGTATGTTCAAGAACCTGATCTGGCTGAAGGAG
XLG3-miniBioID-V5-LITAF BamHI Rev	CGCCGCGGATCCTCACAAACGCTTGTAGGTGCCC

Table 2.4. Primers used for cDNA cloning.

Cycle	Temperature (°C)	Time	Step
1	94	2 minutes	Initial denaturation
12	94	30 seconds	Denaturation
	55	1 minute	Annealing
	72	1 minute/kb	Extension
1	72	10 minutes	Final extension
1	94	2 minutes	Initial denaturation

Table 2.5. KOD HotStart DNA PCR parameters for cDNA cloning.

Alternatively, some constructs could be generated by direct subcloning where plasmids already contained the necessary restriction enzyme recognition sites and could be digested and ligated without performing PCRs.

2.1.8 Restriction digest

30 µl PCR products or DNA vector plasmids were digested overnight at 37°C with 1 µl restriction enzyme(s) (NEB) and the appropriate buffer (NEB). Digested vector plasmid DNA was then treated with calf intestinal alkaline phosphatase (CIP) (NEB) for 1 hour at 37°C. Digested PCR products and vector plasmids in loading buffer (Bioline) were run on a 1% agarose gel. Single separated bands were isolated and purified using the NucleoSpin Gel and PCR clean up kit (Macherey-Nagel) and eluted in 30 µl nuclease-free water.

2.1.9 Ligation

4.5 µl of digested insert DNA and 0.5 µl digested vector DNA were incubated with 1 µl Quick ligase (NEB) in Quick ligase buffer in a total of 20 µl at room temperature for 15 minutes. 5 µl of this ligation reaction was transformed into Top10 cells.

2.1.10 Sanger sequencing

20 µl sequencing reactions contained 100 ng plasmid DNA and 25 pmol appropriate sequencing primer (IDT) (Table 2.6). Samples were sequenced by Sanger sequencing services from GATC Eurofins or Genewiz and analysed using Snapgene.

Primer	Sequence
pEGFP-C1 Fwd	CATGGTCCTGCTGGAGTTCGTG
M13 Rev	CAGGAAACAGCTATGAC
SP6	ATTTAGGTGACACTATAG
T7	TAATACGACTCACTATAGGG
BGH Rev	TAGAAGGCACAGTCGAGG
CMV Fwd	CGCAAATGGGCGGTAGGCGTG
SV40pA-R	GAAATTTGTGATGCTATTGC
Amp-R	ATAATACCGCGCCACATAGC
mRFP Fwd	GCTGAAGCTGAAGGACG
LITAF Rev	ATACGAAGGAGGATTCATGC
BioID2	GGTGCTGCTGAAGGTGCT

Table 2.6. Oligonucleotide sequences for sequencing constructs.

2.2. Cell culture

2.2.1 Cell lines

HeLaM cells, h-telomerase reverse transcriptase (h-TERT) retinal pigment epithelium (RPE)-1 cells, Medical Research Council cell strain 5 (MRC-5) cells, human embryonic kidney (HEK)293 LTV and MDA-MB-231 cell lines were used for experiments. HeLaM and HEK293T LTV cells were maintained at 37°C and 8% CO2 in Dulbecco's Modified Eagle's Medium (DMEM). RPE-1 cells were maintained at 37°C and 5% CO_2 in DMEM/Nutrient mixture F12 HAM supplemented with 2 mM glutamine. MRC5 cells were maintained at 37°C and 8% CO_2 in Eagle's Minimum Essential Medium (EMEM). Media was supplemented with 10% fetal bovine serum (FBS) (HyClone) and 1% non-essential amino acids. These cell lines used in experiments were less than 30 passages and regularly checked for mycoplasma contamination by DAPI staining.

Cell line	Tissue/cell type	Source	Media
HeLaM	Cervix/epithelial	ATCC	DMEM
h-TERT RPE-1	Retinal/epithelial	ATCC	DMEM/F12 Ham
HEK293T-LTV	Kidney	ATCC	DMEM
MRC-5	Lung/fetal	ATCC	EMEM
MDA-MB-231 cells	Breast cancer	ATCC	DMEM

Table 2.7. Summary of human cell lines and cell culture conditions used in this study.

2.2.2 Storage of cells

Cell suspension was centrifuged at 2000 g for 3 minutes. The media was removed and the cell pellet was resuspended in 10% dimethylsuphoxide (DMSO) in FBS (HyClone). This cell suspension was aliquoted into cryovials and stored at -80°C for 24 hours before being transferred into liquid nitrogen and stored at -196°C. Frozen aliquots of cells were thawed by incubation at 37°C until defrosted and transferred into cell culture flasks with the appropriate media.

2.2.3 Poly-D-lysine coating

10cm plates for HEK293T LTV cells were incubated with 5 ml PDL solution for 30 minutes at room temperature. Plates were washed in phosphate-buffered saline (PBS)and used immediately.

2.2.4 DNA transfection

Cells were plated 24-48 hours before transfection. Transient transfections were performed using JetPEI (PolyPlus) using a total DNA:jetPEI ratio of 1 µg:3 µl in 150 mM NaCl, or using GeneJuice (Merck Millipore) using a total DNA:GeneJuice ratio of 1 µg:3 µl in Optimem media following the manufacturer's instructions. For other experiments cells in 10cm plates were transfected using 1 mg/ml branched polyethylenimine (PEI) using a DNA:PEI ratio of 1 µg:3 µl.

2.2.5 siRNA transfection

$0.5x10^5$ cells were plated in a 6 cm plate 24 hours before initial siRNA transfection. 5 µl of 40 nm siRNA oligonucleotide and 5 µl INTERFERin (Polyplus) in 200 µl Optimem was incubated for 10 minutes at room temperature before addition to cells. After 48 hours, $0.3x10^5$ cells were re-plated into a 6 well dish. 24 hours later, cells were transfected a second time with LITAF siRNA. For rescue experiments, siRNA-

resistant GFP-LITAF constructs were transfected 24 hours later using GeneJuice. Cells were analysed 48 hours after DNA transfection, or 72 hours after siRNA transfection, and knockdown efficiency for each experiment was confirmed using Western blotting. Allstars non-targeting siRNA (Qiagen) was used as a control.

siRNA	Target sequence
LITAF	5'-GCAUGAAUCCUCCUUGGUA

Table 2.8. Oligonucleotide sequence used for siRNA-mediated depletion of LITAF. siRNAs were ON-TARGETplus from Dharmacon.

2.2.6 Lentivirus production and transduction

HEK293T LTV cells were plated on PDL-coated 10 cm plates 24 hours before transfection. For each dish, 6 µg pXLG3-LITAF construct, 4.5 µg psPAX2 packaging plasmid and 3 µg pM2G envelope plasmid was transfected into the cells using GeneJuice. After 24 hours, cells were supplemented with 10 mM sodium butyrate (Merck Millipore) for 8 hours. At 72 hours after initial transfection the lentivirus-containing media was harvested and centrifuged for 10 minutes at 4000 rpm and filtered through a 0.45 µM syringe-driven filter unit to remove cell remnants. Lentivirus aliquots were flash frozen in liquid nitrogen and stored at -80°C. For lentivirus transduction, HeLaM cells or RPE-1 cells were transduced with lentivirus stock at a dilution of 1:2-1:20 in the media. All solutions contaminated with virus were treated with 20 minutes UV radiation and then treated with Virkon (DuPont) overnight.

2.3 Immunofluorescence

For immunofluorescence experiments 0.15-0.25x10^5 cells were plated per well containing a 13 mm glass coverslip (Agar) in a 12 well plate or 0.3-0.6x10^5 cells in a 6 well plate.

2.3.1 Formaldehyde fixation and permeabilisation

Cells were washed with PBS prior to fixation in 3% paraformaldehyde (PFA) in PBS for 15 minutes at room temperature. Cells were washed with PBS and excess PFA was quenched with 1M glycine in PBS. Cells were permeabilised in 0.1% Triton X-100 in PBS for 5-10 minutes.

2.3.2 Antibody staining

Cells were washed with PBS and incubated in primary antibody in PBS solution for 30 minutes at room temperature. Cells were washed and incubated in secondary antibody and DAPI (1:500) in PBS solution for 30 minutes. Cells were washed and incubated in ddH_2O. Coverslips were dried and mounted using 7 µl Prolong Gold (Invitrogen) onto glass slides and incubated at room temperature overnight.

2.3.3 Imaging

Cells on coverslips were imaged using an Olympus BX-61 microscope with a 60x 1.4 NA Plan Apo objective. Images were obtained with a CoolSNAP HQ CCD camera (Photometrices) using Metamorph software. Images were processed in ImageJ, Adobe PhotoShop and Adobe Illustrator.

2.3.4 Cargo trafficking

HeLaM cells grown on glass coverslips were serum starved in media lacking FBS for 2 hours. Cells were washed in ice cold PBS containing magnesium and calcium and incubated with CD98 antibody in Leibovitz's L-15 medium for 1 hour at 4°C. Cells were washed in PBS and then incubated at 37°C for 30 minutes or 3 hours. Cells were incubated in stripping buffer (0.5% acetic acid, 500 mM NaCl pH 3.0) for 1 minute at 37°C, washed in PBS and then fixed, permeabilised and stained with secondary antibody.

2.3.5 Quantification of images

A non-biased, object-based method utilising ImageJ was used to determine the co-localisation of endogenous LITAF and overexpressed GFP-LITAF constructs with endosomal markers from fluorescent images. A single wide-field image (from three independent labelling experiments) was superimposed on a grid and GFP-LITAF-containing punctae that lay on grid lines were identified to obtain a random selection of these structures. Each LITAF puncta was then scored for whether it was positive for an endosomal marker. For EEA1 images, a total of 542-854 LITAF punctae were scored in HeLaM cells and a total of 260-304 LITAF punctae were scored in RPE-1 cells. For CD63 images, a total of 484-951 LITAF punctae were scored. To quantify the co-localisation of HA-Arf6 T44N tubules and GFP-LITAF, a grid was superimposed on each image and each tubule that crossed a horizontal grid line was

examined for co-labelling of markers. A total of 291-469 HA-Arf6 T44N tubules were scored per condition.

A non-biased, morphometric technique utilising ImageJ was used to determine density of tubules labelled by different markers from fluorescent images. Tubules were defined as having approximately a minimum length of 1 μm and a minimum width of 0.2 μm. A single wide-field image (from three independent labelling experiments) was superimposed on a grid and the frequency of tubules that crossed horizontal grid lines were identified to estimate the amount of tubules in the cell. The number of grid intersections in each cell was also counted to approximately measure the relative cell area. Each cell was then given a score for the relative density of tubules in the cell. For GFP-LITAF or GFP-SLD-labelled tubules, a total of 23-66 cells were scored for each condition from 3 independent experiments. For CD98 trafficking experiments a total of 130-253 cells were scored per condition. Values were obtained from 20 images from each of 3 independent experiments. For LITAF rescue experiments on Pacsin2-labelled tubules a total of 100–180 cells were scored per condition. Values were obtained from 20 images from each of 3 independent experiments.

2.3.6 Statistics

Values were calculated as overall mean +/- SD, and statistical analysis was performed using Prism 6. For all quantification experiments a Kruskal-Wallis test with Dunn's multiple comparison test was used except for CD98 trafficking experiments where an ordinary one-way ANOVA test was used with Dunnett's multiple comparisons test.

2.5 Cell-based biochemistry

2.5.1 Cell fractionation

HeLaM cells grown in 3x 15 cm plates per condition until they were at ~70% confluency. Cells were washed in PBS and trypsinised and the cell suspension was centrifuged at 4°C at 1500 rpm for 5 minutes. The cells were washed in once in 50 ml buffer A (3 mM Mg-Acetate, 5 mM EGTA, 10 mM HEPES pH 7.4, 250 mM sucrose) and twice in 12 ml buffer A at 4°C and centrifuged again. The cell pellet was resuspended in 2 ml buffer A and cells were lysed mechanically by passing through a ball-bearing cell cracker with 10 μm clearance 5 times. Unbroken cells, nuclei and large debris were removed by centrifugation at 3000 rpm for 10 minutes at 4°C twice.

11 x 34 mm thin-walled centrifuge tubes (Beckman Coulter) were loaded with 800 µl 25% sucrose in buffer A as a cushion followed by 1.5 ml of post-nuclear cell lysate. 100 µl post-nuclear supernatant was retained for input samples. The membrane and cytosolic fractions were separated by ultra-centrifugation for 30 minutes at 40,000 rpm in a TLS-55 rotor at 4°C in the benchtop ultracentrifuge (Beckmann). The pellet was resuspended in buffer A and was taken as the membrane fraction.

2.5.2 Carbonate extraction experiments

A third of the membrane fraction sample from cell fractionation experiments was incubated with 0.1 M Na_2CO_3 (pH 11) on ice for 15 min in 7 x 20 mm thick walled centrifuge tubes, followed by ultra-centrifugation at 100,000 g in a TLA-100 rotor for 10 min. The supernatant was discarded and the pellet resuspended to make a homogeneous suspension in buffer A.

2.5.3 Immunoprecipitation

For immunoprecipitation of biotinylated mCherry-TPD54, HeLaM cells in 10 cm dishes were transduced with lentivirus containing BioID2-V5-LITAF and transfected with mCherry-TPD54 using GeneJuice the following day. 24 hours later, cells were incubated with 50 µM biotin overnight. Cell lysates were prepared in 500 µl 10 mM Tris (pH 7.4), 140 mM NaCl, 0.1% TritonX-100, containing 1 mM phenylmethylsulfonyl fluoride (PMSF) and protease inhibitor cocktail (Roche). A post nuclear supernatant was obtained by centrifugation at 14,000 g for 30 minutes at 4°C and a 10% sample of this was retained for analysis before the remaining supernatant was incubated overnight with 7.5 µl RFP-Trap resin (Chromotek). The resin was then washed 3 times with lysis buffer and then incubated with 20 µl sample buffer, before Western blotting analysis.

2.6 BioID

2.6.1 Streptavidin pulldown

RPE-1 cells were plated onto 15cm plates and incubated until they reached ~50% confluency. Cells were transduced with lentivirus and incubated for 72 hours. Cells were then split into a further 6 15cm plates until they reached ~70% confluency. 50 µM biotin was added in fresh media overnight.

Streptavidin pull-down was performed similar to the published protocol (Roux et al., 2013). Cells were washed twice in ice cold PBS and lysed in 1 ml modified RIPA buffer (50 mM Tris pH 7.4, 1% Triton X-100 (w/v), 0.5% NP-40 (w/v), 0.1% SDS (w/v), 500 mM NaCl, 10 mM $MgCl_2$, 5mM EGTA pH 7.5) containing protease inhibitor cocktail (Roche) and 1 mM PMSF. Cell lysates were scraped and transferred into tubes. Samples were sonicated in the Bioruptor at 4°C for 5 minutes (30 seconds on, 30 seconds off) and centrifuged at 4°C for 30 minutes at 17,000 g. The supernatant was transferred into a fresh tube and the protein concentration was measured using the Biorad assay (Pierce) according to the manufacturer's instructions. Samples were split into 6 equal samples and an input sample was retained for analysis. 25 µl pre-washed Dynabeads™ MyOne™ Streptavidin C1 (Invitrogen) was added to each sample and they were incubated on a roller at 4°C overnight.

The beads were collected on the side of the tube using a magnetic stand. The supernatant was removed and retained as the unbound fraction. Beads were washed by incubating with 1 ml wash buffer on a rotator for 8 minutes at room temperature. Beads were washed in 1 ml wash buffer 1 (2% SDS w/v), then the beads for each sample were pooled and washed again in wash buffer 1. Subsequently, beads were washed in Wash buffer 2 (0.1% deoxycholic acid (w/v), 1% Triton X-100 (w/v), 1 mM EDTA, 500 mM NaCl, 50 mM HEPES, pH 7.4) followed by Wash buffer 3 (0.5% deoxycholic acid (w/v), 0.5% NP-40 (w/v), 1 mM EDTA, 250 mM LiCl, 10 mM TrisCl pH 7.4. Beads were then washed in 50 mM Tris pH7.4, washed in and resuspended in 150 µl 10 mM Tris pH 7.4. 1% pulldown was retained for Western blot analysis. 50 mM ammonium bicarbonate was added to samples sent to Sandford Burnham Prebys Medical Discovery Institute proteomics facility for mass spectrometry analysis.

2.6.2 Sample preparation for mass spectrometry

Beads were resuspended with 8 M urea, 50 mM ammonium bicarbonate, and cysteine disulfide bonds were reduced with 10 mM tris(2-carboxyethyl)phosphine (TCEP) at 30°C for 60 min and cysteines were then alkylated with 30 mM iodoacetamide (IAA) in the dark at room temperature for 30 min. Following alkylation, urea was diluted to 1 M urea, and proteins were subjected to overnight digestion with mass spec grade Trypsin/Lys-C mix (Promega, Madison, WI). Finally, beads were pulled down and the solution with peptides collected into a new tube. Affinity purification was carried out

in a Bravo AssayMap platform (Agilent) using AssayMap streptavidin cartridges (Agilent). Digested peptides were then desalted in a Bravo AssayMap platform (Agilent) using AssayMap C18 cartridges, and dried down in a SpeedVac concentrator.

2.6.3 LC-MS/MS analysis

Prior to LC-MS/MS analysis, dried peptides were reconstituted with 2% ACN, 0.1% FA and concentration was determined using a NanoDrop™ spectrophometer (ThermoFisher). Samples were then analyzed by LC-MS/MS using a Proxeon EASY-nanoLC system (ThermoFisher) coupled to a Q-Exactive Plus mass spectrometer (Thermo Fisher Scientific). Peptides were separated using an analytical C18 Aurora column (75µm x 250 mm, 1.6 µm particles; IonOpticks) at a flow rate of 300 nL/min (60ºC) using a 120-min gradient: 1% to 5% B in 1 min, 6% to 23% B in 72 min, 23% to 34% B in 45 min, and 34% to 48% B in 2 min (A= FA 0.1%; B=80% ACN: 0.1% FA). The mass spectrometer was operated in positive data-dependent acquisition mode. MS1 spectra were measured in the Orbitrap in a mass-to-charge (*m/z*) of 350 – 1700 with a resolution of 70,000 at *m/z* 400. Automatic gain control target was set to 1×10^6 with a maximum injection time of 100 ms. Up to 12 MS2 spectra per duty cycle were triggered, fragmented by HCD, and acquired with a resolution of 17,500 and an AGC target of 5×10^4, an isolation window of 1.6 m/z and a normalized collision energy of 25. The dynamic exclusion was set to 20 seconds with a 10 ppm mass tolerance around the precursor.

2.6.4 Raw data analysis

All mass spectra were analyzed with MaxQuant software version 1.6.11.0 (Cox and Mann, 2008). MS/MS spectra were searched against the *Homo sapiens* Uniprot protein sequence database (downloaded in January 2020) and GPM cRAP sequences (commonly known protein contaminants). Precursor mass tolerance was set to 20ppm and 4.5ppm for the first search where initial mass recalibration was completed and for the main search, respectively. Product ions were searched with a mass tolerance 0.5 Da. The maximum precursor ion charge state used for searching was 7. Carbamidomethylation of cysteine was searched as a fixed modification, while oxidation of methionine and acetylation of protein N-terminal were searched as variable modifications. Enzyme was set to trypsin in a specific mode and a maximum

of two missed cleavages was allowed for searching. The target-decoy-based false discovery rate (FDR) filter for spectrum and protein identification was set to 1%.

2.6.5 Analysis

MaxQuant LFQ intensities were analysed by Perseus (Tyanova et al., 2016). Proteins were filtered to remove proteins only identified by site, or contaminants or proteins identified by the reverse decoy database. Each protein had to be identified by at least 3 spectral counts in 3 replicates of the affinity purification mass spectrometry of one bait. Protein LFQ intensities were $\log_2$ transformed and missing values were imputed from a normal distribution by simulating noise around the lower detection limit using the settings in Perseus (a downshift of 1.8 standard deviations and a width of 0.25 standard deviations). PCA plots and multiscatter correlation plots were generated in Perseus. Two sample Student's t-tests were carried out to identify significant hits in bait pulldowns compared to background (mock condition). The difference between the logarithmised means of the bait against the control ($\log_2$bait/background) and the $-\log_{10}$(p value) was used to generate 'volcano plots' in Graphpad Prism. P values < 0.05 were considered significant.

KEGG and GO term analyses were performed using DAVID (Huang et al., 2009). The default parameters were used, with Benjamin-Hochberg p-value adjustment threshold of 0.05. Protein interaction networks were obtained from STRING database 11.0 (Szklarczyk et al., 2019). Interactions derived from the experiments, databases, and textmining evidence channels were retrieved and a medium confidence score of 0.4 was required. The network was visualised in Cytoscape 3.8.2 (Doncheva et al., 2019, Shannon et al., 2003).

2.7 SDS-PAGE and Western Blotting

2.7.1 Protein expression analysis

For protein expression analysis, cells grown in 6 well plates were washed twice in PBS and lysed in 100 µl/well 2x sample buffer (0.5 M Tris-HCl pH 6.8, 20% glycerol (w/v), 4% SDS (w/v), 0.04% Bromophenol blue (w/v), 100 mM DTT) for 5 minutes. Cells were scraped and transferred into tubes. Samples were incubated at 95°C for 5 minutes and centrifuged at 11,000rpm for 1 minute.

2.7.2 Gel preparation and electrophoresis

Denaturing gels were prepared with a 5% acrylamide upper stacking gel portion and a lower running gel portion with the appropriate % acrylamide (GeneFlow) to resolve proteins of interest using the BioRad Mini-protean system. The stacking gel consisted of 5% acrylamide, 125mM Tris pH 6.8, 0.1% SDS (w/v), 0.1% APS (w/v), 0.1% TEMED (w/v). The running gel usually consisted of 14% acrylamide, 375 mM Tris pH 8.8, 0.1% SDS (w/v), 0.1% APS (w/v), 0.1% TEMED (w/v).

Equal amounts of sample were loaded into lanes of a gel alongside Colour Prestained Protein marker (NEB) as a reference for molecular weights of proteins. Electrophoresis was performed in running buffer (25mM Tris, 192mM glycine, 0.1% SDS (w/v)) at 100V for 10 minutes and then at 180V for up to 60 minutes.

2.7.3 Transfer and Western blotting

SDS-PAGE resolved proteins were transferred onto a polyvinylidene fluoride (PVDF) membrane (Millipore) using the wet transfer BioRad system. Transfer was performed in transfer buffer (20mM Tris, 150mM glycine, 20% MeOH, 0.2% SDS) at 300mA for 2 hours at room temperature.

Membranes were incubated in Casein blocking buffer in TBST (50mM Tris, 150mM NaCl, 0.5% Tween (w/v)) for 30 minutes at room temperature. Membranes were incubated in blocking buffer containing primary antibodies overnight at 4°C. Membranes were washed 3 times in TBST for 5 minutes and incubated in blocking buffer containing secondary antibodies for 1 hour at room temperature. Membranes were washed again 3 times in TBST for 5 minutes.

2.7.4 Imaging and quantification

Washed membranes were scanned using the LI-COR Odyssey CLx or Fc scanner. Band intensities were analysed and quantified using Image Studio Lite Version 5.2.

2.8 Antibodies

Antibody	Host	Source	Product Number	IF	WB
EEA1	Mouse	BD Biosciences	61047	1:200	-
EEA1	Rabbit	Cell Signalling	C45B10	1:200	-
CD63	Mouse	Millipore	RFAC4	1:300	-
GFP	Rabbit	Abcam	ab290	1:500	1:5000
GFP	Mouse	Proteintech	66002-1-1g	1:200	1:2000
V5	Rabbit	Abcam	ab9116	1:200	1:2000
LITAF	Mouse	Santa Cruz	sc-166719	1:200	1:2000
LITAF	Rabbit	Proteintech	16797-1-AP	1:200	1:2000
Pacsin2	Sheep	Lowe Lab	-	1:500	-
MICAL L1	Mouse	Abnova	H00085377BOIP	1:200	-
CD98	Mouse	Biolegend	315602	1:200	-
α5	Mouse	Invitrogen	14-0496-82	1:200	-
Crm1	Rabbit	Bethyl	A300-469A	-	1:5000
Torsin A	Rabbit	Swanton Lab	-	-	1:1000
TfR	Mouse	Zymed	-	-	1:1000
Myc	Goat	Abcam	ab9132	1:200	1:2000
HA	Mouse	Santa Cruz	sc-7392	1:200	
TAT1	Mouse	Keith Gull, University of Oxford	-	-	1:5000
LITAF (*D. rerio*)	Mouse	AbMart	-	-	1:1000

Table 2.9. Primary antibodies used in this study.

Antibody	Host	Source	IF	WB
anti-mouse A488	Donkey	Jackson ImmunoResearch Laboratories	1:200	-
anti-mouse A594	Donkey	Jackson ImmunoResearch Laboratories	1:500	-
anti-rabbit A488	Donkey	Jackson ImmunoResearch Laboratories	1:200	-
anti-rabbit A594	Donkey	Jackson ImmunoResearch Laboratories	1:500	-
anti-sheep A594	Donkey	Jackson ImmunoResearch Laboratories	1:500	-
Streptavidin A594	-	Jackson ImmunoResearch Laboratories	1:1000	-
anti-mouse 680	Donkey	Jackson ImmunoResearch Laboratories	-	1:5000
anti-mouse 800	Donkey	Jackson ImmunoResearch Laboratories	-	1:5000
anti-rabbit 680	Donkey	Jackson ImmunoResearch Laboratories	-	1:5000
anti-mouse 800	Donkey	Jackson ImmunoResearch Laboratories	-	1:5000
anti-sheep 800	Donkey	Jackson ImmunoResearch Laboratories	-	1:5000
Streptavidin 800	-	LiCOR	-	1:5000

Table 2.10. Secondary antibodies used in this study.

2.7 Zebrafish

2.7.1 Maintenance

Zebrafish were raised and maintained at the Biological Services Facility in the University of Manchester under standard conditions (Westerfield, 2000) in accordance with the Animals (Scientific Procedures) Act 1986. Wild type (strain AB Notts) were bred in the University of Manchester. Following breeding embryos were collected and placed in 10 cm dishes with chorion water (60 µg/ml Instant Ocean Sea Salts, $50x10^{-6}$% Methylene Blue and incubated at 28°C.

2.7.2 RNA extraction

For tissue RNA extraction, and embryo RNA extraction, two females and one male AB Notts adult zebrafish or 10 3 or 5 dpf embryos respectively, were terminally anaesthetised with an overdose of MS222 (pH 7). Organs were dissected from adult zebrafish and snap frozen and stored at -80°C (Gupta and Mullins, 2010). 500 µl Trizol (Invitrogen) was added to the samples. Samples were homogenized using IKA Ultra homogeniser on ice for 10 seconds at setting 5 or sonicated in the Bioruptor for 5 minutes at 4°C. A further 500 µl Trizol was added and samples were incubated for 5 minutes. 200 µl chloroform was added and samples were centrifuged at 12,000 rpm for 15 minutes at 4°C. The colourless aqueous phase was transferred to a new tube. 500 µl isopropanol was added and samples were mixed and incubated for 10 minutes. Samples were centrifuged at 12,000 rpm for 15 minutes at 4°C. The supernatant was removed and the pellet was washed with 1 ml 70% ethanol. The samples were mixed by inversion and centrifuged at 7500rpm for 5 minutes at 4°C. Ethanol was removed and the pellet was allowed to dry for 10 minutes. The pellet was resuspended in 30 µl nuclease free water. These samples underwent another clean up using the RNeasy mini kit (Qiagen), using the manufacters instructions, including a DNase digest. Samples were eluted in 20 µl nuclease-free water and stored at -80°C.

2.7.4 cDNA synthesis

For non-quantitative RT-PCR, a total mass of 5ng was used to generate cDNA using Superscript III First strand kit (Invitrogen) according to the manufacturer's instructions.

2.7.5 RT-PCR for expression analysis

Oligonucleotide primers (IDT) were designed using Primer3 (Untergasser et al., 2012) (Table 2.11). RT-PCR was performed on cDNA using GoTaq green master mix (Promega) (Table 2.12).

Gene	Forward Primer	Reverse Primer
EIF1a	CTTCTCAGGCTGACTGTGC	CCGCTAGCATTACCCTCC
LITAF	CTCCATATCCGACACAAGAA CAGTCTATGTTCAGCCTGG	TATGCAGAAGGGAATTAGGC CTCTTGTGCACCCCTAAAA
Si:Ch211-202h22.7	CCTCAGTAATTCAGACGGTT ACAGTAACTCAGACAATGCA	GAAGGGAATCAAACAACACG GAAAATGCCGAGACCAATG
Si:Ch211-202h228	TATGATGCCACCTAGTCTGA TCAACCAAACTCAGTTCACA	TACATGCGTTTGTACAGGAA TGTTGTCTGATTCCCTTCTG
Si:Ch211-202h22.9	GGATCAGACGCAGATTAACT ATTAACTACCCTGTACAGCC	ACAGCATAACCAGCATACAA GATTAACCAGGCCATCAAAC
CDIP1	CCTCATGGTGGTTACTATCC GAGGAGAAGAACGGACAAC	CGACAAAGAAGCAGAACATG CCCATCGTATGAGGAAAGTG
Si:dkeyp-75b4.8	ATGACGAGATAATCCCTCCA GTGACACAACAACAACAAGT	AATACCTGCACACAATGGAT ACTTATTACGACGCACATGA

Table 2.9. Primers used to identify expression of genes present in cDNA isolated from zebrafish.
They were designed to have a length of 18-25bp, GC content 40-60%, and annealing temperature of 55°C.

Number of cycles	Temperature (°C)	Time	Step
1	95	5 minutes	Initial denaturation
35	95	30 seconds	Denaturation
	54	30 seconds	Annealing
	72	30 seconds	Extension
1	72	5 minutes	Final extension

Table 2.10. GoTaq Green master mix PCR parameters.

2.8 CRISPR/Cas9 mutagenesis

2.8.1 sgRNA design

sgRNAs were designed using several online tools including http://crispr.mit.edu/ (Zhang lab, MIT, 2013), CCTop (Stemmer et al., 2015) E-CRISP (Heigwer et al., 2014) and CHOPCHOP (Labun et al., 2016).

sgRNA name	Target exon	Sequence	PAM
LITAF 1	LITAF exon 2	UCAUCGUAUGAUGGAGGAGG	CGG
LITAF 2	LITAF exon 2	GAUGCCUUCAUGUCCGCUGG	AGG
LITAF 3	LITAF exon 2	GGUUGUCCUUGUGCGGUCGG	TGG
CDIP1 1	CDIP1 exon 2	GACCCUCCUCCUCCAUACCC	CGG
CDIP1 2	CDIP1 exon 2	CCGUUCUUCUCCUCGAGGAG	CGG
CDIP1 3	CDIP1 exon 3	GGUGGAGGUCCAUAUUCUGG	AGG

Table 2.11. sgRNAs used in this study.

2.8.2 Cas9 mRNA preparation

pT3TS-nCas9n was linearised by overnight digestion at 37°C by XbaI (NEB). The linear plasmid was isolated by agarose gel extraction (Macherey Nagel). The in vitro transcription reaction was carried out using the mMachine mMessage kit (Ambion). mRNA was cleaned up using MegaClear kit (Invitrogen). RNA integrity was checked by agarose gel electrophoresis.

2.8.3 Single cell embryo injections

The injection mixture containing 1 µl of 20 µM EnGen NLS Cas9 protein (NEB), 500 ng/µl Cas9 mRNA, 20 ng/µl sgRNA, 1 µl of 20 µM tracrRNA and 0.5µl phenol red was prepared on ice. Approximately 2 nl of this mixture was injected into the yolk of single cell stage zebrafish embryos using a microinjector (PLI-90 Pico-Injector, Harvard Apparatus). After injection, embryos were collected and incubated in chorion water at 28°C. After 24 hours, any dead embryos were removed and media was replaced with media containing 0.1% methylene blue was added.

2.8.4 Genomic DNA extraction and Genotyping

3-5dpf embryos were anaesthetised in MS222 (0.2 mg/ml, pH 7) in chorion water. Individual embryos were incubated in 50 µl of 50 mM NaOH for 20 minutes at 95°C and 5 µl 1M Tris was added at 4°C as described in the HotShot method (Meeker et al., 2007). Samples were centrifuged at high speed for 1 minute and cleared supernatants stored at -20°C.

Genotyping PCRs were performed on genomic DNA using GoTaq green master mix (Promega) using conditions as in Table 2.12 and primers as in Table 2.14.

Gene	Forward Primer	Reverse Primer
LITAF Exon 2	TTATGACACAAGACGATGGC	GCACTAGTCAACCAGGTAAG
CDIP1 Exon 2	TTAACGGTGTGTGTTTGTTG	CCACTGCACTTACACATAGT
CDIP1 Exon 3	ATTTCGATTGATCACACAGC	GCCGACCTACTTTGAATCTT

Table 2.12. Genotyping primers used to assess efficiency of CRISPR sgRNAs in injected 3dpf zebrafish embryos.
They were designed to have a length of 18-25bp, GC content 40-60%, and annealing temperature of 55°C.

2.8.5 Blunt PCR cloning

KOD HotStart polymerase was used to amplify regions of interest from zebrafish genomic DNA using primers from Table 2.14 and parameters from Table 2.5. The Zero Blunt PCR Cloning Kit (ThermoFisher) was used to clone blunt end purified PCR products in to the pCR-Blunt vector. Molar ratios of 10:1 insert to vector were used per reaction and were set up according to the manufacturer's instructions. Ligation reactions were performed at room temperature for 30 minutes and half the reaction was transformed into Top10 cells.

2.8.6 Protein extraction

200 µl of RIPA buffer (20mM Tis-HCl, 150mM NaCl, 1mM EGTA, 1% (v/v) NP-40, 1% (w/v) sodium deoxycholate) was then added and samples sonicated using the Bioruptor. Lysates were centrifuged for 20 minutes at 17000 rpm and the supernatant was transferred to a fresh tube. The protein concentration determined using the BCA assay (Pierce). Lysates were snap frozen in liquid nitrogen and stored at -80°C. 50 µg of protein was loaded onto each lane of a 14% gel.

Chapter 3: CMT1c mutations in LITAF affect endosomal recycling tubules

3.1 Introduction

Mutations in LITAF result in CMT1c, a neuropathy which specifically affects the peripheral nervous system (PNS) (Street et al., 2003). Mutation of a range of endocytic regulators results in various forms of CMT, indicating that correct function of this pathway is necessary for Schwann cells to maintain myelin (Azzedine et al., 2012, DiVincenzo et al., 2014). LITAF is a monotopic membrane protein which is integrated into endosomal membranes and interacts with proteins that have roles in endocytic trafficking. These include ESCRT components and Nedd4 family ubiquitin ligases that direct ubiquitinated cargo into lysosomes (Eaton et al., 2011, Shirk et al., 2005), but more recently interactions with recycling endosome machinery have been uncovered (Wunderley et al., 2021). Furthermore, whilst LITAF is known to localise to early and late endosomes, recent studies have shown that LITAF also localises to recycling endosomes (Moriwaki et al., 2018, Wunderley et al., 2021).

Although the interactions and localisation of LITAF provide hints of what its cellular function is, the precise role of LITAF in endocytic trafficking remains to be elucidated. Additionally, in order to understand the pathophysiology of CMT1c disease, it is necessary to appreciate the effect of mutations on LITAF function. Given the location of many of the disease-causing mutations close to the hydrophobic membrane anchor region, and the high degree of conservation of the LITAF domain, it is likely that the membrane association of LITAF is essential for LITAF function. The predicted structure of LITAF containing the pathogenic V144M mutation indicated changes in residues that interact with phosphatidylethanolamine, consistent with the notion that membrane association may be altered in CMT1c disease (Ho et al., 2016).

Several groups have investigated the effect of pathogenic mutations on LITAF localisation. However, studies from different groups have conflicting results. It has been shown that G112S, W116G (Shirk et al., 2005), T115N (Shirk et al., 2005, Zhu et al., 2013) and V144M (Ho et al., 2016) mutations in LITAF did not affect subcellular localisation. However in another study, W116G and P135T mutations caused partial mislocalisation from early endosomes to the cytosol (Lee et al., 2011). In a separate study, A111G, G112S, W116G, and T115N mutations in LITAF resulted in mislocalisation from the late endosome/lysosome to the mitochondria while T49M, L122V, and P135T mutations gave rise to partial mislocalisation to the mitochondria

(Lacerda et al., 2014). In summary, mutations may affect membrane localisation and association but the full range of studies have not reached a consensus. Therefore, it is necessary to clarify the effect of CMT1c mutations on LITAF localisation, as clearly mislocalisation would affect LITAF function, and even partial defects in localisation could direct LITAF away from its normal site of action.

Impaired LITAF function results in endosome vacuolation (Lee et al., 2012, Zhu et al., 2013, Edgar et al., 2020) and increased tubulation of endosomal recycling compartments (Wunderley et al., 2021), which would suggest that LITAF has a role in membrane trafficking. There are reports that LITAF has a role in trafficking of the transferrin receptor (Moriwaki et al., 2018), a well-studied recycling cargo, and in degradative trafficking of EGFR (Lee et al., 2012), but these results have not been replicated (unpublished data and (Wunderley et al., 2021)). It is important to investigate whether patient mutations in LITAF do affect trafficking of cargo, as this may have important implications in the context of polarised delivery of myelin proteins in Schwann cells.

In this section we examined the subcellular localisation of LITAF containing CMT1c mutations and investigated the ability of these mutants to integrate into the membrane. We also looked at the ability of CMT1c mutants to regulate the recycling compartment in the absence of endogenous LITAF and the effect of mutations on trafficking of a clathrin-independent endocytosis (CIE) cargo.

3.2 Results

3.2.1 LITAF containing CMT1c mutations remains localised to endosomes and integrated into the membrane

LITAF has previously been shown to localise to various endosomal membranes but the effect of CMT1c mutations on LITAF membrane integration and localisation remains unclear. Therefore, it was necessary to clarify the localisation of LITAF containing patient mutations in cell lines. We labelled HeLaM cells, RPE-1 cells and MRC-5 cells for endogenous LITAF and also looked at the localisation of overexpressed GFP-LITAF and GFP-LITAF (SLD). We used HeLaM cells as the recycling compartment has a distinct morphology from that of early and late endosomes which can easily be distinguished. We also used RPE-1 cells and MRC-5 cells as they are a non-cancerous diploid cell line and epithelial and fibroblast-derived cells are flat which makes them suitable for imaging studies. Figure 3.1 shows that endogenous LITAF localises to endosomes in the perinuclear region in the three cell lines, and exogenous GFP-LITAF also localises to endosomes. In contrast, the SLD domain of LITAF localises to tubular structures in HeLaM cells, whilst in RPE-1 cells and MRC-5 cells it localises mainly to the plasma membrane but also to endosomes (Figure 3.1). This indicates that LITAF localises to endosomes in different cell lines, whilst expression of the SLD results in an altered distribution.

Additionally, in order to examine the effect of CMT1c mutations on LITAF localisation, cells containing GFP-LITAF and GFP-LITAF containing two patient mutations, P135S and V144M, were labelled with endosomal markers. We selected P135S and V144M patient mutations for further investigation as the P135S mutation is at the edge of the hydrophobic region and the V144M mutations is further away but before the second CXXC motif, and so these are most likely to have an effect on the membrane association of this protein. Previous data indicated that LITAF localises to early endosomes and late endosomes in HeLaM cells (Qin et al., 2016), so we co-labelled HeLaM cells with EEA1 or CD63, markers for early and late endosomes respectively (Figure 3.2). Co-localisation analysis showed that between 30-40% of endogenous and overexpressed GFP-LITAF puncta co-labelled with EEA1, and this did not change with GFP-LITAF containing patient mutations (Figure 3.2B). Furthermore, 50-60% of LITAF puncta co-labelled with CD63 and again this did not

change with two of the CMT1c mutations (Figure 3.3). In RPE-1 cells, 70-80% of LITAF puncta localised to early endosomes indicating that in this cell line there is a slight difference in endosomal distribution of LITAF. Once again, the CMT1c mutations did not affect this co-localisation (Figure 3.4).

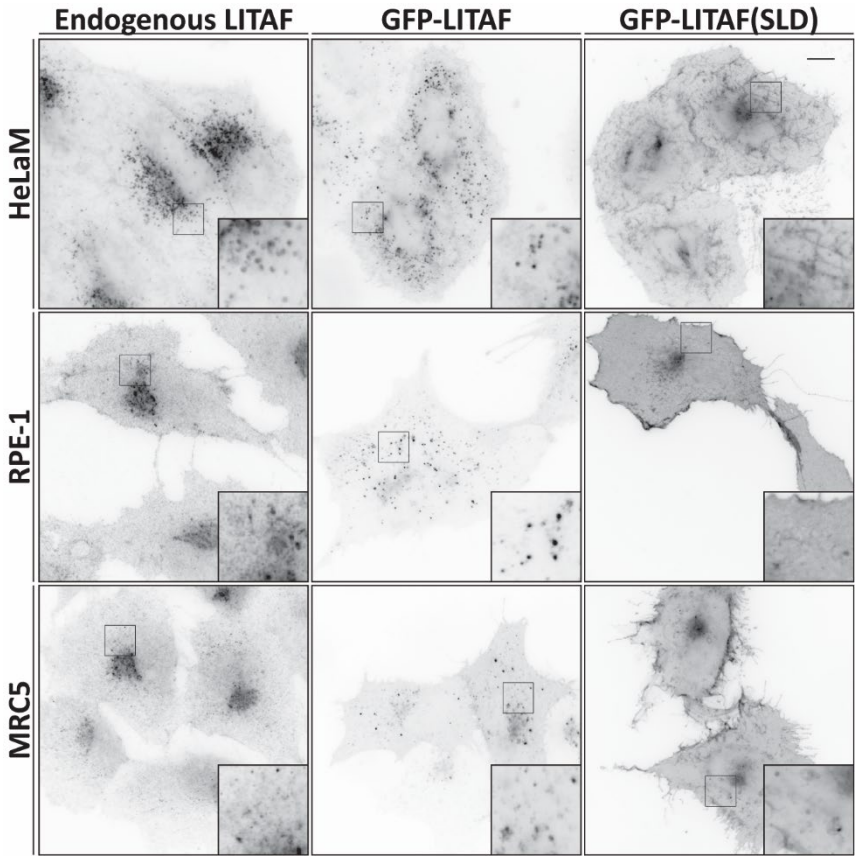

Figure 3.1. Subcellular localisation of LITAF in different cell lines.
HeLaM, RPE-1 and MRC5 cells expressing endogenous LITAF and transiently transfected with GFP-LITAF or GFP-LITAF SLD were analysed by widefield fluorescence microscopy. Scale bar = 10 µm. Insets magnified 3x.

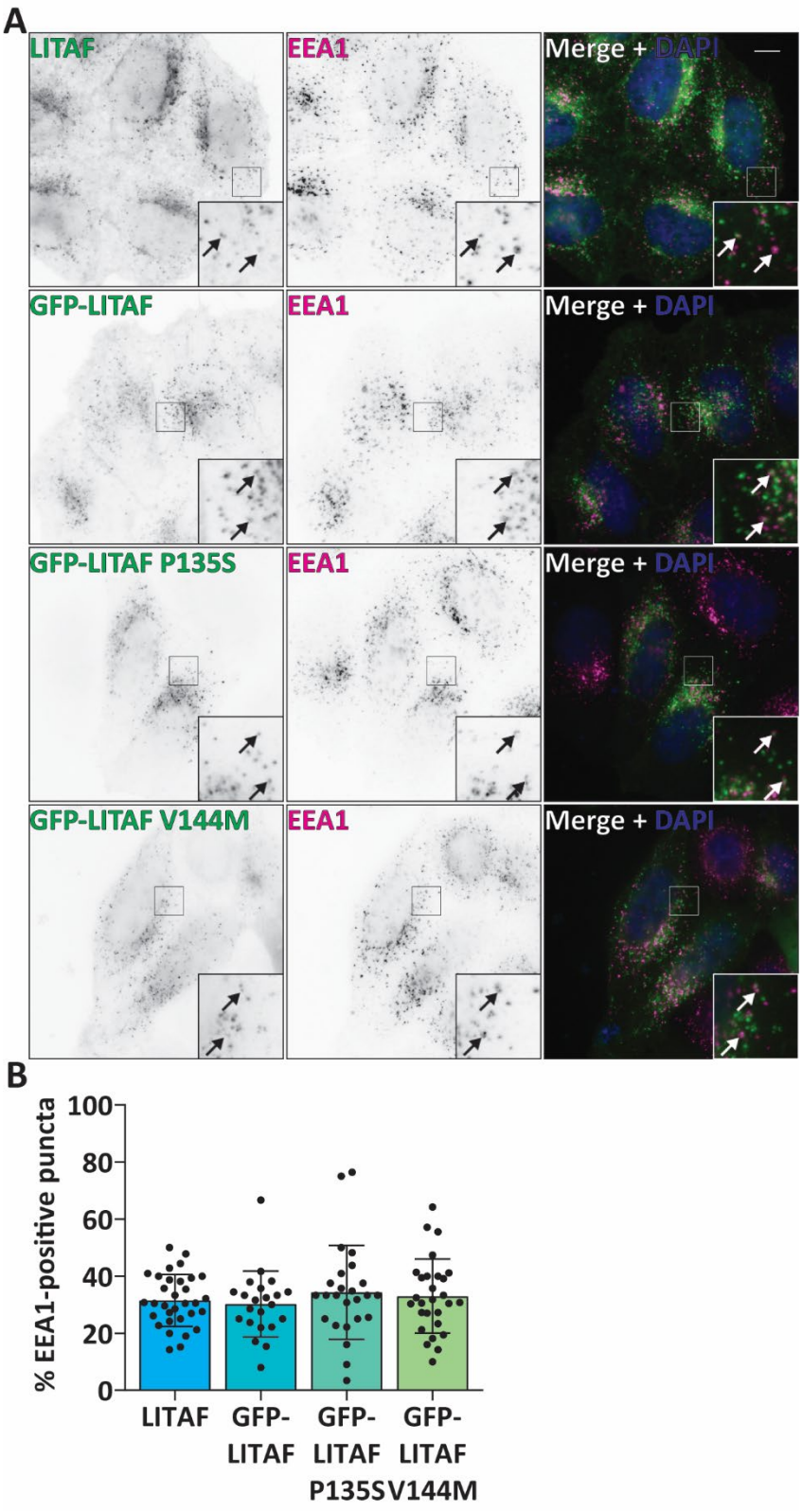

Figure 3.2. LITAF containing patient mutations partially overlapped with early endosomes in HeLaM cells.

A. HeLaM cells stained with LITAF antibody or transiently transfected with GFP-LITAF, GFP-LITAF P135S or GFP-LITAF V144M were stained with anti-EEA1 antibody and analysed by widefield fluorescence microscopy. B. Quantification of co-localisation of LITAF puncta with EEA1. Data were collected from three independent experiments**.** Scale bar = 10 µm. Arrows indicate co-localisation. Insets magnified 3x. Error bars represent standard deviation (SD).

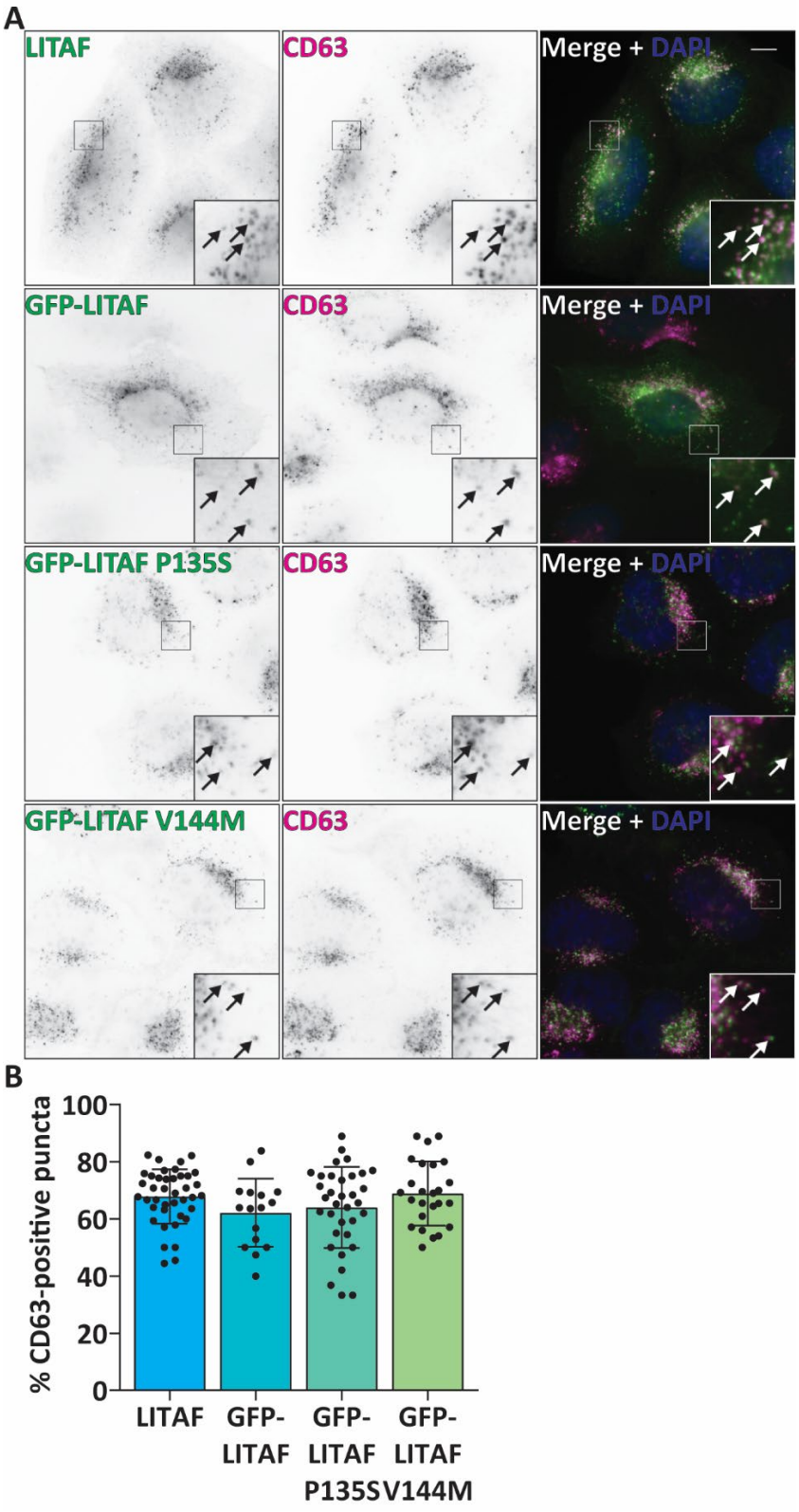

Figure 3.3. LITAF containing patient mutations localised to late endosomes in HeLaM cells.

A. HeLaM cells stained with LITAF antibody or transiently transfected with GFP-LITAF, GFP-LITAF P135S or GFP-LITAF V144M were stained with anti-CD63 antibody and analysed by widefield fluorescence microscopy. B. Quantification of co-localisation of LITAF puncta with CD63. Data were collected from three independent experiments. Scale bar = 10 µm. Arrows indicate co-localisation. Insets magnified 3x. Error bars represent SD.

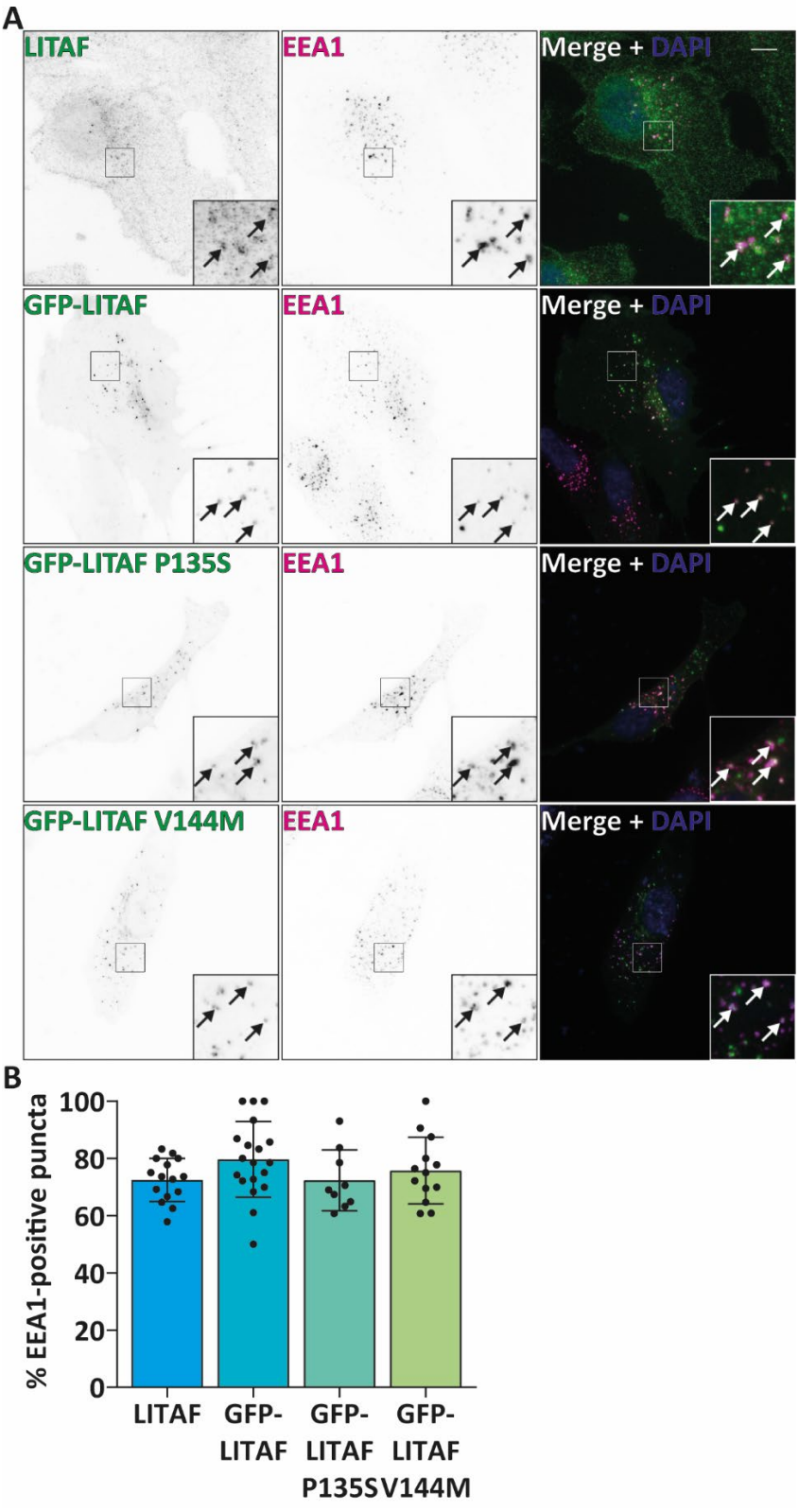

Figure 3.4. LITAF containing patient mutations localised to early endosomes in RPE-1 cells.

A. RPE-1 cells stained with LITAF antibody or transiently transfected with GFP-LITAF, GFP-LITAF P135S or GFP-LITAF V144M were stained with anti-EEA1 antibody and analysed by widefield fluorescence microscopy. B. Quantification of co-localisation of LITAF puncta with EEA1. Data were collected from three independent experiments. Scale bar = 10 µm. Arrows indicate co-localisation. Insets magnified 3x. Error bars represent SD.

LITAF is a monotopic membrane protein, and contains a hydrophobic region that is predicted to form an amphipathic helix and which inserts into the lipid bilayer (Qin et al., 2016, Ho et al., 2016). CMT1c missense mutations localise close to the membrane insertion region. Therefore, it has been suggested that these mutations might affect membrane integration, although LITAF containing CMT1c mutations still localised to endosomes (Figures 3.1-3.3). We tested the membrane integration of CMT1c mutants using cell fractionation. Cell lysates were centrifuged to pellet the membranes. Separation of the membrane fraction from the cell lysate was confirmed by blotting for the soluble nuclear export factor, Crm1 and the transmembrane transferrin receptor (TfR) (Figure 3.5A). The membrane fraction was then subjected to pH 11 carbonate extraction to remove peripheral membrane proteins that do not traverse the membrane. TorsinA, an ER luminal peripheral membrane protein was mostly removed whereas TfR remained in the membrane fraction after incubation with high pH carbonate, indicating successful extraction (Figure 3.5C).

Endogenous LITAF and overexpressed WT LITAF were enriched in the membrane fraction compared to the cell lysate, similar to TfR, while GFP was de-enriched in the membrane fraction (Figure 3.5A, B). Any remaining GFP in the membrane fraction was completely removed following pH 11 carbonate extraction (Figure 3.5C). Interestingly, LITAF C96A, which appears to be cytosolic by immunofluorescence analysis (Qin et al., 2016) was partly localised to the membrane fraction (Figure 3.5A, B). Surprisingly, this pool of LITAF C96A was resistant to extraction (Figure 3.5C, D), suggesting that once LITAF C96A is localised to the membrane, it is integrated. LITAF containing P135S and V144M mutations were also present and integrated into the membrane, albeit at reduced levels compared to WT LITAF (Figure 3.5). Therefore, these data indicate that CMT1c mutations reduce the membrane association of LITAF.

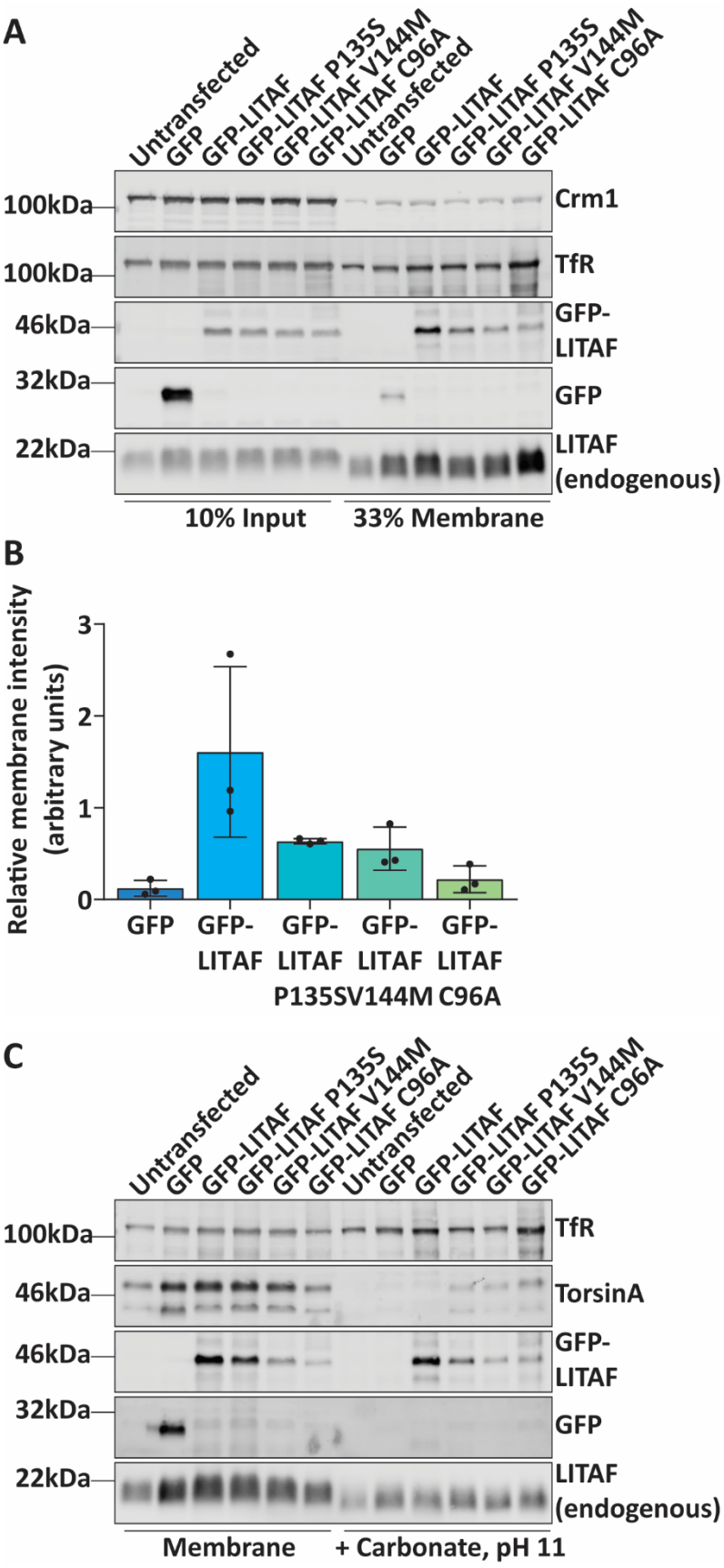
A
Untransfected
GFP
GFP-LITAF
GFP-LITAF P135S
GFP-LITAF V144M
GFP-LITAF C96A
Untransfected
GFP
GFP-LITAF
GFP-LITAF P135S
GFP-LITAF V144M
GFP-LITAF C96A
100kDa
Crm1
100kDa
TfR
46kDa
GFP-LITAF
32kDa
GFP
22kDa
LITAF (endogenous)
10% Input
33% Membrane
B
Relative membrane intensity (arbitrary units)
3
2
1
0
GFP
GFP-LITAF
GFP-LITAF P135S
GFP-LITAF V144M
GFP-LITAF C96A
C
Untransfected
GFP
GFP-LITAF
GFP-LITAF P135S
GFP-LITAF V144M
GFP-LITAF C96A
Untransfected
GFP
GFP-LITAF
GFP-LITAF P135S
GFP-LITAF V144M
GFP-LITAF C96A
100kDa
TfR
46kDa
TorsinA
46kDa
GFP-LITAF
32kDa
GFP
22kDa
LITAF (endogenous)
Membrane
+ Carbonate, pH 11

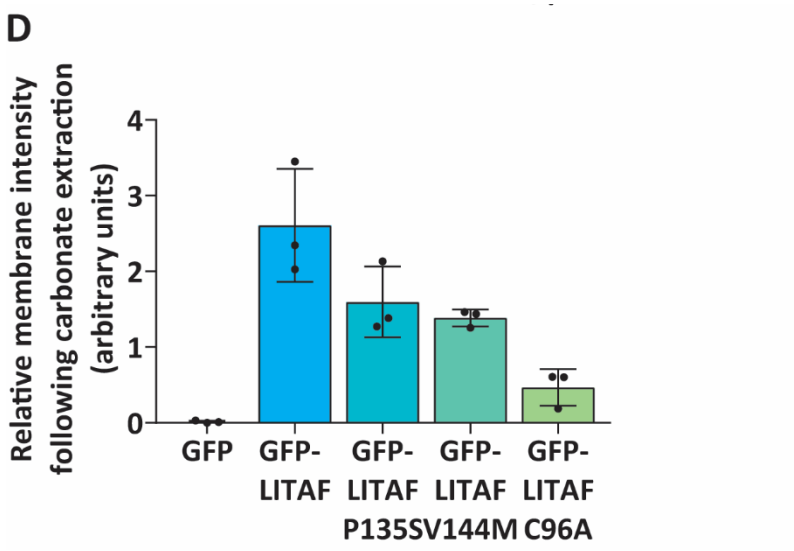

Figure 3.5. CMT1c mutations affected membrane integration.
A. Whole cell lysates and membrane pellet fractions from HeLaM cells were blotted for Crm1, TfR, GFP and LITAF. B. Quantification of the intensity of GFP-LITAF bands in the membrane fraction relative to the input. Band intensities were normalised to endogenous LITAF in each sample. C. The membrane fraction was treated with 100mM pH 11 sodium carbonate, pelleted again, and blotted for TorsinA, TfR, GFP and LITAF. D. Quantification of the intensity of GFP-LITAF bands in the carbonate extraction relative to the membrane input. Band intensities were normalised to endogenous LITAF in each sample. Error bars represent SD.

3.2.2 CMT1c mutations affect the ability of LITAF SLD to partition into recycling tubules in HeLaM cells

Endogenous and overexpressed LITAF partially localises to narrow tubular recycling endosomes that co-label with recycling tubule machinery such as Pacsin2, and recycling cargo such as MHC Class 1 in HeLaM cells (Wunderley et al., 2021). The SLD displays enhanced localisation to these tubules (Wunderley et al., 2021) (Figure 3.1). Another CMT type 1 protein, SH3TC2 localises to recycling endosomes, whilst disease-causing mutations result in SH3TC2 redistributing to early endosomes (Roberts et al., 2010). Therefore, we sought to examine whether CMT1c mutations affect localisation of LITAF to the recycling compartment.

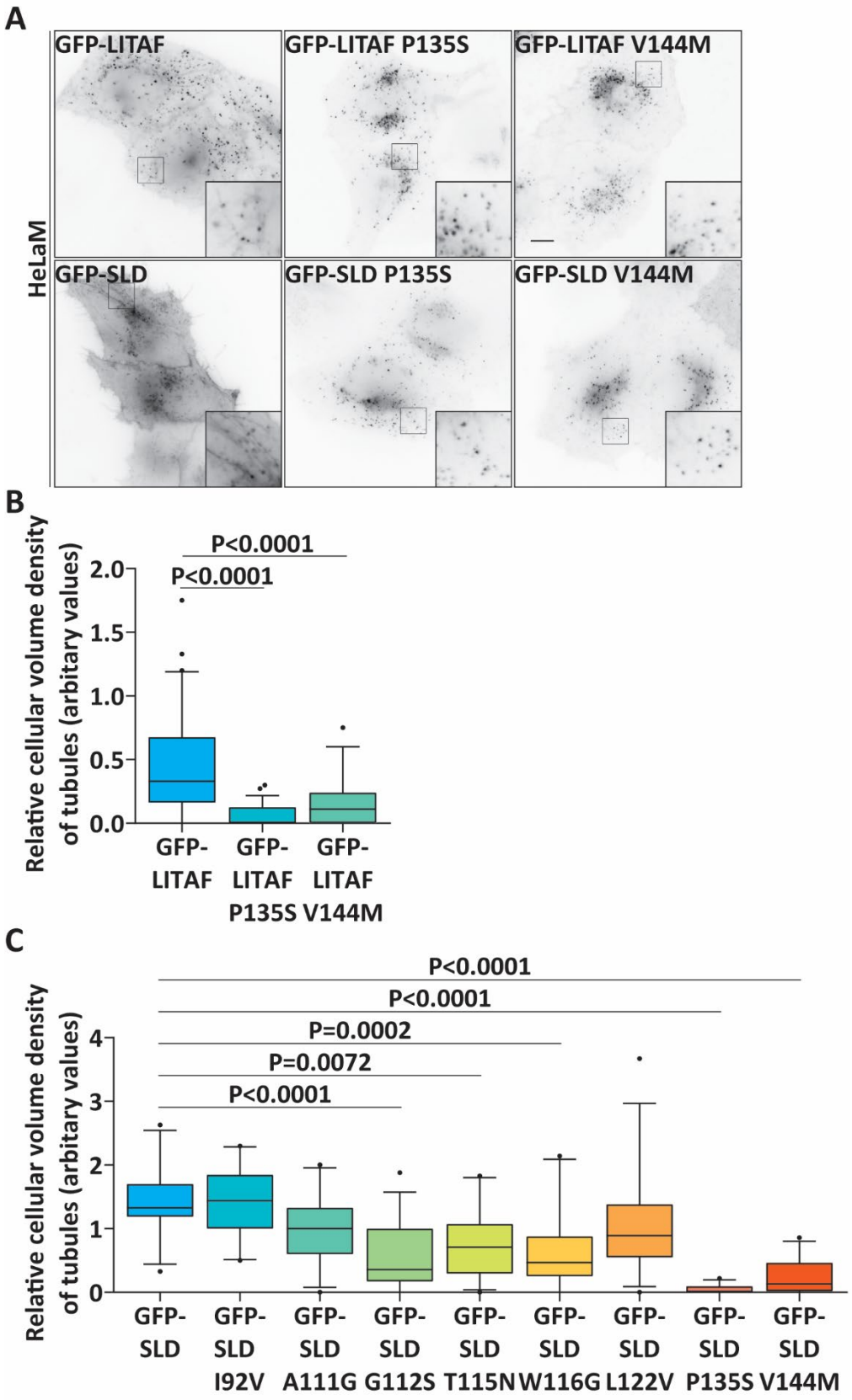
A
HeLaM
GFP-LITAF
GFP-LITAF P135S
GFP-LITAF V144M
GFP-SLD
GFP-SLD P135S
GFP-SLD V144M
B
Relative cellular volume density of tubules (arbitary values)
P<0.0001
P<0.0001
2.0
1.5
1.0
0.5
0.0
GFP-LITAF
GFP-LITAF P135S
GFP-LITAF V144M
C
Relative cellular volume density of tubules (arbitary values)
P<0.0001
P<0.0001
P=0.0002
P=0.0072
P<0.0001
4
3
2
1
0
GFP-SLD
GFP-SLD I92V
GFP-SLD A111G
GFP-SLD G112S
GFP-SLD T115N
GFP-SLD W116G
GFP-SLD L122V
GFP-SLD P135S
GFP-SLD V144M

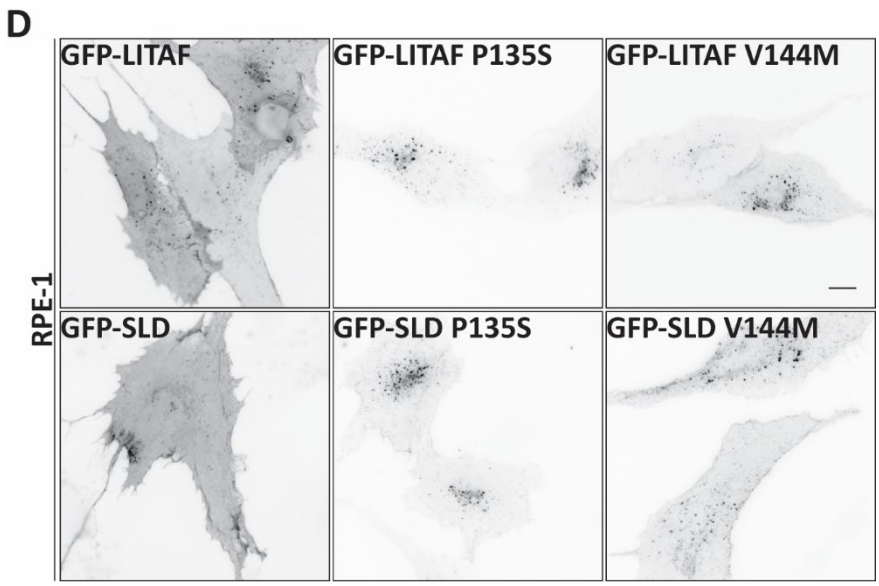

Figure 3.6. Altered distribution of LITAF containing patient mutations in different cell lines.

A. HeLaM cells cells transiently transfected with GFP-LITAF, GFP-LITAF P135S, GFP-LITAF V144M, GFP-SLD, GFP-SLD P135S and GFP-SLD V144M were analysed by widefield fluorescence microscopy. B, C. Quantification of the density of tubules relative to cell area of cells transiently transfected with GFP-tagged full length LITAF and LITAF-containing CMT1c mutations (B) or GFP-tagged SLD and SLD-containing CMT1c mutations (C). Data were collected from three independent experiments. Error bars represent 5-95 percentile. Statistical analysis by Kruskal-Wallis test with Dunn's multiple comparisons test. D. RPE-1 cells transiently transfected with GFP-LITAF, GFP-LITAF P135S, GFP-LITAF V144M, GFP-SLD, GFP-SLD P135S and GFP-SLD V144M were analysed by widefield fluorescence microscopy. Scale bars = 10 µm.

In HeLaM cells, both wild-type and CMT1c mutant LITAF localise mainly to endosomal structures (Figures 3.2-4). However, full-length LITAF also partially localises to tubules, and this tubular localisation is markedly reduced when CMT1c mutations are introduced (Figure 3.6A and B). In addition, the SLD domain mainly localises to tubules, but the SLD containing several CMT1c mutations had markedly reduced tubule vs endosomal labelling (Figure 3.6A and C). This effect varied between different CMT1c causing mutations, indicating that the effect is common to some but not all CMT1c mutations; the density of tubules was decreased in SLD G112S, T115N, W116G, P135S and V144M but not I92V, A111G and L122V (Figure 3.6C). An altered distribution of LITAF mutants is also observed in RPE-1 cells. Full-length LITAF and CMT1c mutant LITAF localised to puncta, and while the SLD domain was more abundant at the plasma membrane, SLD containing CMT1c mutations again remained in punctate structures (Figure 3.6D).

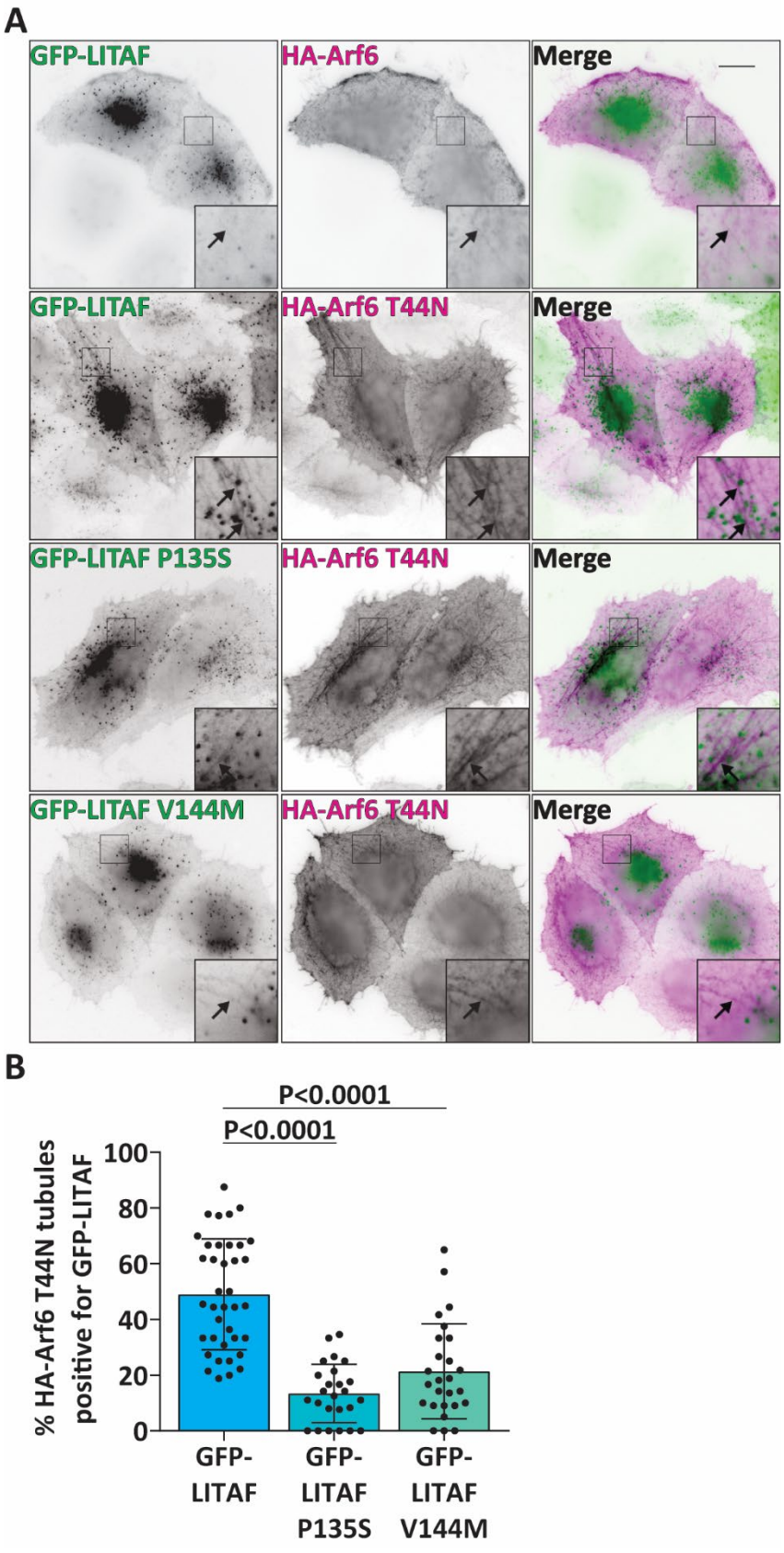
A
GFP-LITAF
HA-Arf6
Merge
GFP-LITAF
HA-Arf6 T44N
Merge
GFP-LITAF P135S
HA-Arf6 T44N
Merge
GFP-LITAF V144M
HA-Arf6 T44N
Merge
B
P<0.0001
P<0.0001
% HA-Arf6 T44N tubules positive for GFP-LITAF
100
80
60
40
20
0
GFP-LITAF
GFP-LITAF P135S
GFP-LITAF V144M

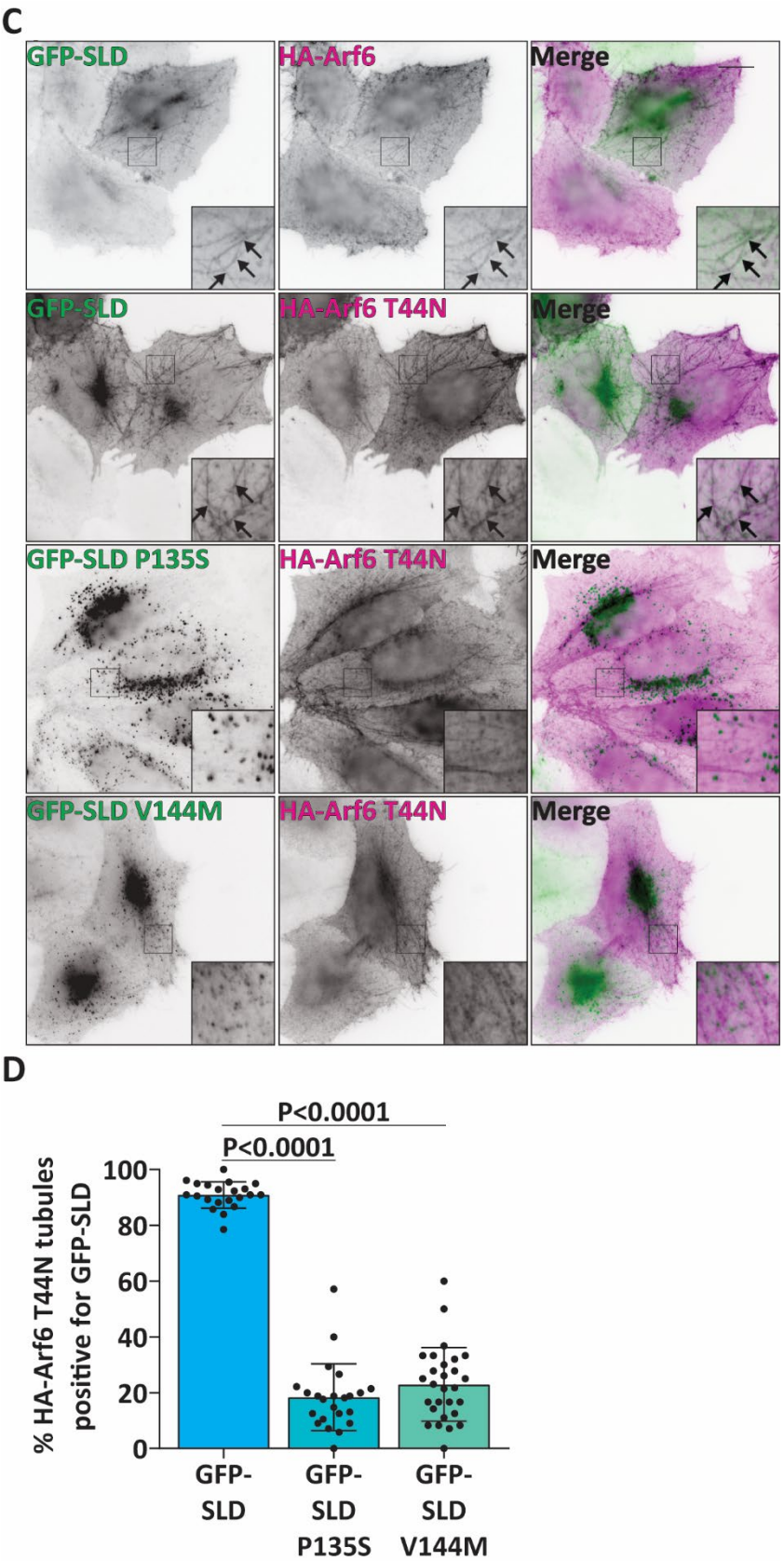

Figure 3.7. LITAF and LITAF SLD containing CMT1c mutations have reduced localisation to Arf6 T44N tubules in HeLaM cells.

A, C. HeLaM cells transiently transfected with HA-tagged Arf6 or Arf6 T44N and either GFP-tagged LITAF, LITAF P135S or LITAF V144M (A) or SLD, SLD P135S or SLD V144M (C) were stained with anti-HA antibody and analysed by widefield fluorescence microscopy. Arrows indicate co-localisation. Scale bars = 10 µm. Insets magnified 3x. B, D. Quantification of co-localisation of HA-Arf6 T44N tubules with GFP-LITAF (B) or GFP-SLD (D). Data were collected from three independent experiments. Error bars represent SD. Statistical analysis by Kruskal-Wallis test with Dunn's multiple comparisons test.

To further investigate the ability of LITAF containing patient mutations to enter into recycling tubules, we examined the effect of dominant-negative Arf6 on LITAF localisation. Arf6 regulates recycling of CIE cargo (Radhakrishna and Donaldson, 1997) and overexpression of Arf6 containing the dominant-negative mutation results in increased abundance of recycling tubules in cells (Macia et al., 2004). Co-expression of Arf6 T44N and LITAF increased the amount of LITAF on tubules compared to WT Arf6 (Figure 3.7A). In contrast, when Arf6 T44N was co-expressed with CMT1c mutants, their localisation was not altered, remaining predominantly on endosomes as opposed to relocating to tubules (Figure 3.7A, B). In addition to this, immunofluorescence analysis of co-expressed SLD with WT Arf6 or Arf6 T44N revealed that wild-type SLD localises on recycling tubules, but again the SLD containing CMT1c mutations remained on endosomes (Figure 3.7C, D). This indicates that while WT LITAF is able to partition into recycling tubules, LITAF containing CMT1c mutations does not localise to the tubular recycling compartment.

3.2.3 CMT1c mutants impair the function of recycling tubules

LITAF normally functions to regulate the recycling compartment, as siRNA-mediated knockdown of LITAF results in increased density of recycling tubules in HeLaM cells. Furthermore, LITAF appears to support scission of recycling tubules via an interaction with EHD1 (Wunderley et al., 2021). Considering that LITAF containing CMT1c mutations was able to insert into the membrane but did not localise to recycling tubules, we next explored whether the CMT1c mutants are able to rescue this LITAF depletion phenotype. In control cells, there were some tubules labelled with endogenous Pacsin2, MICAL L1 and overexpressed GFP-Rab8A, and the density of tubules increased upon LITAF knockdown, as expected (Figure 3.8A). This phenotype was rescued when siRNA-resistant GFP-LITAF was overexpressed in cells, as the density of Pacsin2-labelled tubules returned to control levels (Figure 3.8B, C). However, when GFP-LITAF P135S or GFP-LITAF V144M were expressed in a LITAF knockdown background, the increase in tubule density was not rescued (Figure 3.8B and C). LITAF knockdown efficiency and expression of exogenous LITAF were confirmed by Western blotting (Figure 3.8D). These data indicate that LITAF normally functions to limit expansion of these recycling tubules, while CMT1c mutants are unable to perform this function.

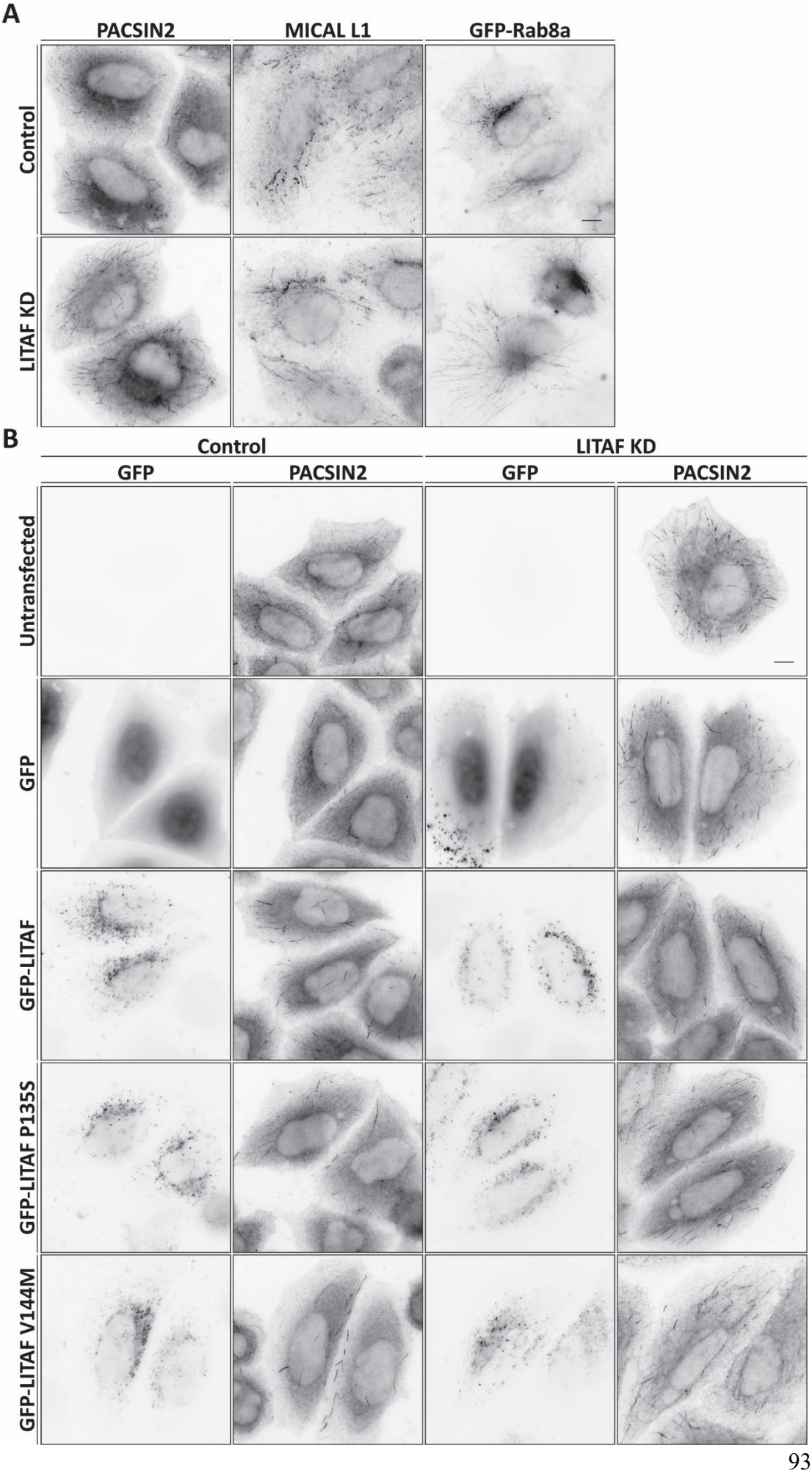
A
PACSIN2
MICAL L1
GFP-Rab8a
Control
LITAF KD
B
Control
LITAF KD
GFP
PACSIN2
GFP
PACSIN2
Untransfected
GFP
GFP-LITAF
GFP-LITAF P135S
GFP-LITAF V144M

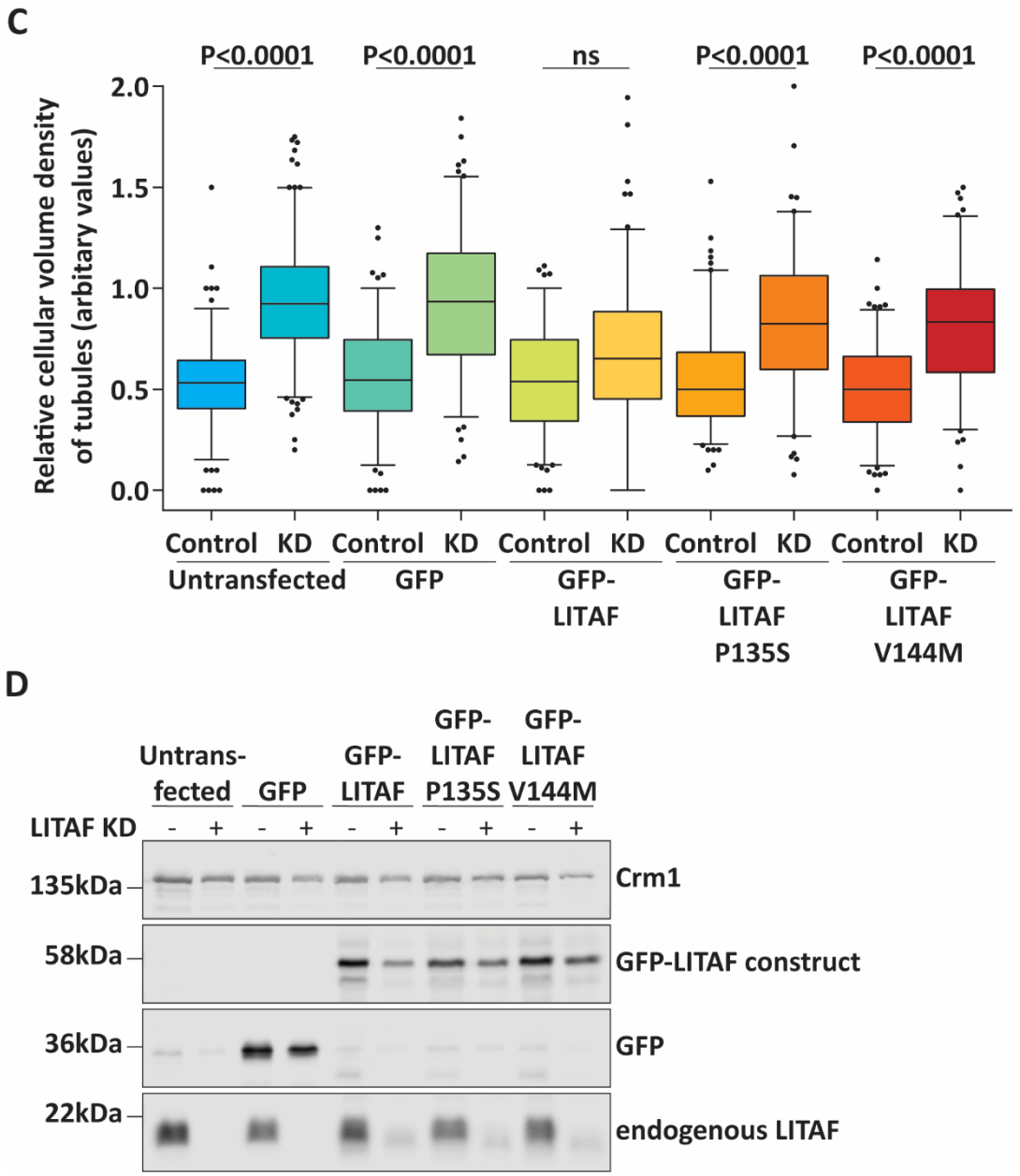

Figure 3.8. LITAF containing CMT1c mutations did not rescue LITAF knockdown recycling tubule phenotype.

A. HeLaM cells treated with control or LITAF-targeting siRNA were stained with Pacsin2 or MICAL L1 antibody or transfected with GFP-Rab8a and analysed by widefield microscopy. B. HeLaM cells treated with control or LITAF-targeting siRNA and untransfected or transiently transfected with GFP, GFP-tagged LITAF, LITAF P135S or LITAF V144M were stained with anti-PACSIN2 antibody and analysed by widefield fluorescence microscopy. Scale bars = 10 µm. C. Quantification of the density of Pacsin2 tubules relative to cell area of cells in B. ns represents P>0.05. Data were collected from three independent experiments. Error bars represent 5-95 percentile. Statistical analysis by Kruskal-Wallis test with Dunn's multiple comparisons test. D. Whole cell lysates were blotted for Crm1, GFP, and LITAF.

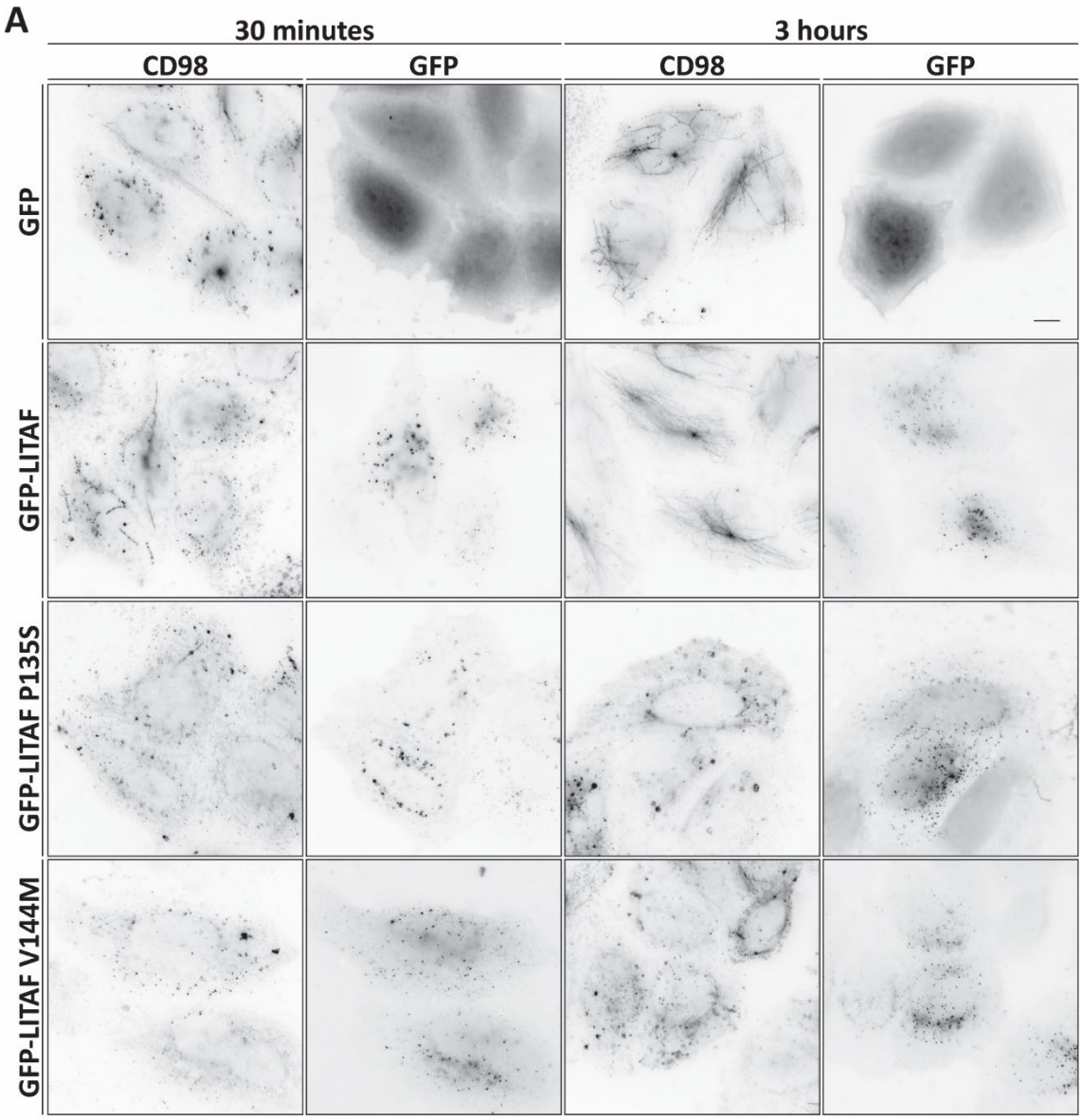
A
30 minutes
3 hours
CD98
GFP
CD98
GFP
GFP
GFP-LITAF
GFP-LITAF P135S
GFP-LITAF V144M

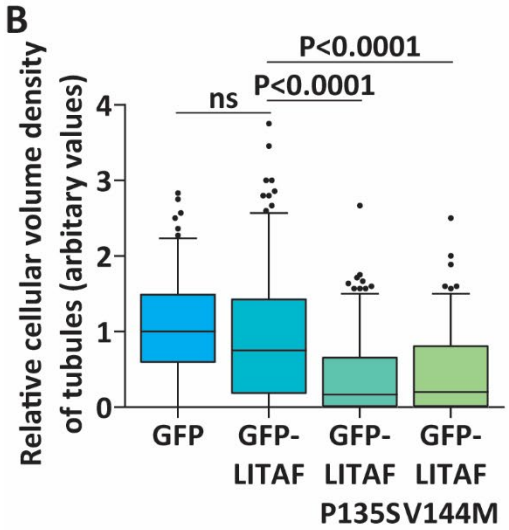
B
Relative cellular volume density of tubules (arbitary values)
P<0.0001
ns
P<0.0001
0
1
2
3
4
GFP
GFP-LITAF
GFP-LITAF P135S
GFP-LITAF V144M

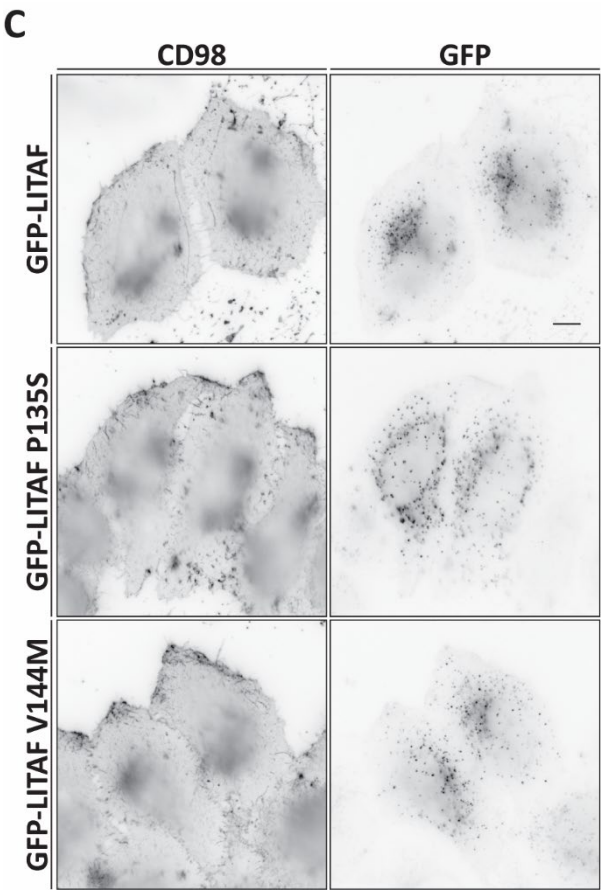

Figure 3.9. CMT1c mutations affected trafficking of CD98.
A. HeLaM cells incubated with CD98 antibody on ice for 30 minutes and then incubated at 37°C for 30 minutes or 3 hours, were stripped and stained with secondary antibody before being analysed by widefield fluorescence microscopy. B. Quantification of the density of CD98 tubules relative to cell area of cells in A. Data were collected from three independent experiments. Error bars represent 5-95 percentile. Statistical analysis by one-way ANOVA with Dunnett's multiple comparison. C. HeLaM cells were transiently transfected with EGFP-LITAF, EGFP-LITAF P135S and EGFP-LITAF V144M and stained with CD98 antibody without permeabilisation and analysed by widefield fluorescence microscopy to show cell surface labelling. Scale bars = 10 µm.

In a knockdown background, CMT1c mutants appear to have a loss of function effect upon the recycling compartment. CMT1c missense mutations are autosomal-dominant, which suggests that they have a deleterious effect in the presence of WT LITAF. Therefore, we assessed whether CMT1c mutations affect trafficking of recycling cargo in this cellular context. Following CIE, CD98 is trafficked through recycling tubules to the plasma membrane in an Arf6-dependent recycling pathway (Eyster et al., 2009). In control cells that expressed GFP or GFP-LITAF, CD98 partially localised to recycling tubules 30 minutes after internalisation, and decorated many tubules after 3 hours (Figure 3.9). In cells where either GFP-LITAF P135S or

GFP-LITAF V144M was expressed, CD98 localised to vacuolar structures and the density of tubules decorated with CD98 was markedly reduced, while the cell surface labelling was not affected (Figure 3.9). This suggests that CMT1c mutants affect trafficking of a cargo that traffics through recycling tubules.

3.3 Discussion

In this chapter, I described how introducing CMT1c mutations into LITAF does not affect early and late endosomal localisation, but does affect the ability of LITAF to localise to recycling tubules. Furthermore, patient mutations affected the membrane integration of LITAF. It also appeared that disease mutations resulted in loss of function in the context of recycling tubules since, in a LITAF knockdown background, CMT1c mutants were not able to rescue the recycling tubule expansion phenotype. Although the effect of LITAF mutations on subcellular localisation appears to be subtle, their expression had a significant functional effect upon trafficking, as trafficking of CD98 cargo to recycling tubules was reduced.

Here, we establish that LITAF containing CMT1c mutations localises to early and late endosomes, which is in agreement with several previous studies (although some of these focused on different mutations in LITAF) (Shirk et al., 2005, Zhu et al., 2013, Ho et al., 2016). We found no evidence to suggest mislocalisation to the mitochondria as others have reported (Lacerda et al., 2014), which could be due to differences in cell type or other technical differences. Differences in subcellular localisation may be caused by differential gene expression of other factors in specific cell types. Furthermore, we present the finding that CMT1c mutations impair the localisation of LITAF to recycling tubules. This compartment is expanded by expression of dominant-negative Arf6, and the propensity of LITAF to localise to these tubules is increased by expressing the SLD alone. However, even under these conditions, LITAF and SLD containing CMT1c mutations do not localise to tubules. Consistent with these results, mutations in SH3TC2 that cause CMT4B (an autosomal recessive form of demyelinating CMT) also cause reduced localisation of the protein to recycling endosomes (Roberts et al., 2010). Taken together, these results suggest that LITAF containing CMT1c mutations may be able to fulfil its function at early and late endosomes but not at the recycling endosome.

We showed that LITAF containing CMT1c mutations can integrate into the membrane, but less efficiently compared to WT LITAF. This reduced membrane integration is consistent with the clustering of CMT1c missense mutations around the hydrophobic region of the SLD that inserts into the membrane. This also supports previous findings that patient mutations cause LITAF to partially mislocalise to the cytosol (Lee et al., 2011).

Furthermore, it has been suggested that the SLD may be able to sense and/or generate membrane curvature and addition of LITAF to liposomes resulted in reduced diameters (Wunderley et al., 2021). The hydrophobic region is predicted to form an amphipathic helix which inserts into the membrane similar to other proteins which sense membrane curvature (Ho et al., 2016). Alternatively, this region may form a hairpin which forms a wedge and contributes to membrane curvature (Qin et al., 2016). Together with evidence that CMT1c mutants have slightly reduced membrane integration, this leads to the question of whether CMT1c mutations are able to perform this function and whether the mutations affect the ability of LITAF to enter into highly curved tubular membranes, which would explain the loss of localisation. Further biochemical analysis of LITAF containing patient mutations is required to address this.

We showed here that CMT1c mutants were unable to rescue expansion of recycling tubules that result from LITAF knockdown and extended these findings to show that CMT1c mutations affected trafficking of a cargo which localises to recycling tubules. These data may be consistent with the hypothesis that CMT1c mutations result in dominant negative loss of function as CMT1c mutants are unable to regulate the morphology of the recycling compartment in these cells and overexpression of CMT1c mutants disrupts trafficking of CD98. Recently, it was shown that CMT1c patient fibroblasts had enlarged and vacuolated late endosomes. This phenotype was not rescued by depletion of LITAF in these cells which provides further evidence for CMT1c mutations causing loss of function (Edgar et al., 2020).

The significance of the effect of LITAF mutations on trafficking of CD98 is highlighted by the evidence for trafficking of PMP22 through the same Arf6-dependent recycling pathway (Chies et al., 2003, Eyster et al., 2009). In addition, recycling of β1 integrin occurs through both Arf6 and Rab11-dependent pathways (Powelka et al., 2004, Arjonen et al., 2012) and correct functioning of β1 integrin is

necessary for Schwann cell interactions with nerve axons and myelination (Feltri et al., 2002, Nodari et al., 2007, Ness et al., 2013). Myelination by Schwann cells requires polarised recycling of myelin proteins, so any defects in recycling of cargo may particularly affect this cell type (Pereira et al., 2012). As HeLaM cells and Schwann cells likely express a different complement of surface proteins, further trafficking experiments following the membrane trafficking pathway of internalised myelin proteins, and the effect of CMT1c mutations on this in Schwann cells, would establish the importance of correct endocytic trafficking in a system more relevant to CMT1c disease.

Chapter 4: Exploring LITAF interactions using BioID

4.1 Introduction

LITAF contains three proline-based protein interaction motifs in its disordered N-terminal region. The PSAP motif facilitates an interaction with the UEV domain of TSG101 (Shirk et al., 2005), a component of ESCRT-I. Previous work has also identified that LITAF interacts with Hrs and STAM1, which comprise ESCRT-0 (Lee et al., 2012). LITAF also contains two PPXY motifs which mediate interactions with WW domain-containing proteins such as ITCH (Eaton et al., 2011) and Nedd4 (Shirk et al., 2005), which are E3 ubiquitin ligases. These proteins have roles in ubiquitin-mediated endosomal trafficking, which is consistent with LITAF's localisation on endosomes. Recent work by our lab and others (Moriwaki et al., 2018) has placed LITAF on recycling endosomes and shown interactions with EHD1 and PACSIN2 (Wunderley et al., 2021). These protein interactions confirm that LITAF likely functions within these pathways. However, its mechanism of action is still incompletely understood.

Any effect of CMT1c mutations on LITAF interactions may indicate how LITAF function is altered in CMT1c disease. Although most CMT1c patient mutations are not located close to motifs required for known protein interactions, it is possible that mutations may affect protein conformation or localisation, which could indirectly affect protein interactions. There have been some studies examining the effect of CMT1c mutations on known interactions. LITAF G112S, T115N and W116G are still able to interact with Nedd4 and TSG101 (Shirk et al., 2005). TSG101 localisation is not affected by LITAF T115N mutation (Li et al., 2015). However, it was shown that LITAF W116G and P135T expression reduced TSG101, STAM1 and Hrs recruitment to endosomal membranes (Lee et al., 2012).

Further analysis of LITAF interaction partners may provide more information on the function of LITAF and how it is dysregulated in disease. Several high-throughput screens have identified a number of potential interactors (Luck et al., 2020, Rolland et al., 2014, Sahni et al., 2015, Huttlin et al., 2017) and these can be viewed using BioGRID alongside experimentally validated interactions (Oughtred et al., 2021). This database shows that there are at least ten proteins which have been identified as possible interactors in more than one screen, while 57 further proteins have been

identified in one screen only. This indicates that there are likely more protein interactions with LITAF that can be explored.

Affinity purification and yeast-two hybrid methods have been used to identify proteins that interact with target proteins of interest, but more recently several approaches have been developed that allow identification of more transiently interacting proteins. BioID is a method which uses proximity-dependent labelling, followed by mass spectrometry, to identify proteins that are proximal to the protein of interest (Roux et al., 2012). A biotin ligase (BirA) was isolated from *Escherichia coli* that normally catalyses the attachment of biotin to a specific target. BirA containing a R118G mutation is more promiscuous, and biotinylates lysine residues on proteins within a 10 nm radius (Roux et al., 2012). A smaller biotin ligase from *Aquifex aeolicus* was humanized and mutated (R40G) to generate BioID2. BioID2 was shown to improve localization and is sensitive to a lower biotin concentration (Kim et al., 2016). When BioID2 fused to a protein of interest is expressed in cells in the presence of 50 μM biotin, there is biotinylation of proximal proteins. Biotinylated proteins can be affinity purified using streptavidin beads and peptides digested off the beads and analysed by mass spectrometry. This results in identification of proteins which may be proximal to the protein of interest (Figure 4.1).

BioID is a useful method to identify interactions of a protein of interest within cells and has several advantages over other methods, including the ability to detect transiently and/or weakly interacting proteins. One of the limitations of BioID is that the proteins identified may not be direct interactors, and there are many commonly identified proteins that may not be specific to the tagged protein of interest. Hits should be validated to ensure they are bona-fide interactors.

In this chapter we wanted to further investigate transient and stable interaction partners of LITAF and also examine whether CMT1c mutations affect these interactions, using BioID2 proximity-dependent labelling. Here we present the use of BioID2 to identify novel proteins that may be proximal to LITAF and show preliminary analysis of some of the hits. The results indicate that BioID is a useful method to identify potential interaction partners of LITAF that have not been studied previously.

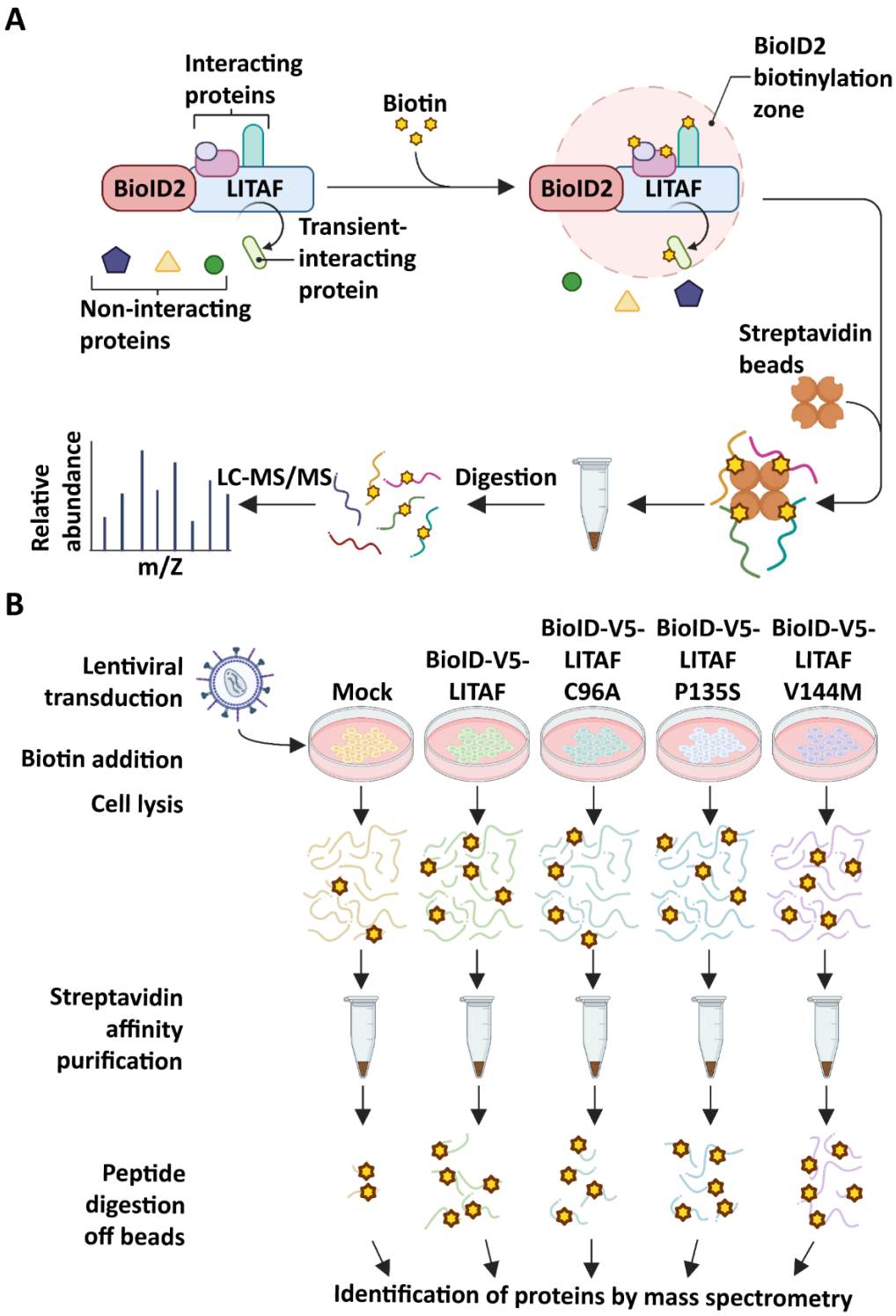

Figure 4.1. BioID method to identify proximal proteins and stable and transient interactors.

A. The Biotin ligase (BirA) is fused to a protein of interest and this construct is expressed in mammalian cells. In the presence of biotin, BirA biotinylates proteins within a 10 nm radius so proximal proteins, but not distal proteins, are biotinylated. Following cell lysis and affinity purification using streptavidin, biotinylated proteins can be identified using mass spectrometry. B. RPE-1 cells transduced with lentivirus containing BioID2-V5-LITAF constructs were plated onto six 15 cm tissue culture plates. 50 µM biotin was added for 18 hours. Cell were lysed under stringent conditions and biotinylated proteins were affinity purified using magnetic streptavidin resin. Identification of enriched proteins was carried out by LC-MS/MS followed by analysis by MaxQuant by the Sanford Burnham proteomics facility and further analysis using Perseus. Figure was made using BioRender.

4.2 Results

4.2.1 Affinity capture of biotinylated proteins from cells expressing BioID2-V5-LITAF

Initially, we wanted to validate lentiviral expression of BioID2-LITAF fusion proteins in RPE-1 cells. Lentivirus generated from just the packaging plasmid and the envelope plasmid, without the lentiviral transfer plasmid, was used as a control condition and is referred to a mock. Additionally, lentivirus containing BioID2-V5-LITAF, BioID2-V5-LITAF C96A, BioID2-V5-LITAF P135S and BioID-V5-LITAF V144M were generated. The C96A mutation disrupts the first CXXC motif in the SLD of LITAF and renders the protein largely cytosolic (Qin et al., 2016). Therefore, this condition was used as a cytosolic control as it is clearly mislocalised. We checked the localisation of these constructs in RPE-1 cells and confirmed that with addition of biotin to the cell media, there was biotinylation of proteins.

The subcellular localisation of BioID-V5-LITAF fusion proteins was assessed using immunofluorescence microscopy by labelling the V5 epitope tag to localise the exogenous protein and using fluorescently-tagged streptavidin to label biotinylated proteins. In the absence of biotin, streptavidin labelled the mitochondria in all conditions (Figure 4.2). This is likely due to the presence of endogenously biotinylated proteins in the mitochondrial matrix, including pyruvate carboxylase, methylcrotonyl-CoA carboxylase subunit α, and propionyl-CoA carboxylase α chain (Hollinshead et al., 1997). In cells transduced with mock lentivirus, V5 labelling showed background staining (Figure 4.2A), whereas expression of BioID-V5-LITAF constructs resulted in increased signal. BioID-V5-LITAF, BioID-V5-LITAF P135S and BioID-V5-LITAF V144M localised to punctate structures, likely endosomes, while BioID-V5-LITAF C96A localised throughout the cytoplasm, as expected (Figure 4.2A). When biotin was added to these cells, streptavidin co-labelled these puncta and also the cytoplasm (Figure 4.2A). Presumably the cytoplasmic staining is due to biotinylation of cytoplasmic proteins.

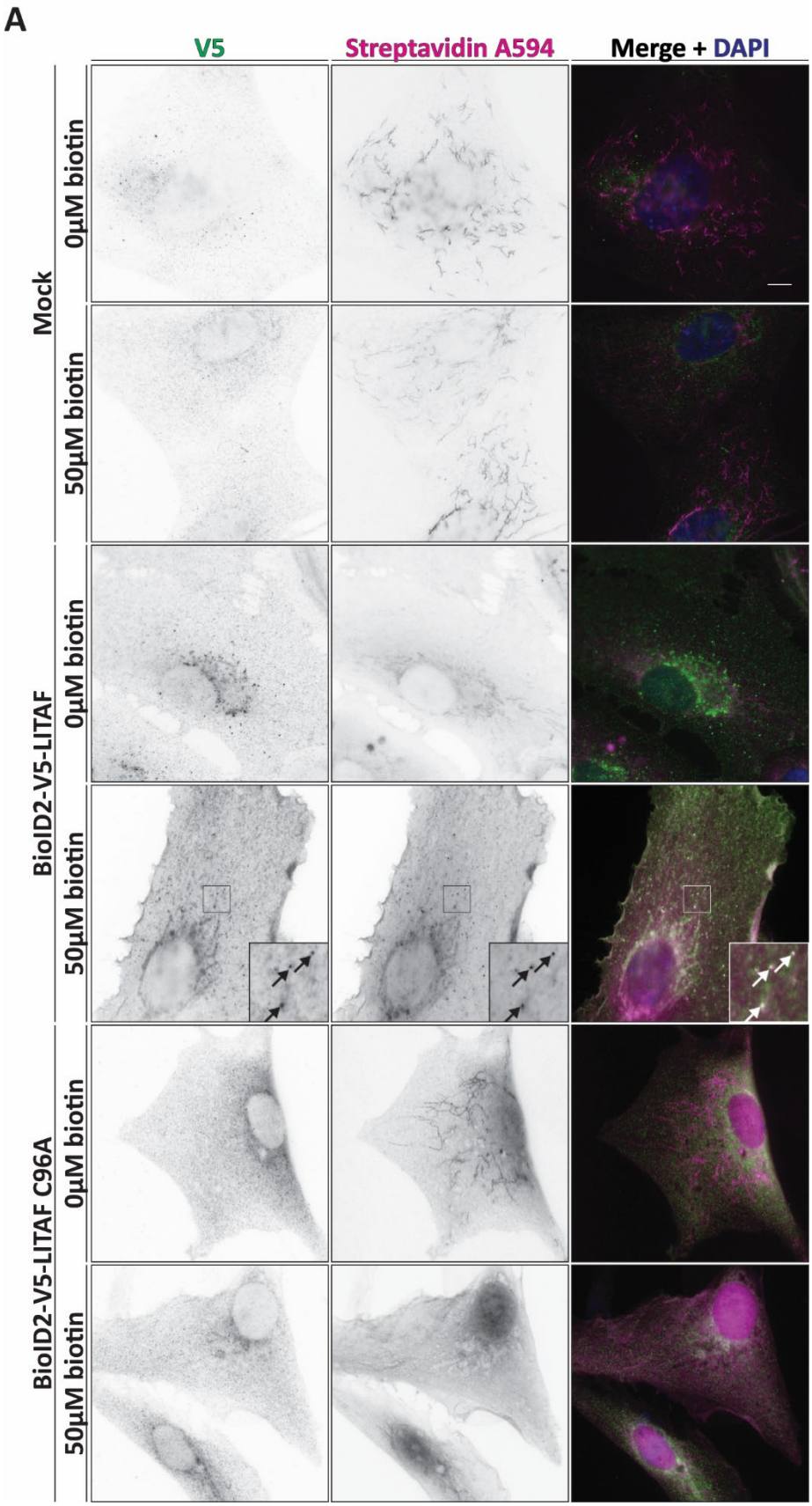
A
V5
Streptavidin A594
Merge + DAPI
Mock
0μM biotin
50μM biotin
BioID2-V5-LITAF
0μM biotin
50μM biotin
BioID2-V5-LITAF C96A
0μM biotin
50μM biotin

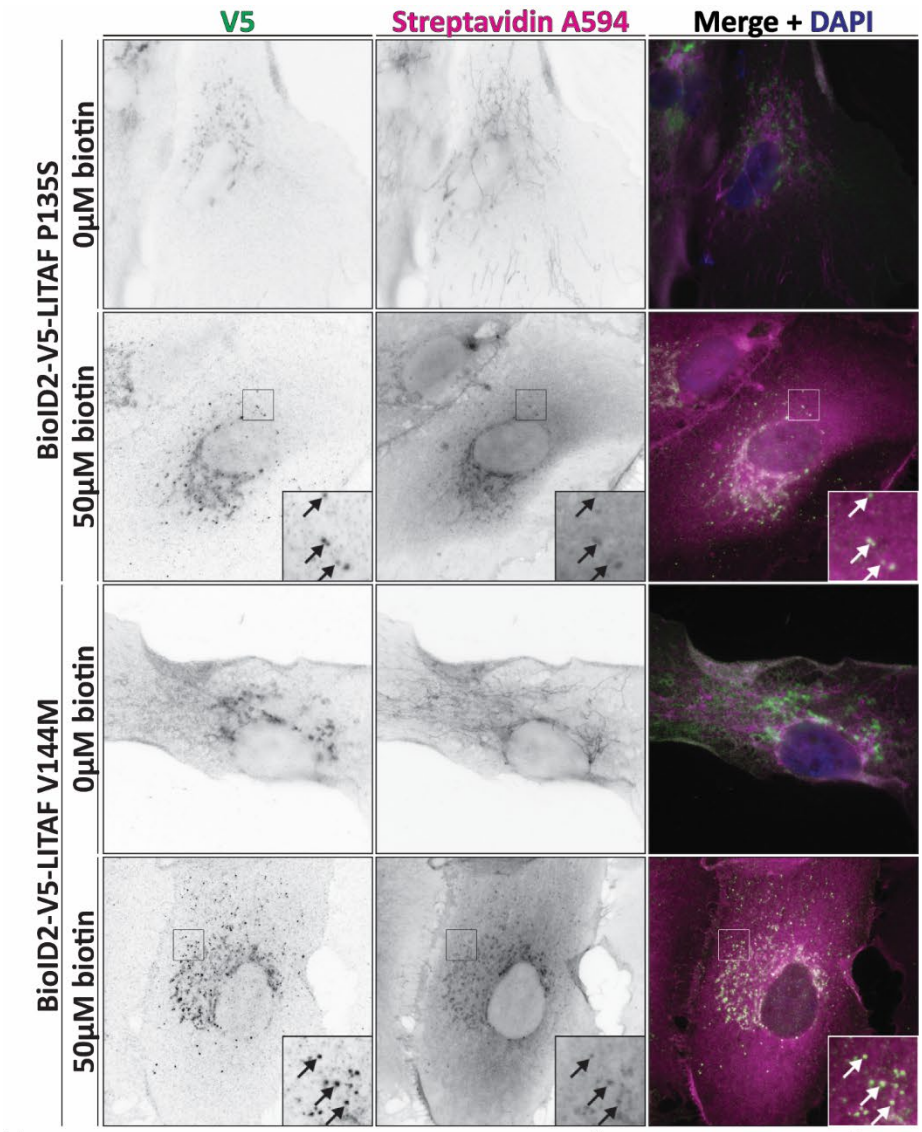
V5
Streptavidin A594
Merge + DAPI
BioID2-V5-LITAF P135S
0μM biotin
50μM biotin
BioID2-V5-LITAF V144M
0μM biotin
50μM biotin

B

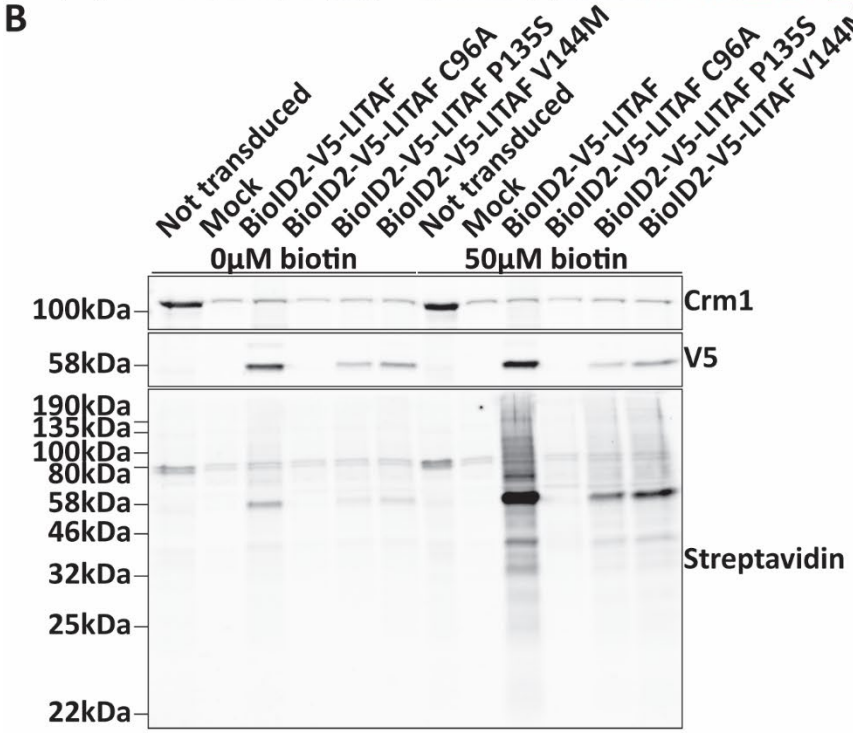
Not transduced
Mock
BioID2-V5-LITAF
BioID2-V5-LITAF C96A
BioID2-V5-LITAF P135S
BioID2-V5-LITAF V144M
Not transduced
Mock
BioID2-V5-LITAF
BioID2-V5-LITAF C96A
BioID2-V5-LITAF P135S
BioID2-V5-LITAF V144M
0μM biotin
50μM biotin
100kDa
58kDa
190kDa
135kDa
100kDa
80kDa
58kDa
46kDa
32kDa
25kDa
22kDa
Crm1
V5
Streptavidin

Figure 4.2. Localisation and expression of lentiviral BioID2 tagged LITAF constructs. RPE-1 cells were left untransduced or were transduced with mock lentivirus or lentivirus containing BioID2-V5-tagged LITAF, LITAF C96A, LITAF P135S and LITAF V144M at a dilution of 1 in 10 for 48 hours and incubated with vehicle or 50 µM biotin overnight. A. Cells on coverslips were fixed and stained with V5 antibody and streptavidin conjugated to A594, and analysed by widefield microscopy. Insets magnified 3x. Scale bar represents 10 µm. B. Cells were lysed and samples were analysed by SDS PAGE and Western blotting analysis. Crm1 antibody was used as a loading control (upper panel). BioID2-V5-tagged proteins were detected with V5 antibody (middle panel) and biotinylated proteins were detected by streptavidin conjugated to IRDye 800CW (lower panel).

Expression of fusion proteins and biotinylation of proteins was also examined by Western blotting analysis (Figure 4.2B). Bands of the appropriate molecular weight were detected by V5 antibody for BioID2-V5-LITAF and the construct containing the CMT1c mutations, P135S and V144M. However, expression of constructs containing CMT1c mutations was reduced compared to the wild type (Figure 4.2B middle panel). Furthermore, expression of BioID2-V5-LITAF C96A was much reduced, although a band could be observed when the intensity was increased. These levels of expression were reflected in the streptavidin labelling of biotinylated proteins in these conditions (Figure 4.2B, lower panel). Few proteins were identified in cells in the absence of supplemental biotin, although there were two bands around 80kDa consistently observed which may again be attributed to endogenously biotinylated enzymes (Figure 4.2B, lower panel).

Together, these results indicate that the BioID2 fusion proteins localise as expected and that with the addition of biotin, there is biotinylation of endogenous proteins. We next tested affinity purification conditions using different streptavidin beads and optimised transduction of the different BioID2-V5-LITAF constructs, which are expressed at variable levels (Figure 4.2B).

Different amounts of magnetic streptavidin-Dynabeads and streptavidin-Sepharose beads were used to affinity-purify biotinylated proteins from cells transduced with mock lentivirus or cells transduced with BioID2-V5-LITAF lentivirus (Figure 4.3A). In the mock condition, there are two bands around 80 kDa that are likely to be endogenously biotinylated proteins, as well as several faint bands in all the samples. With increasing amounts of streptavidin beads, the amount of proteins isolated seems

to slightly increase, but there is not much difference between the magnetic Dynabeads and Sepharose. In contrast, there are many biotinylated proteins affinity-purified by streptavidin beads from cells transduced with BioID2-V5-LITAF and incubated with biotin. The amount of biotinylated proteins pulled down increases with the amount of beads used, and Dynabeads appear to pull-down more proteins than streptavidin Sepharose (Figure 4.3A).

Different dilutions of crude lentivirus preparation were next tested in an attempt to make the expression levels of the BioID2 fusion proteins more equal. At higher dilutions such as 1 in 20, some cells did not express the fusion proteins at levels detectable by immunofluorescence microscopy (data not shown). Therefore, in this titration experiment we used dilutions of 1 in 2, 1 in 5 and 1 in 10 of lentivirus in cell media and examined expression levels by Western blot analysis. Expression levels of cells transduced with GFP and BioID2-V5-LITAF were not affected by the amount of lentivirus used to transduce the cells (Figure 4.3B). Cells transduced with BioID2-V5-LITAF C96A, P135S and V144M expressed most exogenous protein when transduced with lentivirus at a dilution of 1 in 5, but still did not reach the same expression level as BioID2-V5-LITAF (Figure 4.3B).

Therefore, for the large scale BioID mass spectrometry experiment, we scaled up from the test conditions, and used streptavidin-Dynabeads to isolate biotinylated proteins, and a dilution of 1 in 10 of lentivirus to transduce cells with BioID2-V5-LITAF or a dilution of 1 in 5 for BioID2-V5-LITAF C96A, P135S and V144M.

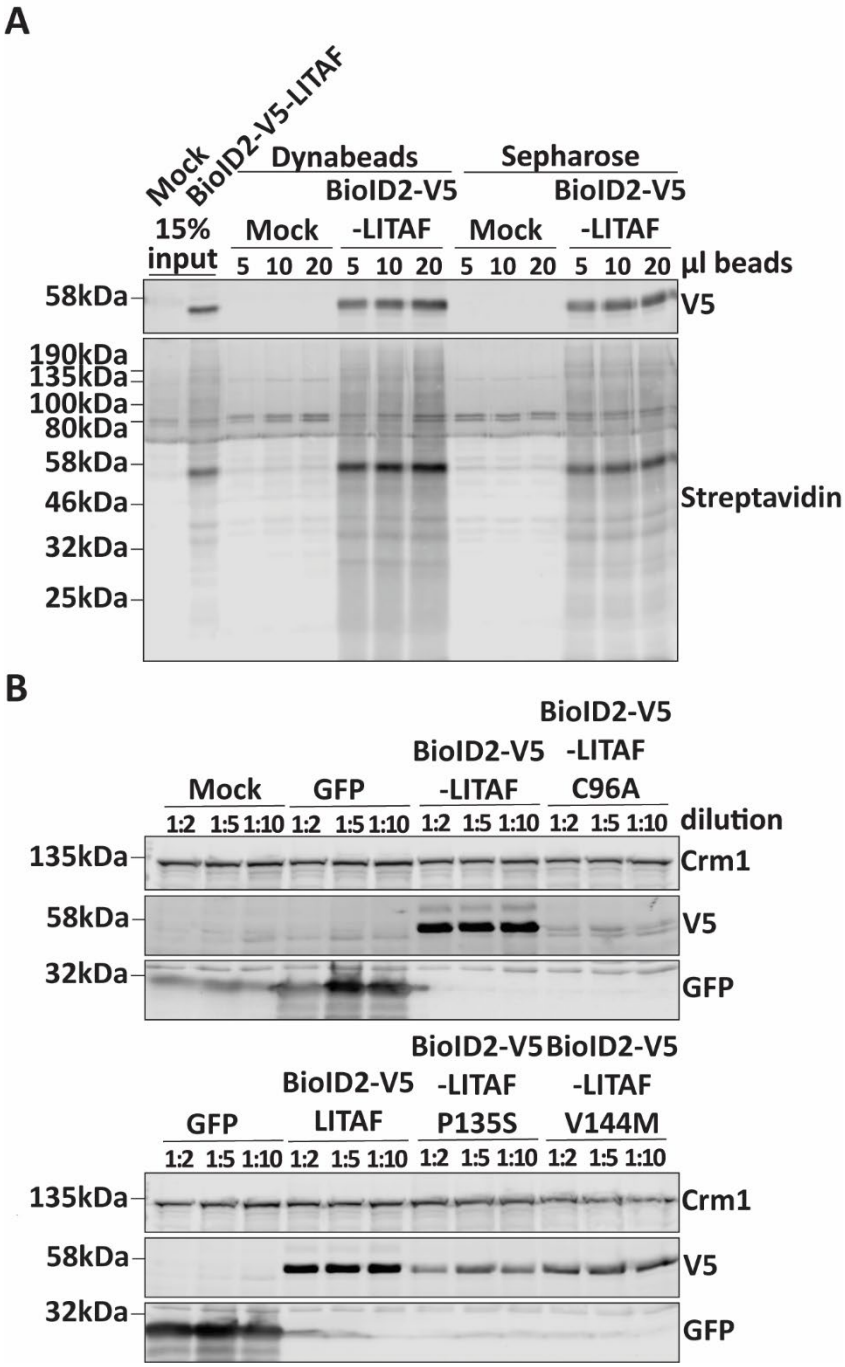

Figure 4.3. Optimisation of streptavidin pulldown of biotinylated proteins and lentiviral expression of BioID2-V5-LITAF constructs.

A. RPE-1 cells were transduced with mock lentivirus or lentivirus containing BioID2-V5-LITAF at a dilution of 1 in 10 for 48 hours and incubated with 50 µM biotin overnight. Biotinylated proteins were affinity purified using increasing amounts (5-20 µl) of Dynabeads MyOne Streptavidin C1 or streptavidin sepharose and eluted after incubation with 2x sample buffer at 95°C for 10 minutes. Samples were analysed by SDS PAGE and Western blotting analysis. BioID2-V5-LITAF was detected with V5 antibody (upper panel) and biotinylated proteins were detected by streptavidin (lower panel). B. RPE-1 cells were transduced with mock lentivirus or with lentivirus containing GFP or BioID2-V5-LITAF WT or containing mutations as indicated, at increasing dilutions. After 72 hours, cell lysates were harvested and analysed by SDS PAGE and Western blotting analysis. Crm1 was detected with Crm1 antibody as a loading control (upper panel), BioID2-V5-LITAF was detected with V5 antibody (middle panel) and GFP was detected with GFP antibody (lower panel).

4.2.2 Analysis of the mass spectrometry dataset

Mass spectrometry was performed on two or three independent repeats of affinity-purified biotinylated proteins isolated from cells transduced with mock lentivirus or lentivirus containing BioID2-V5-LITAF, BioID2-V5-LITAF C96A, BioID2-V5-LITAF P135S or BioID2-V5-LITAF V144M (Figure 4.4A). Western blotting analysis of the streptavidin pull down likely underrepresents the amount of affinity purified biotinylated proteins as the samples were incubated in sample buffer without biotin, which can be added to compete off the biotinylated proteins from the streptavidin beads to increase the yield of biotinylated proteins eluted. The cells transduced with BioID2-V5-LITAF C96A did not grow well in the first repeat so this sample was not included. The first repeat was analysed by mass spectrometry initially while the second and third repeats were analysed by mass spectrometry back-to-back.

Proteins identified by less than 3 spectra were excluded from the analysis. This is an arbitrary threshold used by others in the field to exclude proteins identified at a very low abundance. More than 200 proteins were identified using the 'control' baits (i.e. Mock and LITAF C96A) and more than 500 proteins were identified in the 'experimental' baits (i.e. LITAF WT, LITAF P135S and LITAF V144M) (Figure 4.4B). However, the number of proteins identified in every replicate of a bait experiment was less, between 70-500, indicating that there was some variation between replicates (Figure 4.4C). Spectral intensities were normalised by MaxQuant analysis software using the MaxLFQ algorithm to generate label-free quantification (LFQ) intensities for each protein (Cox et al., 2014). LFQ values are based on the raw intensities but are normalised so that LFQ values represent the relative amounts of proteins between samples. LFQ values were used for further analysis in Perseus (Tyanova et al., 2016).

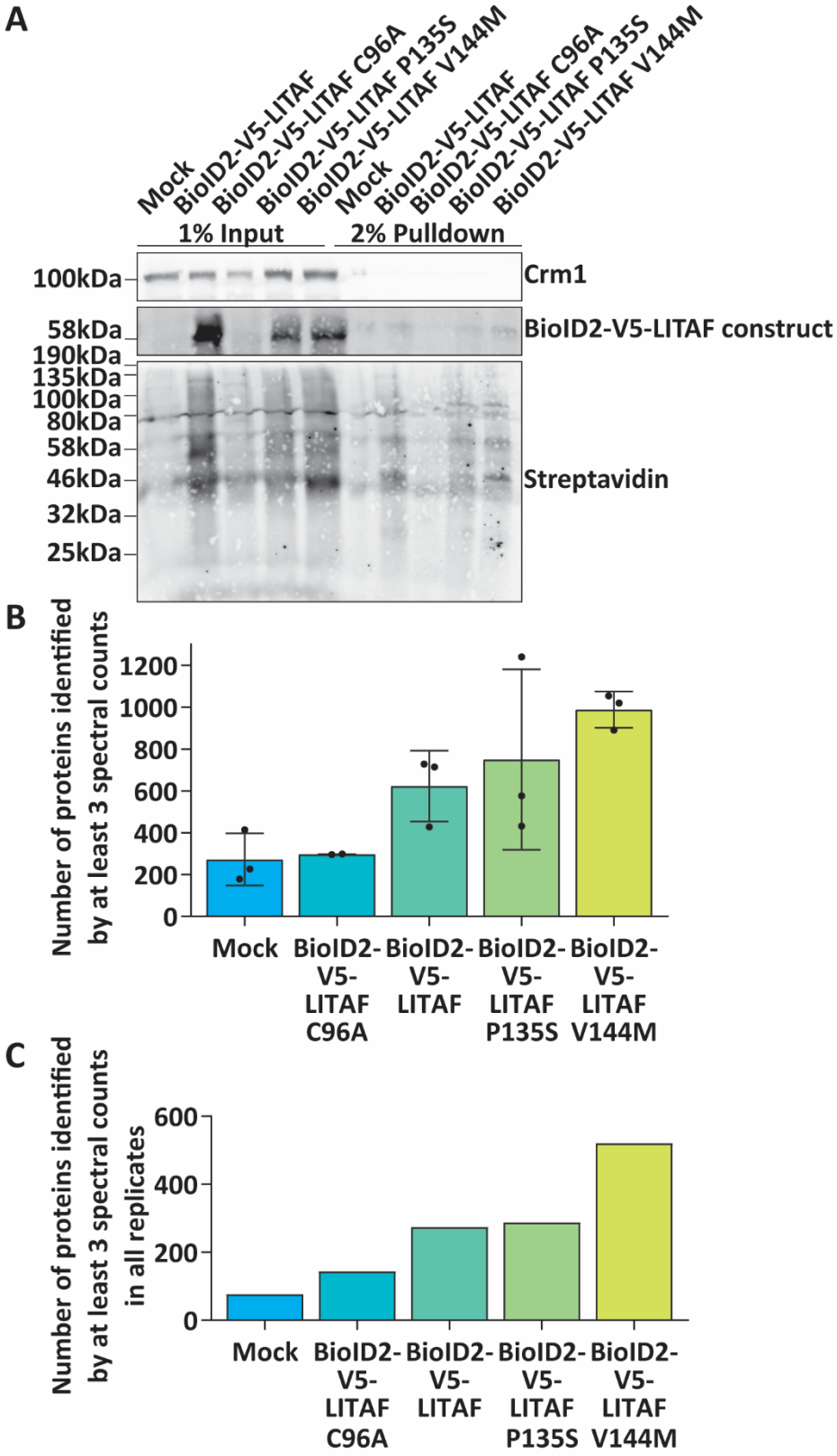

Figure 4.4. BioID2 experiment.

RPE-1 cells were plated onto 6 15cm plates and transduced with lentivirus for 48 hours. 50 µM biotin was added overnight before cells were lysed and biotinylated proteins were affinity purified using streptavidin dynabeads. A. 1% of the input samples and 2% of the pulldown samples were analysed by SDS PAGE and Western blotting. Crm1 was used as a loading control (upper panel). BioID2-V5-LITAF fusion proteins were detected using V5 antibody (middle panel). Biotinylated proteins were detected using streptavidin (lower panel). B. The number of proteins identified by 3 or more peptides in each repeat. C. The number of proteins identified by 3 or more peptides in all repeats of a condition.

Principle component analysis (PCA) of the mass spectrometry data was performed for each sample (Figure 4.5A). The data for the control baits (Mock and C96A) were separated from the experimental baits (LITAF or LITAF containing patient mutations), by principle component 1 (PC1) which represents 41% of the variation in the data (Figure 4.5A). The 'experimental' baits do not separate from each other, indicating that there is no systematic difference in the way each of these LITAF constructs behave. Clearly there are some differences as twice as many proteins were consistently identified in the LITAF V144M condition compared to the other 'experimental' baits (Figure 4.4C). The second variance in the data (PC2) represents the second largest variation of between the data and separates the data obtained from the third repeat from that obtained from the first and second repeats, for each condition (Figure 4.5A). This apparent shift in behaviour is most likely due to technical differences as replicates were prepared on separate occasions. Therefore, principle component analysis indicates that the majority of the variance in the data is due to whether the bait was a control or an experimental sample and there is some variance in the data according to the replicate.

Pairwise comparison analysis was also carried out to compare each sample with every other sample. LFQ intensities for each protein identified in a sample were compared to the LFQ intensities in another sample and a Pearson correlation coefficient was calculated based on this (Figure 4.5B). The Pearson correlation values between replicates for each bait were not especially high. Mass spectrometry experiments where biological replicate samples were prepared in parallel or on the same day might be expected to have Pearson correlation values of 0.9. However, this analysis shows that there is greater correlation between the 'experimental' replicates, (at best from 0.7-0.9) than between experimental baits and control baits (Figure 4.5B). Repeats for each condition should cluster together in PCA analysis and have high Pearson correlation values if the data are reproducible. These analyses show that while the control vs experimental samples are separated, the reproducibility of these experiments is not high. While these results might hinder the evaluation of differences between LITAF WT and CMT1c LITAF, it is still likely to be useful as differences in enrichment in high confidence proteins between conditions may be informative. Additionally, this BioID experiment is useful to explore potential protein interactions of LITAF which can later be examined with LITAF containing CMT1c patient mutations.

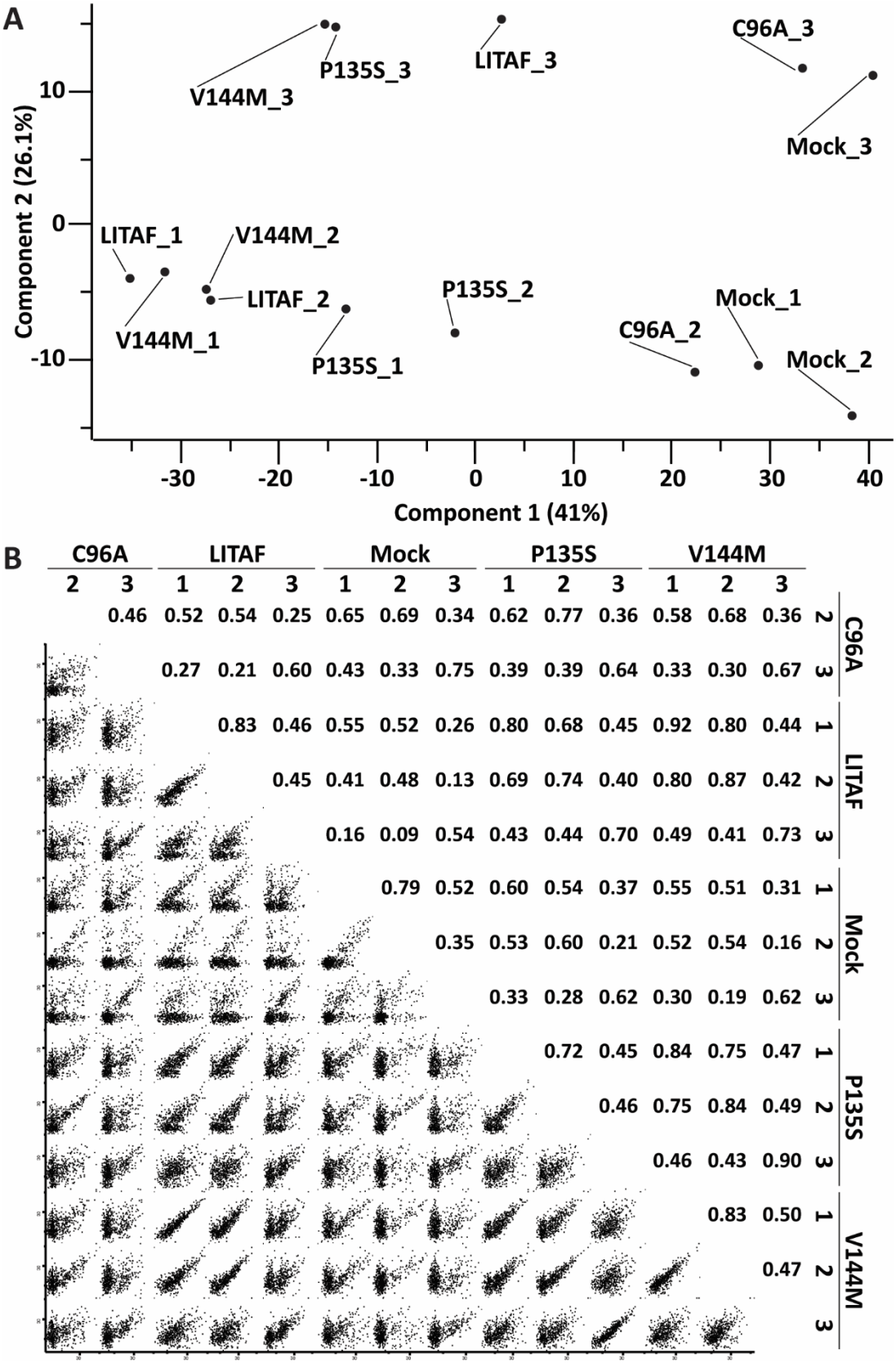

Figure 4.5. Comparison of mass spectrometry data between samples.
A. Principle component analysis was carried out on the LFQ values generated by MaxQuant for the samples analysed by mass spectrometry. Principle component 1 and principle component 2 were plotted against each other for each sample. B. Pairwise comparison of the LFQ values of the proteins identified in each of the samples. Pearson correlation values are displayed.

These data indicate that there is a lot of variation in the proteins detected between replicates and that there is no systematic difference in the proteins identified using WT LITAF as a bait vs LITAF P135S and LITAF V144M. Therefore, criteria used to identify proteins associated with the protein of interest bait were: detection of more than 3 spectral counts in all three (or two for LITAF C96A) biological replicates, significant enrichment compared to mock control sample and presence in less than 40% of the experiments in the contaminant repository for affinity purification (CRAP)ome database (Mellacheruvu et al., 2013).

Using Perseus, missing values were imputed around the detected limits in order to provide a value for proteins without an LFQ intensity so that fold changes could be calculated (Tyanova et al., 2016). LFQ intensities in the replicates of each experimental bait were compared to the intensities obtained in the mock condition, which results in calculation of a fold difference and a statistical value for the confidence of the degree of enrichment. The $\log_2$ fold change can be plotted against the confidence value to produce a volcano plot. Firstly, proteins enriched in the WT LITAF sample compared to proteins identified in the mock condition were investigated (Figure 4.6). 110 proteins were identified as LITAF proximal proteins here using a p-value < 0.05. Three of these proteins were previously known LITAF interactors, NEDD4L, EHD1 and STAM. Surprisingly, some proteins which are known to interact with LITAF including HRS, STAM2 and TSG101 were not identified as significantly enriched (Figure 4.6A).

The significantly enriched proteins were clustered manually according to their known function. Many significantly enriched proteins had roles in endocytosis, including ubiquitin-mediated endocytic trafficking (Figure 4.6B green points) and endocytic recycling (Figure 4.6B orange points), which is as expected given the localisation of LITAF to early, late and recycling endosomes. Additionally, there were several proteins identified which are present at the plasma membrane and are known endocytic cargo (Figure 4.6C). In this subset of proteins there are some whose trafficking has previously been associated with LITAF including EGFR, TFRC (TfR), integrin β1, HLA-A (MHC class 1) as well as solute carrier (SLC) 7A5 and SLC3A2 that together form CD98 (Figure 4.6C, purple points). Interestingly, a large proportion of the proteins identified have roles in cell adhesion (Figure 4.6D).

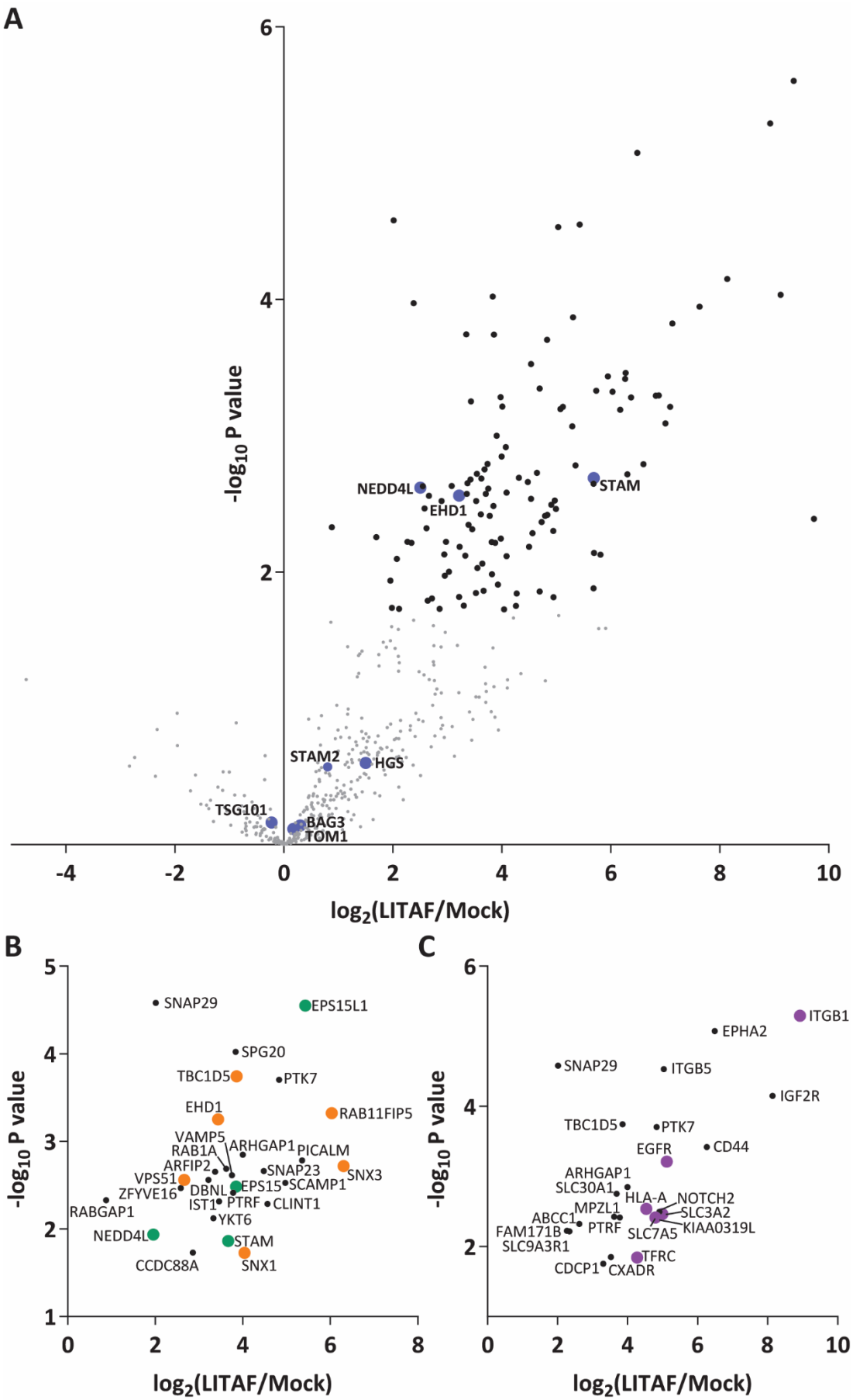
A
-log10 P value
log2(LITAF/Mock)
NEDD4L
EHD1
STAM
STAM2
HGS
TSG101
BAG3
TOM1
B
-log10 P value
log2(LITAF/Mock)
SNAP29
EPS15L1
SPG20
TBC1D5
PTK7
EHD1
RAB11FIP5
VAMP5
RAB1A
ARHGAP1
PICALM
ARFIP2
SNAP23
SNX3
VPS51
EPS15
SCAMP1
ZFYVE16
DBNL
IST1
PTRF
CLINT1
RABGAP1
YKT6
NEDD4L
STAM
CCDC88A
SNX1
C
-log10 P value
log2(LITAF/Mock)
ITGB1
EPHA2
SNAP29
ITGB5
IGF2R
TBC1D5
PTK7
EGFR
CD44
ARHGAP1
SLC30A1
HLA-A
NOTCH2
MPZL1
SLC3A2
ABCC1
PTRF
KIAA0319L
FAM171B
SLC7A5
SLC9A3R1
TFRC
CDCP1
CXADR

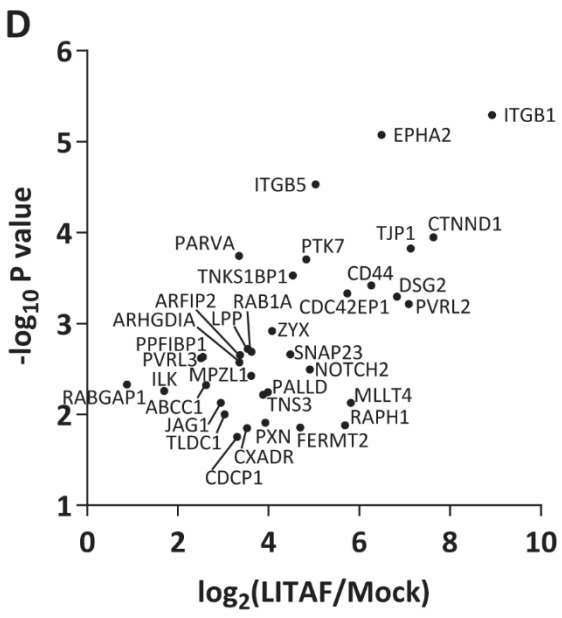

Figure 4.6. Volcano plots showing significantly enriched proteins with LITAF bait compared to the mock control.

Volcano plots comparing the spectral intensities from BioID-LITAF to the mock condition. A. All the spectral intensities are plotted. Significantly enriched proteins are black data points while non-significant proteins are in grey. Known interactors are labelled and shown in blue. B. Significantly enriched proteins with roles in endocytosis are shown. Orange data points indicate proteins involved in recycling while green data points indicate proteins involved in ubiquitin-mediated endocytic trafficking. C. Significantly enriched proteins present on the plasma membrane are shown. Purple data points indicate proteins which have been associated with LITAF. D. Significantly enriched proteins with roles in adhesion are shown.

We also performed t-tests in Perseus to identify significantly enriched or depleted proteins over mock in samples using LITAF P135S and LITAF V144M as baits (Figure 4.7). 78 proteins were identified as LITAF P135S proximal proteins and 210 proteins were identified as LITAF V144M proximal proteins. Similar to the identified LITAF WT proximal proteins, many of these have roles in endocytosis. The most significant hits for LITAF P135S were IGFR2 (CI-MPR) and TPD52L2 (TPD54). The most significant hits for LITAF V144M were ITGB1 (integrin β1), AHNAK2, SQSTM1 and also TPD54. AHNAK2 and AHNAK are commonly identified proteins from biotinylation AP-MS experiments but were not present in more than 40% of control BioID experiments in the CRAPome depository. They were identified in all the experimental conditions as well as LITAF C96A, and so were not followed up for further analysis.

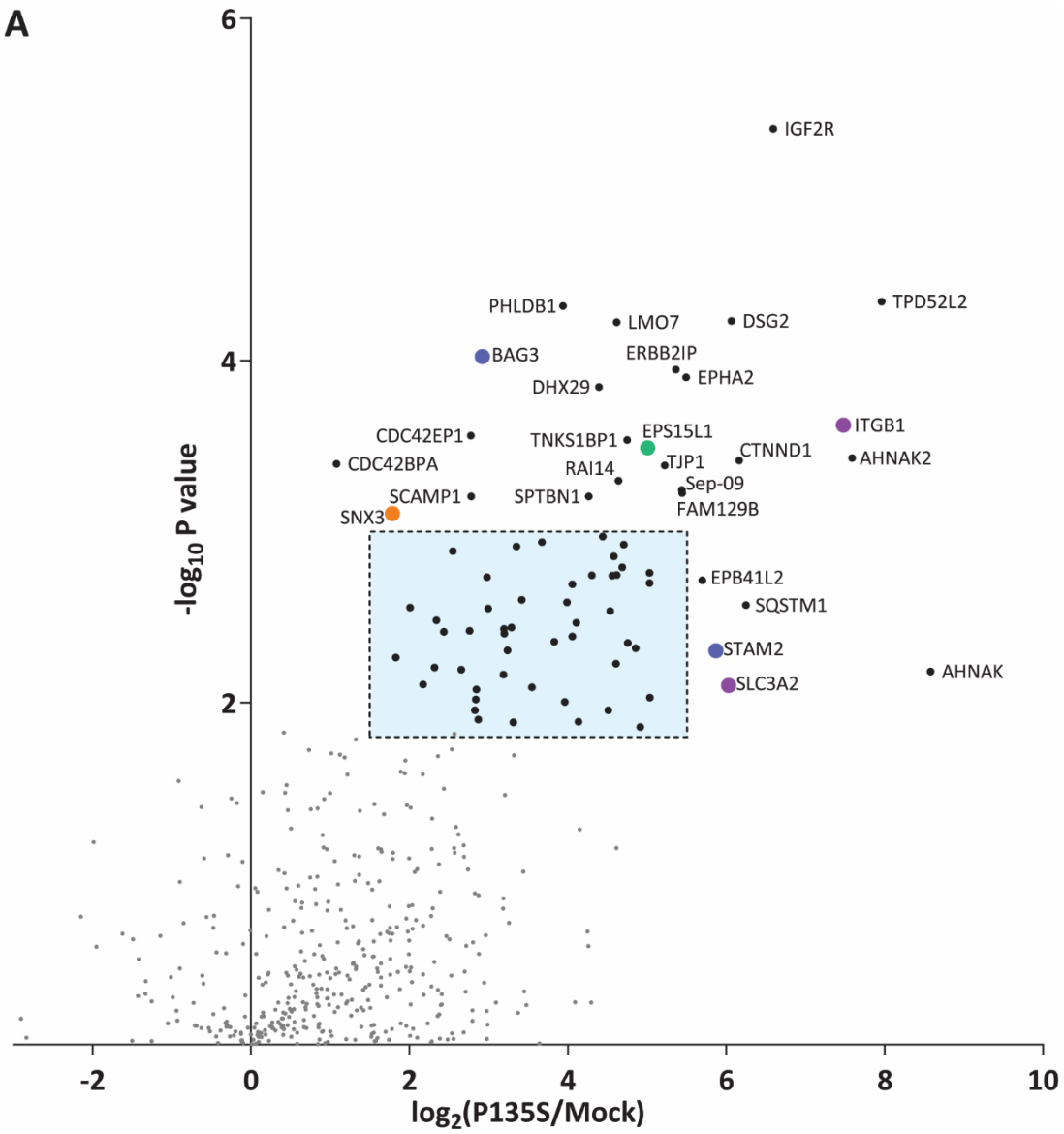
A
6
4
2
-log10 P value
IGF2R
PHLDB1
LMO7
DSG2
TPD52L2
BAG3
ERBB2IP
EPHA2
DHX29
CDC42EP1
TNKS1BP1
EPS15L1
ITGB1
CDC42BPA
RAI14
TJP1
CTNND1
AHNAK2
Sep-09
SCAMP1
SPTBN1
FAM129B
SNX3
EPB41L2
SQSTM1
STAM2
AHNAK
SLC3A2
-2
0
2
4
6
8
10
log2(P135S/Mock)
B
3.0
2.5
2.0
-log10 P value
ZYX
EPB41L3
VPS51
LASP1
SLC7A5
PICALM
ZC3HAV1
NUFIP2
DAB2
STAM
UBAP2
ESYT1
STX7
PVRL2
NOTCH2
TJP2
NSFL1C
RAB11FIP5
EPS15
PRKAR2A
SNX1
ITGB5
ECE1
PDLIM5
CCDC50
SUGT1
GOPC
TNS3
PALLD
ZNF185
RAPH1
TBC1D5
CD44
RBMS2
FERMT2
ADD3
PDLIM1
MLLT4
SNAP23
TLN1
PTPRJ
LIMCH1
LRBA
PAK2
KIAA0319L
BICD2
IST1
CALD1
2
3
4
5
log2(P135S/Mock)

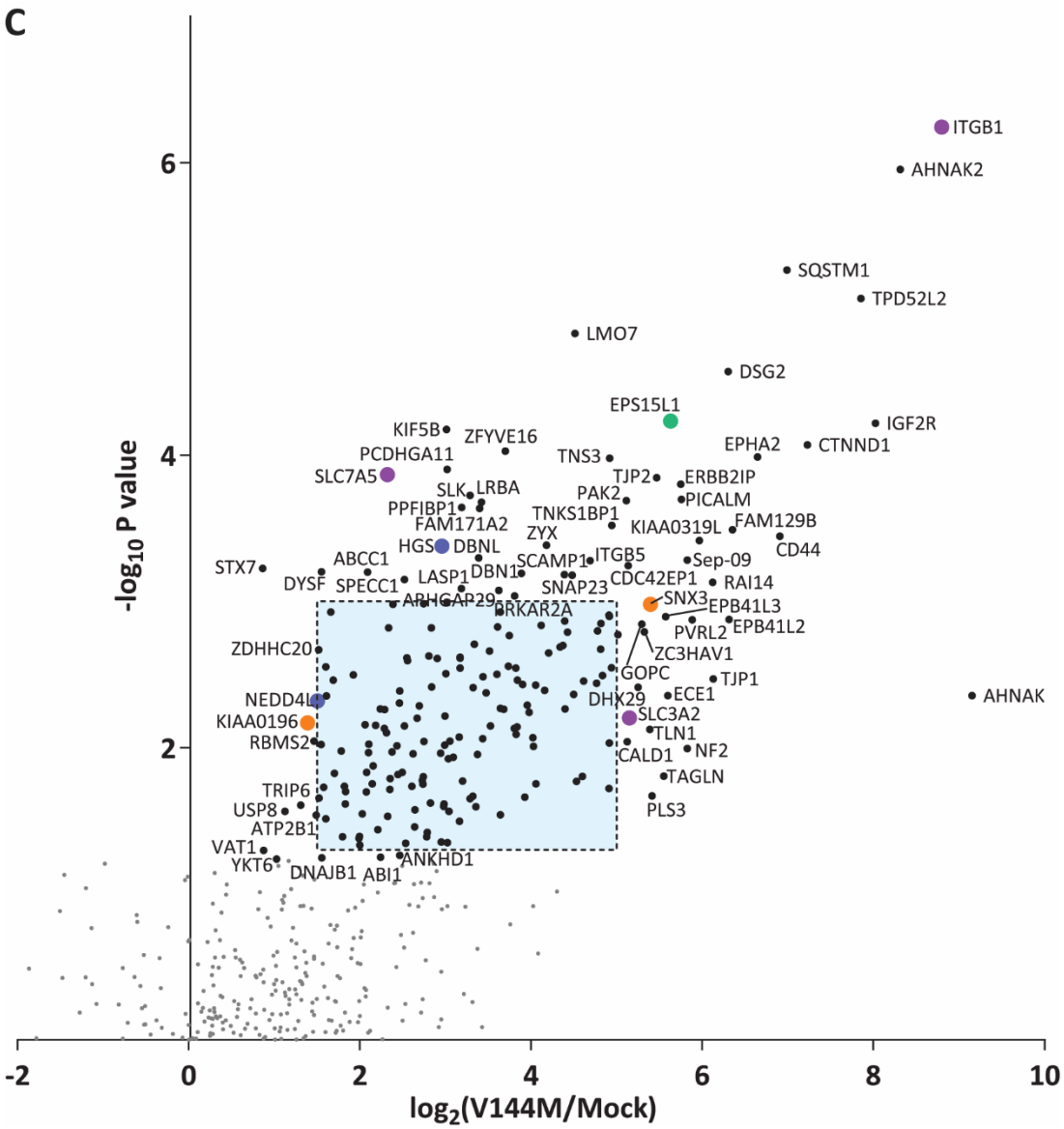
C
ITGB1
AHNAK2
SQSTM1
TPD52L2
LMO7
DSG2
EPS15L1
IGF2R
KIF5B
ZFYVE16
EPHA2
CTNND1
PCDHGA11
TNS3
SLC7A5
TJP2
ERBB2IP
SLK
LRBA
PAK2
PICALM
PPFIBP1
TNKS1BP1
FAM171A2
ZYX
KIAA0319L
FAM129B
HGS
DBNL
CD44
STX7
ABCC1
SCAMP1
ITGB5
Sep-09
DYSF
SPECC1
LASP1
DBN1
CDC42EP1
RAI14
SNAP23
ARHGAP29
SNX3
EPB41L3
PRKAR2A
PVRL2
EPB41L2
ZDHHC20
ZC3HAV1
GOPC
TJP1
AHNAK
NEDD4L
DHX29
ECE1
KIAA0196
SLC3A2
RBMS2
TLN1
CALD1
NF2
TAGLN
TRIP6
PLS3
USP8
ATP2B1
VAT1
YKT6
DNAJB1
ABI1
ANKHD1
-log10 P value
log2(V144M/Mock)
D
PLIN3
Sep-07
AP3B1
TBC1D5
RABGAP1
EPS15
BICD2
AKAP12
AGFG1
EGFR
SUGT1
BAG3
ATP2B4
VAMP3
APBB1
PDLIM1
DCBLD2
SLC30A1
GJA1
NOTCH2
CPD
MPZL1
CCDC50
SHB
ESYT1
FAM171B
STAM2
HLA-A
SH3D19
RFTN1
TLDC1
IST1
SPTBN1
EHD1
COPB1
SPG20
DAB2
PALLD
TXNL1
CAST
EPB41L1
ADD3
FERMT2
GIT1
NUMB
PTK7
RAB11FIP5
YES1
CHMP4B
ARHGAP1
STAM
CCDC88A
CLINT1
VPS51
TFRC
CD2AP
SNAP29
ZNF185
TMEM2
ADD1
SNX1
NSFL1C
ROR1
SLC4A7
DIP2B
SYNJ2
PVRL3
MYO18A
PXN
GNAI2
PSMD4
PRRC2C
RBMS1
RAB23
RASAL2
STAT1
ARFIP2
FAM171A1
FLOT1
ERBB2
SCRIB
FHL2
WDR20
MAP2
PHLDB1
PSMD1
LRRC59
MAP7D3
CSRP1
EIF4G3
CDC42EP3
LNPEP
PDLIM4
CTNNA1
RAPH1
LIMCH1
LIMA1
MAP4K4
UACA
CSDE1
GOLGA4
PARD3B
KLC1
ILK
TRIM25
LPP
FAM21A
MACF1
PTPRJ
MLLT4
SLC9A3R1
HN1L
TGFB1I1
ABCE1
RGS12
TSG101
PDLIM5
SH3GL1
ZDHHC5
PEAK1
NUFIP2
UBAP2
G6PD
PUM1
TNS1
TES
TMEM237
DARS
SNX9
STX5
ARFGAP3
SH3BP4
PLEKHN1
BSG
ROBO1
PDXDC1
MYLK
STAU2
HDLBP
-log10 P value
log2(V144M/Mock)

Figure 4.7. Volcano plots showing significantly enriched proteins using CMT1c baits compared to the mock control.

A. Volcano plots comparing the spectral intensities from BioID-LITAF P135S to the mock condition. All the spectral intensities are plotted. Significantly enriched proteins are labelled with their gene name and are black data points while non-significant proteins are in grey. B. Magnification of the inset shaded in blue in A. C. Volcano plots comparing the spectral intensities from BioID-LITAF V144M to the mock condition. All the spectral intensities are plotted. Significantly enriched proteins are labelled with their gene name and are black data points while non-significant proteins are in grey. D. Magnification of the inset shaded in blue in C. Green indicates proteins involved in ubiquitin mediated endocytosis, orange indicates proteins involved in endocytic recycling, blue indicates known protein interaction with LITAF, purple indicates endocytic cargo.

We performed gene ontology (GO) and Kyoto Encyclopedia of Gene and Genomes (KEGG) pathways analysis and protein interaction network analysis on the 57 significantly enriched proteins over mock which were identified in the LITAF, LITAF P135S and LITAF V144M bait conditions. We observed a strong enrichment for components of cell-cell junctions and proteins involved in cell adhesion (Figure 4.8A). Additionally, the two KEGG pathways which were enriched were endocytosis and adherens junctions (Figure 4.8A). Furthermore, the network of proteins enriched in LITAF WT, LITAF P135S and LITAF V144M shows a cluster of interactions between proteins with roles ubiquitin-mediated endocytic trafficking (shown green) and proteins involved in endocytic recycling (shown in orange) (Figure 4.8B). There was also a cluster of proteins involved in adhesion (shown in pink) and endocytic cargo proteins (shown in purple) (Figure 4.8B). These analyses also showed enrichment of proteins involved in lamellipodia and the actin cytoskeleton (shown in yellow) (Figure 4.8). While LITAF has been associated with endocytosis before, these analyses indicate an association with adherens junctions and cell adhesion as well as the actin cytoskeleton which has not been appreciated previously.

Next, we wanted to compare the abundance of proteins enriched by the different baits, in order to assess whether there are differences in the proteins proximal to WT LITAF and LITAF containing CMT1c mutations. Dot plots were used to compare the relative enrichment of all proteins that were significantly enriched in at least one of the conditions (Figure 4.9). The colour and size of the circle represent the abundance of the protein in the sample, and the outside colour indicates the significance of the enrichment over mock in that sample. The larger and darker the circle, the greater the enrichment and significance of that proximal protein (Figure 4.9E).

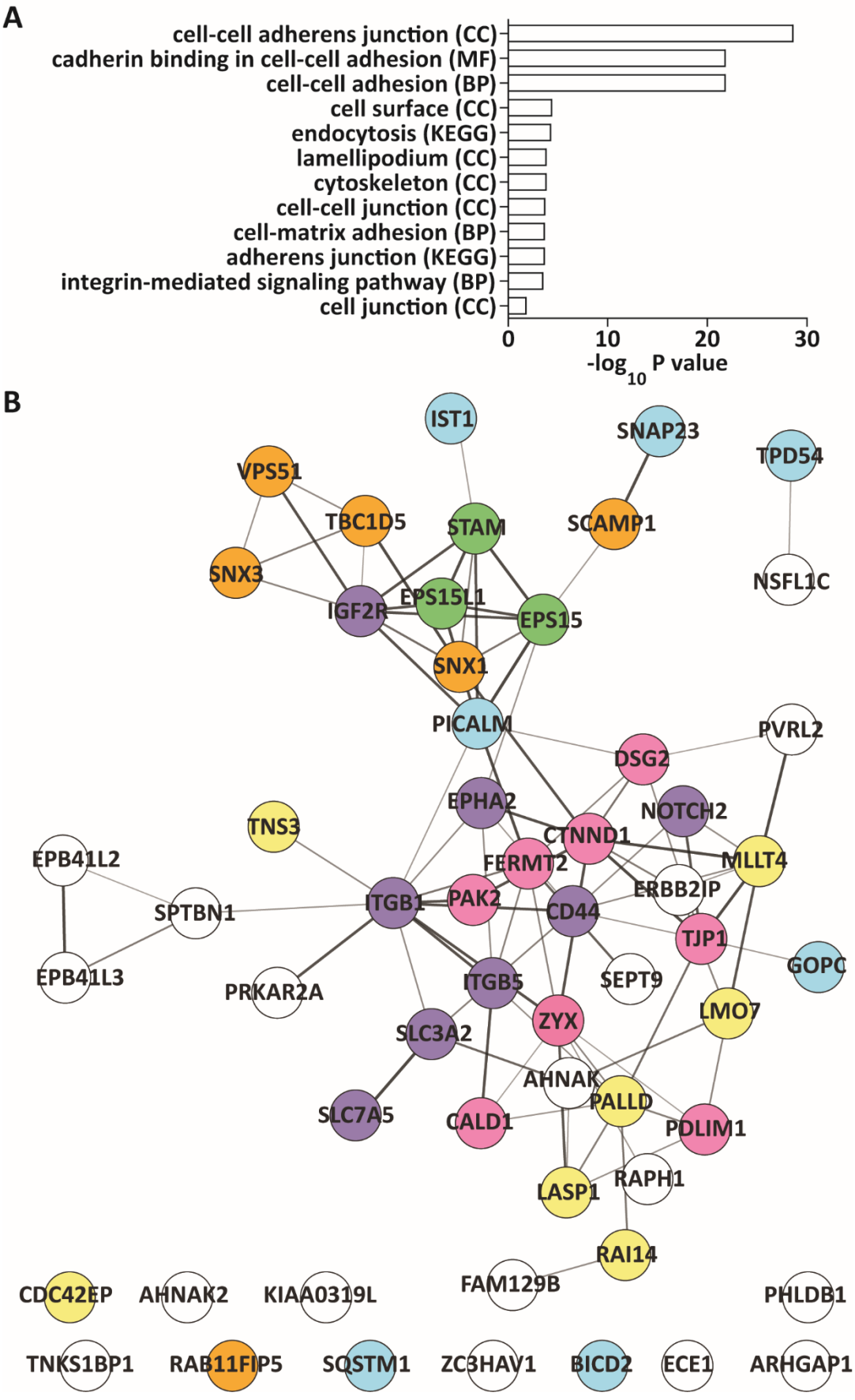
A
cell-cell adherens junction (CC)
cadherin binding in cell-cell adhesion (MF)
cell-cell adhesion (BP)
cell surface (CC)
endocytosis (KEGG)
lamellipodium (CC)
cytoskeleton (CC)
cell-cell junction (CC)
cell-matrix adhesion (BP)
adherens junction (KEGG)
integrin-mediated signaling pathway (BP)
cell junction (CC)
0
10
20
30
-log10 P value
B
IST1
SNAP23
TPD54
VPS51
TBC1D5
STAM
SCAMP1
SNX3
NSFL1C
EPS15L1
IGF2R
EPS15
SNX1
PICALM
PVRL2
DSG2
EPHA2
NOTCH2
TNS3
CTNND1
EPB41L2
FERMT2
MLLT4
ERBB2IP
SPTBN1
ITGB1
PAK2
CD44
TJP1
GOPC
EPB41L3
PRKAR2A
ITGB5
SEPT9
LMO7
ZYX
SLC3A2
AHNAK
PALLD
SLC7A5
CALD1
PDLIM1
RAPH1
LASP1
RAI14
CDC42EP
AHNAK2
KIAA0319L
FAM129B
PHLDB1
TNKS1BP1
RAB11FIP5
SQSTM1
ZC3HAV1
BICD2
ECE1
ARHGAP1

Figure 4.8. Significantly enriched proteins in all experimental conditions.
A. GO terms and KEGG pathway analysis of the 57 proteins enriched in WT LITAF, LITAF P135S and LITAF V144M samples using DAVID (Huang et al., 2009). Significantly over-represented terms are shown. Cellular compartment (CC), molecular function (MF), biological process (BP). B. Network of the enriched proteins in WT LITAF, LITAF P135S and LITAF V144M samples, based on STRING (Szklarczyk et al., 2019) and visualised in Cytoscape (Shannon et al., 2003, Doncheva et al., 2019). Higher confidence interactions are represented by a thicker connecting line. Green indicates proteins involved in ubiquitin mediated endocytosis, orange indicates proteins involved in endocytic recycling, blue indicates other proteins involved in membrane trafficking, purple indicates endocytic cargo, pink indicates proteins involved in adhesion, yellow indicates proteins involved in the actin cytoskeleton.

There are 57 proximal proteins which are significantly enriched by all the experimental baits, and the dot plot shows many of these proteins, which are represented by a circle with a thickened black or dark blue outline (Figure 4.9). There are some proteins which have different levels of abundance between bait conditions. Both STAM and STAM2 are present in increased abundance using the LITAF P135S and LITAF V144M baits, compared to LITAF WT. Additionally, HRS is present in increased abundance in the LITAF V144M sample. Furthermore, strumpellin, a component of the WASH complex, was not enriched in the WT LITAF sample, but was enriched in both LITAF P135S and LITAF V144M samples (Figure 4.8A). Other membrane trafficking proteins identified such as dysferlin, RabGAP1, coatomer subunit β (COPB), LPS-responsive and beige-like anchor protein (LRBA), protein bicaudal D homolog 2 (BICD2), tight junction protein 2 (TJP2) and protocadherin γ A11 (PCDHGA11) are present at increased levels in samples with the CMT1c mutants compared to WT LITAF (Figure 4.9).

Conversely, there are a range of proteins which have roles in membrane trafficking that are de-enriched by the CMT1c mutants compared to WT LITAF. RhoGAP1, spartin and flotillin had reduced abundance in the CMT1c mutant conditions (Figure 4.8A). Snap29, synaptobrevin homologue YKT6, CAVIN1, Rab1A and VAMP5 had lower levels of enrichment in the CMT1c conditions compared to WT LITAF. Tumour protein D54 (TPD54) was also slightly less abundant in the CMT1c conditions but was still one of the most abundant hits in all conditions. EHD1 and Arfaptin-2 were reduced in the LITAF P135S condition compared to both WT LITAF and LITAF V144M baits. (Figure 4.9B).

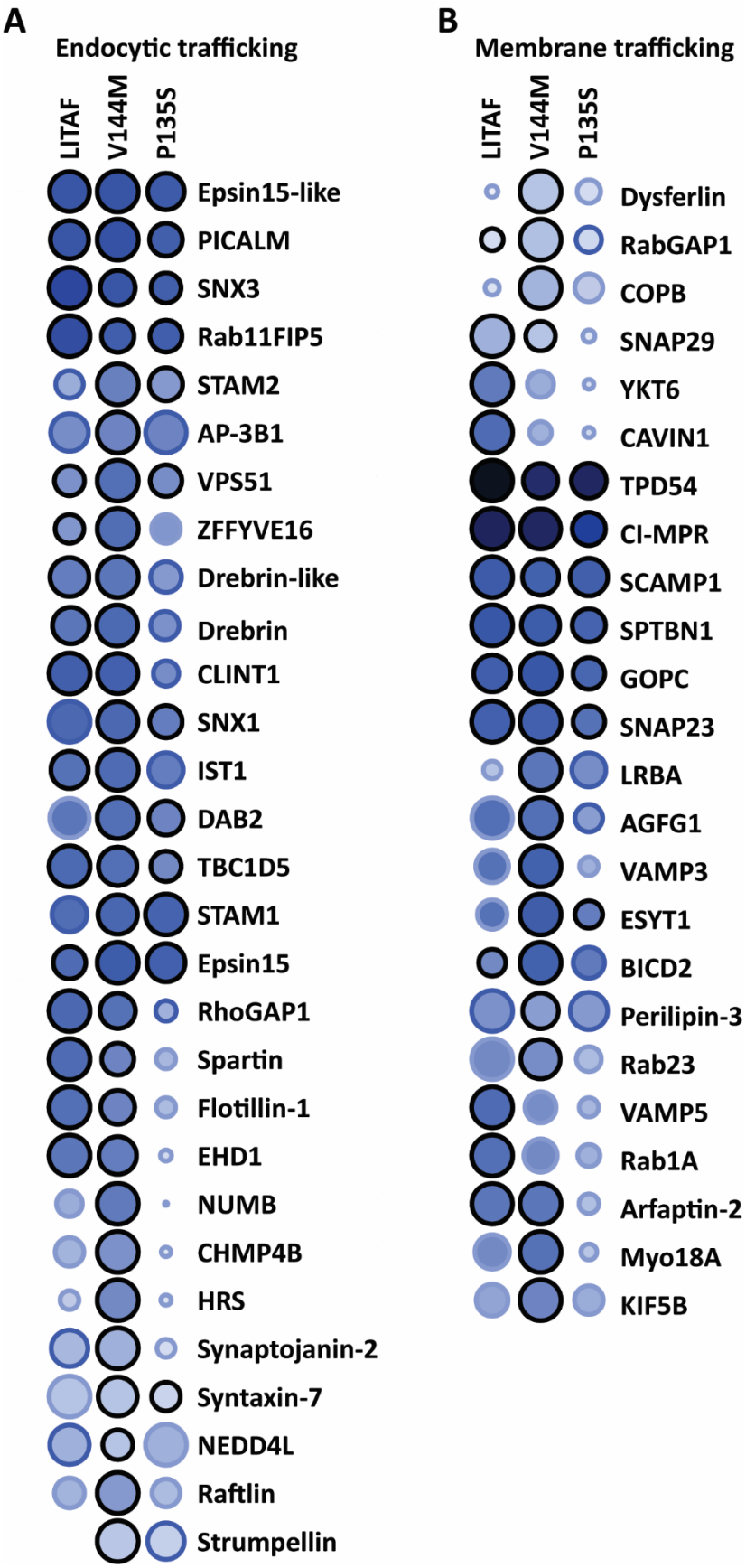
A
Endocytic trafficking
LITAF
V144M
P135S
Epsin15-like
PICALM
SNX3
Rab11FIP5
STAM2
AP-3B1
VPS51
ZFFYVE16
Drebrin-like
Drebrin
CLINT1
SNX1
IST1
DAB2
TBC1D5
STAM1
Epsin15
RhoGAP1
Spartin
Flotillin-1
EHD1
NUMB
CHMP4B
HRS
Synaptojanin-2
Syntaxin-7
NEDD4L
Raftlin
Strumpellin
B
Membrane trafficking
LITAF
V144M
P135S
Dysferlin
RabGAP1
COPB
SNAP29
YKT6
CAVIN1
TPD54
CI-MPR
SCAMP1
SPTBN1
GOPC
SNAP23
LRBA
AGFG1
VAMP3
ESYT1
BICD2
Perilipin-3
Rab23
VAMP5
Rab1A
Arfaptin-2
Myo18A
KIF5B

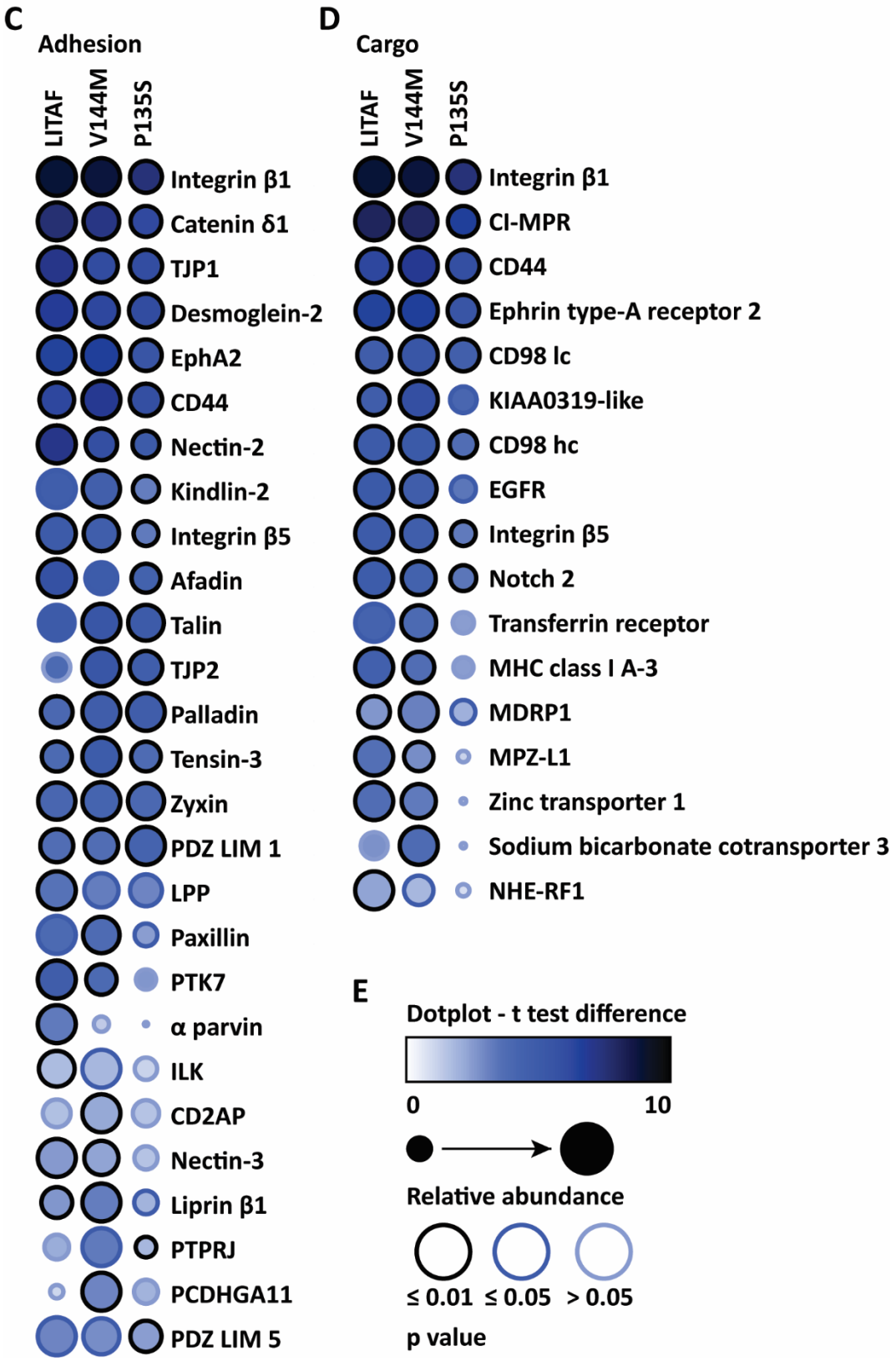

Figure 4.9. Dot plots of enriched proximal proteins for LITAF baits.
Enriched proximal proteins were manually categorised into groups consisting of proteins involved in endocytosis (A), membrane trafficking (B), adhesion (C) and cargo proteins (D). E. Proteins are represented by circles where the size is relative abundance, the colour represents the fold change and the outline refers to the significance of the enrichment. Dot plots were generated using ProHits-Viz online tool (Knight et al., 2017).

A large proportion of the proximal proteins identified also had roles in adhesion (Figure 4.9C). Again, some of these proteins had reduced abundance in the CMT1c mutant conditions compared to LITAF WT. Nectin-2/PVRL2, kindlin-2/FERMT2, afadin/MLLT4, lipoma preferred partner (LPP), protein tyrosine kinase 7 (inactive) (PTK7) and α-parvin were reduced in both V144M and P135S conditions, but the greatest reductions were in the P135S condition (Figure 4.9C). Similarly, when looking at the abundance of cargo proteins, many of them had reduced enrichment in the LITAF P135S condition compared to both the LITAF WT and LITAF V144M condition. Integrin β1 and cation-independent mannose phosphate receptor (CI-MPR) were two proteins with high abundance in all conditions, although slightly reduced in the LITAF P135S condition (Figure 4.9D). Myelin protein zero like 1 (MPZ-L1), major histocompatibility complex (MHC) class 1 and Na^+/H^+ exchange regulatory co-factor 1 (NHE-RF1) had reduced abundance in both CMT1c mutant conditions (Figure 4.9D).

4.2.3 Preliminary analysis of BioID2 hits

Any hits from BioID experiments must be validated as any significantly enriched proteins may just be located close to the bait protein and may not be a specific interactor. Some proteins identified with high confidence were selected for further preliminary analysis to assess whether they might have interactions with LITAF. Firstly, integrin β1 was chosen as it is a cargo that recycles by Arf6 and Rab11-dependent pathways (Arjonen et al., 2012, Powelka et al., 2004) and was significantly enriched in all experimental samples, although slightly reduced in the LITAF P135S condition compared to WT and V144M (Figure 4.9D). Furthermore, many proteins involved in endocytosis and trafficking of integrin β1 were identified as proximal proteins (Figure 4.9), such as EPS15 (Arjonen et al., 2012) Dab2 (Chao and Kunz, 2009), Numb (Nishimura and Kaibuchi, 2007), RabGAP1 (Samarelli et al., 2020) and drebrin (Schiweck et al., 2021). Additionally, TPD54 was identified for further analysis as it is another protein which is involved in many intracellular membrane trafficking pathways and is also involved in integrin β1 recycling (Larocque et al., 2020a, Larocque et al., 2020b). TPD54 was significantly enriched in all conditions, although slightly reduced compared to WT LITAF in the CMT1c mutant conditions (Figure 4.9B). Spartin was also selected for further analysis as its abundance was reduced in the CMT1c conditions (Figure 4.9A). Spartin is associated with the WASH

complex protein strumpellin (Zhao and Hedera, 2015), HECT domain E3 ubiquitin ligases including ITCH and WWP1 (Edwards et al., 2009) and IST1 (Renvoise et al., 2010) and is also associated with EGFR trafficking (Bakowska et al., 2007).

In order to assess whether LITAF and integrins are associated, initial analysis focused on determining co-localisation of WT and mutant LITAF with α5 integrin in MD-MB-231 cells, which are a migratory breast cancer cell line. α5 integrin only heterodimerises with integrin β1 and this forms a fibronectin receptor that is either ubiquitinated and degraded in the lysosome, or recycled to the plasma membrane (Lobert et al., 2010, Arjonen et al., 2012). In permeabilised cells, α5 integrin localised to endosome-like structures and co-localised with WT LITAF and mutant LITAF (Figure 4.10). This confirms that integrin β1 (and associated proteins) is likely to be a proximal protein to LITAF. The co-localisation of LITAF and integrin α5 was not affected by CMT1c mutations at steady state, which is consistent with enrichment with all baits in BioID.

We also examined co-localisation between TPD54 and LITAF. mCherry-TPD54 localised throughout the cytoplasm with increased intensity around the perinuclear region (Figure 4.11A, upper panels) and in some cells localised to distinct puncta (Figure 4.11A lower panels). This difference in localisation may be due to exogenous protein expression levels. GFP-LITAF and GFP-LITAF containing patient mutations partially co-localised with mCherry-TPD54 in both circumstances (Figure 4.11A). Co-immunoprecipitation experiments between GFP-LITAF and mCherry-TPD54 failed to confirm an interaction between these proteins and we hypothesised that this could be due to it being a transient interaction which was not preserved in the IP conditions. Therefore, we used directed BioID to try and establish the validity of TPD54 as a proximal protein to LITAF. In a single preliminary experiment, cells transduced with BioID2-V5-LITAF, transfected with mCherry-TPD54 and incubated with biotin, displayed substantial biotinylation of mCherry-TPD54 (Figure 4.11B). Additionally, when mCherry-TPD54 was immunoprecipitated by RFP-Trap, there was some BioID-V5-LITAF pulled down also (Figure 4.11B) Together, these data extend the mass spectrometry analysis and indicate potential for an interaction between LITAF and TPD54.

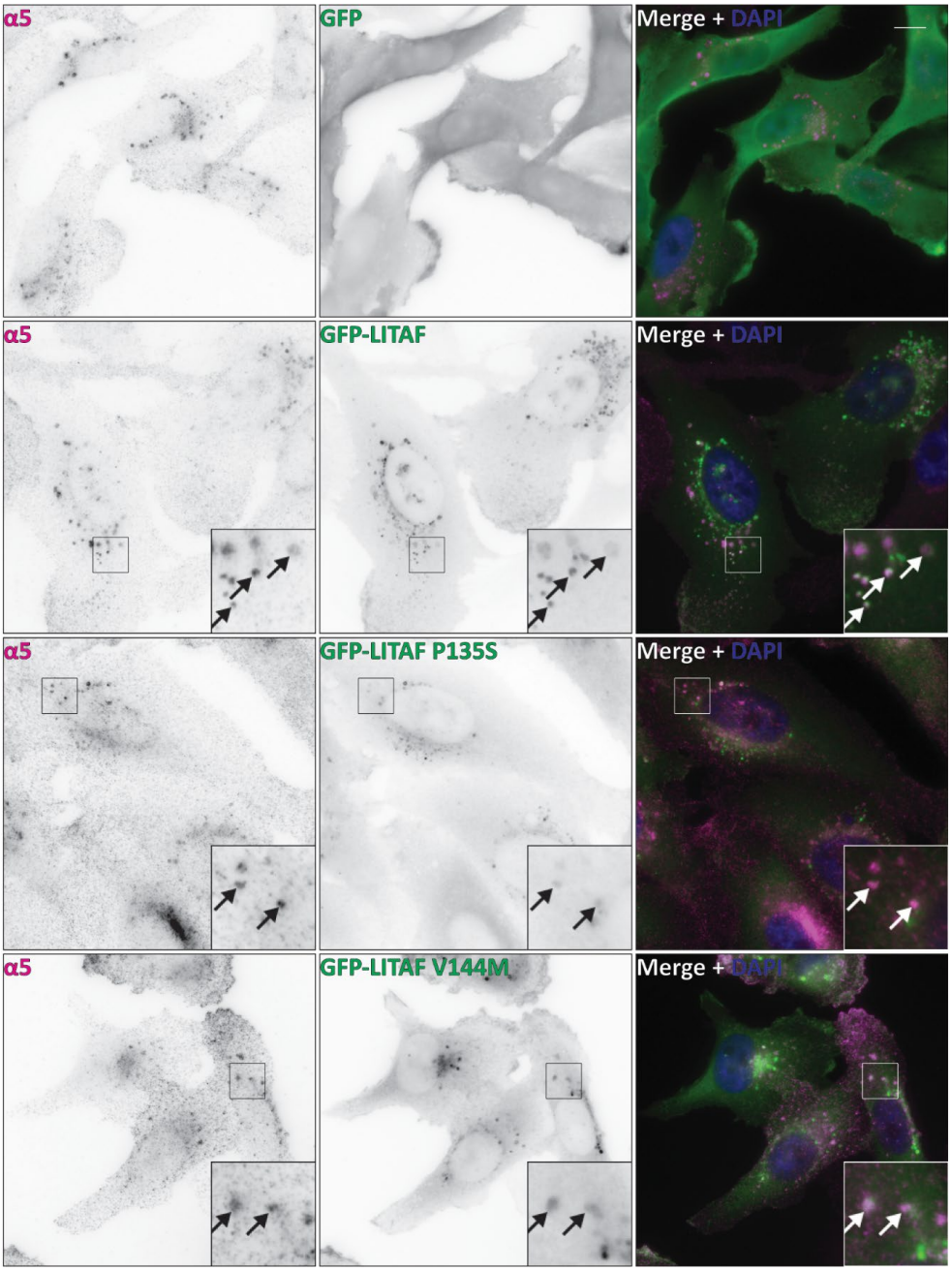

Figure 4.10. Co-localisation of LITAF and integrin in MD-MB-231 cells.
MD-MB-231 cells transduced with lentivirus containing GFP, GFP-LITAF, GFP-LITAF P135S or GFP-LITAF V144M were stained with α5 antibody and analysed by widefield fluorescence microscopy. Arrows indicate co-localisation. Scale bars = 10 µm. Insets magnified 3x.

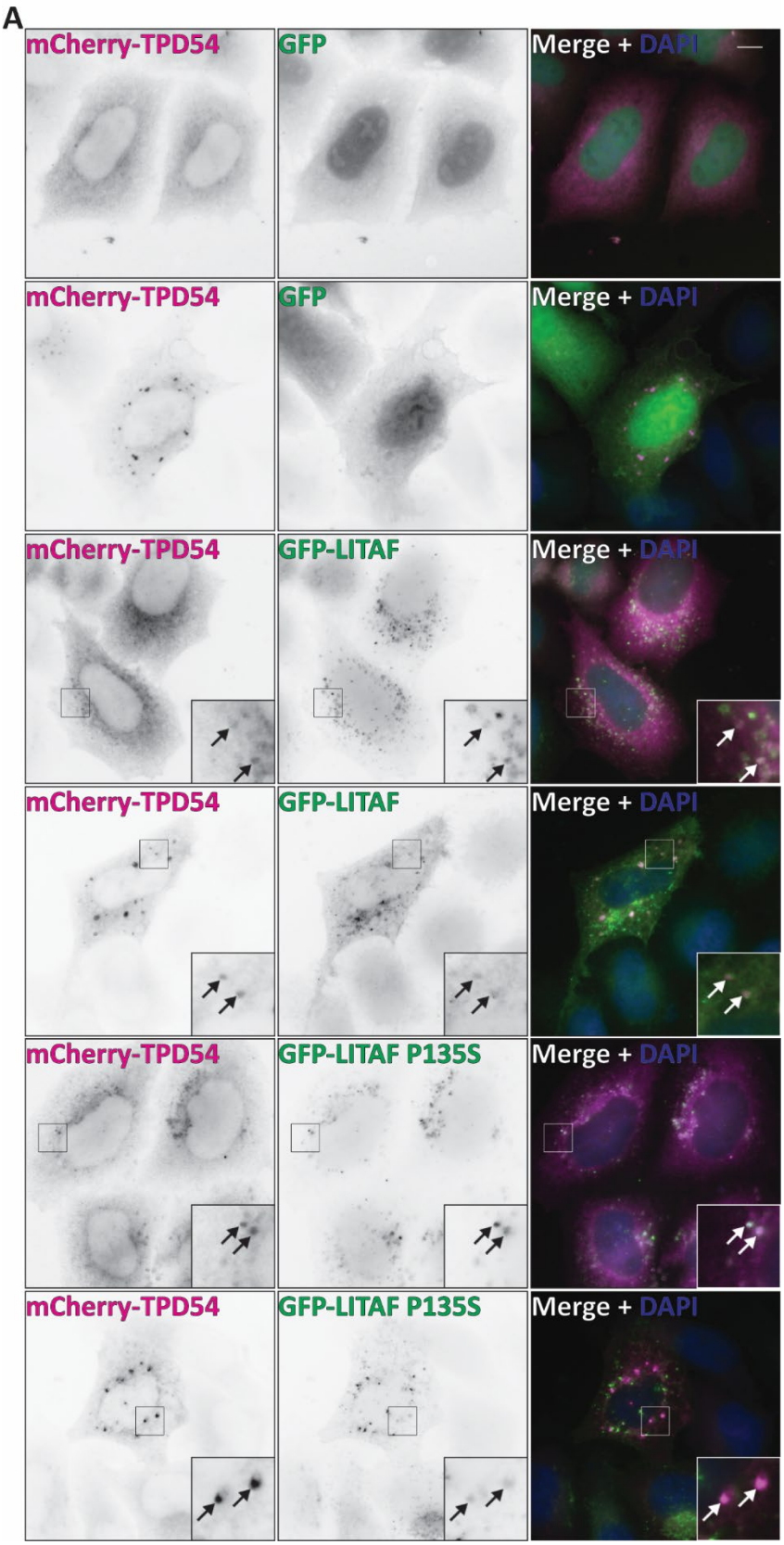
A
mCherry-TPD54
GFP
Merge + DAPI
mCherry-TPD54
GFP
Merge + DAPI
mCherry-TPD54
GFP-LITAF
Merge + DAPI
mCherry-TPD54
GFP-LITAF
Merge + DAPI
mCherry-TPD54
GFP-LITAF P135S
Merge + DAPI
mCherry-TPD54
GFP-LITAF P135S
Merge + DAPI

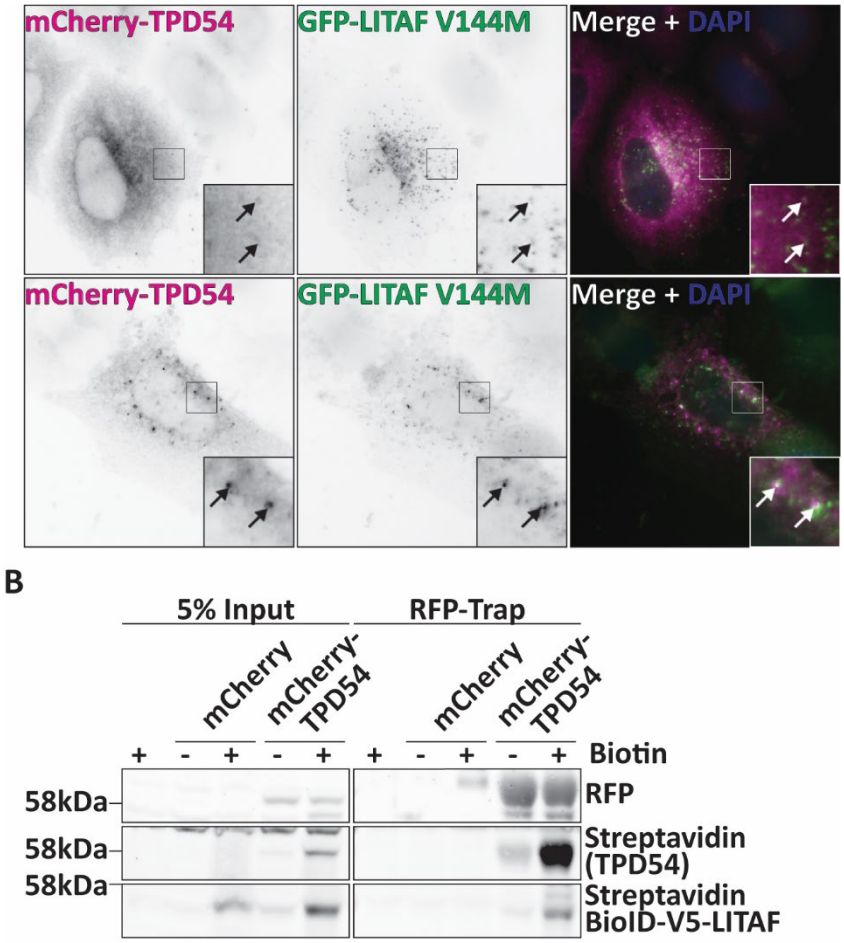

Figure 4.11. Association of TPD54 with LITAF in HeLaM cells.
A. HeLaM cells were transfected with GFP, GFP-LITAF, GFP-LITAF P135S or GFP-LITAF V144M and mCherry-TPD54 were analysed by widefield fluorescence microscopy. Arrows indicate co-localisation. Scale bars = 10 µm. Insets magnified 3x. B. HeLaM cells transduced with BioID-V5-LITAF and transfected with either mCherry or mCherry-TPD54 were incubated with vehicle or 50 µM biotin. Cell lysates were affinity purified using RFP-Trap and 5% input and pulldowns were analysed by SDS PAGE and Western blotting. Biotinylated TPD54 was detected by RFP antibody (upper panel) and streptavidin conjugated to IRDye 800CW (middle panel). BioID-V5-LITAF was detected by streptavidin (lower panel).

In addition to this, we determined whether LITAF and spartin localise to the same subcellular compartment. Exogenous myc-spartin distributed throughout the cytoplasm but in some cells myc-spartin localised to puncta (Figure 4.12). These puncta could be endosomes or lipid droplets, where spartin is known to localise (Edwards et al., 2009). There was some overlap with puncta also containing GFP-LITAF, GFP-LITAF P135S and GFP-LITAF V144M (Figure 4.12). Similar to TPD54, initial co-immunoprecipitation experiments did not confirm a specific interaction between GFP-LITAF and myc-spartin. Again, this could be due to a transient interaction or a lack of direct interaction between these proteins. Altogether, these data provide some evidence that integrin β1, TPD54 and spartin are likely to be proximal proteins to LITAF in cells but further work is required to determine whether they are true interactors.

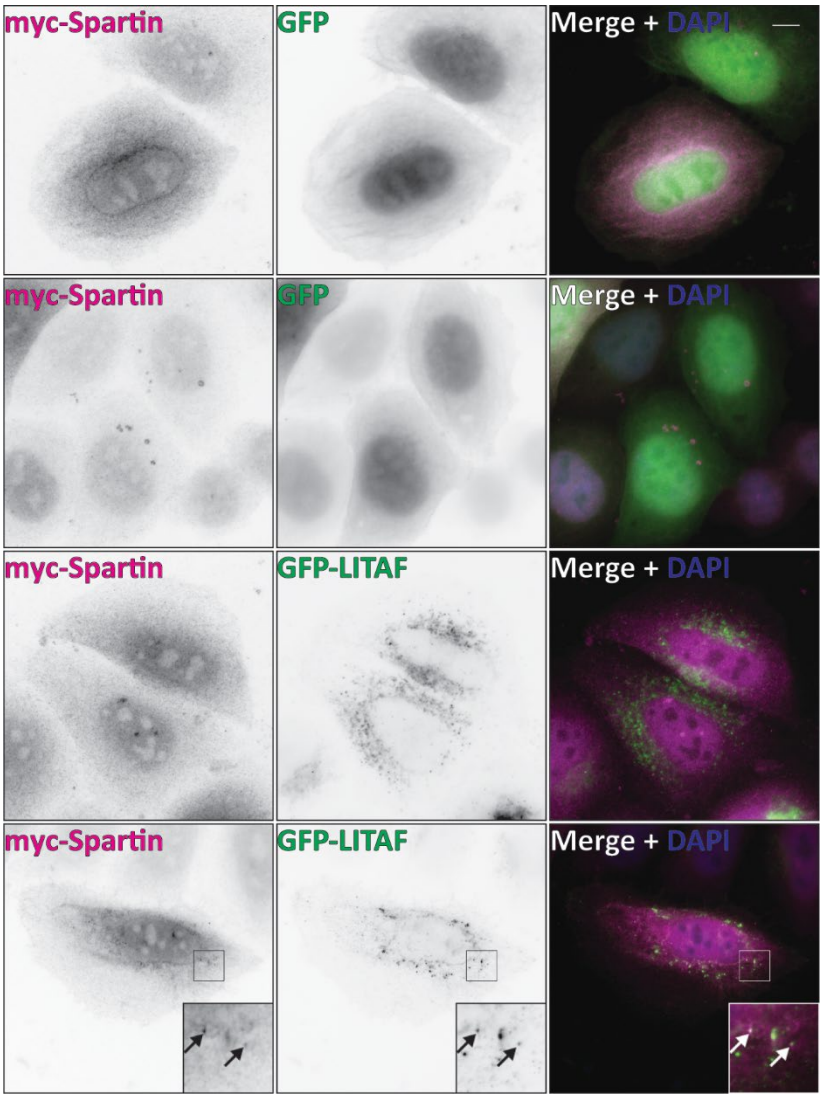

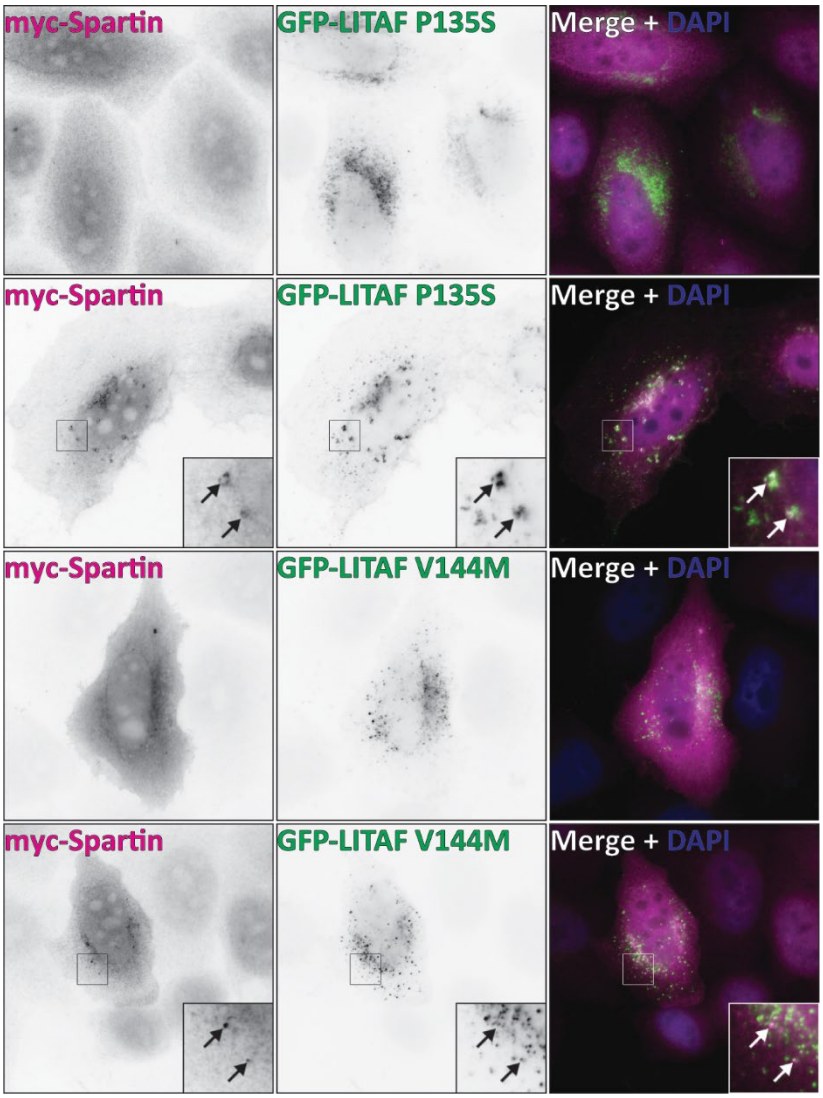

Figure 4.12. Co-localisation of spartin with LITAF in HeLaM cells.
HeLaM cells were transfected with GFP, GFP-LITAF, GFP-LITAF P135S or GFP-LITAF V144M and myc-spartin were stained with myc antibody and analysed by widefield fluorescence microscopy. Arrows indicate co-localisation. Scale bars = 10 µm. Insets magnified 3x.

4.3 Discussion

In this chapter I described the use of BioID to identify proximal proteins to WT LITAF and to LITAF containing CMT1c mutations (P135S and V144M). The enrichment of proteins which are known to be associated with LITAF function indicated successful identification of potential interacting partners. Proteins with a variety of functions were identified, providing plenty of potential novel associations to investigate. Surprisingly, proteins with functions in cell-cell adhesions and the actin cytoskeleton were enriched in the experimental samples. Preliminary analysis of three significantly enriched proteins, integrin β1, TPD54 and spartin suggested that they might indeed be associated with LITAF. Additionally, comparison of the level of enrichment of proximal proteins in LITAF WT, LITAF P135S and LITAF V144M samples suggested that there may be subtle differences in the profile of interacting proteins. Further work is required to test the validity of these potential associations and differences in the proximal proteins identified in WT LITAF vs CMT1c mutant samples should be interrogated further to determine whether they are functionally relevant and if they could inform on the pathophysiology of CMT1c disease.

Analysis of the BioID mass spectrometry data showed that broadly similar proteins were identified by LITAF WT, LITAF P135S and LITAF V144M baits, and that overall, the samples were not significantly different from each other. Considering the experimental set up, it is not surprising that the conditions did not contain major differences in the proximal proteins. The baits are the same protein with the only difference being a single missense mutation, and WT LITAF and CMT1c LITAF localising to early endosomes. Replicate samples might have been more closely correlated if the replicates had been prepared in parallel or on the same day. Additionally, stable cell lines expressing more consistent levels of the different baits might have increased the reproducibility of the mass spectrometry data. Stable isotope labelling with amino acids in cell culture (SILAC)-based BioID could also be used for robust quantitative protein abundance measurements in different conditions. However, the proximal proteins identified here provide useful information on the possible cellular functions of LITAF.

Many membrane trafficking proteins were identified in the BioID experiments. Several of these have known associations with LITAF or are predicted to interact in the BioGRID database. Increased enrichment of STAM, STAM2 and HRS in LITAF P135S and V144M samples may be consistent with the vacuolated endosome phenotype observed in CMT1c patient fibroblasts (Edgar et al., 2020), with increased localisation of LITAF containing CMT1c mutations on endosomes relative to recycling tubules. Observations by Lee *et al* (2012) suggested that LITAF CMT1c mutants may sequester ESCRT components in the cytosol, resulting in disrupted endosomal trafficking (Lee et al., 2012). The validity of the increased association between LITAF mutants and ESCRT-0 should be assessed experimentally and these hypotheses tested.

We showed that LITAF partially overlaps with spartin, which was a significantly enriched proximal protein to LITAF. Spartin functions as an adaptor for ITCH (Edwards et al., 2009) and may have a role in ubiquitin-mediated endocytic trafficking given its localisation to endosomes (Edwards et al., 2009), interactions with ubiquitin (Karlsson et al., 2014), the Rab5 GEF alsin (Cobanoglu et al., 2012) and EPS15 (Bakowska et al., 2005), and its involvement in EGFR trafficking (Bakowska et al., 2007). Spartin also interacts with the WASH complex protein strumpellin (Zhao and Hedera, 2015) which is part of the machinery that generates tubular recycling endosomes. LITAF also interacts with ITCH and may have a similar role to spartin as an adaptor for E3 ubiquitin ligases. Further exploration of this association may shed light on the mechanism of action of LITAF.

LITAF has not previously been associated with cell adhesions. Here, we showed that many proteins involved in focal adhesions were likely to be proximal to LITAF, including integrins β1 and β5, talin, paxillin, kindlin-2, tensin, α-parvin and zyxin. LITAF is likely to have a role in integrin trafficking as loss of LITAF disrupts integrin α5 trafficking and cell migration (Wunderley et al., 2021). Initial experiments shown here indicated overexpression of CMT1c mutants did not affect α5 integrin localisation to endosomes at steady state. This does not exclude the possibility that CMT1c mutants affect the trafficking of integrin β1 bound to α chains other than α5, as this was the only integrin dimer examined here. Preliminary experiments shown here indicate that LITAF may be associated with TPD54, which has a role in trafficking of integrin β1

and in cell migration (Larocque et al., 2020b). This provides further support for a role for LITAF in this pathway. Therefore, despite the lack of high reproducibility between BioID replicates, by narrowing down the list of hits using stringent criteria I believe we were able to identify potential interactors and proximal proteins.

Involvement in integrin trafficking may be a common feature of CMT proteins, since another demyelinating CMT-associated protein, SH3TC2, was found to be associated with integrin α6 using the BioID assay in RPE-1 cells (Vijay et al., 2016). Expression and regulation of integrin β1 in Schwann cells is required for correct interactions with axons and maintenance of myelination (Feltri et al., 2002, Ness et al., 2013) and α6β1 integrin signalling has been shown to be important in the radial sorting of axons before myelination in the PNS (Nodari et al., 2007, Pereira et al., 2009). This indicates the importance of correct trafficking of integrins in Schwann cells for myelination (Pereira et al., 2012). Integrin β1 was one of the most abundant significantly enriched proteins in the LITAF bait sample, indicating that it may be highly associated with LITAF, which supports previous work (Wunderley et al., 2021). This association warrants further investigation into how LITAF affects integrin trafficking considering the importance of integrins in myelination.

Integrins recycle via tubular Arf6 or Rab11-dependent pathways (Powelka et al., 2004). Interestingly, one of the significantly enriched proximal proteins, Drebrin, has been associated with Rab8-dependent recycling tubules and integrin β1 trafficking in neuronal cells (Schiweck et al., 2021). We have shown that LITAF localises to Arf6-positive tubules, and that LITAF regulates Rab8-positive tubules (see section 3.2.3) and Rab11-positive tubules (Wunderley et al., 2021). This places LITAF in the right location to regulate trafficking of integrins. Given the altered distribution of CMT1c mutants away from tubular recycling endosomes, future work should investigate the effect of CMT1c mutations on the recycling of integrins, as well as other cargos, in Schwann cells, as this could inform on the mechanism underlying CMT1c disease.

Chapter 5: Investigating LITAF domain containing proteins in Zebrafish

5.1 Introduction

The correct functioning of LITAF is required for normal physiology as mutation of this protein results in CMT1c disease, a demyelinating peripheral neuropathy (Street et al., 2003). These mutations are autosomal dominant so only one copy of the mutated allele is required for the disease to manifest. This indicates that the disease may be caused by a toxic gain of function mechanism, loss of function due to a dominant negative mechanism, or haploinsufficiency, but it is not yet clear which mechanism accounts for CMT1c disease.

Previous work has shown that the loss of LITAF and CDIP1 in cells has several effects, including expansion of recycling tubules, altered trafficking of α5 integrin and impaired migration (Wunderley et al., 2021). We showed in chapter 3 that CMT1c mutants are unable to rescue LITAF depletion-induced expansion of recycling tubules, which indicates loss of function. In addition, patient fibroblasts containing LITAF T115N and control fibroblasts depleted of LITAF both displayed the same phenotype of vacuolated endosomes. Depletion of LITAF in patient fibroblasts did not rescue the vacuolated endosome phenotype, which further supports a loss of function mechanism (Edgar et al., 2020).

Studies in mouse models of CMT1c disease containing knock-in disease mutations have recapitulated some of the disease phenotypes, such as reduced nerve conduction velocity and myelin infoldings (Lee et al., 2013), as well as other related phenotypes such as increased limb clasping and paralysis in adulthood (Zhu et al., 2013). Myelination was not affected in LITAF knock-out (KO) mice, but after nerve injury there was a delay in the onset of myelination and increased macrophage recruitment to the injury site (Somandin et al., 2012). These studies suggest that CMT1c mutations exert effects due to a toxic gain of function mechanism, as they have different phenotypes to LITAF KO mice (Lee et al., 2013, Zhu et al., 2013). However, the expression of CDIP1 in these mice and possible redundancy with LITAF were not examined.

A genetic interaction between LITAF and CDIP1 was identified recently in a CRISPR-Cas9 screen in mouse B16F10 cells (Liu et al., 2020). LITAF KO cells were found to be four times more resistant than WT to hemolysin BL toxin in terms of cell viability,

while CDIP1 KO did not affect sensitivity to the toxin. This indicates that LITAF may act as a receptor for this toxin. However, LITAF and CDIP1 double KO cells were completely resistant to the toxin, indicating that in the absence of LITAF, CDIP1 can function as a substitute for LITAF (Liu et al., 2020). Although this study did not specifically examine the functions of these proteins in endocytic trafficking or Schwann cells, it does point towards some redundancy between these proteins.

Zebrafish models have been used to study proteins implicated in peripheral neuropathies (Won et al., 2019), including myelin proteins whose mutation results in demyelinating type 1 CMT such as PMP22 (Wulf et al., 1999, Jones et al., 2012), PMP2 (Gonzaga-Jauregui et al., 2015) and MPZ (Preston et al., 2019, Brosamle and Halpern, 2002). Zebrafish represent a useful model system in which to study rare genetic diseases (Adamson et al., 2018) and myelination, due to their high homology with mammals, ease of genetic manipulation and analysis techniques such as imaging (Buckley et al., 2008, Raphael and Talbot, 2011).

Zebrafish have also been used to study two types of axonal CMT caused by mutations in endocytic proteins. A zebrafish model was used to study the effect of Rab7 mutations associated with axonal CMT2B. Rab7 mutants were expressed in spinal sensory neurons and this resulted in defects in axonal development and reduced vesicle transport speeds, suggesting altered vesicle trafficking in this disease (Ponomareva et al., 2016). Additionally, zebrafish have also been used to model CMT2M that is caused by mutations in dynamin 2 (Bragato et al., 2016). Embryos expressing exogenous dynamin 2 containing a CMT mutation did not form secondary motor axons. Additionally, these embryos had more disordered muscle tissue (Bragato et al., 2016).

As yet, there have been several studies looking at LITAF function *in vivo*, but there have not been many studies examining the role of CDIP1 *in vivo,* or members of the LITAF domain family in zebrafish. Moreover, redundancy between LITAF domain containing proteins has not been studied *in vivo*. Therefore, in this chapter we aimed to determine the level of conservation within the LITAF domain protein family in zebrafish compared to humans and carry out preliminary characterisation of these genes. We also set out to determine the consequence of organismal loss of LITAF and CDIP1 in founder zebrafish embryos and stable homozygous knockout lines.

5.2 Results

5.2.1 Identification of LITAF domain containing genes in zebrafish

Zebrafish often have multiple orthologues of mammalian genes due to a whole genome duplication event which occurred in the teleost lineage (Glasauer and Neuhauss, 2014). As such, it is important to examine and characterise related genes to identify the most relevant gene for further study in this model organism. Therefore, we looked at the protein similarity, gene synteny, presence of conserved motifs and mRNA expression of genes with similarity to LITAF and CDIP1 in zebrafish.

The mammalian genome encodes two LITAF domain containing proteins; LITAF and CDIP1. To identify LITAF and CDIP1 orthologues in zebrafish, the nucleotide and protein sequence of human LITAF SLD was searched against *Danio rerio* nucleotide and protein collections using BLAST. Additionally, Uniprot and PFAM databases were searched for LITAF domain containing proteins in zebrafish. These analyses identified 9 proteins that contain a LITAF domain in zebrafish (Figure 5.1A). Two orthologues have been annotated as LITAF and CDIP1 but 7 additional LITAF family members have been retained in zebrafish. Interestingly, one of the LITAF orthologues, ubald1a, has a ubiquitin binding associated (UBA) like domain at the N-terminus. The other 8 proteins have similarity to human LITAF and CDIP1 in their N-terminal regions, including some conservation of the proline protein interaction motifs (Figure 5.1A).

The SLD domains are very highly conserved between zebrafish proteins (Figure 5.1B) and many residues are 100% conserved, including C96 and C149 that are essential for membrane integration (Qin et al., 2016). Interestingly, several residues which are mutated in CMT1c have high levels of conservation. G112, P135 and R160 residues are completely conserved, and W116, L122 and V144 residues are mostly conserved in all the zebrafish SLD-containing proteins. Conservation of the residues that are mutated in CMT1c disease indicates that they may also be important for the function of LITAF in zebrafish. Conversely, I92, A111 and T115 residues are not very well conserved (Figure 5.2B).

In order to determine expression of SLD-containing genes across tissues in zebrafish, we performed semi-quantitative RT-PCR on cDNA prepared from dissected tissues (pooled from two males and one female adult zebrafish). Zebrafish LITAF was expressed in all tissues examined. si:ch211-202h22.7 appeared to have lower expression than LITAF in all tissues, but was expressed at a relatively higher level in the skin. si:ch211-202h22.8 was expressed in most tissues except the liver. si:ch211-202h22.9 was expressed in most tissues, except the ovary, brain and liver. Zebrafish CDIP1 had ubiquitous expression, and was slightly more highly expressed in the brain, whereas si:dkeyp-75b4.8 was also ubiquitously expressed but at an apparently lower level (Figure 5.1C).

We also performed multiple sequence alignment and phylogenetic analysis of the LITAF domain-containing genes in humans and zebrafish in order to ascertain how closely related these variants are. Ubald1a appeared to be the most distantly related, while human and zebrafish LITAF and CDIP1 are the most closely related between species (Figure 5.1D). Zebrafish CDIP1 and human CDIP1 are the most similar of all the LITAF domain containing proteins with 72.9% similarity. Zebrafish LITAF is the most similar to human LITAF as they share 53.7% similarity, which is 7.5% greater than the next most similar protein, si:ch211-202h22.9 (Table 5.1).

Furthermore, conservation of chromosomal regions surrounding human LITAF and CDIP1 genes in zebrafish was also assessed by synteny analysis (Table 5.1). This comparison indicates whether the order and direction of genes on a chromosome is conserved between species. A duplicated gene which has a high level of synteny between species is more likely to have retained the same function but this isn't definite. The highest level of synteny exists between human LITAF and CDIP1 on chromosome 16 with zebrafish LITAF and CDIP1 on chromosome 3, and human LITAF with si:ch211-157c3.4 on chromosome 3. There is also limited synteny between human LITAF on chromosome 16 with si:dkeyp-75b4.8 on chromosome 1. si:ch211-202h22.7, si:ch211-202h22.8 and si:ch211-202h22.9 are present consecutively on zebrafish chromosome 1 and show no synteny with human LITAF or CDIP1.

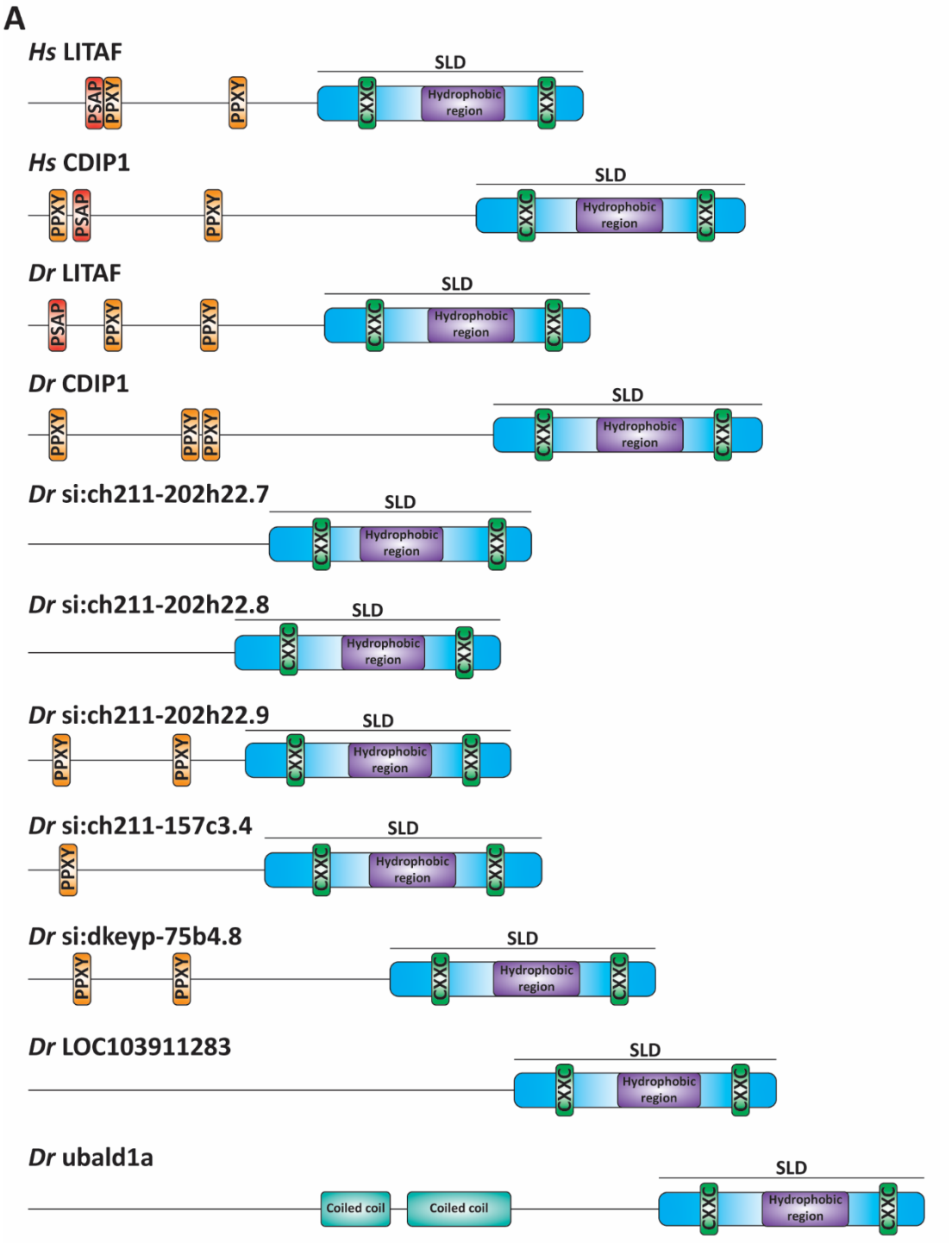
A
Hs LITAF
PSAP
PPXY
PPXY
SLD
CXXC
Hydrophobic region
CXXC
Hs CDIP1
PPXY
PSAP
PPXY
SLD
CXXC
Hydrophobic region
CXXC
Dr LITAF
PSAP
PPXY
PPXY
SLD
CXXC
Hydrophobic region
CXXC
Dr CDIP1
PPXY
PPXY
PPXY
SLD
CXXC
Hydrophobic region
CXXC
Dr si:ch211-202h22.7
SLD
CXXC
Hydrophobic region
CXXC
Dr si:ch211-202h22.8
SLD
CXXC
Hydrophobic region
CXXC
Dr si:ch211-202h22.9
PPXY
PPXY
SLD
CXXC
Hydrophobic region
CXXC
Dr si:ch211-157c3.4
PPXY
SLD
CXXC
Hydrophobic region
CXXC
Dr si:dkeyp-75b4.8
PPXY
PPXY
SLD
CXXC
Hydrophobic region
CXXC
Dr LOC103911283
SLD
CXXC
Hydrophobic region
CXXC
Dr ubald1a
Coiled coil
Coiled coil
SLD
CXXC
Hydrophobic region
CXXC
B
90
100
110
120
130
140
150
160
Hs_LITAF PITFLDRPIQMCCPSCNKMIVSQLSYNAGALTWLSCGSLCLLGCIAGCCFIPFCVDALQDVDHYCPNCRALLGTYKRL---
Hs_CDIP1 GEIFEGAPVQTVCPHCQQAITTKISYEIGLMNFVLGFFCCFMGCDLGCCLIPCLINDFKDVTHTCPSCKAYIYTYKRLC--
Dr_litaf GLVFGNVPVQAHCPVCSQSVITRLEYSSGPLVWLSCAGLAVFGCIYGCCLIPFCIEDLKDVTHHCPNCSSVLGVHKRF---
Dr_cdip1 GEMFQSAPVQTVCPHCQQPIITRISHDIGLMNTLVCMFCFFVGCDLGCCLIPCLIDDLKDVTHTCPNCKGYIYTYKRIC--
Dr_si:dkeyp-75b4.8 STTLDDTPASIVCRYCHQSIVTHVEYKPGVISWLMCVVISFLGGICGCCVIPFFVRGFLDAHHSCPLCKRHIGIYTRK---
Dr_si:ch211-157c3.4 SYELGRKPAMATCTSCQQQVLTNVTYKVGVYAWLMCILIFFCGFVLGCCLIPFFMKFFKDAYHSCPRCNKILHVEKKRCCH
Dr_si:ch211-202h22.8 PPSLSDVPGQTKCPHCQQQIITETRYVNGLLTWLICGGLGILLI-WPCCLIPFCVSACKDVEHRCPNCKHVVFLYKRM---
Dr_si:ch211-202h22.7 PSRLGECPGQMRCPHCQQQVVTETTYVNGLLVWGICIGLGIFGI-WPCCLIPFCVDSCKDVQHRCPGCKSLVYVYKRS---
Dr_si:ch211-202h22.9 LTSLTDVPGRITCPHCLTEVITETEHVSGLMAWLICGTLALFVC-WLCCCIPFCLDACKDVKHTCPNCRNIIRIYKRIQ--
Dr_LOC103911283 MPNLSDLPAQTMCPHCKLQVITITEHFSGLSAWVACGCLALIGC-WPCCLMPFWMDSCKDVEHRCPNCNNILCYYKRL---
Dr_ubald1a LDEVTMSPAKVKCPSCHKIVTTEIQYKLSSNAFLFCCLLSVVGCVAGCCLVPFCLNRFKDVAHSCPSCNKEICAVNRI---
Consensus
+++LGDVPAQTVCPHCQQQVITETEY+SGLLAWLICGGLAF+GCIWGCCLIPFCVD++KDVTH+CPNCK+II++YKR+CCH

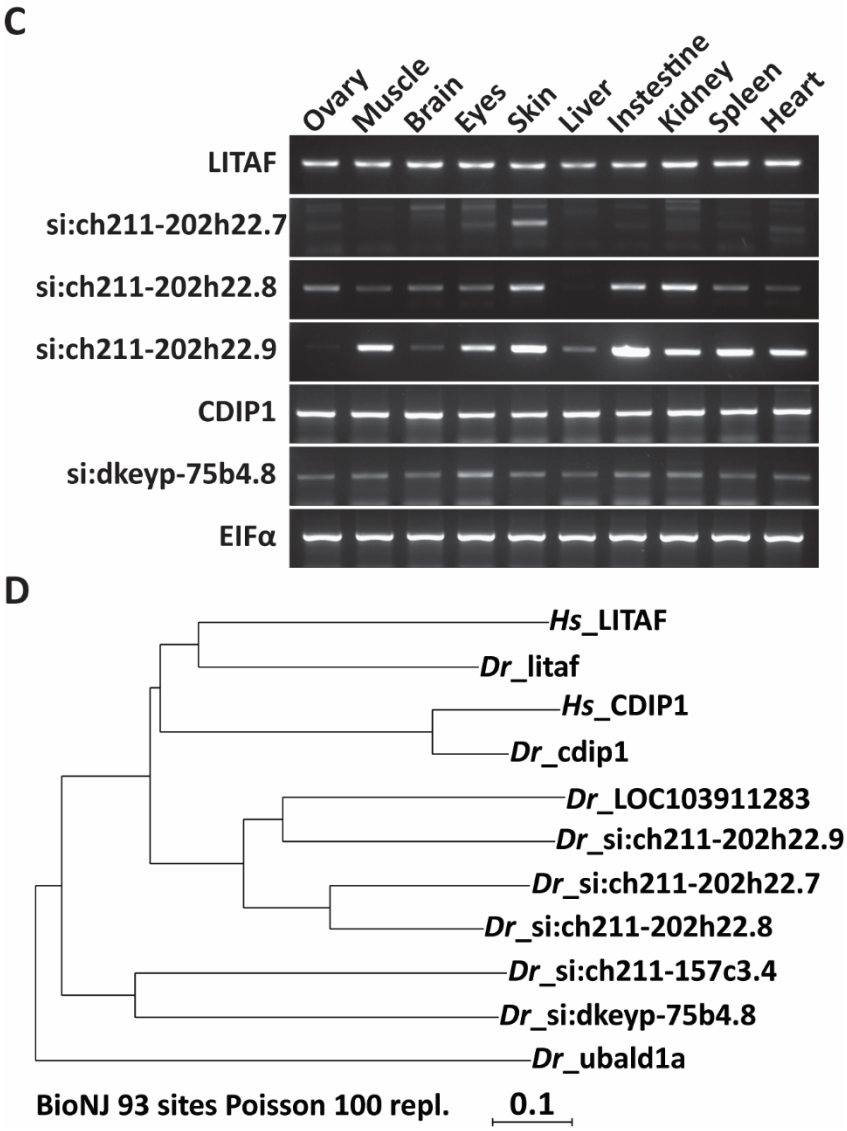

Figure 5.1. LITAF domain containing genes in zebrafish.
A. Schematic showing the structural organisation of LITAF domain containing genes in humans and zebrafish. B. Alignment of human and zebrafish LITAF SLD with consensus sequence and identity histogram shown below. Sequences were obtained from Uniprot and aligned using TCoffee WS using Jalview to generate the figure with Clustal colouring. Residue numbering refers to human LITAF reference sequence (first line). C. RT-PCR expression analysis of zebrafish genes with homology to human LITAF. Using cDNA prepared from RNA extracts of adult zebrafish tissues, expression of zebrafish genes containing the LITAF domain was examined by RT-PCR. Results are representative of 2 experiments using different primer sets. EIF1A was used as a loading control. si:ch211-157c3.4 and LOC103911283 were not included in this analysis as these genes had not been identified when the experiment was performed. D. Phylogenetic tree of human and zebrafish LITAF domain containing genes generated using TCoffee protein alignment. Seaview was used to generate the figure (Gouy et al., 2010).

Gene Name	Protein identity (similarity) to human LITAF	Protein identity (similarity) to human CDIP1	Motifs	Tissue expression	Synteny
LITAF	**40.1% (53.7%)**	29.9% (37.1%)	✓	Ubiquitous high	✓
si:ch211-202h22.7	29.1% (40.6%)	25.3% (31.2%)	✗	Low	✗
si:ch211-202h22.8	34.8% (46.6%)	25.9% (34.4%)	✗	Variable	✗
si:ch211-202h22.9	35.7% (46.2%)	28.8% (36.8%)	2x PPXY	Variable	✗
CDIP1	28.1% (35.5%	**63.3% (72.9%)**	3x PPXY	Ubiquitous high	✓
si:dkeyp-75b4.8	29.1% (38.6%)	25.1% (36.6%)	2x PPXY	Ubiquitous low	Some
si:ch211-157c3.4	25.1% (36.1%)	19.8% (27.7)	2x PPXY	-	✓
LOC103911283	22.65 (31.4%	25.7% (34.4%)	✗	-	✗
Ubald1	15.4% (26.2%)	13.5% (20.2%)	✗	-	✗

Table 5.1. Similarity and identity of zebrafish LITAF domain containing proteins compared to human LITAF and CDIP1.
Protein identity and similarity to human LITAF and CDIP1 score was obtained from alignments generated by Emboss Needle. The highest score for each is highlighted in bold. The presence of the PT/SAP and two PPXY motifs found in human LITAF and CDIP1 in zebrafish proteins was indicated. Tissue expression information was summarised from Figure 5.1. Synteny compared to human LITAF and CDIP1 on chromosome 16 was assessed using Synteny database.

Zebrafish proteins similar to LITAF and CDIP1 all contain highly conserved C-terminal LITAF domains (Figure 5.1A, B), but zebrafish LITAF and CDIP1 appear to be most closely related, have the greatest protein identity and similarity, and have synteny with human LITAF and CDIP1 (Figure 5.1, Table 5.1). Zebrafish LITAF and CDIP1 have the most similar tissue expression profile compared to mammals (Figure 5.1C). Zebrafish LITAF contains all three N-terminal proline interaction motifs found in human LITAF. Zebrafish CDIP1 contains three PPXY motifs, compared to the two present in human CDIP1, but not the PT/SAP motif found in human CDIP1 (Figure 5.1). In summary, it appears that zebrafish LITAF and CDIP1 have most similar features to human LITAF and CDIP1.

5.2.2 Generating LITAF and CDIP1 knockout zebrafish using CRISPR-Cas9 gene editing

In order to determine the effect of loss of function of LITAF in zebrafish we performed gene editing to knock-out the function of this gene. We also targeted CDIP1 as this similar protein may perform a redundant function or potentially could be involved in an adaptive response when LITAF is lost. As zebrafish LITAF and CDIP1 orthologues share the most similarity with human proteins (see above), we hypothesised that these proteins may perform similar functions in zebrafish, so we targeted these genes in gene editing experiments.

To generate knockout mutants, we used CRISPR-Cas9 gene editing (Figure 5.2). Single guide RNAs (sgRNAs) were designed using several online tools and selected manually so that formation of an indel in the target cleavage site was likely to disrupt a restriction enzyme recognition site in the genomic DNA. Three sgRNAs for each gene of interest was assessed for efficiency (Figure 5.3A, C). Genomic DNA from embryos injected at the single cell stage with the CRISPR-Cas9 mixture was extracted and the genomic region of interest was amplified by PCR. Restriction digest using the appropriate enzyme was performed, and PCR products resistant to digest suggested that indels in that region had been produced, indicating successful Cas9-mediated cleavage of the target DNA (Figure 5.3B, D). Some of these embryos showed complete resistance to digestion indicating that they might be F0 null for the targeted gene (Figure 5.3B, D). For LITAF, sgRNA2 was the most efficient, while for CDIP1, sgRNA3 was most efficient, and resistance to digestion was clearly observed in all embryos (Figure 5.3B, D). Therefore, these two sgRNAs were selected to generate CRISPR LITAF, CDIP1 and LITAF and CDIP1 double knockout zebrafish lines.

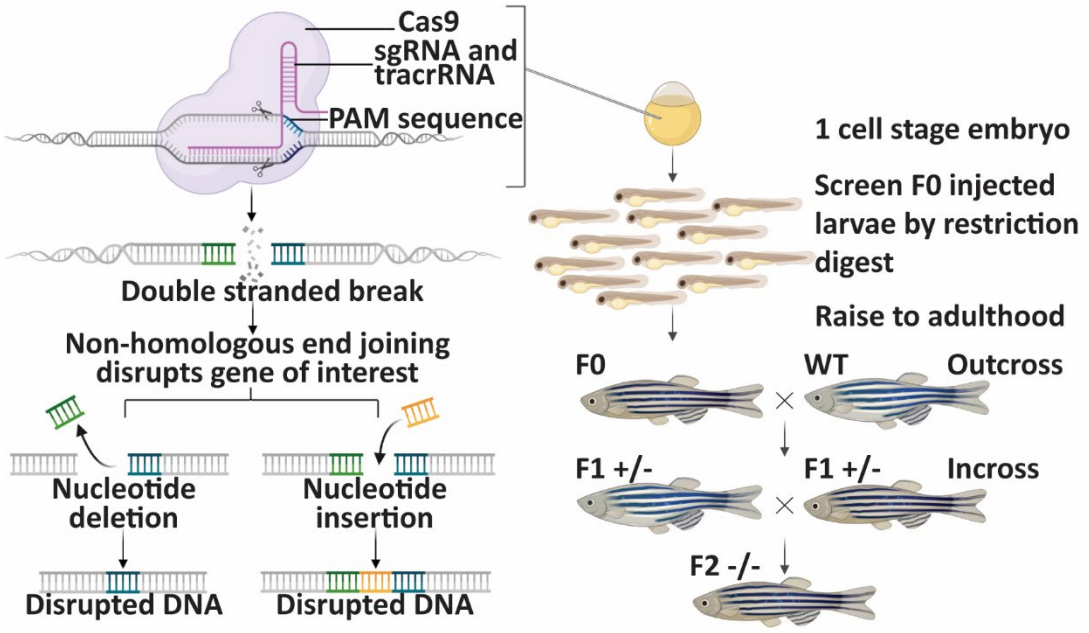

Figure 5.2. CRISPR-Cas9 genetic knock-out experimental design.
Cas9 endonuclease binds to single guide RNAs which are targeted to genes of interest where it catalyses cleavage of double stranded DNA. Cellular machinery facilitates non homologous end joining which results in the insertion or deletion of nucleotides and results in disrupted DNA. Single cell embryos injected with sgRNA, tracrRNA, Cas9 mRNA and protein were assessed for guide efficiency. F0 injected embryos were raised to adulthood, screened for mutations by restriction digest and outcrossed to WT zebrafish. Genomic DNA from F1 heterozygote zebrafish containing gene disruption was sequenced and zebrafish harbouring mutations predicted to cause loss of protein were incrossed to produce F2 homozygous knockout zebrafish. Figure created using Biorender.

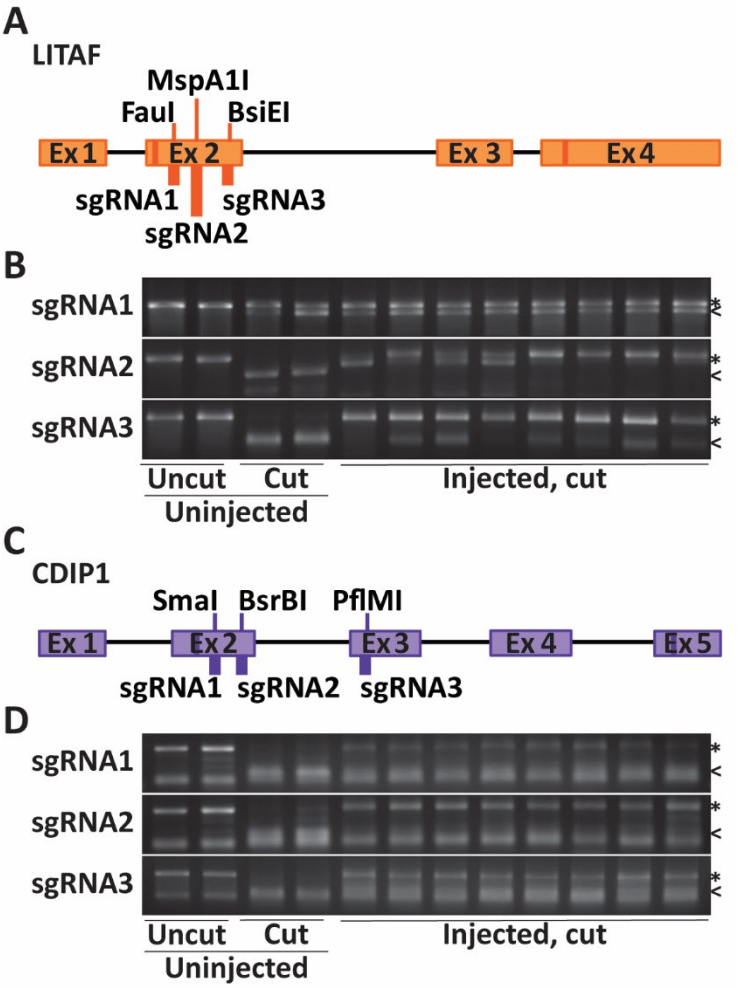

Figure 5.3. LITAF and CDIP1 CRISPR-Cas9.
A, C. Three sgRNAs for LITAF (A) and CDIP1 (C) were designed to target a region in the first coding exons of the gene that would disrupt a specific restriction enzyme recognition site if there was disruption due to Cas9 endonuclease activity. B, D. Genomic DNA was extracted from control uninjected (left) and injected 3 or 4dpf embryos and PCR was performed to amplify the region flanking the sgRNA target site. Following incubation with the appropriate restriction enzyme, electrophoresis was used to determine the resistance to restriction enzyme digest and efficacy of the different sgRNAs. * indicates resistant PCR product while < indicates digested PCR product.

Considering the efficient disruption of the gene resulting from CRISPR-Cas9, we wanted to determine whether acute loss of LITAF and/or CDIP1 from zebrafish embryos had any deleterious effects or affected development. Therefore, we examined the gross morphological development of founder embryos with mosaic disruption of the gene. Firstly, we examined the efficacy of the CRISPR-Cas9 in 10 embryos from each condition using restriction digest (Figure 5.4A). The degree of PCR product digestion was scored and indicated that all of the control injected embryo PCR

products were not resistant to digestion, as expected (Figure 5.4A arrows, B). A proportion of the PCR products from embryos injected with LITAF and CDIP1 guides were fully resistant to digestion and the majority were partially resistant, indicating mosaic disruption of the target gene (Figure 5.4A asterisks, B).

The survival of these embryos over the first 5 days post fertilisation (dpf) was assessed, and this showed that there were similar rates of survival of around 75% in this time period between embryos injected with control CRISPR-Cas9 mixture and embryos injected with CRISPR-Cas9 targeting the indicated gene (Figure 5.4C). Further to this, the gross morphology of embryos was monitored and images taken at the indicated time points (Figure 5.4D). There was no obvious difference in the development of these embryos compared to WT (Figure 5.4D). Additionally, to determine whether growth was altered in embryos with disrupted LITAF and/or CDIP1 genes, the length of larvae was measured. Again, this showed no difference between control injected embryos and LITAF and CDIP1 sgRNA injected embryos (Figure 5.4E).

Together these data suggest that disruption of LITAF and CDIP1 genes, individually or together, did not affect larval development of zebrafish. Evidently, in these embryos there was not complete disruption of the gene in all embryos and any mutations induced by CRISPR-Cas9 may not result in loss of protein expression. Furthermore, these embryos contain maternally deposited mRNA, which is present through to the gastrula stage at around 5.5 hpf (Newport and Kirschner, 1982, Kimmel et al., 1995), and may provide wild-type protein in early development. Therefore, the effect of loss of LITAF and CDIP1 at very early developmental time points is still not known.

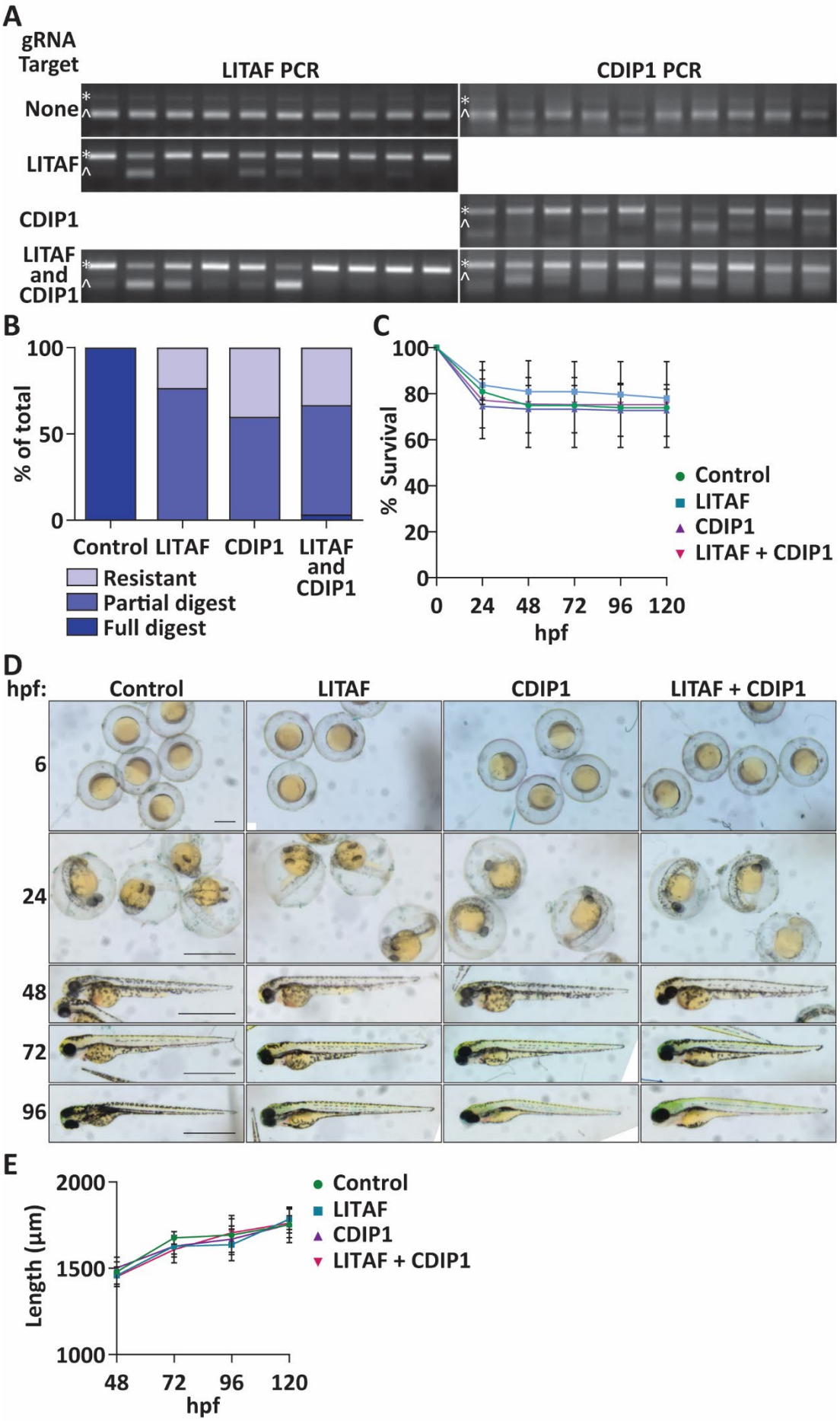
A
gRNA Target
LITAF PCR
CDIP1 PCR
None
LITAF
CDIP1
LITAF and CDIP1
B
% of total
100
50
0
Control
LITAF
CDIP1
LITAF and CDIP1
Resistant
Partial digest
Full digest
C
% Survival
100
80
60
40
20
0
0
24
48
72
96
120
hpf
Control
LITAF
CDIP1
LITAF + CDIP1
D
hpf:
Control
LITAF
CDIP1
LITAF + CDIP1
6
24
48
72
96
E
Length (µm)
2000
1500
1000
48
72
96
120
hpf
Control
LITAF
CDIP1
LITAF + CDIP1

Figure 5.4. Analysis of F0 CRISPR embryos.
A. Restriction digest of PCR amplicons of the gene of interest from the genomic DNA of injected embryos. * indicates resistant PCR product while < indicates digested PCR product. B. Scoring of CRISPR-Cas9 efficiency from restriction digests of 20-30 embryos per condition. C. Survival of embryos up to 5dpf injected with sgRNAs targeting the indicated genes. 199-316 embryos were analysed per condition. D. Larvae were imaged on a brightfield dissecting microscope and assessed for any gross morphological abnormalities at the indicated time points. Scale bars represent 500 µm. E. The body length from images in D were measured to determine any defects in growth. Error bars represent SD.

In order to investigate the consequence of total loss of LITAF and CDIP1 at the organismal level, we generated LITAF knockout, CDIP1 knockout and LITAF and CDIP1 knockout zebrafish lines. We raised injected F0 embryos to adulthood, screened them for gene disruption and outcrossed F0 null zebrafish with WT zebrafish to generate offspring with single mutations (Figure 5.2, Figure 5.5). The proportions of genotypes from F0 LITAF knockout outcrosses were slightly skewed towards LITAF+/- genotype and the proportion of genotypes from F0 CDIP1 knockout outcrosses was more skewed towards CDIP1+/- genotype (Figure 5.5E). The expected Mendelian ratio from this cross is 50:50 WT:heterozygote. The reason for this discrepancy is unknown. Additionally, most of the adult offspring from F0 LITAF knockout zebrafish outcrosses and F0 LITAF and CDIP1 knockout zebrafish outcrosses were males so these crosses were repeated to generate F1 generations with better female to male ratios.

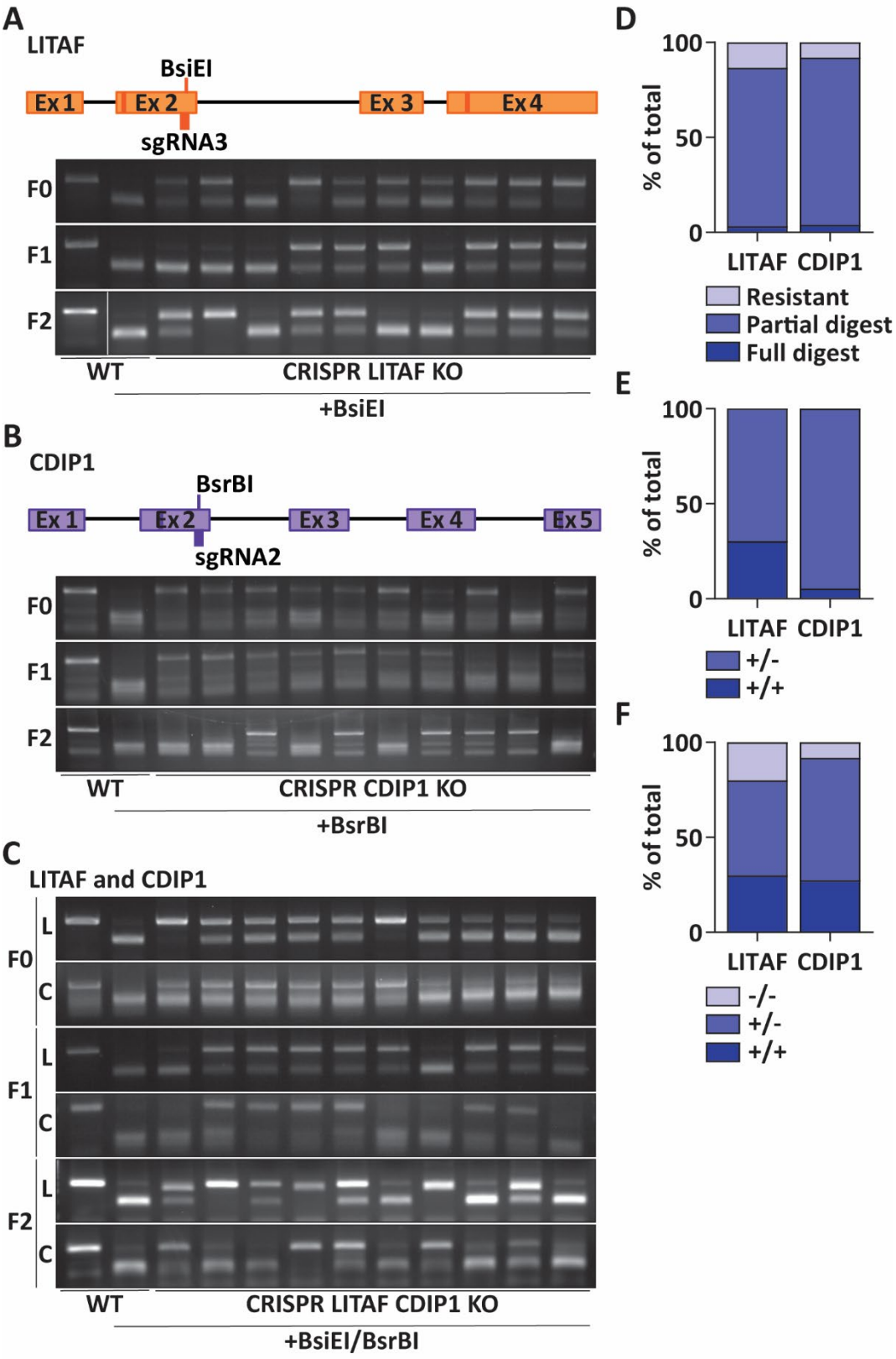

Figure 5.5. Generation of homozygous LITAF and CDIP1 knockout zebrafish.
A-C. Genotyping by PCR and restriction digest of genomic DNA extracted from F0, F1 and F2 generations of LITAF KO (A), CDIP1 KO (B) or LITAF and CDIP1 KO (C) zebrafish. D-F. Proportions of LITAF KO and CDIP1 KO F0 (D), F1 (E) or F2 (F) generation zebrafish with the indicated mutations.

	LITAF +/+	LITAF +/-	LITAF -/-
CDIP1 +/+	29.6 (6.3)	6.5 (12.5)	1.9 (6.3)
CDIP1 +/-	3.7 (12.5)	33.3 (25)	13.0 (12.5)
CDIP1 -/-	0 (6.3)	4.6 (12.5)	7.4 (6.3)

Table 5.2. Ratio of genotype in LITAF and CDIP1 double knockout F2 zebrafish.
The percentage of 108 adult zebrafish with the indicated genotype obtained from two LITAF+/- CDIP1+/- incrosses are shown, with the expected percentage in brackets.

Adult F1 zebrafish containing gene disruptions were sequenced and mutations that were predicted to cause loss of LITAF or CDIP1 protein were identified. F1 zebrafish from the same outcross that contained the same mutation were incrossed to generate F2 zebrafish, a proportion of which were homozygous mutants (Figure 5.5F, Table 5.2). The genotypes of single LITAF KO F2 zebrafish matches the expected mendelian ratio and the genotypes of single CDIP1 KO F2 are close to the expected mendelian ratio, although there were fewer homozygous mutants than expected (Figure 5.5F). The proportions of genotypes resulting from double mutant LITAF+/- CDIP1+/- incrosses were broadly similar to expected proportions with the exception of the much larger proportion of WT offspring than would be expected (Table 5.2). There was no significant amount of mortality in these clutches so it is unclear as to the reason behind this skewed proportion.

Similarly, from single mutant LITAF +/- incrosses and double mutant LITAF+/- CDIP1+/- incrosses, most of the zebrafish raised to adulthood were male. The lack of females in these populations is unlikely to be due to a loss of viability of females lacking LITAF, as the WT and heterozygote siblings also had very low female to male ratios. Inbreeding of the WT zebrafish line may have caused a predisposition to produce male offspring, or it may be a result of environmental conditions in the aquarium. Outcrossing of these lines to WT populations may restore a normal sex ratio. Unfortunately, a lack of homozygous knockout breeding pairs precluded further experiments on F3 homozygous zebrafish embryos.

In LITAF KO zebrafish, a 4 base pair (bp) deletion was detected which would result in the presence of an early stop codon. (Figure 5.6A). CDIP1 KO zebrafish had a 4bp deletion and a single base substitution, which would also result in frameshift and formation of an early stop codon. (Figure 5.6B). Furthermore, LITAF and CDIP1 double knockout zebrafish were obtained that contained frameshift mutations in both genes. There was the same 4bp deletion in LITAF and a 7bp deletion in CDIP1 in these double KO zebrafish (Figure 5.6A, B). All these mutations are predicted to result in truncated protein products if the mRNA is not degraded by nonsense mediated decay.

We wanted to test whether these mutations do in fact result in loss of protein so we analysed muscle tissue protein extracts from WT, LITAF KO, CDIP1 KO and LITAF and CDIP1 KO zebrafish. An antibody raised to zebrafish LITAF detected a band between 25 and 32kDa in WT and CDIP1 KO zebrafish protein samples that was absent in LITAF KO and double LITAF and CDIP1 KO protein samples (Figure 5.6C, arrow). This indicates that full-length LITAF protein is lost in both LITAF KO and LITAF and CDIP1 KO zebrafish. However, this does not rule out the possibility of a shorter truncated form being expressed from a downstream alternate start codon as the antibody was identified using three peptides from the N-terminus, central region and C-terminus. We could not verify the loss of CDIP1 protein due to lack of an antibody that detected zebrafish CDIP1.

Despite the apparent lack of LITAF protein in LITAF KO and double LITAF and CDIP1 KO zebrafish, there was no obvious phenotype resulting from loss of LITAF. Mature homozygous adults were viable up to at least 4 months of age, had no difference in growth compared to heterozygote clutch mates and had no gross morphological abnormalities. Males were able to breed with WT females to produce viable offspring. This indicates that loss of LITAF and most likely also CDIP1 is compatible with zebrafish life up to 4 months.

A

```
WT          181 ATGTACCCACCGACCGCACAAGGACAACCTGTCACCAGTCCC 223
LITAF KO    181 ATGTACCCA----CCGCACAAGGACAACCTGTCACCAGTCCC 219
LITAF +
CDIP1 KO    181 ATGTACCCA----CCGCACAAGGACAACCTGTCACCAGTCCC 219
```

WT

```
MAMPMPTAPPMENTTLVGHPPPPSYDEISGANPYYPAGPYPPADMKASGPPPYPTQ
EYNQMYPPTAQGQPVTSPVVAVQTVYVQPGLVFGNVPVQAHCPVCSQSVITRLEYS
SGPLVWLSCAGLAVFGCIYGCCLIPFCIEDLKDVTHHCPNCSSVLGVHKRF* 163
```

LITAF KO

```
MAMPMPTAPPMENTTLVGHPPPPSYDEISGANPYYPAGPYPPADMKASGPPPYPTQ
EYNQMYPPHKDNLSPVPS* 74
```

B

```
WT          16 CTCCTCCATACCCCGGGGGCCCCAATGCTCCGCTCCTCGAGGAG 60
CDIP1 KO    16 CTCCTCCATACCCCGGGGGCCCCAATGCTCCG----TtCAGGAG 56
LITAF +
CDIP1 KO    16 CTCCTCCATACCCCGGGGGCCCCAATGCTCCG-------AGGAG 53
```

WT

```
MSSDPPPPYPGGPNAPLLEEKNGQPLHSAGTAPVMTGPPQGHPLPPEYGPPPYEAT
QQPGFVPPHVPGEGPIPKPMHMPMPMPHPHGGYYPPLGHFPHTMGEYAGPGPSHFA
PGHTATVLAPPGAATTTVTVLQGEMFQSAPVQTVCPHCQQPIITRISHDIGLMNTL
VCMFCFFVGCDLGCCLIPCLIDDLKDVTHTCPNCKGYIYTYKRIC* 213
```

CDIP1 KO

```
MSSDPPPPYPGGPNAPFRRRTDNLCILQALLQ*  32
```

C

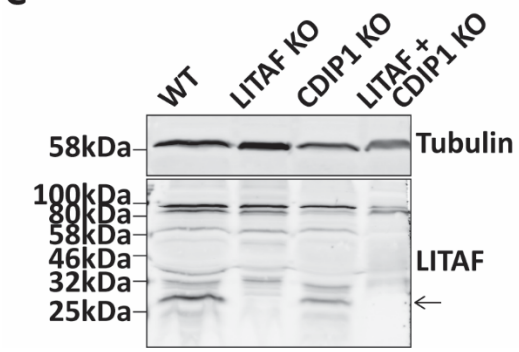

Figure 5.6. CRISPR-Cas9 induced mutations in LITAF result in loss of protein.
A, B. Sequence alignments of regions of LITAF (A) or CDIP1 (B) genomic DNA containing mutations from WT, LITAF KO, CDIP1 KO and LITAF and CDIP1 KO zebrafish as indicated. The predicted protein sequence is shown below. C. Protein extracts from muscle tissue of WT, LITAF KO, CDIP1 KO or double LITAF and CDIP1 KO zebrafish were analysed by SDS PAGE and Western blotting analysis. Tubulin was used as a loading control and was detected by TAT1 antibody (top panel). Zebrafish LITAF antibody was used to detect LITAF (bottom panel). The arrow indicates the LITAF band.

5.3 Discussion

In this chapter, I described the identification of LITAF domain containing proteins in zebrafish and the selection of zebrafish LITAF and CDIP1 as the most closely related genes to human LITAF and CDIP1, following bioinformatics and adult tissue expression analysis. We analysed F0 zebrafish with disruptions in the gene for any developmental defects and generated F2 homozygous knockout zebrafish for LITAF, CDIP1 and both LITAF and CDIP1. Zebrafish lacking LITAF and CDIP1, either alone or together, did not have any obvious phenotypes. However, further analysis at older ages and interrogation of any cellular phenotypes is necessary to more completely assess any defects that may be present in these zebrafish.

Zebrafish have retained up to 20% of duplicated genes from the whole genome duplication event which occurred in the teleost lineage (Postlethwait et al., 2000). However, phylogenetic analysis indicates that the LITAF domain proteins were present before the divergence of human and zebrafish LITAF, which suggests that they are not products of this genome duplication. Other model organisms contain multiple LITAF domain containing proteins; there are 19 in *Drosophila melanogaster* and 14 in *Caenorhabditis elegans*. Zebrafish have 9 genes which code for the LITAF domain, one of these also contains a UBA domain. The LITAF domain is very highly conserved between species and within the LITAF domain proteins in zebrafish. In particular, cysteine residues critical for the structure and membrane association of the LITAF domain are conserved in all genes. If any variants did have mutations in these residues, then clearly they would be likely to be non-functional or have a different function.

We used bioinformatics and expression analysis to identify the possible functional orthologues of LITAF and CDIP1 in zebrafish. We concluded that zebrafish LITAF and CDIP1 were likely to be the relevant genes due to the high sequence similarity (53.7% and 72.9% respectively) with the mammalian proteins, ubiquitous expression, which is also seen with the mammalian proteins, and the presence of protein interaction motifs that are conserved in the mammalian proteins. Other studies on LITAF in zebrafish have identified the same LITAF orthologue as the one described here (Moshal et al., 2019, Chen et al., 2021) Morpholino treatment to knock-down this protein resulted in increased calcium ion transients in zebrafish embryos similar to those attributed to LITAF in rabbit cardiomyocytes (Moshal et al., 2019). This was

attributed to the ubiquitin ligase adaptor function with Nedd4 which ubiquitinates and downregulates ion channels (Moshal et al., 2019). This indicates that LITAF has a necessary function in multiple cell types. We did not observe an obvious phenotype in the heart of LITAF KO zebrafish but a closer examination of this organ was not undertaken. LITAF was shown to be ubiquitously expressed and highly expressed in gills and also upregulated by lipopolysaccharides (LPS) and infection similar to human LITAF (Chen et al., 2021). This likely relates to the role of LITAF in immune responses in mammalian cells (Tang et al., 2005). These data indicate that zebrafish LITAF is a functional gene and is likely to have a similar function to human LITAF as a ubiquitin ligase adaptor and in the immune response following stimulation by LPS.

There is a lack of functional data on zebrafish CDIP1 so it is not completely certain whether it has retained the same function as human CDIP1. Zebrafish CDIP1 contains three PPXY motifs compared to the two found in human CDIP1, but the significance of this protein interaction motif for CDIP1 function is unknown. Zebrafish CDIP1 lacks the PS/TAP motif found in the mammalian protein and this motif in LITAF was shown to facilitate an interaction with TSG101 (Shirk et al., 2005). It has also been proposed that the TSG101 UEV domain may bind to the ubiquitin moiety conjugated to CDIP1 which could conserve this interaction in zebrafish (Inukai et al., 2021)

A recent study by Inukai *et al* (2021) identified protein interaction motifs in human CDIP1 which facilitate protein interactions that have not been studied previously (Inukai et al., 2021). The ALG-2-binding motif 2 (ABM-2) -like motif PQPGF, which is necessary for interaction with ALG-2 in human cells, is not completely conserved in zebrafish, as the first proline is substituted with glutamine, but there is an ABM-3-like motif (MPMPMP) just after, which may mediate an interaction with ALG-2 in zebrafish (Inukai et al., 2021). This interaction is calcium ion-dependent and may function to increase cell death induced by overexpression of CDIP1. Additionally, ALG-2 may act as adaptor for CDIP1 association with ESCRT-I. CDIP1 contains a FFAT-like motif which facilitates an interaction with VAP-A and VAP-B (Inukai et al., 2021). An aspartic acid residue which is critical for this interaction is conserved in all LITAF domain containing proteins in zebrafish (Inukai et al., 2021). Further studies on these LITAF domain proteins are required to definitively assess whether they have retained a functional role.

The other LITAF proteins in zebrafish and other orthologues in *C. elegans* and *D. melanogaster* may have subfunctionalised, gained new functions or lost their function (Glasauer and Neuhauss, 2014). Some of the LITAF domain containing proteins in zebrafish appeared to have a different tissue expression profile indicating that they may potentially have subfunctionalised and may have a specific function in these tissues. With the exception of zebrafish LITAF, they have all lost the PT/SAP motif indicating that this protein interaction motif is not required for their function and they may have a slightly different function to human LITAF. Zebrafish Ubald1a has a UBA domain and two coiled coil domains in its N-terminal region which indicates that it has a different function to LITAF.

Orthologues in *C. elegans* and *D. melanogaster* have also gained other modular domains which are likely to give the protein a different cellular function. The high level of conservation in the LITAF domain between these species indicates that this region is likely to have the same properties as in human LITAF. This region mediates membrane integration and generates membrane curvature (Wunderley et al., 2021). This indicates that membrane association and even membrane curvature may be a common feature which may be modulated by the function of the N-terminal region. Membrane curvature is a requirement in various membrane trafficking events so these proteins could have alternative roles in this pathway, and this could explain why there are so many in these species compared to mammals. As yet, the function of these orthologues has not been studied.

Using CRISPR-Cas9 we generated a LITAF knock-out zebrafish strain, a CDIP1 knock-out zebrafish strain and a double LITAF and CDIP1 knock-out zebrafish strain. The loss of LITAF protein was confirmed in single LITAF KO and double LITAF and CDIP1 KO zebrafish by Western blotting, but the loss of CDIP1 protein was not verified as an antibody against zebrafish CDIP1 is not available. The zebrafish LITAF antibody was obtained from AbMart which uses Proteome Epitope Tag Antibody Library (PETAL) technology to screen monoclonal antibodies against peptides from a protein of interest (Wang et al., 2020). Knock-out of LITAF and CDIP1 alone or together did not result in any developmental or morphological differences in embryos, larvae or adult zebrafish. Additionally, there was no explicit effect upon movement or behavioural responses. Maternally deposited RNA may compensate for the loss of

these genes in very early development and incrosses of homozygous mutant zebrafish would be required address this outstanding question. These data support the view that LITAF and CDIP1 are dispensable for normal development and growth of zebrafish, which is in line with the effect of knockout of LITAF and CDIP1 in mice, which were also viable (Somandin et al., 2012, Zhu et al., 2013, Namba et al., 2013).

It is plausible that while LITAF and CDIP1 are dispensable in zebrafish up to 4 months of age, deleterious effects might only manifest in older fish, as the age of onset of CMT1c disease and the severity of the disease in humans is variable. This is likely to be due to variation in disease penetrance between individuals. Further analysis of adult homozygous KO zebrafish is required to determine whether these proteins have a necessary functional role in this species. Specifically, studies in endocytic trafficking in the peripheral nervous system would be informative as LITAF is likely to have a specific role in this specialised tissue. It would be interesting to carry out ultrastructural analysis of the peripheral myelin in these zebrafish, as myelin structural defects such as myelin infolding are observed in mice containing CMT1c mutations (Lee et al., 2013), or onion bulb formation, which was detected in CMT1c patient nerve biopsy (Street et al., 2003). Furthermore, in the absence of an obvious phenotype, transcriptomics may provide insight into molecular changes that occur when these genes are lost, or any adaptive mechanisms that take place. Importantly, the expression of LITAF domain family members should be examined as they are likely candidates for genes which may be upregulated to compensate for loss of LITAF and CDIP1. LITAF KO may not give the same phenotype as CMT1c disease as the mutations may give rise to a dominant effect. Therefore, it would be interesting to knock-in patient mutations to generate a disease model.

Chapter 6: Discussion

Missense mutations in the highly conserved SLD of LITAF cause CMT1c disease (Street et al., 2003). Defective regulation of endocytic trafficking, in particular endocytic recycling, has been linked to several types of demyelinating CMT disease indicating that there is a common underlying pathophysiological mechanism (Lee et al., 2017). The lack of clarity of the role of LITAF in this pathway has hindered understanding of the molecular mechanism that results in CMT1c disease. In this thesis we have further explored the cellular role of LITAF, the effect of CMT1c mutations on LITAF function in cells, and generated a zebrafish model in which we have begun to examine the consequence of loss of LITAF *in vivo*.

6.1 Endocytic trafficking

LITAF has been implicated in several endocytic trafficking roles, such as functioning as a ubiquitin ligase adaptor (Eaton et al., 2011, Moshal et al., 2019, Turan et al., 2020), facilitating ubiquitin-mediated endocytic trafficking through interactions with ESCRTs (Lee et al., 2012), and more recently in regulation of the tubular recycling endosome (Moriwaki et al., 2018, Wunderley et al., 2021). In agreement with previous studies, the results presented here confirm a role for LITAF at early and late endosomes, and we showed that CMT1c mutations do not affect localisation to these compartments. We focused on the effect of CMT1c mutations on LITAF function at the tubular recycling endosome in the light of mounting evidence of dysregulation of this compartment in CMT disease (Roberts et al., 2010, Pietiainen et al., 2013, Kachhap et al., 2007, Stendel et al., 2010).

We showed for the first time that two CMT1c mutations have reduced localisation to Arf6-positive recycling tubules and that overexpression of these CMT1c mutants does not rescue the expansion of recycling tubules that occurs upon LITAF knockdown. Furthermore, there is a functional effect of expressing these mutants on CD98 trafficking, which is Arf6-dependent (Eyster et al., 2009). The importance of these findings in relation to CMT1c demyelinating disease is highlighted by the role of Arf6 in myelination. Knockdown of Arf6 inhibits myelination in oligodendrocyte-neuronal co-cultures (Miyamotoa et al., 2014) and loss of cytohesin-2, an Arf6-GEF, in mouse Schwann cells results in reduced myelin thickness in the sciatic nerve (Toni et al., 2015). Therefore, it is possible that loss of regulation of the Arf6 recycling pathway in cells expressing CMT1c mutants may lead to demyelination in CMT1c disease.

Although previous studies have suggested that LITAF has a role in trafficking of EGFR (Lee et al., 2012) and transferrin receptor (Moriwaki et al., 2018), these results have not been replicated in our lab (unpublished data, (Wunderley et al., 2021)). However, here we showed that trafficking of CD98 was altered in cells expressing CMT1c mutants. Association of LITAF with CD98 was also inferred by enrichment of both CD98 heavy and light chains in a BioID screen, which provides some degree of validation for the BioID results.

Several other cargo proteins were also identified by the BioID screen, notably β1 and β5 integrins, which were two of the most abundant hits. Interestingly, CD98 and β1 integrin have been associated previously (Cai et al., 2005, Miyamoto et al., 2003, Zent et al., 2000, Prager et al., 2007) and β1 integrin is also recycled by the Arf6-dependent pathway (Powelka et al., 2004). Several proteins associated with β1 integrin endocytosis and trafficking were significantly enriched in the BioID experiments, such as integrin-like kinase (ILK), EPS15 (Arjonen et al., 2012), Dab2 (Chao and Kunz, 2009), Numb (Nishimura and Kaibuchi, 2007), RabGAP1 (Samarelli et al., 2020), drebrin (Schiweck et al., 2021) and TPD54 (Larocque et al., 2020a). Identification of integrins was particularly interesting because these proteins are known to have a functional role in Schwann cells and during myelination (Feltri et al., 2002, Nodari et al., 2007, Pereira et al., 2009, Ness et al., 2013). Furthermore, another integrin, α6, was picked up in a BioID screen of another demyelinating CMT protein, SH3TC2 (Vijay et al., 2016). If CMT1c mutations result in dysregulated trafficking of integrins, then, again, this could provide a link to demyelination in Schwann cells.

Identification of a large number of membrane trafficking proteins by BioID using LITAF as a bait provides further support for the role of LITAF on endocytic compartments. Members of large protein complexes involved in endocytic trafficking such as ESCRTs, retromer, WASH, FERARI and GARP/EARP were identified as significant hits. ESCRTs function to direct ubiquitinated cargo into endosome subdomains and remodel the membrane to generate ILV's in MVBs. Retromer functions to sort specific cargo into tubular domains that extend from the sorting endosome for recycling. SNX3 and TBC1D5 were enriched in the BioID screen. SNX3 associates with retromer and may target it to the membrane by interacting with PI3P (Carlton et al., 2005, Harterink et al., 2011, Chandra et al., 2019), as well as binding

to specific cargo that are sorted by this complex (Harterink et al., 2011, Kovtun et al., 2018). TBC1D5 is a Rab7-GAP that interacts with the cargo selective complex of retromer (Seaman et al., 2009). SNX1 was another enriched protein, which is a component of ESCPE-1 that also functions alongside retromer to sort cargo from endosomes to the *trans*-Golgi network (Simonetti et al., 2019, Evans et al., 2020).

Retromer associates with the WASH complex, which promotes actin nucleation and polymerisation by activating Arp2/3 (Simonetti and Cullen, 2019, Derivery et al., 2012, Gomez and Billadeau, 2009) and also regulates endosomal fission (Derivery et al., 2009). This association with the actin cytoskeleton is thought to provide the mechanical force required for biogenesis of vesicles. Generation and stabilisation of tubular membranes requires dynamic rearrangement of the actin and microtubule cytoskeleton (Anitei and Hoflack, 2012, Puthenveedu et al., 2010). Furthermore, there is a requirement for membrane curvature generation and LITAF may have a function in this process (see below). We found that LITAF may be proximal to several cytoskeleton regulating proteins including the WASH complex protein FAM21A (Gomez and Billadeau, 2009), and this may be consistent with coupling of membrane curvature generation to the cytoskeleton. Another WASH complex protein, strumpellin, was only identified in samples with CMT1c LITAF mutants and not in the WT LITAF sample, but the exact function of this protein in the WASH complex is not clear (Freeman et al., 2013, Tyrrell et al., 2016).

Another way of sorting cargo at recycling endosomes is by a ‘kiss and run’ mechanism facilitated by the FERARI complex. FERARI co-ordinates fusion of recycling endosomes with sorting endosomes, so that cargo can be transferred into the recycling endosome portion. The FERARI complex then mediates scission to separate the recycling endosome from the sorting endosome so it can be transported back to the plasma membrane (Solinger et al., 2020). Rab11FIP5 and EHD1 are FERARI complex members identified in our BioID screen. Recycling vesicles are targeted to their acceptor compartments by tethering complexes such as GARP and EARP, which interact with SNAREs on the Golgi and plasma membrane respectively. VPS51 is a component of GARP and EARP and was identified by BioID. SNAREs including SNAP23 and SNAP29, as well as vesicle associated proteins VAMP3 and VAMP5,

were also identified as proximal proteins to LITAF. These proteins function in the fusion of vesicles with their specific target compartment.

There is interplay between machinery that directs cargo towards degradation and complexes that sort cargo to recycling tubules. The proximity of LITAF to these complexes infers that LITAF may have a role in several of these processes and might be placed at the junction of these sorting and trafficking events. We identified a novel association between LITAF and TPD54, but the functional significance of this association is still unknown. Similar to our hypothesis that LITAF is likely to cycle between endocytic compartments, TPD54 localises to intracellular nanovesicles that are proposed to be carriers that traffic between organelles (Larocque et al., 2020a). Additionally, TPD54 is involved in trafficking of integrin β1 and required for migration of cells in a 3D matrix (Larocque et al., 2020b). The BioID screen revealed many membrane trafficking proteins as well as adhesion proteins and regulators of the actin cytoskeleton but the interaction of LITAF with these proteins must be validated before any functional information can be inferred.

6.2 Membrane association

In this study we showed that two patient CMT1c mutations affect the membrane integration of LITAF, but the reduction was not as severe as it was for the C96A mutation that abolishes the zinc finger. The P135S and V144M mutations lie at the C-terminal end of the membrane insertion region and could plausibly affect the conformation of this region. One possibility is that the CMT1c mutations affect LITAF structure so that it is unable to insert into very highly curved membranes, such as recycling tubules, but still competent to insert into less curved membranes, such as early endosomes. This would explain the effect of CMT1c mutations on LITAF localisation as well as membrane integration. *In vitro* experiments looking at incorporation of LITAF mutants into liposomes would address whether the mutations have the same curvature sensitivity as WT LITAF (Wunderley et al., 2021). Furthermore, it is possible that LITAF regulates the morphology of the recycling compartment by supporting the scission of tubules via its association with EHD1. LITAF containing CMT1c mutations was unable to perform this function which suggests that there could be scission defect.

LITAF binds to phosphatidylinositol-4-phosphate (PI4P), which is enriched on recycling tubules (Moriwaki et al., 2018), and this may contribute towards the localisation of the protein to recycling tubule membranes. The BioID screen identified two palmitoyltransferases ZDHHC20 and ZDHHC5. ZDHHC20 and ZDHHC5 were present in all samples but were only enriched in the LITAF V144M bait sample. A search using the SwissPalm S-palmitoylation database (Blanc et al., 2019) shows that LITAF (Thinon et al., 2018) and CDIP1 (Dowal et al., 2011) have both been identified by proteomic screens of palmitoylated proteins. LITAF and CDIP1 both have several predicted sites and LITAF has a palmitoyl-proteome site at C137 (Thinon et al., 2018). Palmitoylation could also contribute to the membrane recruitment of LITAF. Mutation of two conserved cysteine residues (which are not in the CXXC motifs) in the SLD of LITAF resulted in loss of tubule labelling; instead they labelled endosomes (Wunderley et al., 2021). One of these sites is a predicted palmitoylation site but this has not been shown experimentally. This effect is similar to what was observed with CMT1c mutations in the SLD. The effect of palmitoylation on LITAF localisation could be tested using a protein palmitoylation inhibitor such as 2-Br-palmitate as well as mutation of candidate sites. Additionally, the effect of patient mutations on palmitoylation should be assessed as this could affect the efficiency of membrane integration. Palmitoylation increases the membrane affinity and can stabilise the oligomerisation of a protein and is a feature of hairpin anchor proteins such as caveolin (Monier et al., 1996) and flotillin (Morrow et al., 2002). Palmitoylation of LITAF could have a similar effect and be required for correct cellular function.

Solution of the structure of full-length LITAF is precluded by the highly hydrophobic membrane insertion region. This core hydrophobic region may form a short amphipathic helix or it may form a hairpin-like structure but the structure is still not defined (Qin et al., 2016). In both cases, an asymmetric insertion into the lipid bilayer forms a wedge which deforms the membrane and generates curvature (Kozlov et al., 2014). One model for the induction of membrane curvature by LITAF is a mechanism similar to that employed by flotillin (Morrow et al., 2002), caveolin (Monier et al., 1995) and ER-shaping reticulons (Hu et al., 2008). These proteins contain a hairpin anchor and form oligomers. LITAF is able to self-associate (Lee et al., 2012) and the SLD may form a zinc ion stabilised hairpin where the hydrophobic region inserts into the membrane (Qin et al., 2016).

Another possibility is that this hydrophobic region forms an amphipathic helix similar to epsin N-terminal homology (ENTH) domain proteins (Ford et al., 2002). The predicted structure by Ho *et al* (2016) suggests that this region forms a very shallow amphipathic helix which may induce membrane curvature (Campelo et al., 2008, Kozlov et al., 2014). However, this region only has a small dipole and is very hydrophobic. It might not be sufficiently strong an amphipathic helix to direct membrane integration and membrane curvature alone, but the addition of the CXXC knuckle clamp (Qin et al., 2016) and self-association of LITAF (Lee et al., 2012) might support the interaction of the predicted amphipathic helix with the membrane and thus also be requisites for inducing membrane curvature. A very shallow insertion might even augment the membrane curvature generation (Kozlov et al., 2014).

It has been proposed that LITAF may support the scission of recycling tubules by associating with EHD1 (Wunderley et al., 2021). The membrane insertion region could destabilise the membrane and contribute to scission, similar to amphipathic helix containing Sar1 (Hariri et al., 2014). Many proteins that contain amphipathic helices have been linked to membrane fission events (Zhukovsky et al., 2019), and LITAF may also function in this way. Further work is required to elucidate the nature of membrane integration of LITAF and the configuration of the membrane integration region and the effect of mutations on the structure of this region.

6.3 Loss of function or gain of function mechanism

One of our aims was to investigate the consequence of loss of LITAF and CDIP1 *in vivo* to shed light on the function of these proteins in a physiological context, assess the degree of functional redundancy between these proteins and whether the disease results from a loss of function. This study was complicated by the presence of multiple LITAF domain family members in zebrafish. We found that acute loss of either LITAF or CDIP1 proteins in F0 null zebrafish larvae as well as stable individual loss of these proteins in homozygous mutant adults did not adversely affect gross development or growth, similar to LITAF KO mice (Somandin et al., 2012, Zhu et al., 2013) and CDIP1 KO mice (Namba et al., 2013). However, it is possible that the function of LITAF and CDIP1 may be able to compensate for each other as they are likely to have overlapping functions. Therefore, we also generated zebrafish lacking both LITAF and CDIP1 in order to determine whether these proteins have redundancy. These double

knock-out zebrafish did not have any developmental or obvious phenotype, similar to the single LITAF or CDIP1 knock-out zebrafish. However, we were unable to further investigate any possible cellular phenotypes in zebrafish embryos due to a lack of homozygous knock-out females and so we did not carry out Schwann cell and motor neuron staining and further analysis of movement and other possible phenotypes.

There are several possible reasons why LITAF and CDIP1 knock-out zebrafish do not exhibit a phenotype. Zebrafish have several other LITAF domain proteins, which could have a compensatory effect in this organism, potentially even in the double knock-out background. Additionally, LITAF and CDIP1 single or double knock-out zebrafish may develop a phenotype over time, as any cellular changes may take time to manifest as a deleterious organismal phenotype, as is seen in the progressive nature of CMT1c disease. Alternatively, LITAF and CDIP1 may not have an essential function in this organism. We attempted to knock in a CMT1c mutation into zebrafish LITAF using a base editing version of Cas9 (Zhang et al., 2017) but our efforts were unsuccessful. Technical advances may make this aim more achievable, and this could provide a useful model of CMT1c disease in which further studies could be done.

It is possible that CMT1c occurs by a loss of function mechanism due to haploinsufficiency or a dominant negative effect or pathogenesis could occur due to a toxic gain of function effect. Loss of function due to reduced protein levels and haploinsufficiency is unlikely as the abundance of LITAF in patient cells and WT cells is similar (Street et al., 2003). Additionally, mice overexpressing LITAF W116G in the presence of endogenous WT LITAF developed structural myelin defects (Lee et al., 2013), which also argues against haploinsufficiency. So far it has been difficult to distinguish between a dominant negative effect and a toxic gain of function effect.

Some of the data from mouse models indicate that CMT1c disease may occur by a toxic gain of function mechanism as LITAF knock-out mice did not have any deleterious effects (Somandin et al., 2012). In addition, LITAF knock-out and LITAF T115N had distinct ultrastructural effects in cells from transgenic mice. Cells lacking LITAF had multilamellar cisternal compartments while cells containing LITAF T115N had vacuolated structures (Zhu et al., 2013). One possibility suggested by Lee *et al* (2012) is that mutated LITAF may be able to sequester ESCRT-0 components in the cytosol, which would be a toxic gain of function effect.

This is in contrast to a recent report which concluded that CMT1c is likely to result from a dominant negative loss of function effect as fibroblasts depleted of LITAF and patient fibroblasts containing LITAF T115N had the same vacuolated endosome phenotype (Edgar et al., 2020). We showed that CMT1c mutant LITAF could not rescue the recycling tubule expansion phenotype, which further supports a loss of function mechanism. Additionally, overexpressed CMT1c mutants in a WT LITAF background were unable to regulate trafficking of CD98 to recycling tubules which indicates a dominant negative effect or a toxic gain of function. LITAF is able oligomerise (Lee et al., 2012), hence mutant LITAF might instead sequester wild-type LITAF away from its site of action. This results in a dominant negative loss of function effect as the mutant protein negatively affects the function of the WT protein leading to overall loss of function. The data presented here point to CMT1c mutations sequestering WT LITAF away from recycling tubules where its function is required for correct trafficking of specific cargo.

LITAF may have several functions in different endosomal compartments such that CMT1c mutations may cause a loss of function in one place (such as recycling endosomes), while functioning normally in a different context (i.e. on endosomes), which could alter the homeostasis within this pathway. Thus, CMT1c disease may result from a combination of dominant negative effects and toxic gain of function.

6.4 Future Directions

One of the major questions that remains to be addressed is why Schwann cells are uniquely susceptible to dysregulated LITAF function when this protein is ubiquitously expressed. Several explanations have been proposed, such as the requirement for polarised delivery of myelin proteins to the apical surface for myelin sheath formation (Pereira et al., 2012). Alternatively, the balance of trafficking of myelin proteins and their turnover requires a delicate homeostasis and Schwann cells are particularly vulnerable to any defects in this, which is highlighted by the overabundance of PMP22 which causes the majority of CMT1 disease (Azzedine et al., 2012). Potentially the ability of CDIP1 to compensate for LITAF function in CMT1c disease in this specialised cell type is impaired so Schwann cells are disproportionately affected. This could be due to CDIP1 not being expressed in this cell type, or the specific function of LITAF in Schwann cells cannot be compensated for by CDIP1. Therefore, future

studies on the effect of CMT1c mutations on Schwann cell-specific trafficking processes will be well positioned to address this outstanding question. There are some potential protein interactions with LITAF which may be implicated in disease, such as the association with β1 integrin and the Arf6 recycling pathway, which should be investigated further in Schwann cells. The effect of CMT1c mutations on LITAF function in Schwann cells would provide more insight into the pathophysiology of CMT1c disease.

Bibliography

ACCONCIA, F., SIGISMUND, S. & POLO, S. 2009. Ubiquitin in trafficking: The network at work. *Experimental Cell Research,* 315**,** 1610-1618.

ADAMSON, K. I., SHERIDAN, E. & GRIERSON, A. J. 2018. Use of zebrafish models to investigate rare human disease. *Journal of Medical Genetics,* 55**,** 641-649.

ADELL, M. A. Y., VOGEL, G. F., PAKDEL, M., MULLER, M., LINDNER, H., HESS, M. W. & TEIS, D. 2014. Coordinated binding of Vps4 to ESCRT-III drives membrane neck constriction during MVB vesicle formation. *Journal of Cell Biology,* 205**,** 33-49.

AGROMAYOR, M., CARLTON, J. G., PHELAN, J. P., MATTHEWS, D. R., CARLIN, L. M., AMEER-BEG, S., BOWERS, K. & MARTIN-SERRANO, J. 2009. Essential Role of hIST1 in Cytokinesis. *Molecular Biology of the Cell,* 20**,** 1374-1387.

AGROMAYOR, M., SOLER, N., CABALLE, A., KUECK, T., FREUND, S. M., ALLEN, M. D., BYCROFT, M., PERISIC, O., YE, Y., MCDONALD, B., SCHEEL, H., HOFMANN, K., NEIL, S. J. D., MARTIN-SERRANO, J. & WILLIAMS, R. L. 2012. The UBAP1 Subunit of ESCRT-I Interacts with Ubiquitin via a SOUBA Domain. *Structure,* 20**,** 414-428.

ALI, N., ZHANG, L., TAYLOR, S., MIRONOV, A., URBE, S. & WOODMAN, P. 2013. Recruitment of UBPY and ESCRT Exchange Drive HD-PTP-Dependent Sorting of EGFR to the MVB. *Current Biology,* 23**,** 453-461.

ALLISON, R., LUMB, J. H., FASSIER, C., CONNELL, J. W., TEN MARTIN, D., SEAMAN, M. N. J., HAZAN, J. & REID, E. 2013. An ESCRT-spastin interaction promotes fission of recycling tubules from the endosome. *Journal of Cell Biology,* 202**,** 527-543.

ANITEI, M. & HOFLACK, B. 2012. Bridging membrane and cytoskeleton dynamics in the secretory and endocytic pathways. *Nature Cell Biology,* 14**,** 11-19.

ARIGHI, C. N., HARTNELL, L. M., AGUILAR, R. C., HAFT, C. R. & BONIFACINO, J. S. 2004. Role of the mammalian retromer in sorting of the cation-independent mannose 6-phosphate receptor. *Journal of Cell Biology,* 165**,** 123-133.

ARJONEN, A., ALANKO, J., VELTEL, S. & IVASKA, J. 2012. Distinct Recycling of Active and Inactive ss 1 Integrins. *Traffic,* 13**,** 610-625.

ASAO, H., SASAKI, Y., ARITA, T., TANAKA, N., ENDO, K., KASAI, H., TAKESHITA, T., ENDO, Y., FUJITA, T. & SUGAMURA, K. 1997. Hrs is associated with STAM, a signal-transducing adaptor molecule - Its suppressive effect on cytokine-induced cell growth. *Journal of Biological Chemistry,* 272**,** 32785-32791.

AZZEDINE, H., BOLINO, A., TAIEB, T., BIROUK, N., DI DUCA, M., BOUHOUCHE, A., BENAMOU, S., MRABET, A., HAMMADOUCHE, T., CHKILI, T., GOUIDER, R., RAVAZZOLO, R., BRICE, A., LAPORTE, J. & LEGUERN, E. 2003. Mutations in MTMR13, a new pseudophosphatase homologue of MTMR2 and Sbf1, in two families with an autosomal recessive demyelinating form of Charcot-Marie-Tooth disease associated with early-onset glaucoma. *American Journal of Human Genetics,* 72**,** 1141-1153.

AZZEDINE, H., SENDEREK, J., RIVOLTA, C. & CHRAST, R. 2012. Molecular Genetics of Charcot-Marie-Tooth Disease: From Genes to Genomes. *Molecular Syndromology,* 3**,** 204–214.

BABST, M., KATZMANN, D. J., ESTEPA-SABAL, E. J., MEERLOO, T. & EMR, S. D. 2002a. ESCRT-III: An endosome-associated heterooligomeric protein complex required for MVB sorting. *Developmental Cell,* 3**,** 271-282.

BABST, M., KATZMANN, D. J., SNYDER, W. B., WENDLAND, B. & EMR, S. D. 2002b. Endosome-associated complex, ESCRT-II, recruits transport machinery for protein sorting at the multivesicular body. *Developmental Cell,* 3**,** 283-289.

BABST, M., ODORIZZI, G., ESTEPA, E. J. & EMR, S. D. 2000. Mammalian tumor susceptibility gene 101 (TSG101) and the yeast homologue, Vps23p, both function in late endosomal trafficking. *Traffic,* 1**,** 248-258.

BABST, M., WENDLAND, B., ESTEPA, E. J. & EMR, S. D. 1998. The Vps4p AAA ATPase regulates membrane association of a Vps protein complex required for normal endosome function. *Embo Journal,* 17**,** 2982-2993.

BACHE, K. G., SLAGSVOLD, T., CABEZAS, A., ROSENDAL, K. R., RAIBORG, C. & STENMARK, H. 2004. The growth-regulatory protein HCRP1/hVps37A is a subunit of mammalian ESCRT-I and mediates receptor down-regulation. *Molecular Biology of the Cell,* 15**,** 4337-4346.

BAETS, J., DE JONGHE, P. & TIMMERMAN, V. 2014. Recent advances in Charcot-Marie-Tooth disease. *Current Opinion in Neurology,* 27**,** 532-540.

BAIETTI, M. F., ZHANG, Z., MORTIER, E., MELCHIOR, A., DEGEEST, G., GEERAERTS, A., IVARSSON, Y., DEPOORTERE, F., COOMANS, C., VERMEIREN, E., ZIMMERMANN, P. & DAVID, G. 2012. Syndecan-syntenin-ALIX regulates the biogenesis of exosomes. *Nature Cell Biology,* 14**,** 677-685.

BAKOWSKA, J. C., JENKINS, R., PENDLETON, J. & BLACKSTONE, C. 2005. The Troyer syndrome (SPG20) protein spartin interacts with Eps15. *Biochemical and Biophysical Research Communications,* 334**,** 1042-1048.

BAKOWSKA, J. C., JUPILLE, H., FATHEDDIN, P., PUERTOLLANO, R. & BLACKSTONE, C. 2007. Troyer syndrome protein spartin is mono-ubiquitinated and functions in EGF receptor trafficking. *Molecular Biology of the Cell,* 18**,** 1683-1692.

BARRETO, L., OLIVEIRA, F. S., NUNES, P. S., COSTA, I., GARCEZ, C. A., GOES, G. M., NEVES, E. L. A., QUINTANS, J. D. S. & ARAUJO, A. A. D. 2016. Epidemiologic Study of Charcot-Marie-Tooth Disease: A Systematic Review. *Neuroepidemiology,* 46**,** 157-165.

BENNETT, C. L., SHIRK, A. J., HUYNH, H. M., STREET, V. A., NELIS, E., VAN MALDERGEM, L., DE JONGHE, P., JORDANOVA, A., GUERGUELTCHEVA, V., TOURNEV, I., VAN DEN BERGH, P., SEEMAN, P., MAZANEC, R., PROCHAZKA, T., KREMENSKY, I., HABERLOVA, J., WEISS, M. D., TIMMERMAN, V., BIRD, T. D. & CHANCE, P. F. 2004. SIMPLE mutation in demyelinating neuropathy and distribution in sciatic nerve. *Annals of Neurology,* 55**,** 713-720.

BERGER, P., BONNEICK, S., WILLI, S., WYMANN, M. & SUTER, U. 2002a. Loss of phosphatase activity in myotubularin-related protein 2 is associated with Charcot-Marie-Tooth disease type 4B1. *Human Molecular Genetics,* 11**,** 1569-1579.

BERGER, P., YOUNG, P. & SUTER, U. 2002b. Molecular cell biology of Charcot-Marie-Tooth disease. *Neurogenetics,* 4**,** 1-15.

BERGOFFEN, J., SCHERER, S. S., WANG, S., SCOTT, M. O., BONE, L. J., PAUL, D. L., CHEN, K., LENSCH, M. W., CHANCE, P. F. & FISCHBECK, K. H. 1993. CONNEXIN MUTATIONS IN X-LINKED CHARCOT-MARIE-TOOTH DISEASE. *Science,* 262**,** 2039-2042.

BHALLA, K., EYRE, H. J., WHITMORE, S. A., SUTHERLAND, G. R. & CALLEN, D. F. 1999. C160rf5, a novel proline-rich gene at 16p13.3, is highly expressed in the brain. *Journal of Human Genetics,* 44**,** 383-387.

BHARADWAJ, R., CUNNINGHAM, K. M., ZHANG, K. & LLOYD, T. E. 2016. FIG4 regulates lysosome membrane homeostasis independent of phosphatase function. *Human Molecular Genetics,* 25**,** 681-692.

BISHOP, N. & WOODMAN, P. 2001. TSG101/mammalian VPS23 and mammalian VPS28 interact directly and are recruited to VPS4-induced endosomes. *Journal of Biological Chemistry,* 276**,** 11735-11742.

BLANC, M., DAVID, F. P. A. & VAN DER GOOT, F. G. 2019. SwissPalm 2: Protein S-Palmitoylation Database. *Protein Lipidation: Methods and Protocols,* 2009**,** 203-214.

BOLINO, A., MUGLIA, M., CONFORTI, F. L., LEGUERN, E., SALIH, M. A. M., GEORGIOU, D. M., CHRISTODOULOU, K., HAUSMANOWA-PETRUSEWICZ, I., MANDICH, P., SCHENONE, A., GAMBARDELLA, A., BONO, F., QUATTRONE, A., DEVOTO, M. & MONACO, A. P. 2000. Charcot-Marie-Tooth type 4B is caused by mutations in the gene encoding myotubularin-related protein-2. *Nature Genetics,* 25**,** 17-19.

BONIFACINO, J. S. & HURLEY, J. H. 2008. Retromer. *Current Opinion in Cell Biology,* 20**,** 427-436.

BONIFACINO, J. S. & TRAUB, L. M. 2003. Signals for sorting of transmembrane proteins to endosomes and lysosomes. *Annual Review of Biochemistry,* 72**,** 395-447.

BRAGATO, C., GAUDENZI, G., BLASEVICH, F., PAVESI, G., MAGGI, L., GIUNTA, M., COTELLI, F. & MORA, M. 2016. Zebrafish as a Model to Investigate Dynamin 2-Related Diseases. *Scientific Reports,* 6.

BRAUN, A., PINYOL, R., DAHLHAUS, R., KOCH, D., FONAREV, P., GRANT, B. D., KESSELS, M. M. & QUALMANN, B. 2005. EHD proteins associate with syndapin I and II and such interactions play a crucial role in endosomal recycling. *Molecular Biology of the Cell,* 16**,** 3642-3658.

BROSAMLE, C. & HALPERN, M. E. 2002. Characterization of myelination in the developing zebrafish. *Glia,* 39**,** 47-57.

BROWN, L., ONGUSAHA, P. P., KIM, H. G., NUTI, S., MANDINOVA, A., LEE, J. W., KHOSRAVI-FAR, R., AARONSON, S. A. & LEE, S. W. 2007. CDIP, a novel pro-apoptotic gene, regulates TNF alpha-mediated apoptosis in a p53-dependent manner. *Embo Journal,* 26**,** 3410-3422.

BROWN-ENDRES, L., SCHOENFELD, D., TIAN, F., KIM, H. G., NAMBA, T., MUNOZ-FONTELA, C., MANDINOVA, A., AARONSON, S. A. & LEE, S. W. 2012. Expression of the p53 Target CDIP Correlates with Sensitivity to TNF alpha-Induced Apoptosis in Cancer Cells. *Cancer Research,* 72**,** 2373-2382.

BUCHKOVICH, N. J., HENNE, W. M., TANG, S. G. & EMR, S. D. 2013. Essential N-Terminal Insertion Motif Anchors the ESCRT-III Filament during MVB Vesicle Formation. *Developmental Cell,* 27**,** 201-214.

BUCKLEY, C. E., GOLDSMITH, P. & FRANKLIN, R. J. M. 2008. Zebrafish myelination: a transparent model for remyelination? *Disease Models & Mechanisms,* 1**,** 221-228.

BURD, C. & CULLEN, P. J. 2014. Retromer: A Master Conductor of Endosome Sorting. *Cold Spring Harbor Perspectives in Biology,* 6.

CAI, B. S., GIRIDHARAN, S. S. P., ZHANG, J., SAXENA, S., BAHL, K., SCHMIDT, J. A., SORGEN, P. L., GUO, W., NASLAVSKY, N. & CAPLAN, S. 2013. Differential Roles of C-terminal Eps15 Homology Domain Proteins as Vesiculators and Tubulators of Recycling Endosomes. *Journal of Biological Chemistry,* 288**,** 30172-30180.

CAI, S., BULUS, N., FONSECA-SIESSER, P. M., CHEN, D., HANKS, S. K., POZZI, A. & ZENT, R. 2005. CD98 modulates integrin beta 1 function in polarized epithelial cells. *Journal of Cell Science,* 118**,** 889-899.

CAMPELO, F., MCMAHON, H. T. & KOZLOV, M. M. 2008. The hydrophobic insertion mechanism of membrane curvature generation by proteins. *Biophysical Journal,* 95**,** 2325-2339.

CARLTON, J., BUJNY, M., RUTHERFORD, A. & CULLEN, P. 2005. Sorting nexins - Unifying trends and new perspectives. *Traffic,* 6**,** 75-82.

CASWELL, P. & NORMAN, J. 2008. Endocytic transport of integrins during cell migration and invasion. *Trends in Cell Biology,* 18**,** 257-263.

CHANDRA, M., CHIN, Y. K. Y., MAS, C., FEATHERS, J. R., PAUL, B., DATTA, S., CHEN, K. E., JIA, X. Y., YANG, Z., NORWOOD, S. J., MOHANTY, B., BUGARCIC, A., TEASDALE, R. D., HENNE, W. M., MOBLI, M. & COLLINS, B. M. 2019. Classification of the human phox homology (PX) domains based on their phosphoinositide binding specificities. *Nature Communications,* 10.

CHAO, W. T. & KUNZ, J. 2009. Focal adhesion disassembly requires clathrin-dependent endocytosis of integrins. *Febs Letters,* 583**,** 1337-1343.

CHEN, G., ZHANG, Z. J., WEI, Z. Y., CHENG, Q., LI, X., LI, W., DUAN, S. M. & GU, X. S. 2012. Lysosomal exocytosis in Schwann cells contributes to axon remyelination. *Glia,* 60**,** 295-305.

CHEN, K., TIAN, J., WANG, J., JIA, Z., ZHANG, Q., HUANG, W., ZHAO, X., GAO, Z., GAO, Q. & ZOU, J. 2021. Lipopolysaccharide-induced TNFα factor (LITAF) promotes inflammatory responses and activates apoptosis in zebrafish Danio rerio. *Gene,* 780**,** 145487.

CHEN, K.-E., HEALY, M. D. & COLLINS, B. M. 2019. Towards a molecular understanding of endosomal trafficking by Retromer and Retriever. *Traffic,* 20**,** 465-478.

CHEN, Y. S., CHEN, N. N., QIN, X. W., MI, S., HE, J., LIN, Y. F., GAO, M. S., WENG, S. P., GUO, C. J. & HE, J. G. 2016. Tiger frog virus ORF080L protein interacts with LITAF and impairs EGF-induced EGFR degradation. *Virus Research,* 217**,** 133-142.

CHIES, R., NOBBIO, L., EDOMI, P., SCHENONE, A., SCHNEIDER, C. & BRANCOLINI, C. 2003. Alterations in the Arf6-regulated plasma membrane endosomal recycling pathway in cells overexpressing the tetraspan protein Gas3/PMP22. *Journal of Cell Science,* 116**,** 987-999.

CHRISTOFORIDIS, S., MIACZYNSKA, M., ASHMAN, K., WILM, M., ZHAO, L. Y., YIP, S. C., WATERFIELD, M. D., BACKER, J. M. & ZERIAL, M. 1999. Phosphatidylinositol-3-OH kinases are Rab5 effectors. *Nature Cell Biology,* 1**,** 249-252.

CIOTTI, P., LUIGETTI, M., GEROLDI, A., CAPPONI, S., PEZZINI, I., GULLI, R., PAZZAGLIA, C., PADUA, L., MASSA, R., MANDICH, P. & BELLONE, E. 2014. A novel LITAF/SIMPLE mutation within a family with a demyelinating form of Charcot-Marie-Tooth disease. *Journal of the Neurological Sciences,* 343**,** 183-186.

CLAIRFEUILLE, T., MAS, C., CHAN, A. S. M., YANG, Z., TELLO-LAFOZ, M., CHANDRA, M., WIDAGDO, J., KERR, M. C., PAUL, B., MERIDA, I., TEASDALE, R. D., PAVLOS, N. J., ANGGONO, V. & COLLINS, B. M. 2016. A molecular code for endosomal recycling of phosphorylated cargos by the SNX27-retromer complex. *Nature Structural & Molecular Biology,* 23**,** 921-932.

COBANOGLU, G., OZANSOY, M. & BASAK, A. N. 2012. Are alsin and spartin novel interaction partners? *Biochemical and Biophysical Research Communications,* 427**,** 1-4.

COLLINS, B. M., NORWOOD, S. J., KERR, M. C., MAHONY, D., SEAMAN, M. N. J., TEASDALE, R. D. & OWEN, D. J. 2008. Structure of Vps26B and mapping of its interaction with the retromer protein complex. *Traffic,* 9**,** 366-379.

COX, J., HEIN, M. Y., LUBER, C. A., PARON, I., NAGARAJ, N. & MANN, M. 2014. Accurate Proteome-wide Label-free Quantification by Delayed Normalization and Maximal Peptide Ratio Extraction, Termed MaxLFQ. *Molecular & Cellular Proteomics,* 13**,** 2513-2526.

COX, J. & MANN, M. 2008. MaxQuant enables high peptide identification rates, individualized p.p.b.-range mass accuracies and proteome-wide protein quantification. *Nature Biotechnology,* 26**,** 1367-1372.

CULLEN, P. & STEINBERG, F. 2018. To degrade or not to degrade: mechanisms and significance of endocytic recycling. *Nat Rev Mol Cell Biol,* 19**,** 679-696.

DAUMKE, O., LUNDMARK, R., VALLIS, Y., MARTENS, S., BUTLER, P. J. G. & MCMAHON, H. T. 2007. Architectural and mechanistic insights into an EHD ATPase involved in membrane remodelling. *Nature,* 449**,** 923-U15.

DEO, R., KUSHWAH, M. S., KAMERKAR, S. C., KADAM, N. Y., DAR, S., BABU, K., SRIVASTAVA, A. & PUCADYIL, T. J. 2018. ATP-dependent membrane remodeling links EHD1 functions to endocytic recycling. *Nature Communications,* 9.

DERIVERY, E., HELFER, E., HENRIOT, V. & GAUTREAU, A. 2012. Actin Polymerization Controls the Organization of WASH Domains at the Surface of Endosomes. *Plos One,* 7.

DERIVERY, E., SOUSA, C., GAUTIER, J. J., LOMBARD, B., LOEW, D. & GAUTREAU, A. 2009. The Arp2/3 Activator WASH Controls the Fission of Endosomes through a Large Multiprotein Complex. *Developmental Cell,* 17**,** 712-723.

DIKIC, I., WAKATSUKI, S. & WALTERS, K. J. 2009. Ubiquitin-binding domains - from structures to functions. *Nature Reviews Molecular Cell Biology,* 10**,** 659-671.

DIVINCENZO, C., ELZINGA, C. D., MEDEIROS, A. C., KARBASSI, I., JONES, J. R., EVANS, M. C., BRAASTAD, C. D., BISHOP, C. M., JAREMKO, M., WANG, Z., LIAQUAT, K., HOFFMAN, C. A., YORK, M. D., BATISH, S. D., LUPSKI, J. R. & HIGGINS, J. J. 2014. The allelic spectrum of Charcot–Marie–Tooth disease in over 17,000 individuals with neuropathy. *Molecular Genetics & Genomic Medicine,* 2**,** 522–529.

DONALDSON, J. G. & JACKSON, C. L. 2011. ARF family G proteins and their regulators: roles in membrane transport, development and disease. *Nature Reviews Molecular Cell Biology,* 12**,** 362-375.

DONCHEVA, N. T., MORRIS, J. H., GORODKIN, J. & JENSEN, L. J. 2019. Cytoscape StringApp: Network Analysis and Visualization of Proteomics Data. *Journal of Proteome Research,* 18**,** 623-632.

DOVE, K. K. & KLEVIT, R. E. 2017. RING-Between-RING E3 Ligases: Emerging Themes amid the Variations. *Journal of Molecular Biology,* 429**,** 3363-3375.

DOWAL, L., YANG, W., FREEMAN, M. R., STEEN, H. & FLAUMENHAFT, R. 2011. Proteomic analysis of palmitoylated platelet proteins. *Blood,* 118**,** E62-E73.

EASTMAN, S. W., MARTIN-SERRANO, J., CHUNG, W., ZANG, T. & BIENIASZ, P. D. 2005. Identification of human VPS37C, a component of endosomal sorting complex

required for transport-I important for viral budding. *Journal of Biological Chemistry,* 280**,** 628-636.

EATON, H. E., DESROCHERS, G., DRORY, S. B., METCALF, J., ANGERS, A. & BRUNETTI, C. R. 2011. SIMPLE/LITAF Expression Induces the Translocation of the Ubiquitin Ligase Itch towards the Lysosomal Compartments. *Plos One,* 6.

EATON, H. E., LACERDA, A. F., DESROCHERS, G., METCALF, J., ANGERS, A. & BRUNETTI, C. R. 2013. Cellular LITAF Interacts with Frog Virus 3 75L Protein and Alters Its Subcellular Localization. *Journal of Virology,* 87**,** 716-723.

EATON, H. E., METCALF, J., LACERDA, A. F. & BRUNETTI, C. R. 2012. Accumulation of Endogenous LITAF in Aggresomes. *Plos One,* 7.

EDGAR, J. R., HO, A. K., LAURA, M., HORVATH, R., REILLY, M. M., LUZIO, J. P. & ROBERTS, R. C. 2020. A dysfunctional endolysosomal pathway common to two sub-types of demyelinating Charcot-Marie-Tooth disease. *Acta Neuropathologica Communications,* 8.

EDWARDS, T. L., CLOWES, V. E., TSANG, H. T. H., CONNELL, J. W., SANDERSON, C. M., LUZIO, J. P. & REID, E. 2009. Endogenous spartin (SPG20) is recruited to endosomes and lipid droplets and interacts with the ubiquitin E3 ligases AIP4 and AIP5. *Biochemical Journal,* 423**,** 31-39.

EL-GEBALI, S., MISTRY, J., BATEMAN, A., EDDY, S. R., LUCIANI, A., POTTER, S. C., QURESHI, M., RICHARDSON, L. J., SALAZAR, G. A., SMART, A., SONNHAMMER, E. L. L., HIRSH, L., PALADIN, L., PIOVESAN, D., TOSATTO, S. C. E. & FINN, R. D. 2019. The Pfam protein families database in 2019. *Nucleic Acids Research,* 47**,** D427-D432.

EVANS, A. J., DALY, J. L., ANUAR, A. N. K., SIMONETTI, B. & CULLEN, P. J. 2020. Acute inactivation of retromer and ESCPE-1 leads to time-resolved defects in endosomal cargo sorting. *Journal of Cell Science,* 133.

EVERETT, L. M., LI, A. X., DEVARAJU, G., CAPERELLGRANT, A. & BIGSBY, R. M. 1997. A novel estrogen-enhanced transcript identified in the rat uterus by differential display. *Endocrinology,* 138**,** 3836-3841.

EYSTER, C. A., HIGGINSON, J. D., HUEBNER, R., PORAT-SHLIOM, N., WEIGERT, R., WU, W. W., SHEN, R. F. & DONALDSON, J. G. 2009. Discovery of New Cargo Proteins that Enter Cells through Clathrin-Independent Endocytosis. *Traffic,* 10**,** 590-599.

FELTRI, M. L., PORTA, D. G., PREVITALI, S. C., NODARI, A., MIGLIAVACCA, B., CASSETTI, A., LITTLEWOOD-EVANS, A., REICHARDT, L. F., MESSING, A., QUATTRINI, A., MUELLER, U. & WRABETZ, L. 2002. Conditional disruption of beta 1 integrin in Schwann cells impedes interactions with axons. *Journal of Cell Biology,* 156**,** 199-209.

FORD, M. G. J., MILLS, I. G., PETER, B. J., VALLIS, Y., PRAEFCKE, G. J. K., EVANS, P. R. & MCMAHON, H. T. 2002. Curvature of clathrin-coated pits driven by epsin. *Nature,* 419**,** 361-366.

FRANKEL, E. B. & AUDHYA, A. 2018. ESCRT-dependent cargo sorting at multivesicular endosomes. *Seminars in Cell & Developmental Biology,* 74**,** 4-10.

FREEMAN, C., SEAMAN, M. N. J. & REID, E. 2013. The hereditary spastic paraplegia protein strumpellin: Characterisation in neurons and of the effect of disease mutations on WASH complex assembly and function. *Biochimica Et Biophysica Acta-Molecular Basis of Disease,* 1832**,** 160-173.

FREEMAN, C. L., HESKETH, G. & SEAMAN, M. N. J. 2014. RME-8 coordinates the activity of the WASH complex with the function of the retromer SNX dimer to control endosomal tubulation. *Journal of Cell Science,* 127**,** 2053-2070.

FREEMAN, M. R. & DOHERTY, J. 2006. Glial cell biology in Drosophila and vertebrates. *Trends in Neurosciences,* 29**,** 82-90.

GERDING, W. M., KOETTING, J., EPPLEN, J. T. & NEUSCH, C. 2009. Hereditary motor and sensory neuropathy caused by a novel mutation in LITAF. *Neuromuscular Disorders,* 19**,** 701-703.

GILLOOLY, D. J., MORROW, I. C., LINDSAY, M., GOULD, R., BRYANT, N. J., GAULLIER, J. M., PARTON, R. G. & STENMARK, H. 2000. Localization of phosphatidylinositol 3-phosphate in yeast and mammalian cells. *Embo Journal,* 19**,** 4577-4588.

GIRIDHARAN, S. S. P., CAI, B. S., VITALE, N., NASLAVSKY, N. & CAPLAN, S. 2013. Cooperation of MICAL-L1, syndapin2, and phosphatidic acid in tubular recycling endosome biogenesis. *Molecular Biology of the Cell,* 24**,** 1776-1790.

GLASAUER, S. M. K. & NEUHAUSS, S. C. F. 2014. Whole-genome duplication in teleost fishes and its evolutionary consequences. *Molecular Genetics and Genomics,* 289**,** 1045-1060.

GOKOOL, S., TATTERSALL, D. & SEAMAN, M. N. J. 2007. EHD1 interacts with retromer to stabilize SNX1 tubules and facilitate endosome-to-golgi retrieval. *Traffic,* 8**,** 1873-1886.

GOLDENRING, J. R. 2015. Recycling endosomes. *Current Opinion in Cell Biology,* 35**,** 117-122.

GOMEZ, T. S. & BILLADEAU, D. D. 2009. A FAM21-Containing WASH Complex Regulates Retromer-Dependent Sorting. *Developmental Cell,* 17**,** 699-711.

GONZAGA-JAUREGUI, C., HAREL, T., GAMBIN, T., KOUSI, M., GRIFFIN, L. B., FRANCESCATTO, L., OZES, B., KARACA, E., JHANGIANI, S. N., BAINBRIDGE, M. N., LAWSON, K. S., PEHLIVAN, D., OKAMOTO, Y., WITHERS, M., MANCIAS, P., SLAVOTINEK, A., REITNAUER, P. J., GOKSUNGUR, M. T., SHY, M., CRAWFORD, T. O., KOENIG, M., WILLER, J., FLORES, B. N., PEDIADITRAKIS, I., US, O., WISZNIEWSKI, W., PARMAN, Y., ANTONELLIS, A., MUZNY, D. M., KATSANIS, N., BATTALOGLU, E., BOERWINKLE, E., GIBBS, R. A., LUPSKI, J. R. & BAYLOR-HOPKINS CTR MENDELIAN, G. 2015. Exome Sequence Analysis Suggests that Genetic Burden Contributes to Phenotypic Variability and Complex Neuropathy. *Cell Reports,* 12**,** 1169-1183.

GOUY, M., GUINDON, S. & GASCUEL, O. 2010. SeaView Version 4: A Multiplatform Graphical User Interface for Sequence Alignment and Phylogenetic Tree Building. *Molecular Biology and Evolution,* 27**,** 221-224.

GRANT, B. D. & DONALDSON, J. G. 2009. Pathways and mechanisms of endocytic recycling. *Nature Reviews Molecular Cell Biology,* 10**,** 597-608.

GUIMARAES-COSTA, R., FERFOGLIA, R., LEONARD-LOUIS, S., ZIEGLER, F., MAGY, L., FOURNIER, E., DUBOURG, O., BOUCHE, P., MAISONOBE, T., LACOUR, A., MOERMAN, A., LATOUR, P. & STOJKOVIC, T. 2017. Phenotypic spectrum of Charcot-Marie-Tooth disease due to LITAF/SIMPLE mutations: a study of 18 patients. *European Journal of Neurology,* 24**,** 530-538.

GUPTA, T. & MULLINS, M. C. 2010. Dissection of Organs from the Adult Zebrafish. *Journal of Visualized Experiments***,** e1717.

HAGLUND, K. & DIKIC, I. 2012. The role of ubiquitylation in receptor endocytosis and endosomal sorting. *Journal of cell science,* 125**,** 265-275.

HANSON, P. I., ROTH, R., LIN, Y. & HEUSER, J. E. 2008. Plasma membrane deformation by circular arrays of ESCRT-III protein filaments. *Journal of Cell Biology,* 180**,** 389-402.

HARBOUR, M. E., BREUSEGEM, S. Y. & SEAMAN, M. N. J. 2012. Recruitment of the endosomal WASH complex is mediated by the extended 'tail' of Fam21 binding to the retromer protein Vps35. *Biochemical Journal,* 442**,** 209-220.

HARIRI, H., BHATTACHARYA, N., JOHNSON, K., NOBLE, A. J. & STAGG, S. M. 2014. Insights into the Mechanisms of Membrane Curvature and Vesicle Scission by the Small GTPase Sar1 in the Early Secretory Pathway. *Journal of Molecular Biology,* 426**,** 3811-3826.

HARTERINK, M., PORT, F., LORENOWICZ, M. J., MCGOUGH, I. J., SILHANKOVA, M., BETIST, M. C., VAN WEERING, J. R. T., VAN HEESBEEN, R., MIDDELKOOP, T. C., BASLER, K., CULLEN, P. J. & KORSWAGEN, H. C. 2011. A SNX3-dependent retromer pathway mediates retrograde transport of the Wnt sorting receptor Wntless and is required for Wnt secretion. *Nature Cell Biology,* 13**,** 914-U358.

HAYASAKA, K., HIMORO, M., SATO, W., TAKADA, G., UYEMURA, K., SHIMIZU, N., BIRD, T. D., CONNEALLY, P. M. & CHANCE, P. F. 1993. CHARCOT-MARIE-TOOTH NEUROPATHY TYPE-1B IS ASSOCIATED WITH MUTATIONS OF THE MYELIN-P(0) GENE. *Nature Genetics,* 5**,** 31-34.

HE, S. P., TAN, G. H., LIU, Q., HUANG, K. W., REN, J., ZHANG, X., YU, X. C., HUANG, P. & AN, C. C. 2011. The LSD1-Interacting Protein GILP Is a LITAF Domain Protein That Negatively Regulates Hypersensitive Cell Death in Arabidopsis. *Plos One,* 6.

HEIGWER, F., KERR, G. & BOUTROS, M. 2014. E-CRISP: fast CRISPR target site identification. *Nature Methods,* 11**,** 122-124.

HENNE, W. M., BUCHKOVICH, N. J., ZHAO, Y. Y. & EMR, S. D. 2012. The Endosomal Sorting Complex ESCRT-II Mediates the Assembly and Architecture of ESCRT-III Helices. *Cell,* 151**,** 356-371.

HICKE, L. & RIEZMAN, H. 1996. Ubiquitination of a yeast plasma membrane receptor signals its ligand-stimulated endocytosis. *Cell,* 84**,** 277-287.

HIERRO, A., ROJAS, A. L., ROJAS, R., MURTHY, N., EFFANTIN, G., KAJAVA, A. V., STEVEN, A. C., BONIFACINO, J. S. & HURLEY, J. H. 2007. Functional architecture of the retromer cargo-recognition complex. *Nature,* 449**,** 1063-U8.

HO, A. K., WAGSTAFF, J. L., MANNA, P. T., WARTOSCH, L., QAMAR, S., GARMAN, E., F., FREUND, S. M. V. & ROBERTS, R. C. 2016. The topology, structure and PE interaction of LITAF underpin a Charcot-Marie-Tooth disease type 1C *BMC Biology,* 14**,** 109.

HOLLINSHEAD, M., SANDERSON, J. & VAUX, D. J. 1997. Anti-biotin antibodies offer superior organelle-specific labeling of mitochondria over avidin or streptavidin. *Journal of Histochemistry & Cytochemistry,* 45**,** 1053-1057.

HONG, Y. B., JOO, J., HYUN, Y. S., KWAK, G., CHOI, Y. R., YEO, H. K., JWA, D. H., KIM, E. J., MO, W. M., NAM, S. H., KIM, S. M., YOO, J. H., KOO, H., PARK, H. T., CHUNG, K. W. & CHOI, B. O. 2016. A Mutation in PMP2 Causes Dominant Demyelinating Charcot-Marie-Tooth Neuropathy. *Plos Genetics,* 12.

HU, J. J., SHIBATA, Y., VOSS, C., SHEMESH, T., LI, Z. L., COUGHLIN, M., KOZLOV, M. M., RAPOPORT, T. A. & PRINZ, W. A. 2008. Membrane proteins of the endoplasmic reticulum induce high-curvature tubules. *Science,* 319**,** 1247-1250.

HUANG, D. W., SHERMAN, B. T. & LEMPICKI, R. A. 2009. Bioinformatics enrichment tools: paths toward the comprehensive functional analysis of large gene lists. *Nucleic Acids Research,* 37**,** 1-13.

HUANG, Y. Z. & BENNETT, C. L. 2007. Litaf/simple protein is increased in intestinal tissues from patients with CD and UC, but is unlikely to function as a transcription factor. *Inflammatory Bowel Diseases,* 13**,** 120-121.

HUIZING, M., DIDIER, A., WALENTA, J., ANIKSTER, Y., GAHL, W. A. & KRAMER, H. 2001. Molecular cloning and characterization of human VPS18, VPS 11, VPS16, and VPS33. *Gene,* 264**,** 241-247.

HUOTARI, J. & HELENIUS, A. 2011. Endosome maturation. *Embo Journal,* 30**,** 3481-3500.

HURLEY, J. H. & HANSON, P. I. 2010. Membrane budding and scission by the ESCRT machinery: it's all in the neck. *Nature Reviews Molecular Cell Biology,* 11**,** 556-566.

HUTTLIN, E. L., BRUCKNER, R. J., PAULO, J. A., CANNON, J. R., TING, L., BALTIER, K., COLBY, G., GEBREAB, F., GYGI, M. P., PARZEN, H., SZPYT, J., TAM, S., ZARRAGA, G., PONTANO-VAITES, L., SWARUP, S., WHITE, A. E., SCHWEPPE, D. K., RAD, R., ERICKSON, B. K., OBAR, R. A., GURUHARSHA, K. G., LI, K., RTAVANIS-TSAKONAS, S. A., GYGI, S. P. & HARPER, J. W. 2017. Architecture of the human interactome defines protein communities and disease networks. *Nature,* 545**,** 505-+.

ICHIOKA, F., TAKAYA, E., SUZUKI, H., KAJIGAYA, S., BUCHMAN, V. L., SHIBATA, H. & MAKI, M. 2007. HD-PTP and Alix share some membrane-traffic related proteins that interact with their Bro1 domains or proline-rich regions. *Archives of Biochemistry and Biophysics,* 457**,** 142-149.

INUKAI, R., MORI, K., KUWATA, K., SUZUKI, C., MAKI, M., TAKAHARA, T. & SHIBATA, H. 2021. The Novel ALG-2 Target Protein CDIP1 Promotes Cell Death by Interacting with ESCRT-I and VAPA/B. *International Journal of Molecular Sciences,* 22.

ISHII, A., FURUSHO, M., DUPREE, J. L. & BANSAL, R. 2016. Strength of ERK1/2 MAPK Activation Determines Its Effect on Myelin and Axonal Integrity in the Adult CNS. *Journal of Neuroscience,* 36**,** 6471-6487.

JANVIER, K. & BONIFACINO, J. S. 2005. Role of the endocytic machinery in the sorting of lysosome-associated membrane proteins. *Molecular Biology of the Cell,* 16**,** 4231-4242.

JAO, L. E., WENTE, S. R. & CHEN, W. B. 2013. Efficient multiplex biallelic zebrafish genome editing using a CRISPR nuclease system. *Proceedings of the National Academy of Sciences of the United States of America,* 110**,** 13904-13909.

JERATH, N. U. & SHY, M. E. 2017. Charcot-Marie-Tooth disease type 1C: Clinical and electrophysiological findings for the c.334G > a (p.Gly112Ser) Litaf/Simple mutation. *Muscle & Nerve,* 56**,** 1092-1095.

JESSEN, K. R. & MIRSKY, R. 2016. The repair Schwann cell and its function in regenerating nerves. *Journal of Physiology-London,* 594**,** 3521-3531.

JOLLIFFE, C. N., HARVEY, K. F., HAINES, B. P., PARASIVAM, G. & KUMAR, S. 2000. Identification of multiple proteins expressed in murine embryos as binding partners for the WW domains of the ubiquitin-protein ligase Nedd4. *Biochemical Journal,* 351**,** 557-565.

JONES, E. A., BREWER, M. H., SRINIVASAN, R., KRUEGER, C., SUN, G., CHARNEY, K. N., KELES, S., ANTONELLIS, A. & SVAREN, J. 2012. Distal enhancers upstream of the Charcot-Marie-Tooth type 1A disease gene PMP22. *Human Molecular Genetics,* 21**,** 1581-1591.

JORDANOVA, A., DE JONGHE, P., BOERKOEL, C. F., TAKASHIMA, H., DE VRIENDT, E., CEUTERICK, C., MARTIN, J. J., BUTLER, I. J., MANCIAS, P., PAPASOZOMENOS, S. C., TERESPOLSKY, D., POTOCKI, L., BROWN, C. W., SHY, M., RITA, D. A., TOURNEV, I., KREMENSKY, I., LUPSKI, J. R. & TIMMERMAN, V. 2003. Mutations in the neurofilament light chain gene (NEFL) cause early onset severe Charcot-Marie-Tooth disease. *Brain,* 126**,** 590-597.

JOVIC, M., KIEKEN, F., NASLAVSKY, N., SORGEN, P. L. & CAPLAN, S. 2009. Eps15 Homology Domain 1-associated Tubules Contain Phosphatidylinositol-4-Phosphate and Phosphatidylinositol-(4,5)-Bisphosphate and Are Required for Efficient Recycling. *Molecular Biology of the Cell,* 20**,** 2731-2743.

KACHHAP, S. K., FAITH, D., QIAN, D. Z., SHABBEER, S., GALLOWAY, N. L., PILI, R., DENMEADE, S. R., DEMARZO, A. M. & CARDUCCI, M. A. 2007. The N-Myc Down Regulated Gene1 (NDRG1) Is a Rab4a Effector Involved in Vesicular Recycling of E-Cadherin. *Plos One,* 2.

KARLSSON, A. B., WASHINGTON, J., DIMITROVA, V., HOOPER, C., SHEKHTMAN, A. & BAKOWSKA, J. C. 2014. The role of spartin and its novel ubiquitin binding region in DALIS occurrence. *Molecular Biology of the Cell,* 25**,** 1355-1365.

KATZMANN, D. J., BABST, M. & EMR, S. D. 2001. Ubiquitin-dependent sorting into the multivesicular body pathway requires the function of a conserved endosomal protein sorting complex, ESCRT-I. *Cell,* 106**,** 145-155.

KELSALL, I. R., ZHANG, J. Z., KNEBEL, A., ARTHUR, J. S. C. & COHEN, P. 2019. The E3 ligase HOIL-1 catalyses ester bond formation between ubiquitin and components of the Myddosome in mammalian cells. *Proceedings of the National Academy of Sciences of the United States of America,* 116**,** 13293-13298.

KIDD, G. J., OHNO, N. & TRAPP, B. D. 2013. Biology of Schwann cells. *Peripheral Nerve Disorders,* 115**,** 55-79.

KIEKEN, F., SHARMA, M., JOVIC, M., GIRIDHARAN, S. S. P., NASLAVSKY, N., CAPLAN, S. & SORGEN, P. L. 2010. Mechanism for the Selective Interaction of C-terminal Eps15 Homology Domain Proteins with Specific Asn-Pro-Phe-containing Partners. *Journal of Biological Chemistry,* 285**,** 8687-8694.

KIM, B. Y., KRAMER, H., YAMAMOTO, A., KOMINAMI, E., KOHSAKA, S. & AKAZAWA, C. 2001. Molecular characterization of mammalian homologues of class CVPS proteins that interact with syntaxin-7. *Journal of Biological Chemistry,* 276**,** 29393-29402.

KIM, D. I., JENSEN, S. C., NOBLE, K. A., BIRENDRA, K. C., ROUX, K. H., MOTAMEDCHABOKI, K. & ROUX, K. J. 2016. An improved smaller biotin ligase for BioID proximity labeling. *Molecular Biology of the Cell,* 27**,** 1188-1196.

KIM, S. A., VACRATSIS, P. O., FIRESTEIN, R., CLEARY, M. L. & DIXON, J. E. 2003. Regulation of myotubularin-related (MTMR)2 phosphatidylinositol phosphatase by MTMR5, a catalytically inactive phosphatase. *Proceedings of the National Academy of Sciences of the United States of America,* 100**,** 4492-4497.

KIMMEL, C. B., BALLARD, W. W., KIMMEL, S. R., ULLMANN, B. & SCHILLING, T. F. 1995. STAGES OF EMBRYONIC-DEVELOPMENT OF THE ZEBRAFISH. *Developmental Dynamics,* 203**,** 253-310.

KLEIN, C. J., MIDDHA, S., DUAN, X. H., WU, Y. H., LITCHY, W. J., GU, W. H., DYCK, P. J. B., GAVRILOVA, R. H., SMITH, D. I., KOCHER, J. P. & DYCK, P. J. 2014. Application of whole exome sequencing in undiagnosed inherited polyneuropathies. *Journal of Neurology Neurosurgery and Psychiatry,* 85**,** 1265-1272.

KNIGHT, J. D. R., CHOI, H., GUPTA, G. D., PELTETIER, L., RAUGHT, B., NESVIZHSKII, A. I. & GINGRAS, A. C. 2017. ProHits-viz: a suite of web tools for visualizing interaction proteomics data. *Nature Methods,* 14**,** 645-646.

KOOIJMAN, E. E., CHUPIN, V., DE KRUIJFF, B. & BURGER, K. N. J. 2003. Modulation of membrane curvature by phosphatidic acid and lysophosphatidic acid. *Traffic,* 4**,** 162-174.

KOSTELANSKY, M. S., SUN, J., LEE, S. H., KIM, J., GHIRLANDO, R., HIERRO, A., EMR, S. D. & HURLEY, J. H. 2006. Structural and functional organization of the ESCRT-I trafficking complex. *Cell,* 125**,** 113-126.

KOVACH, M. J., LIN, J. P., BOYADJIEV, S., CAMPBELL, K., MAZZEO, L., HERMAN, K., RIMER, L. A., FRANK, W., LLEWELLYN, B., JABS, E. W., GELBER, D. & KIMONIS, V. E. 1999. A unique point mutation in the PMP22 gene is associated with Charcot-Marie-Tooth disease and deafness. *American Journal of Human Genetics,* 64**,** 1580-1593.

KOVTUN, O., LENEVA, N., BYKOV, Y. S., ARIOTTI, N., TEASDALE, R. D., SCHAFFER, M., ENGEL, B. D., OWEN, D. J., BRIGGS, J. A. G. & COLLINS, B. M. 2018. Structure of the membrane-assembled retromer coat determined by cryo-electron tomography. *Nature,* 561**,** 561-+.

KOZLOV, M. M., CAMPELO, F., LISKA, N., CHERNOMORDIK, L. V., MARRINK, S. J. & MCMAHON, H. T. 2014. Mechanisms shaping cell membranes. *Current Opinion in Cell Biology,* 29**,** 53-60.

KUMAR, C. V., SWETHA, R. G., RAMAIAH, S. & ANBARASU, A. 2015. Tryptophan to Glycine mutation in the position 116 leads to protein aggregation and decreases the stability of the LITAF protein. *Journal of Biomolecular Structure & Dynamics,* 33**,** 1695-1709.

KVAINICKAS, A., JIMENEZ-ORGAZ, A., NAGELE, H., HU, Z. H., DENGJEL, J. & STEINBERG, F. 2017. Cargo-selective SNX-BAR proteins mediate retromer trimer independent retrograde transport. *Journal of Cell Biology,* 216**,** 3677-3693.

LABUN, K., MONTAGUE, T. G., GAGNON, J. A., THYME, S. B. & VALEN, E. 2016. CHOPCHOP v2: a web tool for the next generation of CRISPR genome engineering. *Nucleic Acids Research,* 44**,** W272-W276.

LACERDA, A. F., HARTJES, E. & BRUNETTI, C. R. 2014. LITAF Mutations Associated with Charcot-Marie-Tooth Disease 1C Show Mislocalization from the Late Endosome/Lysosome to the Mitochondria. *Plos One,* 9.

LAROCQUE, G., LA-BORDE, P. J., CLARKE, N. I., CARTER, N. J. & ROYLE, S. J. 2020a. Tumor protein D54 defines a new class of intracellular transport vesicles. *Journal of Cell Biology,* 219.

LAROCQUE, G., LA-BORDE, P. J., WILSON, B. J., CLARKE, N. I., MOORE, D. J., CASWELL, P. T. & ROYLE, S. J. 2020b. Intracellular nanovesicles mediate integrin trafficking during cell migration. *bioRxiv***,** 2020.08.19.257287.

LATOUR, P., GONNAUD, P. M., OLLAGNON, E., CHAN, V., PERELMAN, S., STOJKOVIC, T., STOLL, C., VIAL, C., ZIEGLER, F., VANDENBERGHE, A. & MAIRE, I. 2006. SIMPLE mutation analysis in dominant demyelinating Charcot-Marie-Tooth disease: three novel mutations. *Journal of the Peripheral Nervous System,* 11**,** 148-155.

LAUFFER, B. E. L., MELERO, C., TEMKIN, P., LEI, C., HONG, W. J., KORTEMME, T. & VON ZASTROW, M. 2010. SNX27 mediates PDZ-directed sorting from endosomes to the plasma membrane. *Journal of Cell Biology,* 190**,** 565-574.

LEE, S. M., CHIN, L. S. & LI, L. 2012. Charcot-Marie-Tooth disease-linked protein SIMPLE functions with the ESCRT machinery in endosomal trafficking. *Journal of Cell Biology,* 199**,** 799-816.

LEE, S. M., CHIN, L. S. & LI, L. 2017. Dysregulation of ErbB Receptor Trafficking and Signaling in Demyelinating Charcot-Marie-Tooth Disease. *Molecular Neurobiology,* 54**,** 87-100.

LEE, S. M., OLZMANN, J. A., CHIN, L. S. & LI, L. 2011. Mutations associated with Charcot-Marie-Tooth disease cause SIMPLE protein mislocalization and degradation by the proteasome and aggresome-autophagy pathways. *Journal of Cell Science,* 124**,** 3319-3331.

LEE, S. M., SHA, D., MOHAMMED, A. A., ASRESS, S., GLASS, J. D., CHIN, L. S. & LI, L. 2013. Motor and sensory neuropathy due to myelin infolding and paranodal damage in a transgenic mouse model of Charcot-Marie-Tooth disease type 1C. *Human Molecular Genetics,* 22**,** 1755-1770.

LENK, G. M., FERGUSON, C. J., CHOW, C. Y., JIN, N., JONES, J. M., GRANT, A. E., ZOLOV, S. N., WINTERS, J. J., GIGER, R. J., DOWLING, J. J., WEISMAN, L. S. & MEISLER, M. H. 2011. Pathogenic Mechanism of the FIG4 Mutation Responsible for Charcot-Marie-Tooth Disease CMT4J. *Plos Genetics,* 7.

LEON, S. & HAGUENAUER-TSAPIS, R. 2009. Ubiquitin ligase adaptors: Regulators of ubiquitylation and endocytosis of plasma membrane proteins. *Experimental Cell Research,* 315**,** 1574-1583.

LI, W., BENGTSON, M. H., ULBRICH, A., MATSUDA, A., REDDY, V. A., ORTH, A., CHANDA, S. K., BATALOV, S. & JOAZEIRO, C. A. P. 2008. Genome-Wide and Functional Annotation of Human E3 Ubiquitin Ligases Identifies MULAN, a Mitochondrial E3 that Regulates the Organelle's Dynamics and Signaling. *Plos One,* 3.

LI, W. J., ZHU, H., ZHAO, X. L., BRANCHO, D., LIANG, Y. X., ZOU, Y. Y., BENNETT, C. & CHOW, C. W. 2015. Dysregulated Inflammatory Signaling upon Charcot-Marie-Tooth Type 1C Mutation of SIMPLE Protein. *Molecular and Cellular Biology,* 35**,** 2464-2478.

LI, X. R., WANG, X., ZHANG, X. L., ZHAO, M. K., TSANG, W. L., ZHANG, Y. L., YAU, R. G. W., WEISMAN, L. S. & XU, H. X. 2013. Genetically encoded fluorescent probe to visualize intracellular phosphatidylinositol 3,5-bisphosphate localization and dynamics. *Proceedings of the National Academy of Sciences of the United States of America,* 110**,** 21165-21170.

LI, X. Y. & DIFIGLIA, M. 2012. The recycling endosome and its role in neurological disorders. *Progress in Neurobiology,* 97**,** 127-141.

LIU, J., ZUO, Z. H., SASTALLA, I., LIU, C. Y., JANG, J. Y., SEKINE, Y., LI, Y. S., PIROOZNIA, M., LEPPLA, S. H., FINKEL, T. & LIU, S. H. 2020. Sequential CRISPR-Based Screens Identify LITAF and CDIP1 as the Bacillus cereus Hemolysin BL Toxin Host Receptors. *Cell Host & Microbe,* 28**,** 402-+.

LOBERT, V. H., BRECH, A., PEDERSEN, N. M., WESCHE, J., OPPELT, A., MALERØD, L. & STENMARK, H. 2010. Ubiquitination of alpha 5 beta 1 integrin controls fibroblast migration through lysosomal degradation of fibronectin-integrin complexes. *Dev Cell,* 19**,** 148-59.

LOGAN, A. M., MAMMEL, A. E., ROBINSON, D. C., CHIN, A. L., CONDON, A. F. & ROBINSON, F. L. 2017. Schwann cell-specific deletion of the endosomal PI 3-kinase Vps34 leads to delayed radial sorting of axons, arrested myelination, and abnormal ErbB2-ErbB3 tyrosine kinase signaling. *Glia,* 65**,** 1452-1470.

LU, Q., HOPE, L. W. Q., BRASCH, M., REINHARD, C. & COHEN, S. N. 2003. TSG101 interaction with HRS mediates endosomal trafficking and receptor down-regulation. *Proceedings of the National Academy of Sciences of the United States of America,* 100**,** 7626-7631.

LUCK, K., KIM, D. K., LAMBOURNE, L., SPIROHN, K., BEGG, B. E., BIAN, W. T., BRIGNALL, R., CAFARELLI, T., CAMPOS-LABORIE, F. J., CHARLOTEAUX, B., CHOI, D., COTE, A. G., DALEY, M., DEIMLING, S., DESBULEUX, A., DRICOT, A., GEBBIA, M., HARDY, M. F., KISHORE, N., KNAPP, J. J., KOVACS, I. A., LEMMENS, I., MEE, M. W., MELLOR, J. C., POLLIS, C., PONS, C., RICHARDSON, A. D., SCHLABACH, S., TEEKING, B., YADAV, A., BABOR, M., BALCHA, D., BASHA, O., BOWMAN-COLIN, C., CHIN, S. F., CHOI, S. G., COLABELLA, C., COPPIN, G., D'AMATA, C., DE RIDDER, D., DE ROUCK, S., DURAN-FRIGOLA, M., ENNAJDAOUI, H., GOEBELS, F., GOEHRING, L., GOPAL, A., HADDAD, G., HATCHI, E., HELMY, M., JACOB, Y., KASSA, Y., LANDINI, S., LI, R. J., VAN LIESHOUT, N., MACWILLIAMS, A., MARKEY, D., PAULSON, J. N., RANGARAJAN, S., RASLA, J., RAYHAN, A., ROLLAND, T., SAN-MIGUEL, A., SHEN, Y., SHEYKHKARIMLI, D., SHEYNKMAN, G. M., SIMONOVSKY, E., TASAN, M., TEJEDA, A., TROPEPE, V., TWIZERE, J. C., WANG, Y., WEATHERITT, R. J., WEILE, J., XIA, Y., YANG, X. P., YEGER-LOTEM, E., ZHONG, Q., ALOY, P., BADER, G. D., RIVAS, J. D. L., GAUDET, S., HAO, T., RAK, J., TAVERNIER, J., HILL, D. E., VIDAL, M., ROTH, F. P. & CALDERWOOD, M. A. 2020. A reference map of the human binary protein interactome. *Nature,* 580**,** 402-+.

LUDES-MEYERS, J. H., KIL, H., BEDNAREK, A. K., DRAKE, J., BEDFORD, M. T. & ALDAZ, C. M. 2004. WWOX binds the specific proline-rich ligand PPXY: identification of candidate interacting proteins. *Oncogene,* 23**,** 5049-5055.

LUIGETTI, M., FABRIZI, G. M., TAIOLI, F., DEL GRANDE, A. & LO MONACO, M. 2014. A novel LITAF/SIMPLE variant within a family with minimal demyelinating Charcot-Marie-Tooth disease. *Neurological Sciences,* 35**,** 2005-2007.

LUMB, J. H., LEUNG, K. F., DUBOIS, K. N. & FIELD, M. C. 2011. Rab28 function in trypanosomes: interactions with retromer and ESCRT pathways. *Journal of Cell Science,* 124**,** 3771-3783.

LYONS, D. A., POGODA, H. M., VOAS, M. G., WOODS, I. G., DIAMOND, B., NIX, R., ARANA, N., JACOBS, J. & TALBOT, W. S. 2005. erbb3 and erbb2 are essential for Schwann cell migration and myelination in zebrafish. *Current Biology,* 15**,** 513-524.

MACDONALD, E., BROWN, L., SELVAIS, A., LIU, H., WARING, T., NEWMAN, D., BITHELL, J., GRIMES, D., URBE, S., CLAGUE, M. J. & ZECH, T. 2018. HRS-WASH axis governs actin-mediated endosomal recycling and cell invasion. *Journal of Cell Biology,* 217**,** 2549-2564.

MACIA, E., LUTON, F., PARTISANI, M., CHERFILS, J., CHARDIN, P. & FRANCO, M. 2004. The GDP-bound form of Arf6 is located at the plasma membrane. *Journal of Cell Science,* 117**,** 2389-2398.

MACIAS, M. J., WIESNER, S. & SUDOL, M. 2002. WW and SH3 domains, two different scaffolds to recognize proline-rich ligands. *Febs Letters,* 513**,** 30-37.

MARCHESE, A., RAIBORG, C., SANTINI, F., KEEN, J. H., STENMARK, H. & BENOVIC, J. L. 2003. The E3 ubiquitin ligase AIP4 mediates ubiquitination and sorting of the G protein-coupled receptor CXCR4. *Developmental Cell,* 5**,** 709-722.

MATSUMURA, Y., NISHIGORI, C., HORIO, T. & MIYACHI, Y. 2004. PIG7/LITAF gene mutation and overexpression of its gene product in extramammary Paget's disease. *International Journal of Cancer,* 111**,** 218-223.

MATSUO, H., CHEVALLIER, J., MAYRAN, N., LE BLANC, I., FERGUSON, C., FAURE, J., BLANC, N. S., MATILE, S., DUBOCHET, J., SADOUL, R., PARTON, R. G., VILBOIS, F. & GRUENBERG, J. 2004. Role of LBPA and Alix in multivesicular liposome formation and endosome organization. *Science,* 303**,** 531-534.

MAUREL, P. & SALZER, J. L. 2000. Axonal regulation of Schwann cell proliferation and survival and the initial events of myelination requires PI 3-kinase activity. *Journal of Neuroscience,* 20**,** 4635-4645.

MAXFIELD, F. R. & MCGRAW, T. E. 2004. Endocytic recycling. *Nature Reviews Molecular Cell Biology,* 5**,** 121-132.

MCBRIDE, H. M., RYBIN, V., MURPHY, C., GINER, A., TEASDALE, R. & ZERIAL, M. 1999. Oligomeric complexes link Rab5 effectors with NSF and drive membrane fusion via interactions between EEA1 and syntaxin 13. *Cell,* 98**,** 377-386.

MCGOURTY, C. A., AKOPIAN, D., WALSH, C., GORUR, A., WERNER, A., SCHEKMAN, R., BAUTISTA, D. & RAPE, M. 2016. Regulation of the CUL3 Ubiquitin Ligase by a Calcium-Dependent Co-adaptor. *Cell,* 167**,** 525-+.

MCMAHON, H. T. & GALLOP, J. L. 2005. Membrane curvature and mechanisms of dynamic cell membrane remodelling. *Nature,* 438**,** 590-596.

MCNALLY, K. E., FAULKNER, R., STEINBERG, F., GALLON, M., GHAI, R., PIM, D., LANGTON, P., PEARSON, N., DANSON, C. M., NAGELE, H., MORRIS, L. L., SINGLA, A., OVERLEE, B. L., HEESOM, K. J., SESSIONS, R., BANKS, L., COLLINS, B. M., BERGER, I., BILLADEAU, D. D., BURSTEIN, E. & CULLEN, P. J. 2017. Retriever is a multiprotein complex for retromer-independent endosomal cargo recycling. *Nature Cell Biology,* 19**,** 1214-+.

MEEKER, N. D., HUTCHINSON, S. A., HO, L. & TRECLE, N. S. 2007. Method for isolation of PCR-ready genomic DNA from zebrafish tissues. *Biotechniques,* 43**,** 610-+.

MEGGOUH, F., DE VISSER, M., ARTS, W. F. M., DE COO, R., VAN SCHAIK, I. N. & BAAS, F. 2005. Early onset neuropathy in a compound form of Charcot-Marie-Tooth disease. *Annals of Neurology,* 57**,** 589-591.

MELLACHERUVU, D., WRIGHT, Z., COUZENS, A. L., LAMBERT, J. P., ST-DENIS, N. A., LI, T., MITEVA, Y. V., HAURI, S., SARDIU, M. E., LOW, T. Y., HALIM, V. A., BAGSHAW, R. D., HUBNER, N. C., AL-HAKIM, A., BOUCHARD, A., FAUBERT, D., FERMIN, D., DUNHAM, W. H., GOUDREAULT, M., LIN, Z. Y., BADILLO, B. G., PAWSON, T., DUROCHER, D., COULOMBE, B., AEBERSOLD, R., SUPERTI-FURGA, G., COLINGE, J., HECK, A. J. R., CHOI, H., GSTAIGER, M., MOHAMMED, S., CRISTEA, I. M., BENNETT, K. L., WASHBURN, M. P., RAUGHT, B., EWING, R. M., GINGRAS, A. C. & NESVIZHSKII, A. I. 2013. The CRAPome: a contaminant repository for affinity purification-mass spectrometry data. *Nature Methods,* 10**,** 730-+.

MELLMAN, I. & YARDEN, Y. 2013. Endocytosis and Cancer. *Cold Spring Harbor Perspectives in Biology,* 5.

MERRILL, J. C., YOU, J., CONSTABLE, C., LEEMAN, S. E. & AMAR, S. 2011. Whole-body deletion of LPS-induced TNF-alpha factor (LITAF) markedly improves

experimental endotoxic shock and inflammatory arthritis. *Proceedings of the National Academy of Sciences of the United States of America,* 108**,** 21247-21252.

METZGER, M. B., HRISTOVA, V. A. & WEISSMAN, A. M. 2012. HECT and RING finger families of E3 ubiquitin ligases at a glance. *Journal of Cell Science,* 125**,** 531-537.

MIYAMOTO, Y. J., MITCHELL, J. S. & MCINTYRE, B. W. 2003. Physical association and functional interaction between beta 1 integrin and CD98 on human T lymphocytes. *Molecular Immunology,* 39**,** 739-751.

MIYAMOTOA, Y., YAMAMORI, N., TORII, T., TANOUE, A. & YAMAUCHI, J. 2014. Rab35, acting through ACAP2 switching off Arf6, negatively regulates oligodendrocyte differentiation and myelination. *Molecular Biology of the Cell,* 25**,** 1532-1542.

MONIER, S., DIETZEN, D. J., HASTINGS, W. R., LUBLIN, D. M. & KURZCHALIA, T. V. 1996. Oligomerization of VIP21-caveolin in vitro is stabilized by long chain fatty acylation or cholesterol. *Febs Letters,* 388**,** 143-149.

MONIER, S., PARTON, R. G., VOGEL, F., BEHLKE, J., HENSKE, A. & KURZCHALIA, T. V. 1995. VIP21-CAVEOLIN, A MEMBRANE-PROTEIN CONSTITUENT OF THE CAVEOLAR COAT, OLIGOMERIZES IN-VIVO AND IN-VITRO. *Molecular Biology of the Cell,* 6**,** 911-927.

MORITA, E., SANDRIN, V., ALAM, S. L., ECKERT, D. M., GYGI, S. P. & SUNDQUIST, W. I. 2007. Identification of human MVB12 proteins as ESCRT-I Subunits that function in HIV budding. *Cell Host & Microbe,* 2**,** 41-53.

MORIWAKI, Y., BEGUM, N. A., KOBAYASHI, M., MATSUMOTO, M., TOYOSHIMA, K. & SEYA, T. 2001. Mycobacterium bovis bacillus Calmette-Guerin and its cell wall complex induce a novel lysosomal membrane protein, SIMPLE, that bridges the missing link between lipopolysaccharide and p53-inducible gene, LITAF(PIG7), and estrogen-inducible gene, EET-1. *Journal of Biological Chemistry,* 276**,** 23065-23076.

MORIWAKI, Y., OHNO, Y., ISHII, T., TAKAMURA, Y., KITA, Y., WATABE, K., SANGO, K., TSUJI, S. & MISAWA, H. 2018. SIMPLE binds specifically to PI4P through SIMPLE-like domain and participates in protein trafficking in the trans-Golgi network and/or recycling endosomes. *Plos One,* 13.

MORROW, I. C., REA, S., MARTIN, S., PRIOR, I. A., PROHASKA, R., HANCOCK, J. F., JAMES, D. E. & PARTON, R. G. 2002. Flotillin-1/Reggie-2 traffics to surface raft domains via a novel Golgi-independent pathway - Identification of a novel membrane targeting domain and a role for palmitoylation. *Journal of Biological Chemistry,* 277**,** 48834-48841.

MOSHAL, K. S., RODER, K., KABAKOV, A. Y., WERDICH, A. A., CHIANG, D. Y. E., TURAN, N. N., XIE, A., KIM, T. Y., COOPER, L. L., LU, Y. C., ZHONG, M. W., LI, W. Y., TERENTYEV, D., CHOI, B. R., KARMA, A., MACRAE, C. A. & KOREN, G. 2019. LITAF (Lipopolysaccharide-Induced Tumor Necrosis Factor) Regulates Cardiac L-Type Calcium Channels by Modulating NEDD (Neural Precursor Cell Expressed Developmentally Downregulated Protein) 4-1 Ubiquitin Ligase. *Circulation-Genomic and Precision Medicine,* 12**,** 407-420.

MUND, T. & PELHAM, H. R. B. 2009. Control of the activity of WW-HECT domain E3 ubiquitin ligases by NDFIP proteins. *Embo Reports,* 10**,** 501-507.

MYOKAI, F., TAKASHIBA, S., LEBO, R. & AMAR, S. 1999. A novel lipopolysaccharide-induced transcription factor regulating tumor necrosis factor alpha gene expression: Molecular cloning, sequencing, characterization, and chromosomal assignment. *Proceedings of the National Academy of Sciences of the United States of America,* 96**,** 4518-4523.

NAKHRO, K., PARK, J. M., HONG, Y. B., PARK, J. H., NAM, S. H., YOON, B. R., YOO, J. H., KOO, H., JUNG, S. C., KIM, H. L., KIM, J. Y., CHOI, K. G., CHOI, B. O. & CHUNG, K. W. 2013. SET binding factor 1 (SBF1) mutation causes Charcot-Marie-Tooth disease type 4B3. *Neurology,* 81**,** 165-173.

NAMBA, T., TIAN, F., CHU, K. K., HWANG, S. Y., YOON, K. W., BYUN, S., HIRAKI, M., MANDINOVA, A. & LEE, S. W. 2013. CDIP1-BAP31 Complex Transduces Apoptotic Signals from Endoplasmic Reticulum to Mitochondria under Endoplasmic Reticulum Stress. *Cell Reports,* 5**,** 331-339.

NESS, J. K., SNYDER, K. M. & TAPINOS, N. 2013. Lck tyrosine kinase mediates beta 1-integrin signalling to regulate Schwann cell migration and myelination. *Nature Communications,* 4.

NEWPORT, J. & KIRSCHNER, M. 1982. A MAJOR DEVELOPMENTAL TRANSITION IN EARLY XENOPUS-EMBRYOS .2. CONTROL OF THE ONSET OF TRANSCRIPTION. *Cell,* 30**,** 687-696.

NEWTON-CHEH, C., EIJGELSHEIM, M., RICE, K. M., DE BAKKER, P. I. W., YIN, X. Y., ESTRADA, K., BIS, J. C., MARCIANTE, K., RIVADENEIRA, F., NOSEWORTHY, P. A., SOTOODEHNIA, N., SMITH, N. L., ROTTER, J. I., KORS, J. A., WITTEMAN, J. C. M., HOFMAN, A., HECKBERT, S. R., O'DONNELL, C. J., UITTERLINDEN, A. G., PSATY, B. M., LUMLEY, T., LARSON, M. G. & STRICKER, B. H. C. 2009. Common variants at ten loci influence QT interval duration in the QTGEN Study. *Nature Genetics,* 41**,** 399-406.

NISHIMURA, T. & KAIBUCHI, K. 2007. Numb controls integrin endocytosis for directional cell migration with aPKC and PAR-3. *Developmental Cell,* 13**,** 15-28.

NODARI, A., ZAMBRONI, D., QUATTRINI, A., COURT, F. A., D'URSO, A., RECCHIA, A., TYBULEWICZ, V. L. J., WRABETZ, L. & FELTRI, M. L. 2007. beta 1 integrin activates Rac1 in Schwann cells to generate radial lamellae during axonal sorting and myelination. *Journal of Cell Biology,* 177**,** 1063-1075.

NORRIS, A., TAMMINENI, P., WANG, S., GERDES, J., MURR, A., KWAN, K. Y., CAI, Q. & GRANT, B. D. 2017. SNX-1 and RME-8 oppose the assembly of HGRS-1/ESCRT-0 degradative microdomains on endosomes. *Proceedings of the National Academy of Sciences of the United States of America,* 114**,** E307-E316.

OGATA, T., IIJIMA, S., HOSHIKAWA, S., MIURA, T., YAMAMOTO, S., ODA, H., NAKAMURA, K. & TANAKA, S. 2004. Opposing extracellular signal-regulated kinase and Akt pathways control Schwann cell myelination. *Journal of Neuroscience,* 24**,** 6724-6732.

OUGHTRED, R., RUST, J., CHANG, C., BREITKREUTZ, B. J., STARK, C., WILLEMS, A., BOUCHER, L., LEUNG, G., KOLAS, N., ZHANG, F., DOLMA, S., COULOMBE-HUNTINGTON, J., CHATR-ARYAMONTRI, A., DOLINSKI, K. & TYERS, M. 2021. The BioGRID database: A comprehensive biomedical resource of curated protein, genetic, and chemical interactions. *Protein Science,* 30**,** 187-200.

PATZIG, J., JAHN, O., TENZER, S., WICHERT, S. P., DE MONASTERIO-SCHRADER, P., ROSFA, S., KUHAREV, J., YAN, K., BORMUTH, I., BREMER, J., AGUZZI, A., ORFANIOTOU, F., HESSE, D., SCHWAB, M. H., MOBIUS, W., NAVE, K. A. & WERNER, H. B. 2011. Quantitative and Integrative Proteome Analysis of Peripheral Nerve Myelin Identifies Novel Myelin Proteins and Candidate Neuropathy Loci. *Journal of Neuroscience,* 31**,** 16369-16386.

PEPLOWSKA, K., MARKGRAF, D. F., OSTROWICZ, C. W., BANGE, G. & UNGERMANN, C. 2007. The CORVET tethering complex interacts with the yeast

Rab5 homolog Vps21 and is involved in endo-lysosomal biogenesis. *Developmental Cell,* 12**,** 739-750.

PEREIRA, J. A., BENNINGER, Y., BAUMANN, R., GONCALVES, A. F., OZCELIK, M., THURNHERR, T., TRICAUD, N., MEIJER, D., FASSLER, R., SUTER, U. & RELVAS, J. B. 2009. Integrin-linked kinase is required for radial sorting of axons and Schwann cell remyelination in the peripheral nervous system. *Journal of Cell Biology,* 185**,** 147-161.

PEREIRA, J. A., LEBRUN-JULIEN, F. & SUTER, U. 2012. Molecular mechanisms regulating myelination in the peripheral nervous system. *Trends in Neurosciences,* 35**,** 123-134.

PERINI, E. D., SCHAEFER, R., STOTER, M., KALAIDZIDIS, Y. & ZERIAL, M. 2014. Mammalian CORVET Is Required for Fusion and Conversion of Distinct Early Endosome Subpopulations. *Traffic,* 15**,** 1366-1389.

PFEFFER, S. R. 2017. Rab GTPases: master regulators that establish the secretory and endocytic pathways. *Molecular Biology of the Cell,* 28**,** 712-715.

PFEUFER, A., SANNA, S., ARKING, D. E., MULLER, M., GATEVA, V., FUCHSBERGER, C., EHRET, G. B., ORRU, M., PATTARO, C., KOTTGEN, A., PERZ, S., USALA, G., BARBALIC, M., LI, M., PUTZ, B., SCUTERI, A., PRINEAS, R. J., SINNER, M. F., GIEGER, C., NAJJAR, S. S., KAO, W. H. L., MUHLEISEN, T. W., DEI, M., HAPPLE, C., MOHLENKAMP, S., CRISPONI, L., ERBEL, R., JOCKEL, K. H., NAITZA, S., STEINBECK, G., MARRONI, F., HICKS, A. A., LAKATTA, E., MULLER-MYHSOK, B., PRAMSTALLER, P. P., WICHMANN, H. E., SCHLESSINGER, D., BOERWINKLE, E., MEITINGER, T., UDA, M., CORESH, J., KAAB, S., ABECASIS, G. R. & CHAKRAVARTI, A. 2009. Common variants at ten loci modulate the QT interval duration in the QTSCD Study. *Nature Genetics,* 41**,** 407-414.

PHILLIPS-KRAWCZAK, C. A., SINGLA, A., STAROKADOMSKYY, P., DENG, Z. H., OSBORNE, D. G., LI, H. Y., DICK, C. J., GOMEZ, T. S., KOENECKE, M., ZHANG, J. S., DAI, H. M., SIFUENTES-DOMINGUEZ, L. F., GENG, L. N., KAUFMANN, S. H., HEIN, M. Y., WALLIS, M., MCGAUGHRAN, J., GECZ, J., DE SLUIS, B. V., BILLADEAU, D. D. & BURSTEIN, E. 2015. COMMD1 is linked to the WASH complex and regulates endosomal trafficking of the copper transporter ATP7A. *Molecular Biology of the Cell,* 26**,** 91-103.

PIETIAINEN, V., VASSILEV, B., BLOM, T., WANG, W., NELSON, J., BITTMAN, R., BACK, N., ZELCER, N. & IKONEN, E. 2013. NDRG1 functions in LDL receptor trafficking by regulating endosomal recycling and degradation. *Journal of Cell Science,* 126**,** 3961-3971.

PINEDA-MOLINA, E., BELRHALI, H., PIEFER, A. J., AKULA, I., BATES, P. & WEISSENHORN, W. 2006. The crystal structure of the C-terminal domain of Vps28 reveals a conserved surface required for Vps20 recruitment. *Traffic,* 7**,** 1007-1016.

PIPER, R. C., DIKIC, I. & LUKACS, G. L. 2014. Ubiquitin-Dependent Sorting in Endocytosis. *Cold Spring Harbor Perspectives in Biology,* 6.

PODINOVSKAIA, M. & SPANG, A. 2018. The Endosomal Network: Mediators and Regulators of Endosome Maturation. *Endocytosis and Signaling,* 57**,** 1-38.

POLS, M. S., BRINK, C., GOSAVI, P., OORSCHOT, V. & KLUMPERMAN, J. 2013. The HOPS Proteins hVps41 and hVps39 Are Required for Homotypic and Heterotypic Late Endosome Fusion. *Traffic,* 14**,** 219-232.

POLYAK, K., XIA, Y., ZWEIER, J. L., KINZLER, K. W. & VOGELSTEIN, B. 1997. A model for p53-induced apoptosis. *Nature,* 389**,** 300-305.

PONOMAREVA, O. Y., ELICEIRI, K. W. & HALLORAN, M. C. 2016. Charcot-Marie-Tooth 2b associated Rab7 mutations cause axon growth and guidance defects during vertebrate sensory neuron development. *Neural Development,* 11.

PONTING, C. P., MOTT, R., BORK, P. & COPLEY, R. R. 2001. Novel protein domains and repeats in Drosophila melanogaster: Insights into structure, function, and evolution. *Genome Research,* 11**,** 1996-2008.

POSTLETHWAIT, J. H., WOODS, I. G., NGO-HAZELETT, P., YAN, Y. L., KELLY, P. D., CHU, F., HUANG, H., HILL-FORCE, A. & TALBOT, W. S. 2000. Zebrafish comparative genomics and the origins of vertebrate chromosomes. *Genome Research,* 10**,** 1890-1902.

POTERYAEV, D., DATTA, S., ACKEMA, K., ZERIAL, M. & SPANG, A. 2010. Identification of the Switch in Early-to-Late Endosome Transition. *Cell,* 141**,** 497-508.

POWELKA, A. M., SUN, J. L., LI, J., GAO, M. G., SHAW, L. M., SONNENBERG, A. & HSU, V. W. 2004. Stimulation-dependent recycling of integrin beta 1 regulated by ARF6 and Rab11. *Traffic,* 5**,** 20-36.

PRAGER, G. W., FERAL, C. C., KIM, C., HAN, J. & GINSBERG, M. H. 2007. CD98hc (SLC3A2) interaction with the integrin beta subunit cytoplasmic domain mediates adhesive signaling. *Journal of Biological Chemistry,* 282**,** 24477-24484.

PRESTON, M. A., FINSETH, L. T., BOURNE, J. N. & MACKLIN, W. B. 2019. A novel myelin protein zero transgenic zebrafish designed for rapid readout of in vivo myelination. *Glia,* 67**,** 650-667.

PROGIDA, C., SPINOSA, M. R., DE LUCA, A. & BUCCI, C. 2006. RILP interacts with the VPS22 component of the ESCRT-II complex. *Biochemical and Biophysical Research Communications,* 347**,** 1074-1079.

PURUSHOTHAMAN, L. K., ARLT, H., KUHLEE, A., RAUNSER, S. & UNGERMANN, C. 2017. Retromer-driven membrane tubulation separates endosomal recycling from Rab7/Ypt7-dependent fusion. *Molecular Biology of the Cell,* 28**,** 783-791.

PUTHENVEEDU, M. A., LAUFFER, B., TEMKIN, P., VISTEIN, R., CARLTON, P., THORN, K., TAUNTON, J., WEINER, O. D., PARTON, R. G. & VON ZASTROW, M. 2010. Sequence-Dependent Sorting of Recycling Proteins by Actin-Stabilized Endosomal Microdomains. *Cell,* 143**,** 761-773.

QIN, W. X., WUNDERLEY, L., BARRETT, A. L., HIGH, S. & WOODMAN, P. G. 2016. The Charcot Marie Tooth disease protein LITAF is a zinc-binding monotopic membrane protein. *Biochemical Journal,* 473**,** 3965-3978.

RADHAKRISHNA, H. & DONALDSON, J. G. 1997. ADP-ribosylation factor 6 regulates a novel plasma membrane recycling pathway. *Journal of Cell Biology,* 139**,** 49-61.

RAHAJENG, J., GIRIDHARAN, S. S. P., CAI, B. S., NASLAVSKY, N. & CAPLAN, S. 2012. MICAL-L1 is a Tubular Endosomal Membrane Hub that Connects Rab35 and Arf6 With Rab8a. *Traffic,* 13**,** 82-93.

RAIBORG, C., BACHE, K. G., GILLOOLY, D. J., MADSHUSH, I. H., STANG, E. & STENMARK, H. 2002. Hrs sorts ubiquitinated proteins into clathrin-coated microdomains of early endosomes. *Nature Cell Biology,* 4**,** 394-398.

RAIBORG, C., BACHE, K. G., MEHLUM, A., STANG, E. & STENMARK, H. 2001a. Hrs recruits clathrin to early endosomes. *Embo Journal,* 20**,** 5008-5021.

RAIBORG, C., BREMNES, B., MEHLUM, A., GILLOOLY, D. J., D'ARRIGO, A., STANG, E. & STENMARK, H. 2001b. FYVE and coiled-coil domains determine the specific localisation of Hrs to early endosomes. *Journal of Cell Science,* 114**,** 2255-2263.

RAIBORG, C. & STENMARK, H. 2009. The ESCRT machinery in endosomal sorting of ubiquitylated membrane proteins. *Nature,* 458**,** 445-452.

RAPHAEL, A. R. & TALBOT, W. S. 2011. NEW INSIGHTS INTO SIGNALING DURING MYELINATION IN ZEBRAFISH. *Growth Factors in Development,* 97**,** 1-19.

REID, E., CONNELL, J., DULEY, S., BROWN, S. E. & SANDERSON, C. M. 2005. The hereditary spastic paraplegia protein spastin interacts with the ESCRT-III complex-associated endosomal protein CHMP1B. *Human Molecular Genetics,* 14**,** 19-38.

RENVOISE, B., PARKER, R. L., YANG, D., BAKOWSKA, J. C., HURLEY, J. H. & BLACKSTONE, C. 2010. SPG20 Protein Spartin Is Recruited to Midbodies by ESCRT-III Protein Ist1 and Participates in Cytokinesis. *Molecular Biology of the Cell,* 21**,** 3293-3303.

RICHARDSON, S. C. W., WINISTORFER, S. C., POUPON, V., LUZIO, J. P. & PIPER, R. C. 2004. Mammalian late vacuole protein sorting orthologues participate in early endosomal fusion and interact with the cytoskeleton. *Molecular Biology of the Cell,* 15**,** 1197-1210.

RINK, J., GHIGO, E., KALAIDZIDIS, Y. & ZERIAL, M. 2005. Rab conversion as a mechanism of progression from early to late endosomes. *Cell,* 122**,** 735-749.

ROBERTS, R. C., PEDEN, A. A., BUSS, F., BRIGHT, N. A., LATOUCHE, M., REILLY, M. M., KENDRICK-JONES, J. & LUZIO, J. P. 2010. Mistargeting of SH3TC2 away from the recycling endosome causes Charcot-Marie-Tooth disease type 4C. *Human Molecular Genetics,* 19**,** 1009-1018.

ROBINSON, F. L. & DIXON, J. E. 2005. The phosphoinositide-3-phosphatase MTMR2 associates with MTMR13, a membrane-associated pseudophosphatase also mutated in type 4B Charcot-Marie-Tooth disease. *Journal of Biological Chemistry,* 280**,** 31699-31707.

ROJAS, R., VAN VLIJMEN, T., MARDONES, G. A., PRABHU, Y., ROJAS, A. L., MOHAMMED, S., HECK, A. J. R., RAPOSO, G., VAN DER SLUIJS, P. & BONIFACINO, J. S. 2008. Regulation of retromer recruitment to endosomes by sequential action of Rab5 and Rab7. *Journal of Cell Biology,* 183**,** 513-526.

ROLLAND, T., TASAN, M., CHARLOTEAUX, B., PEVZNER, S. J., ZHONG, Q., SAHNI, N., YI, S., LEMMENS, I., FONTANILLO, C., MOSCA, R., KAMBUROV, A., GHIASSIAN, S. D., YANG, X. P., GHAMSARI, L., BALCHA, D., BEGG, B. E., BRAUN, P., BREHME, M., BROLY, M. P., CARVUNIS, A. R., CONVERY-ZUPAN, D., COROMINAS, R., COULOMBE-HUNTINGTON, J., DANN, E., DREZE, M., DRICOT, A., FAN, C. Y., FRANZOSA, E., GEBREAB, F., GUTIERREZ, B. J., HARDY, M. F., JIN, M., KANG, S. L., KIROS, R., LIN, G. N., LUCK, K., MACWILLIAMS, A., MENCHE, J. R., MURRAY, R. R., PALAGI, A., POULIN, M. M., RAMBOUT, X., RASLA, J., REICHERT, P., ROMERO, V., RUYSSINCK, E., SAHALIE, J. M., SCHOLZ, A., SHAH, A. A., SHARMA, A., SHEN, Y., SPIROHN, K., TAM, S., TEJEDA, A. O., TRIGG, S. A., TWIZERE, J. C., VEGA, K., WALSH, J., CUSICK, M. E., XIA, Y., BARABASI, A. L., IAKOUCHEVA, L. M., ALOY, P., DE LAS RIVAS, J., TAVERNIER, J., CALDERWOOD, M. A., HILL, D. E., HAO, T., ROTH, F. P. & VIDAL, M. 2014. A Proteome-Scale Map of the Human Interactome Network. *Cell,* 159**,** 1212-1226.

ROUX, K. J., KIM, D. I. & BURKE, B. 2013. BioID: A Screen for Protein-Protein Interactions. *Current Protocols in Protein Science,* 74**,** 19.23.1-19.23.14.

ROUX, K. J., KIM, D. I., RAIDA, M. & BURKE, B. 2012. A promiscuous biotin ligase fusion protein identifies proximal and interacting proteins in mammalian cells. *Journal of Cell Biology,* 196**,** 801-810.

SAHNI, N., YI, S., TAIPALE, M., BASS, J. I. F., COULOMBE-HUNTINGTON, J., YANG, F., PENG, J., WEILE, J., KARRAS, G. I., WANG, Y., KOVACS, I. A., KAMBUROV, A., KRYKBAEVA, I., LAM, M. H., TUCKER, G., KHURANA, V., SHARMA, A., LIU, Y. Y., YACHIE, N., ZHONG, Q., SHEN, Y., PALAGI, A., SAN-MIGUEL, A., FAN, C. Y., BALCHA, D., DRICOT, A., JORDAN, D. M., WALSH, J. M., SHAH, A. A., YANG, X. P., STOYANOVA, A. K., LEIGHTON, A., CALDERWOOD, M. A., JACOB, Y., CUSICK, M. E., SALEHI-ASHTIANI, K., WHITESELL, L. J., SUNYAEV, S., BERGER, B., BARABASI, A. L., CHARLOTEAUX, B., HILL, D. E., HAO, T., ROTH, F. P., XIA, Y., WALHOUT, A. J. M., LINDQUIST, S. & VIDAL, M. 2015. Widespread Macromolecular Interaction Perturbations in Human Genetic Disorders. *Cell,* 161**,** 647-660.

SAIFI, G. M., SZIGETI, K., WISZNIEWSKI, W., SHY, M. E., KRAJEWSKI, K., HAUSMANOWA-PETRUSEWICZ, I., KOCHANSKI, A., REESER, S., MANCIAS, P., BUTLER, I. & LUPSKI, J. R. 2005. SIMPLE mutations in Charcot-Marie-Tooth disease and the potential role of its protein product in protein degradation. *Human Mutation,* 25**,** 372-383.

SAKAI, R., FUKUDA, R., UNIDA, S., AKI, M., ONO, Y., ENDO, A., KUSUMI, S., KOGA, D., FUKUSHIMA, T., KOMADA, M. & OKIYONEDA, T. 2019. The integral function of the endocytic recycling compartment is regulated by RFFL-mediated ubiquitylation of Rab11 effectors. *Journal of Cell Science,* 132.

SAKSENA, S., WAHLMAN, J., TEIS, D., JOHNSON, A. E. & EMR, S. D. 2009. Functional reconstitution of ESCRT-III assembly and disassembly. *Cell,* 136**,** 97-109.

SALEEB, R. S., KAVANAGH, D. M., DUN, A. R., DALGARNO, P. A. & DUNCAN, R. R. 2019. A VPS33A-binding motif on syntaxin 17 controls autophagy completion in mammalian cells. *Journal of Biological Chemistry,* 294**,** 4188-4201.

SALZER, J. L. 2015. Schwann Cell Myelination. *Cold Spring Harbor Perspectives in Biology,* 7.

SAMARELLI, A. V., ZIEGLER, T., MEVES, A., FASSLER, R. & BOTTCHER, R. T. 2020. Rabgap1 promotes recycling of active beta 1 integrins to support effective cell migration. *Journal of Cell Science,* 133.

SBRISSA, D., IKONOMOV, O. C., FU, Z. Y., IJUIN, T., GRUENBERG, J., TAKENAWA, T. & SHISHEVA, A. 2007. Core protein machinery for mammalian phosphatidylinositol 3,5-bisphosphate synthesis and turnover that regulates the progression of endosomal transport - Novel sac phosphatase joins the arpikfyve-pikfyve complex. *Journal of Biological Chemistry,* 282**,** 23878-23891.

SCHINDLER, C., CHEN, Y., PU, J., GUO, X. L. & BONIFACINO, J. S. 2015. EARP is a multisubunit tethering complex involved in endocytic recycling. *Nature Cell Biology,* 17**,** 639-U229.

SCHIWECK, J., MURK, K., LEDDEROSE, J., MÜNSTER-WANDOWSKI, A., ORNAGHI, M., VIDA, I. & EICKHOLT, B. J. 2021. Drebrin controls scar formation and astrocyte reactivity upon traumatic brain injury by regulating membrane trafficking. *Nature Communications,* 12**,** 1490.

SCHMIDT, O. & TEIS, D. 2012. The ESCRT machinery. *Current Biology,* 22**,** R116-R120.

SCHONEBERG, J., LEE, I. H., IWASA, J. H. & HURLEY, J. H. 2017. Reverse-topology membrane scission by the ESCRT proteins. *Nature Reviews Molecular Cell Biology,* 18**,** 5-17.

SEAMAN, M. N. J. 2004. Cargo-selective endosomal sorting for retrieval to the Golgi requires retromer. *Journal of Cell Biology,* 165**,** 111-122.

SEAMAN, M. N. J., HARBOUR, M. E., TATTERSALL, D., READ, E. & BRIGHT, N. 2009. Membrane recruitment of the cargo-selective retromer subcomplex is catalysed by the small GTPase Rab7 and inhibited by the Rab-GAP TBC1D5. *Journal of Cell Science,* 122**,** 2371-2382.

SEAMAN, M. N. J., MARCUSSON, E. G., CEREGHINO, J. L. & EMR, S. D. 1997. Endosome to Golgi retrieval of the vacuolar protein sorting receptor, Vps10p, requires the function of the VPS29, VPS30, and VPS35 gene products. *Journal of Cell Biology,* 137**,** 79-92.

SENDEREK, J., BERGMANN, C., WEBER, S., KETELSEN, U. P., SCHORLE, H., RUDNIK-SCHONEBORN, S., BUTTNER, R., BUCHHEIM, E. & ZERRES, K. 2003. Mutation of the SBF2 gene, encoding a novel member of the myotubularin family, in Charcot-Marie-Tooth neuropathy type 4B2/11p15. *Human Molecular Genetics,* 12**,** 349-356.

SHANNON, P., MARKIEL, A., OZIER, O., BALIGA, N. S., WANG, J. T., RAMAGE, D., AMIN, N., SCHWIKOWSKI, B. & IDEKER, T. 2003. Cytoscape: A software environment for integrated models of biomolecular interaction networks. *Genome Research,* 13**,** 2498-2504.

SHARMA, M., GIRIDHARAN, S. S. P., RAHAJENG, J., NASLAVSKY, N. & CAPLAN, S. 2009. MICAL-L1 Links EHD1 to Tubular Recycling Endosomes and Regulates Receptor Recycling. *Molecular Biology of the Cell,* 20**,** 5181-5194.

SHEARWIN-WHYATT, L., DALTON, H. E., FOOT, N. & KUMAR, S. 2006. Regulation of functional diversity within the Nedd4 family by accessory and adaptor proteins. *Bioessays,* 28**,** 617-628.

SHEARWIN-WHYATT, L. M., BROWN, D. L., WYLIE, F. G., STOW, J. L. & KUMAR, S. 2004. N4WBP5A (Ndfip2), a Nedd4-interacting protein, localizes to multivesicular bodies and the Golgi, and has a potential role in protein trafficking. *Journal of Cell Science,* 117**,** 3679-3689.

SHI, A. B., SUN, L., BANERJEE, R., TOBIN, M., ZHANG, Y. H. & GRANT, B. D. 2009. Regulation of endosomal clathrin and retromer-mediated endosome to Golgi retrograde transport by the J-domain protein RME-8. *Embo Journal,* 28**,** 3290-3302.

SHI, H., ROJAS, R., BONIFACINO, J. S. & HURLEY, J. H. 2006. The retromer subunit Vps26 has an arrestin fold and binds Vps35 through its C-terminal domain. *Nature Structural & Molecular Biology,* 13**,** 540-548.

SHIRK, A. J., ANDERSON, S. K., HASHEMI, S. H., CHANCE, P. F. & BENNETT, C. L. 2005. SIMPLE interacts with NEDD4 and TSG101: Evidence for a role in lysosomal sorting and implications for Charcot-Marie-Tooth disease. *Journal of Neuroscience Research,* 82**,** 43-50.

SIDIROPOULOS, P. N. M., MIEHE, M., BOCK, T., TINELLI, E., OERTLI, C. I., KUNER, R., MEIJER, D., WOLLSCHEID, B., NIEMANN, A. & SUTER, U. 2012. Dynamin 2 mutations in Charcot-Marie-Tooth neuropathy highlight the importance of clathrin-mediated endocytosis in myelination. *Brain,* 135**,** 1395-1411.

SIMONETTI, B. & CULLEN, P. J. 2019. Actin-dependent endosomal receptor recycling. *Current Opinion in Cell Biology,* 56**,** 22-33.

SIMONETTI, B., DANSON, C. M., HEESOM, K. J. & CULLEN, P. J. 2017. Sequence-dependent cargo recognition by SNX-BARs mediates retromer-independent transport of CI-MPR. *Journal of Cell Biology,* 216**,** 3695-3712.

SIMONETTI, B., PAUL, B., CHAUDHARI, K., WEERATUNGA, S., STEINBERG, F., GORLA, M., HEESOM, K. J., BASHAW, G. J., COLLINS, B. M. & CULLEN, P. J.

2019. Molecular identification of a BAR domain-containing coat complex for endosomal recycling of transmembrane proteins. *Nature Cell Biology,* 21**,** 1219-+.

SIMONS, M. & TROTTER, J. 2007. Wrapping it up: the cell biology of myelination. *Current Opinion in Neurobiology,* 17**,** 533-540.

SIMONSEN, A., GAULLIER, J. M., D'ARRIGO, A. & STENMARK, H. 1999. The Rab5 effector EEA1 interacts directly with syntaxin-6. *Journal of Biological Chemistry,* 274**,** 28857-28860.

SIMONSEN, A., LIPPE, R., CHRISTOFORIDIS, S., GAULLIER, J. M., BRECH, A., CALLAGHAN, J., TOH, B. H., MURPHY, C., ZERIAL, M. & STENMARK, H. 1998. EEA1 links PI(3)K function to Rab5 regulation of endosome fusion. *Nature,* 394**,** 494-498.

SINKIEWICZ-DAROL, E., LACERDA, A. F., KOSTERA-PRUSZCZYK, A., POTULSKA-CHROMIK, A., SOKOLOWSKA, B., KABZINSKA, D., BRUNETTI, C. R., HAUSMANOWA-PETRUSEWICZ, I. & KOCHANSKI, A. 2015. The LITAF/SIMPLE I92V sequence variant results in an earlier age of onset of CMT1A/HNPP diseases. *Neurogenetics,* 16**,** 27-32.

SKRE, H. 1974. GENETIC AND CLINICAL ASPECTS OF CHARCOT-MARIE-TOOTHS DISEASE. *Clinical Genetics,* 6**,** 98-118.

SLAGSVOLD, T., AASLAND, R., HIRANO, S., BACHE, K. G., RAIBORG, C., TRAMBAIOLO, D., WAKATSUKI, S. & STENMARK, H. 2005. Eap45 in mammalian ESCRT-II binds ubiquitin via a phosphoinositide-interacting GLUE domain. *Journal of Biological Chemistry,* 280**,** 19600-19606.

SOLINGER, J. A., RASHID, H. O., PRESCIANOTTO-BASCHONG, C. & SPANG, A. 2020. FERARI is required for Rab11-dependent endocytic recycling. *Nature Cell Biology,* 22**,** 213-+.

SOMANDIN, C., GERBER, D., PEREIRA, J. A., HORN, M. & SUTER, U. 2012. LITAF (SIMPLE) regulates Wallerian degeneration after injury but is not essential for peripheral nerve development and maintenance: Implications for Charcot-Marie-Tooth disease. *Glia,* 60**,** 1518-1528.

SONNICHSEN, B., DE RENZIS, S., NIELSEN, E., RIETDORF, J. & ZERIAL, M. 2000. Distinct membrane domains on endosomes in the recycling pathway visualized by multicolor imaging of Rab4, Rab5 and Rab11. *Journal of Cell Biology,* 149**,** 901-913.

SORKIN, A. 2004. Cargo recognition during clathrin-mediated endocytosis: a team effort. *Current Opinion in Cell Biology,* 16**,** 392-399.

SPANG, A. 2016. Membrane Tethering Complexes in the Endosomal System. *Frontiers in Cell and Developmental Biology,* 4.

SRINIVASAN, S., LEEMAN, S. E. & AMAR, S. 2010. Beneficial Dysregulation of the Time Course of Inflammatory Mediators in Lipopolysaccharide-Induced Tumor Necrosis Factor Alpha Factor-Deficient Mice. *Clinical and Vaccine Immunology,* 17**,** 699-704.

STEFANI, F., ZHANG, L., TAYLOR, S., DONOVAN, J., ROLLINSON, S., DOYOTTE, A., BROWNHILL, K., BENNION, J., PICKERING-BROWN, S. & WOODMAN, P. 2011. UBAP1 Is a Component of an Endosome-Specific ESCRT-I Complex that Is Essential for MVB Sorting. *Current Biology,* 21**,** 1245-1250.

STEINBERG, F., GALLON, M., WINFIELD, M., THOMAS, E. C., BELL, A. J., HEESOM, K. J., TAVARE, J. M. & CULLEN, P. J. 2013. A global analysis of SNX27-retromer assembly and cargo specificity reveals a function in glucose and metal ion transport. *Nature Cell Biology,* 15**,** 461-+.

STEMMER, M., THUMBERGER, T., KEYER, M. D., WITTBRODT, J. & MATEO, J. L. 2015. CCTop: An Intuitive, Flexible and Reliable CRISPR/Cas9 Target Prediction Tool. *Plos One,* 10**,** 11.

STENDEL, C., ROOS, A., KLEINE, H., ARNAUD, E., OZCELIK, M., SIDIROPOULOS, P. N. M., ZENKER, J., SCHUPFER, F., LEHMANN, U., SOBOTA, R. M., LITCHFIELD, D. W., LUSCHER, B., CHRAST, R., SUTER, U. & SENDEREK, J. 2010. SH3TC2, a protein mutant in Charcot-Marie-Tooth neuropathy, links peripheral nerve myelination to endosomal recycling. *Brain,* 133**,** 2462-2474.

STREET, V. A., BENNETT, C. L., GOLDY, J. D., SHIRK, A. J., KLEOPA, K. A., TEMPEL, B. L., LIPE, H. P., SCHERER, S. S., BIRD, T. D. & CHANCE, P. F. 2003. Mutation of a putative protein degradation gene LITAF/SIMPLE in Charcot-Marie-Tooth disease 1C. *Neurology,* 60**,** 22-26.

STUCHELL, M. D., GARRUS, J. E., MULLER, B., STRAY, K. M., GHAFFARIAN, S., MCKINNON, R., KRAUSSLICH, H. G., MORHAM, S. G. & SUNDQUIST, W. I. 2004. The human endosomal sorting complex required for transport (ESCRT-I) and its role in HIV-1 budding. *Journal of Biological Chemistry,* 279**,** 36059-36071.

STUFFERS, S., BRECH, A. & STENMARK, H. 2009. ESCRT proteins in physiology and disease. *Experimental Cell Research,* 315**,** 1619-1626.

SZKLARCZYK, D., GABLE, A. L., LYON, D., JUNGE, A., WYDER, S., HUERTA-CEPAS, J., SIMONOVIC, M., DONCHEVA, N. T., MORRIS, J. H., BORK, P., JENSEN, L. J. & MERING, C. 2019. STRING v11: protein-protein association networks with increased coverage, supporting functional discovery in genome-wide experimental datasets. *Nucleic Acids Research,* 47**,** D607-D613.

TABUCHI, M., YANATORI, I., KAWAI, Y. & KISHI, F. 2010. Retromer-mediated direct sorting is required for proper endosomal recycling of the mammalian iron transporter DMT1. *Journal of Cell Science,* 123**,** 756-766.

TAKAHASHI, S., KUBO, K., WAGURI, S., YABASHI, A., SHIN, H. W., KATOH, Y. & NAKAYAMA, K. 2012. Rab11 regulates exocytosis of recycling vesicles at the plasma membrane. *Journal of Cell Science,* 125**,** 4049-4057.

TAKATORI, S., TATEMATSU, T., CHENG, J. L., MATSUMOTO, J., AKANO, T. & FUJIMOTO, T. 2016. Phosphatidylinositol 3,5-Bisphosphate-Rich Membrane Domains in Endosomes and Lysosomes. *Traffic,* 17**,** 154-167.

TANG, X. R., MARCIANO, D. L., LEEMAN, S. E. & AMAR, S. 2005. LPS induces the interaction of a transcription factor, LPS-induced TNF-alpha factor, and STAT6(B) with effects on multiple cytokines. *Proceedings of the National Academy of Sciences of the United States of America,* 102**,** 5132-5137.

TANG, X. R., METZGER, D., LEEMAN, S. & AMAR, S. 2006. LPS-induced TNF-alpha factor (LITAF)-deficient mice express reduced LPS-induced cytokine: Evidence for LITAF-dependent LPS signaling pathways. *Proceedings of the National Academy of Sciences of the United States of America,* 103**,** 13777-13782.

TEMKIN, P., LAUFFER, B., JAGER, S., CIMERMANCIC, P., KROGAN, N. J. & VON ZASTROW, M. 2011. SNX27 mediates retromer tubule entry and endosome-to-plasma membrane trafficking of signalling receptors. *Nature Cell Biology,* 13**,** 715-U199.

TEO, H. L., GILL, D. J., SUN, J., PERISIC, O., VEPRINTSEV, D. B., VALLIS, Y., EMR, S. D. & WILLIAMS, R. L. 2006. ESCRT-I core and ESCRT-II GLUE domain structures reveal role for GLUE in linking to ESCRT-I and membranes. *Cell,* 125**,** 99-111.

THINON, E., FERNANDEZ, J. P., MOLINA, H. & HANG, H. C. 2018. Selective Enrichment and Direct Analysis of Protein S-Palmitoylation Sites. *Journal of Proteome Research,* 17**,** 1907-1922.

TONI, T., OHNO, N., MIYAMOTO, Y., KAWAHARA, K., SAITOH, Y., NAKAMURA, K., TAKASHIMA, S., SAKAGAMI, H., TANOUE, A. & YAMAUCHI, J. 2015. Arf6 guanine-nucleotide exchange factor cytohesin-2 regulates myelination in nerves. *Biochemical and Biophysical Research Communications,* 460**,** 819-825.

TRAJKOVIC, K., DHAUNCHAK, A. S., GONCALVES, J. T., WENZEL, D., SCHNEIDER, A., BUNT, G., NAVE, K. A. & SIMONS, M. 2006. Neuron to glia signaling triggers myelin membrane exocytosis from endosomal storage sites. *Journal of Cell Biology,* 172**,** 937-948.

TURAN, N. N., MOSHAL, K. S., RODER, K., BAGGETT, B. C., KABAKOV, A. Y., DHAKAL, S., TERAMOTO, R., CHIANG, D. Y. E., ZHONG, M. W., XIE, A., LU, Y. C., DUDLEY, S. C., MACRAE, C. A., KARMA, A. & KOREN, G. 2020. The endosomal trafficking regulator LITAF controls the cardiac Nav1.5 channel via the ubiquitin ligase NEDD4-2. *Journal of Biological Chemistry,* 295**,** 18148-18159.

TYANOVA, S., TEMU, T., SINITCYN, P., CARLSON, A., HEIN, M. Y., GEIGER, T., MANN, M. & COX, J. 2016. The Perseus computational platform for comprehensive analysis of (prote)omics data. *Nature Methods,* 13**,** 731-740.

TYRRELL, B. J., WOODHAM, E. F., SPENCE, H. J., STRATHDEE, D., INSALL, R. H. & MACHESKY, L. M. 2016. Loss of strumpellin in the melanocytic lineage impairs the WASH Complex but does not affect coat colour. *Pigment Cell & Melanoma Research,* 29**,** 559-571.

UNTERGASSER, A., CUTCUTACHE, I., KORESSAAR, T., YE, J., FAIRCLOTH, B. C., REMM, M. & ROZEN, S. G. 2012. Primer3-new capabilities and interfaces. *Nucleic Acids Research,* 40.

VALENTIJN, L. J., BAAS, F., WOLTERMAN, R. A., HOOGENDIJK, J. E., VANDENBOSCH, N. H. A., ZORN, I., GABREELSFESTEN, A. W. M., DEVISSER, M. & BOLHUIS, P. A. 1992. IDENTICAL POINT MUTATIONS OF PMP-22 IN TREMBLER-J MOUSE AND CHARCOT-MARIE-TOOTH DISEASE TYPE-1A. *Nature Genetics,* 2**,** 288-291.

VAN DER KANT, R., JONKER, C. T. H., WIJDEVEN, R. H., BAKKER, J., JANSSEN, L., KLUMPERMAN, J. & NEEFJES, J. 2015. Characterization of the Mammalian CORVET and HOPS Complexes and Their Modular Restructuring for Endosome Specificity. *Journal of Biological Chemistry,* 290**,** 30280-30290.

VAN WEERING, J. R. T., VERKADE, P. & CULLEN, P. J. 2012. SNX-BAR-Mediated Endosome Tubulation is Co-ordinated with Endosome Maturation. *Traffic,* 13**,** 94-107.

VERHOEVEN, K., DE JONGHE, P., COEN, K., VERPOORTEN, N., AUER-GRUMBACH, M., KWON, J. M., FITZPATRICK, D., SCHMEDDING, E., DE VRIENDT, E., JACOBS, A., VAN GERWEN, V., WAGNER, K., HARTUNG, H. P. & TIMMERMAN, V. 2003. Mutations in the small GTP-ase late endosomal protein RAB7 cause Charcot-Marie-Tooth type 2B neuropathy. *American Journal of Human Genetics,* 72**,** 722-727.

VIJAY, S., CHIU, M., DACKS, J. B. & ROBERTS, R. C. 2016. Exclusive expression of the Rab11 effector SH3TC2 in Schwann cells links integrin-alpha(6) and myelin maintenance to Charcot-Marie-Tooth disease type 4C. *Biochimica Et Biophysica Acta-Molecular Basis of Disease,* 1862**,** 1279-1290.

WALLROTH, A. & HAUCKE, V. 2018. Phosphoinositide conversion in endocytosis and the endolysosomal system. *Journal of Biological Chemistry,* 293**,** 1526-1535.

WANG, T. L. & HONG, W. J. 2006. RILP interacts with VPS22 and VPS36 of ESCRT-II and regulates their membrane recruitment. *Biochemical and Biophysical Research Communications,* 350**,** 413-423.

WANG, Z. H., LI, Y., HOU, B., PRONOBIS, M. I., WANG, M. Q., WANG, Y. M., CHENG, G. C., WENG, W. N., WANG, Y. Q., TANG, Y. F., XU, X. F., PAN, R., LIN, F., WANG, N., CHEN, Z. Q., WANG, S. W., MA, L. Z., LI, Y. R., HUANG, D. L., JIANG, L., WANG, Z. Q., ZENG, W. F., ZHANG, Y., DU, X. M., LIN, Y., LI, Z. Q., XIA, Q. Y., GENG, J., DAI, H. P., YU, Y., ZHAO, X. D., YUAN, Z., YAN, J., NIE, Q. H., ZHANG, X. Q., WANG, K., CHEN, F. L., ZHANG, Q., ZHU, Y. X., ZHENG, S. S., POSS, K. D., TAO, S. C. & MENG, X. 2020. An array of 60,000 antibodies for proteome-scale antibody generation and target discovery. *Science Advances,* 6.

WARNER, L. E., MANCIAS, P., BUTLER, I. J., MCDONALD, C. M., KEPPEN, L., KOOB, K. G. & LUPSKI, J. R. 1998. Mutations in the early growth response 2 (EGR2) gene are associated with hereditary myelinopathies. *Nature Genetics,* 18**,** 382-384.

WEERATUNGA, S., PAUL, B., COLLINS, B. M. & PA, A. L. O. O. 2020. Recognising the signals for endosomal trafficking. *Current Opinion in Cell Biology,* 65**,** 17-27.

WERTZ, I. E., O'ROURKE, K. M., ZHOU, H. L., EBY, M., ARAVIND, L., SESHAGIRI, S., WU, P., WIESMANN, C., BAKER, R., BOONE, D. L., MA, A., KOONIN, E. V. & DIXIT, V. M. 2004. De-ubiquitination and ubiquitin ligase domains of A20 downregulate NF-kappa B signalling. *Nature,* 430**,** 694-699.

WESTERFIELD, M. 2000. *The Zebrafish Book. A Guide for the Laboratory Use of Zebrafish (Danio rerio)*, University of Oregon Press, Eugene.

WHITLEY, P., REAVES, B. J., HASHIMOTO, M., RILEY, A. M., POTTER, B. V. L. & HOLMAN, G. D. 2003. Identification of mammalian Vps24p as an effector of phosphatidylinositol 3,5-bisphosphate-dependent endosome compartmentalization. *Journal of Biological Chemistry,* 278**,** 38786-38795.

WON, S. Y., CHOI, B. O., CHUNG, K. W. & LEE, J. E. 2019. Zebrafish is a central model to dissect the peripheral neuropathy. *Genes & Genomics,* 41**,** 993-1000.

WULF, P., BERNHARDT, R. R. & SUTER, U. 1999. Characterization of peripheral myelin protein 22 in zebrafish (zPMP22) suggests an early role in the development of the peripheral nervous system. *Journal of Neuroscience Research,* 57**,** 467-478.

WUNDERLEY, L., ZHANG, L., YARWOOD, R., QIN, W., LOWE, M. & WOODMAN, P. 2021. Endosomal recycling tubule scission and integrin recycling involve the membrane curvature supporting protein LITAF. *Journal of Cell Science,* Online ahead of print.

XHABIJA, B., TAYLOR, G. S., FUJIBAYASHI, A., SEKIGUCHI, K. & VACRATSIS, P. O. 2011. Receptor mediated endocytosis 8 is a novel PI(3)P binding protein regulated by myotubularin-related 2. *Febs Letters,* 585**,** 1722-1728.

XIE, S. W., BAHL, K., REINECKE, J. B., HAMMOND, G. R. V., NASLAVSKY, N. & CAPLAN, S. 2016. The endocytic recycling compartment maintains cargo segregation acquired upon exit from the sorting endosome. *Molecular Biology of the Cell,* 27**,** 108-126.

YORIKAWA, C., SHIBATA, H., WAGURI, S., HATTA, K., HORII, M., KATOH, K., KOBAYASHI, T., UCHIYAMA, Y. & MAKI, M. 2005. Human CHMP6, a myristoylated ESCRT-III protein, interacts directly with an ESCRT-II component EAP20 and regulates endosomal cargo sorting. *Biochemical Journal,* 387**,** 17-26.

YOSHIDA, A., HAYASHI, H., TANABE, K. & FUJITA, A. 2017. Segregation of phosphatidylinositol 4-phosphate and phosphatidylinositol 4,5-bisphosphate into distinct microdomains on the endosome membrane. *Biochimica Et Biophysica Acta-Biomembranes,* 1859**,** 1880-1890.

YOSHIMURA, S., GERONDOPOULOS, A., LINFORD, A., RIGDEN, D. J. & BARR, F. A. 2010. Family-wide characterization of the DENN domain Rab GDP-GTP exchange factors. *Journal of Cell Biology,* 191**,** 367-381.

ZENT, R., FENCZIK, C. A., CALDERWOOD, D. A., LIU, S. C., DELLOS, M. & GINSBERG, M. H. 2000. Class- and splice variant-specific association of CD98 with integrin beta cytoplasmic domains. *Journal of Biological Chemistry,* 275**,** 5059-5064.

ZHANG, J. B., LIU, J. C., NORRIS, A., GRANT, B. D. & WANG, X. C. 2018. A novel requirement for ubiquitin-conjugating enzyme UBC-13 in retrograde recycling of MIG-14/Wntless and Wnt signaling. *Molecular Biology of the Cell,* 29**,** 2098-2112.

ZHANG, Y. H., QIN, W., LU, X. C., XU, J. S., HUANG, H. G., BAI, H. P., LI, S. & LIN, S. 2017. Programmable base editing of zebrafish genome using a modified CRISPR-Cas9 system. *Nature Communications,* 8.

ZHAO, J. & HEDERA, P. 2015. Strumpellin and Spartin, Hereditary Spastic Paraplegia Proteins, are Binding Partners. *Journal of Experimental Neuroscience,* 9**,** 15-25.

ZHU, H., GUARIGLIA, S., YU, R. Y. L., LI, W. J., BRANCHO, D., PEINADO, H., LYDEN, D., SALZER, J., BENNETT, C. & CHOW, C. W. 2013. Mutation of SIMPLE in Charcot-Marie-Tooth 1C alters production of exosomes. *Molecular Biology of the Cell,* 24**,** 1619-1637.

ZHU, J. H., JIANG, J. Y., ZHOU, W. J., ZHU, K. C. & CHEN, X. B. 1999. Differential regulation of cellular target genes by p53 devoid of the PXXP motifs with impaired apoptotic activity. *Oncogene,* 18**,** 2149-2155.

ZHUKOVSKY, M. A., FILOGRANA, A., LUINI, A., CORDA, D. & VALENTE, C. 2019. Protein Amphipathic Helix Insertion: A Mechanism to Induce Membrane Fission. *Frontiers in Cell and Developmental Biology,* 7.

ZIMMERBERG, J. & KOZLOV, M. M. 2006. How proteins produce cellular membrane curvature. *Nature Reviews Molecular Cell Biology,* 7**,** 9-19.

Appendix

Protein names	Gene names	Mock (Log2 LFQ Intensity)			Mean Mock (log2 LFQ Intensity)	LITAF (Log2 LFQ Intensity)			Mean LITAF (log2 LFQ Intensity)	-Log (p-value)	Fold change
Tumor protein D54	TPD52L2	23.28	23.14	22.71	23.04	32.58	32.07	32.55	32.40	5.60	9.36
Integrin beta-1	ITGB1	23.38	23.69	23.25	23.44	32.38	31.95	32.77	32.37	5.29	8.93
Ephrin type-A receptor 2	EPHA2	23.08	22.49	22.99	22.85	29.20	29.23	29.59	29.34	5.07	6.49
Synaptosomal-associated protein 29	SNAP29	24.03	23.90	24.17	24.03	26.08	26.11	25.95	26.05	4.58	2.01
Epidermal growth factor receptor substrate 15-like 1	EPS15L1	22.28	22.32	22.77	22.45	27.49	28.12	28.05	27.88	4.55	5.43
Integrin beta-5	ITGB5	22.93	22.91	23.53	23.12	28.15	27.95	28.38	28.16	4.53	5.04
Cation-independent mannose-6-phosphate receptor	IGF2R	22.57	23.11	23.04	22.91	31.87	30.93	30.33	31.05	4.15	8.14
Protein AHNAK2	AHNAK2	23.01	22.93	23.30	23.08	31.07	32.83	32.68	32.19	4.03	9.12
Spartin	SPG20	23.39	23.59	22.80	23.26	27.01	27.10	27.17	27.10	4.02	3.83
Cytospin-B	SPECC1	23.77	23.34	23.68	23.60	26.13	25.99	25.83	25.98	3.97	2.38
Catenin delta-1	CTNND1	21.89	22.31	22.15	22.12	30.60	29.76	28.90	29.75	3.95	7.63
Serine/threonine-protein kinase PAK 2	PAK2	22.61	23.61	23.06	23.10	28.03	28.81	28.37	28.40	3.87	5.31
Tight junction protein ZO-1	TJP1	23.13	23.64	22.94	23.24	31.17	30.38	29.56	30.37	3.82	7.13
Alpha-parvin	PARVA	23.70	23.85	23.66	23.74	27.55	26.72	26.98	27.08	3.74	3.35
TBC1 domain family member 5	TBC1D5	23.37	23.45	22.80	23.21	26.90	27.47	26.82	27.06	3.74	3.86
Inactive tyrosine-protein kinase 7	PTK7	22.51	22.32	22.45	22.43	27.64	26.53	27.60	27.26	3.70	4.83
182 kDa tankyrase-1-binding protein	TNKS1BP1	24.30	23.03	23.36	23.56	27.98	28.16	28.16	28.10	3.53	4.54
Niban-like protein 1	FAM129B	22.85	22.49	24.11	23.15	28.91	29.75	29.61	29.42	3.46	6.27
Ankycorbin	RAI14	22.50	22.40	22.92	22.61	29.26	28.83	27.56	28.55	3.44	5.95
CD44 antigen	CD44	22.06	23.69	23.21	22.99	28.89	29.02	29.84	29.25	3.42	6.26
Band 4.1-like protein 1	EPB41L1	22.52	23.66	22.65	22.94	28.12	27.24	27.56	27.64	3.35	4.69
Cdc42 effector protein 1	CDC42EP1	24.10	23.18	23.05	23.44	28.38	29.88	29.27	29.18	3.33	5.73
Rab11 family-interacting protein 5	RAB11FIP5	22.37	22.67	23.62	22.89	29.33	29.38	28.05	28.92	3.32	6.03

Protein names	Gene names	Mock (Log2 LFQ Intensity)			Mean Mock (log2 LFQ Intensity)	LITAF (Log2 LFQ Intensity)			Mean LITAF (log2 LFQ Intensity)	-Log (p-value)	Fold change
Protein LAP2	ERBB2IP	23.11	23.08	23.85	23.34	29.36	29.89	31.43	30.23	3.30	6.88
Desmoglein-2	DSG2	22.20	22.83	22.51	22.51	28.24	29.32	30.46	29.34	3.29	6.83
LIM and SH3 domain protein 1	LASP1	23.95	23.11	22.93	23.33	27.55	26.84	27.53	27.31	3.28	3.98
Endothelin-converting enzyme 1	ECE1	22.41	24.04	22.59	23.01	30.06	28.85	29.26	29.39	3.28	6.37
EH domain-containing protein 1	EHD1	22.58	23.41	22.73	22.91	26.79	26.04	26.20	26.34	3.25	3.43
Nectin-2	PVRL2	24.55	22.31	23.23	23.36	30.41	29.91	31.02	30.45	3.21	7.09
Epidermal growth factor receptor	EGFR	23.34	21.59	22.29	22.41	27.70	27.28	27.60	27.53	3.21	5.12
Discoidin, CUB and LCCL domain-containing protein 2	DCBLD2	23.72	22.97	22.91	23.20	27.77	27.88	29.18	28.27	3.20	5.08
Band 4.1-like protein 3	EPB41L3	23.44	24.65	23.26	23.78	30.61	30.20	29.06	29.95	3.19	6.17
Band 4.1-like protein 2	EPB41L2	22.49	23.06	22.88	22.81	30.89	30.20	28.37	29.82	3.09	7.01
Spectrin beta chain, non-erythrocytic 1	SPTBN1	23.74	24.42	23.78	23.98	30.36	28.87	28.59	29.27	3.07	5.29
Zyxin	ZYX	23.38	24.34	23.99	23.90	28.37	28.41	27.16	27.98	2.92	4.07
Rho GTPase-activating protein 1	ARHGAP1	24.06	23.72	22.84	23.54	28.25	27.26	27.11	27.54	2.85	4.00
Phosphatidylinositol-binding clathrin assembly protein	PICALM	24.25	23.97	23.16	23.79	30.13	29.33	27.97	29.14	2.78	5.35
Zinc transporter 1	SLC30A1	24.07	22.79	23.50	23.45	26.73	27.79	26.89	27.14	2.75	3.68
A-kinase anchor protein 12	AKAP12	24.38	23.10	22.72	23.40	27.34	28.69	28.10	28.04	2.73	4.64
Lipoma-preferred partner	LPP	23.76	22.66	24.18	23.53	26.81	27.00	27.41	27.07	2.72	3.54
Sorting nexin-3	SNX3	22.91	21.62	23.04	22.52	30.11	28.82	27.54	28.83	2.72	6.31
Amyloid beta A4 precursor protein-binding family B member 1	APBB1	22.55	22.17	24.13	22.95	27.36	27.12	27.30	27.26	2.69	4.31
Zinc finger CCCH-type antiviral protein 1	ZC3HAV1	22.98	22.89	24.04	23.30	29.59	29.80	27.58	28.99	2.69	5.69
Ras-related protein Rab-1A	RAB1A	23.43	22.20	22.23	22.62	26.66	25.64	26.44	26.24	2.69	3.62
Drebrin	DBN1	23.62	22.36	23.25	23.07	26.18	27.11	26.21	26.50	2.68	3.43

Protein names	Gene names	Mock (Log2 LFQ Intensity)			Mean Mock (log2 LFQ Intensity)	LITAF (Log2 LFQ Intensity)			Mean LITAF (log2 LFQ Intensity)	-Log (p-value)	Fold change
Synaptosomal-associated protein 23	SNAP23	22.87	24.29	23.62	23.59	28.78	28.30	27.13	28.07	2.66	4.48
Arfaptin-2	ARFIP2	22.71	22.86	23.68	23.08	27.18	26.27	25.90	26.45	2.65	3.37
Septin-9	Sep-09	24.08	22.69	22.57	23.12	29.51	29.40	27.49	28.80	2.65	5.68
cAMP-dependent protein kinase type II-alpha regulatory subunit	PRKAR2A	23.28	23.24	24.33	23.62	27.12	26.78	26.20	26.70	2.63	3.08
Liprin-beta-1	PPFIBP1	22.40	23.14	22.94	22.83	25.04	25.12	25.97	25.38	2.63	2.55
Nectin-3	PVRL3	22.97	23.23	24.05	23.42	25.58	26.13	26.06	25.92	2.62	2.51
Vesicle-associated membrane protein 5	VAMP5	22.82	22.72	23.58	23.04	25.99	26.72	27.66	26.79	2.61	3.75
Carboxypeptidase D	CPD	22.45	23.51	24.52	23.49	27.61	27.81	27.33	27.58	2.58	4.09
PDZ and LIM domain protein 1	PDLIM1	23.89	23.34	22.48	23.24	27.66	26.81	26.37	26.95	2.57	3.71
Rho GDP-dissociation inhibitor 1	ARHGDIA	22.50	23.96	23.83	23.43	26.65	26.53	27.17	26.78	2.57	3.36
Drebrin-like protein	DBNL	23.16	23.13	23.24	23.18	27.21	26.43	25.53	26.39	2.56	3.22
Vacuolar protein sorting-associated protein 51 homolog	VPS51	22.85	22.47	22.33	22.55	25.46	25.70	24.48	25.21	2.56	2.66
HLA class I histocompatibility antigen, A-3 alpha chain	HLA-A	21.81	22.35	23.51	22.55	27.97	27.00	26.29	27.09	2.54	4.54
Secretory carrier-associated membrane protein 1	SCAMP1	22.14	23.42	23.10	22.89	28.13	28.86	26.59	27.86	2.53	4.97
Protein bicaudal D homolog 2	BICD2	22.80	23.58	24.03	23.47	25.87	26.79	26.44	26.37	2.52	2.90
LIM domain only protein 7	LMO7	22.69	23.18	23.14	23.00	26.90	27.20	25.50	26.53	2.52	3.53
Neurogenic locus notch homolog protein 2	NOTCH2	22.86	23.74	22.28	22.96	27.70	29.07	26.84	27.87	2.49	4.91
Epidermal growth factor receptor substrate 15	EPS15	23.42	23.73	23.52	23.56	26.29	28.38	27.55	27.40	2.48	3.85
Zinc finger FYVE domain-containing protein 16	ZFYVE16	23.36	22.99	23.14	23.16	25.27	26.54	25.42	25.75	2.47	2.58
4F2 cell-surface antigen heavy chain	SLC3A2	23.78	22.26	23.93	23.32	28.68	29.13	27.13	28.32	2.46	5.00

Protein names	Gene names	MOCK (Log2 LFQ Intensity)			Mean Mock (log2 LFQ Intensity)	LITAF (Log2 LFQ Intensity)			Mean LITAF (log2 LFQ Intensity)	-Log (p-value)	Fold change
Myelin protein zero-like protein 1	MPZL1	22.74	23.09	23.25	23.02	27.76	25.83	26.33	26.64	2.42	3.62
Dyslexia-associated protein KIAA0319-like protein	KIAA0319L	22.86	23.25	23.28	23.13	28.93	28.56	26.40	27.96	2.42	4.84
Polymerase I and transcript release factor	PTRF	24.43	22.58	23.02	23.34	27.65	27.07	26.64	27.12	2.41	3.78
Large neutral amino acids transporter small subunit 1	SLC7A5	22.75	22.43	23.07	22.75	27.28	29.01	26.36	27.55	2.41	4.80
Neuroblast differentiation-associated protein AHNAK	AHNAK	26.84	23.82	29.26	26.64	35.43	36.94	36.75	36.37	2.39	9.73
Golgi-associated PDZ and coiled-coil motif-containing protein	GOPC	22.96	23.72	23.40	23.36	29.15	28.55	26.57	28.09	2.37	4.73
Rho GTPase-activating protein 29	ARHGAP29	23.96	24.03	23.80	23.93	28.08	27.71	26.17	27.32	2.35	3.39
Rab GTPase-activating protein 1	RABGAP1	23.05	22.93	22.91	22.96	23.93	24.04	23.55	23.84	2.33	0.88
Multidrug resistance-associated protein 1	ABCC1	22.67	22.14	22.82	22.54	25.61	25.55	24.34	25.16	2.32	2.62
IST1 homolog	IST1	24.33	23.41	22.51	23.41	27.33	26.27	27.03	26.87	2.32	3.46
Pleckstrin homology-like domain family B member 1	PHLDB1	22.56	22.83	22.39	22.59	27.76	28.93	25.93	27.54	2.30	4.94
Clathrin interactor 1	CLINT1	24.37	22.30	24.52	23.73	29.08	28.07	27.73	28.29	2.28	4.56
Integrin-linked protein kinase	ILK	23.53	23.06	22.73	23.10	25.15	24.43	24.82	24.80	2.26	1.70
Palladin	PALLD	24.95	23.82	23.19	23.99	28.86	28.03	27.03	27.97	2.24	3.98
Cdc42 effector protein 3	CDC42EP3	22.31	23.27	24.05	23.21	25.80	26.65	26.11	26.19	2.22	2.98
Protein FAM171B	FAM171B	22.55	23.16	23.83	23.18	25.30	25.87	25.18	25.45	2.22	2.27
Septin-7	Sep-07	23.53	23.04	22.57	23.05	28.13	25.90	26.56	26.86	2.22	3.81
Tensin-3	TNS3	23.18	22.73	23.70	23.20	26.53	28.43	26.29	27.08	2.21	3.88
Na(+)/H(+) exchange regulatory cofactor NHE-RF1	SLC9A3R1	23.09	22.44	23.78	23.10	25.11	25.84	25.37	25.44	2.21	2.34
Gap junction alpha-1 protein	GJA1	23.69	23.27	22.61	23.19	27.48	25.82	25.94	26.41	2.19	3.23

Protein names	Gene names	MOCK (Log2 LFQ Intensity)			Mean Mock (log2 LFQ Intensity)	LITAF (Log2 LFQ Intensity)			Mean LITAF (log2 LFQ Intensity)	-Log (p-value)	Fold change
Sequestosome-1	SQSTM1	22.67	22.74	23.07	22.83	29.34	29.92	26.30	28.52	2.14	5.69
Protein jagged-1	JAG1	23.09	23.01	23.07	23.06	24.85	26.78	26.38	26.00	2.13	2.94
Afadin	MLLT4	22.17	23.08	23.66	22.97	30.21	29.47	26.67	28.78	2.13	5.81
Synaptobrevin homolog YKT6	YKT6	23.30	24.01	23.66	23.66	27.98	27.18	25.80	26.99	2.12	3.33
NSFL1 cofactor p47	NSFL1C	23.29	24.67	23.74	23.90	25.76	26.16	26.01	25.98	2.10	2.08
Flotillin-1	FLOT1	21.99	23.59	24.05	23.21	27.37	27.20	25.99	26.85	2.06	3.64
Plasma membrane calcium-transporting ATPase 4	ATP2B4	22.41	23.97	23.69	23.35	27.58	27.39	25.74	26.91	2.03	3.55
TLD domain-containing protein 1	TLDC1	23.33	23.16	23.88	23.46	27.51	26.59	25.36	26.49	2.00	3.03
Pseudopodium-enriched atypical kinase 1	PEAK1	23.04	23.96	22.56	23.18	27.69	27.79	25.54	27.01	1.98	3.82
Hematological and neurological expressed 1-like protein	HN1L	23.09	23.88	22.25	23.07	25.83	25.36	26.89	26.03	1.97	2.96
E3 ubiquitin-protein ligase NEDD4-like	NEDD4L	23.70	23.53	24.06	23.76	24.89	26.21	26.05	25.71	1.94	1.95
Paxillin	PXN	22.77	23.98	23.93	23.56	28.97	27.33	26.16	27.48	1.91	3.93
Ras-associated and pleckstrin homology domains-containing protein 1	RAPH1	23.78	22.65	23.03	23.15	30.15	30.11	26.24	28.84	1.88	5.68
Signal transducing adapter molecule 1	STAM	22.24	24.13	23.09	23.15	25.48	27.24	27.73	26.82	1.86	3.67
Fermitin family homolog 2	FERMT2	24.09	23.07	22.38	23.18	29.11	28.63	25.88	27.87	1.86	4.69
Coxsackievirus and adenovirus receptor	CXADR	23.89	23.50	22.49	23.29	28.21	25.70	26.54	26.81	1.85	3.52
Transferrin receptor protein 1	TFRC	20.64	22.81	22.12	21.86	24.74	26.10	27.54	26.13	1.84	4.27
Transcriptional coactivator YAP1	YAP1	23.03	21.39	23.92	22.78	26.28	26.27	25.43	25.99	1.82	3.21
Caldesmon	CALD1	26.25	23.05	23.39	24.23	30.43	28.98	28.12	29.18	1.82	4.95
Perilipin-3	PLIN3	23.18	23.75	22.92	23.28	24.78	26.37	26.85	26.00	1.81	2.72
Guanine nucleotide-binding protein G(i) subunit alpha-2	GNAI2	23.84	22.41	23.07	23.11	26.39	24.73	26.13	25.75	1.79	2.64

Protein names	Gene names	MOCK (Log2 LFQ Intensity)			Mean Mock (log2 LFQ Intensity)	LITAF (Log2 LFQ Intensity)			Mean LITAF (log2 LFQ Intensity)	-Log (p-value)	Fold change
CUB domain-containing protein 1	CDCP1	21.84	23.07	24.07	23.00	26.71	26.98	25.21	26.30	1.75	3.30
SH2 domain-containing adapter protein B	SHB	23.25	21.95	23.47	22.89	28.92	27.03	25.50	27.15	1.75	4.26
Girdin	CCDC88A	23.28	22.84	22.54	22.89	25.07	27.17	25.00	25.75	1.73	2.86
Sorting nexin-1	SNX1	22.93	23.55	23.09	23.19	28.13	28.40	25.16	27.23	1.73	4.04

Table A.1. Significantly enriched proteins in the LITAF WT condition vs. Mock. The table shows the results of label-free quantitative analysis of mass spectrometry proteomics by MaxQuant and Perseus following BioID.

Protein names	Gene names	Mock (Log2 LFQ Intensity)			Mean Mock (log2 LFQ Intensity)	LITAF P135S (Log2 LFQ Intensity)			Mean LITAF P135S (log2 LFQ Intensity)	-Log (p-value)	Fold change
Cation-independent mannose-6-phosphate receptor	IGF2R	22.57	23.11	23.04	22.91	29.34	29.52	29.65	29.50	5.36	6.60
Tumor protein D54	TPD52L2	23.28	23.14	22.71	23.04	31.65	30.32	31.05	31.01	4.34	7.96
Pleckstrin homology-like domain family B member 1	PHLDB1	22.56	22.83	22.39	22.59	26.72	26.68	26.20	26.54	4.32	3.94
Desmoglein-2	DSG2	22.20	22.83	22.51	22.51	28.13	28.48	29.12	28.58	4.23	6.06
LIM domain only protein 7	LMO7	22.69	23.18	23.14	23.00	28.03	27.47	27.36	27.62	4.22	4.62
BAG family molecular chaperone regulator 3	BAG3	23.73	23.40	23.58	23.57	26.71	26.58	26.18	26.49	4.02	2.92
Protein LAP2	ERBB2IP	23.11	23.08	23.85	23.34	28.20	28.94	28.98	28.71	3.95	5.36
Ephrin type-A receptor 2	EPHA2	23.08	22.49	22.99	22.85	27.70	28.74	28.59	28.34	3.90	5.49
ATP-dependent RNA helicase DHX29	DHX29	22.43	22.59	22.77	22.60	26.99	26.67	26.09	26.58	3.85	3.99
Integrin beta-1	ITGB1	23.38	23.69	23.25	23.44	29.99	30.77	32.00	30.92	3.62	7.48
Cdc42 effector protein 1	CDC42EP1	24.10	23.18	23.05	23.44	28.22	28.60	29.18	28.67	3.56	5.22
182 kDa tankyrase-1-binding protein	TNKS1BP1	24.30	23.03	23.36	23.56	28.57	28.18	28.19	28.31	3.54	4.75
Epidermal growth factor receptor substrate 15-like 1	EPS15L1	22.28	22.32	22.77	22.45	27.50	28.14	26.74	27.46	3.49	5.01
Protein AHNAK2	AHNAK2	23.01	22.93	23.30	23.08	29.44	31.76	30.80	30.67	3.43	7.59
Catenin delta-1	CTNND1	21.89	22.31	22.15	22.12	29.37	27.83	27.65	28.28	3.42	6.16
Serine/threonine-protein kinase MRCK alpha	CDC42BPA	22.23	22.96	22.52	22.57	27.38	26.83	26.25	26.82	3.40	4.25
Tight junction protein ZO-1	TJP1	23.13	23.64	22.94	23.24	30.02	29.50	28.28	29.27	3.39	6.03
Ankycorbin	RAI14	22.50	22.40	22.92	22.61	26.87	28.09	26.78	27.25	3.30	4.64
Septin-9	Sep-09	24.08	22.69	22.57	23.12	28.75	28.06	28.86	28.55	3.24	5.44
Niban-like protein 1	FAM129B	22.85	22.49	24.11	23.15	28.44	28.25	29.10	28.59	3.22	5.44
Spectrin beta chain, non-erythrocytic 1	SPTBN1	23.74	24.42	23.78	23.98	28.32	28.86	27.55	28.24	3.21	4.26

Protein names	Gene names	Mock (Log2 LFQ Intensity)			Mean Mock (log2 LFQ Intensity)	LITAF P135S (Log2 LFQ Intensity)			Mean LITAF P135S (log2 LFQ Intensity)	-Log (p-value)	Fold change
Secretory carrier-associated membrane protein 1	SCAMP1	22.14	23.42	23.10	22.89	27.74	27.70	26.91	27.45	3.20	4.56
Sorting nexin-3	SNX3	22.91	21.62	23.04	22.52	27.16	26.75	27.50	27.14	3.10	4.62
Band 4.1-like protein 3	EPB41L3	23.44	24.65	23.26	23.78	27.94	28.80	27.93	28.22	2.97	4.44
Zyxin	ZYX	23.38	24.34	23.99	23.90	28.58	27.25	27.76	27.86	2.94	3.96
Vacuolar protein sorting-associated protein 51 homolog	VPS51	22.85	22.47	22.33	22.55	25.39	25.83	24.79	25.33	2.92	2.78
Large neutral amino acids transporter small subunit 1	SLC7A5	22.75	22.43	23.07	22.75	26.92	26.73	28.42	27.36	2.91	4.61
LIM and SH3 domain protein 1	LASP1	23.95	23.11	22.93	23.33	27.45	26.39	26.78	26.87	2.89	3.55
Phosphatidylinositol-binding clathrin assembly protein	PICALM	24.25	23.97	23.16	23.79	29.19	27.52	28.40	28.37	2.86	4.58
Nuclear fragile X mental retardation-interacting protein 2	NUFIP2	22.51	22.92	22.97	22.80	25.18	26.32	25.44	25.64	2.79	2.84
Zinc finger CCCH-type antiviral protein 1	ZC3HAV1	22.98	22.89	24.04	23.30	29.30	28.37	27.33	28.33	2.76	5.03
Extended synaptotagmin-1	ESYT1	22.89	22.25	23.07	22.73	25.89	25.33	26.55	25.92	2.75	3.19
Signal transducing adapter molecule 1	STAM	22.24	24.13	23.09	23.15	27.46	27.80	27.09	27.45	2.74	4.30
Syntaxin-7	STX7	23.01	23.19	22.95	23.05	23.89	24.17	24.33	24.13	2.74	1.08
Disabled homolog 2	DAB2	22.95	23.42	24.26	23.55	26.74	26.56	26.27	26.52	2.73	2.98
Band 4.1-like protein 2	EPB41L2	22.49	23.06	22.88	22.81	30.04	27.60	27.90	28.51	2.72	5.70
Nectin-2	PVRL2	24.55	22.31	23.23	23.36	28.31	27.98	28.89	28.39	2.70	5.03
Ubiquitin-associated protein 2	UBAP2	23.31	23.45	22.88	23.21	25.57	26.03	25.07	25.55	2.69	2.34
Neurogenic locus notch homolog protein 2	NOTCH2	22.86	23.74	22.28	22.96	25.99	26.13	26.81	26.31	2.60	3.35
Rab11 family-interacting protein 5	RAB11FIP5	22.37	22.67	23.62	22.89	28.54	27.68	26.51	27.58	2.59	4.69
Sequestosome-1	SQSTM1	22.67	22.74	23.07	22.83	28.13	30.95	28.15	29.08	2.57	6.25

Protein names	Gene names	Mock (Log2 LFQ Intensity)			Mean Mock (log2 LFQ Intensity)	LITAF P135S (Log2 LFQ Intensity)			Mean LITAF P135S (log2 LFQ Intensity)	-Log (p-value)	Fold change
Tight junction protein ZO-2	TJP2	22.77	21.93	22.63	22.45	27.70	25.82	27.93	27.15	2.56	4.71
NSFL1 cofactor p47	NSFL1C	23.29	24.67	23.74	23.90	26.98	27.21	26.50	26.90	2.55	3.00
Epidermal growth factor receptor substrate 15	EPS15	23.42	23.73	23.52	23.56	27.01	29.38	27.88	28.09	2.54	4.53
cAMP-dependent protein kinase type II-alpha regulatory subunit	PRKAR2A	23.28	23.24	24.33	23.62	25.96	26.34	26.84	26.38	2.48	2.76
Endothelin-converting enzyme 1	ECE1	22.41	24.04	22.59	23.01	27.71	26.32	27.34	27.12	2.47	4.11
Integrin beta-5	ITGB5	22.93	22.91	23.53	23.12	26.40	25.55	27.28	26.41	2.44	3.29
Sorting nexin-1	SNX1	22.93	23.55	23.09	23.19	27.34	26.11	25.70	26.38	2.43	3.19
Coiled-coil domain-containing protein 50	CCDC50	22.41	23.39	22.75	22.85	26.15	25.06	25.29	25.50	2.42	2.65
PDZ and LIM domain protein 5	PDLIM5	24.77	24.34	25.62	24.91	27.05	27.51	27.48	27.35	2.41	2.44
Suppressor of G2 allele of SKP1 homolog	SUGT1	23.34	24.19	23.48	23.67	25.29	25.81	25.39	25.50	2.40	1.83
Golgi-associated PDZ and coiled-coil motif-containing protein	GOPC	22.96	23.72	23.40	23.36	27.76	28.33	26.16	27.42	2.39	4.06
Tensin-3	TNS3	23.18	22.73	23.70	23.20	26.17	26.75	28.18	27.03	2.36	3.83
Palladin	PALLD	24.95	23.82	23.19	23.99	30.03	28.15	28.05	28.74	2.35	4.76
Zinc finger protein 185	ZNF185	21.78	24.19	23.18	23.05	28.62	28.15	26.94	27.90	2.32	4.85
TBC1 domain family member 5	TBC1D5	23.37	23.45	22.80	23.21	25.98	25.32	26.93	26.08	2.31	2.87
Signal transducing adapter molecule 2	STAM2	22.59	22.69	23.35	22.88	24.65	25.87	25.75	25.42	2.30	2.55
Ras-associated and pleckstrin homology domains-containing protein 1	RAPH1	23.78	22.65	23.03	23.15	28.39	27.15	26.09	27.21	2.26	4.06
RNA-binding motif, single-stranded-interacting protein 2	RBMS2	22.28	24.14	21.75	22.72	28.27	26.91	26.82	27.33	2.23	4.61
CD44 antigen	CD44	22.06	23.69	23.21	22.99	28.95	27.07	30.55	28.86	2.21	5.87
Gamma-adducin	ADD3	23.35	22.50	22.16	22.67	27.15	25.29	25.82	26.09	2.19	3.42
Neuroblast differentiation-associated protein AHNAK	AHNAK	26.84	23.82	29.26	26.64	34.31	36.09	35.27	35.22	2.18	8.58

Protein names	Gene names	Mock (Log2 LFQ Intensity)			Mean Mock (log2 LFQ Intensity)	LITAF P135S (Log2 LFQ Intensity)			Mean LITAF P135S (log2 LFQ Intensity)	-Log (p-value)	Fold change
Fermitin family homolog 2	FERMT2	24.09	23.07	22.38	23.18	26.31	25.80	27.14	26.42	2.16	3.24
PDZ and LIM domain protein 1	PDLIM1	23.89	23.34	22.48	23.24	28.92	27.20	26.34	27.49	2.10	4.25
4F2 cell-surface antigen heavy chain	SLC3A2	23.78	22.26	23.93	23.32	27.67	27.35	25.96	26.99	2.10	3.67
Afadin	MLLT4	22.17	23.08	23.66	22.97	28.88	26.96	26.24	27.36	2.09	4.39
Synaptosomal-associated protein 23	SNAP23	22.87	24.29	23.62	23.59	27.90	25.93	27.32	27.05	2.08	3.46
Talin-1	TLN1	25.28	22.35	25.36	24.33	29.11	30.18	28.81	29.36	2.03	5.04
Receptor-type tyrosine-protein phosphatase eta	PTPRJ	22.42	22.26	23.24	22.64	24.88	24.31	24.08	24.42	2.02	1.79
LIM and calponin homology domains-containing protein 1	LIMCH1	22.26	22.67	23.42	22.78	24.38	24.98	25.51	24.95	2.00	2.17
Serine/threonine-protein kinase PAK 2	PAK2	22.61	23.61	23.06	23.10	28.91	25.72	28.20	27.61	1.96	4.51
Lipopolysaccharide-responsive and beige-like anchor protein	LRBA	23.41	23.22	23.61	23.41	25.08	27.20	26.44	26.24	1.96	2.83
Dyslexia-associated protein KIAA0319-like protein	KIAA0319L	22.86	23.25	23.28	23.13	26.97	29.03	25.78	27.26	1.90	4.13
IST1 homolog	IST1	24.33	23.41	22.51	23.41	26.34	25.85	27.64	26.61	1.89	3.20
Protein bicaudal D homolog 2	BICD2	22.80	23.58	24.03	23.47	27.23	27.69	25.43	26.78	1.88	3.31
Caldesmon	CALD1	26.25	23.05	23.39	24.23	30.29	28.28	28.86	29.14	1.86	4.92
Rho GTPase-activating protein 1	ARHGAP1	24.06	23.72	22.84	23.54	24.90	25.75	26.00	25.55	1.82	2.01
LIM domain and actin-binding protein 1	LIMA1	22.21	23.64	24.05	23.30	26.31	25.30	26.61	26.07	1.82	2.78

Table A.2. Significantly enriched proteins in the LITAF P135S condition vs. Mock. The table shows the results of label-free quantitative analysis of mass spectrometry proteomics by MaxQuant and Perseus following BioID.

Protein names	Gene names	Mock (Log2 LFQ Intensity)			Mean Mock (log2 LFQ Intensity)	LITAF V144M (Log2 LFQ Intensity)			Mean LITAF V144M (log2 LFQ Intensity)	-Log (p-value)	Fold change
Integrin beta-1	ITGB1	23.38	23.69	23.25	23.44	32.36	32.07	32.22	32.22	6.24	8.78
Protein AHNAK2	AHNAK2	23.01	22.93	23.30	23.08	31.52	31.47	31.11	31.37	5.95	8.29
Sequestosome-1	SQSTM1	22.67	22.74	23.07	22.83	29.64	30.15	29.59	29.79	5.26	6.97
Tumor protein D54	TPD52L2	23.28	23.14	22.71	23.04	31.27	30.82	30.55	30.88	5.07	7.83
LIM domain only protein 7	LMO7	22.69	23.18	23.14	23.00	27.37	27.65	27.47	27.50	4.83	4.49
Desmoglein-2	DSG2	22.20	22.83	22.51	22.51	28.37	28.88	29.13	28.79	4.57	6.28
Epidermal growth factor receptor substrate 15-like 1	EPS15L1	22.28	22.32	22.77	22.45	27.93	28.59	27.67	28.06	4.23	5.61
Cation-independent mannose-6-phosphate receptor	IGF2R	22.57	23.11	23.04	22.91	31.70	30.77	30.26	30.91	4.22	8.00
Kinesin-1 heavy chain	KIF5B	23.31	23.00	23.55	23.29	26.41	26.26	26.17	26.28	4.17	2.99
Catenin delta-1	CTNND1	21.89	22.31	22.15	22.12	30.15	29.11	28.72	29.33	4.07	7.21
Zinc finger FYVE domain-containing protein 16	ZFYVE16	23.36	22.99	23.14	23.16	26.53	27.23	26.76	26.84	4.03	3.68
Ephrin type-A receptor 2	EPHA2	23.08	22.49	22.99	22.85	29.80	29.92	28.70	29.48	3.99	6.63
Tensin-3	TNS3	23.18	22.73	23.70	23.20	27.93	28.40	27.97	28.10	3.98	4.90
Protocadherin gamma-A11	PCDHGA11	23.51	23.79	23.20	23.50	26.71	26.33	26.45	26.50	3.90	3.00
Large neutral amino acids transporter small subunit 1	SLC7A5	22.75	22.43	23.07	22.75	28.04	28.75	27.63	28.14	3.87	5.39
Tight junction protein ZO-2	TJP2	22.77	21.93	22.63	22.45	28.14	27.33	28.20	27.89	3.84	5.44
Protein LAP2	ERBB2IP	23.11	23.08	23.85	23.34	29.67	28.53	29.01	29.07	3.80	5.73
STE20-like serine/threonine-protein kinase	SLK	23.86	23.86	23.27	23.66	27.04	27.11	26.63	26.93	3.72	3.27
Phosphatidylinositol-binding clathrin assembly protein	PICALM	24.25	23.97	23.16	23.79	29.56	30.03	29.00	29.53	3.70	5.74
Serine/threonine-protein kinase PAK 2	PAK2	22.61	23.61	23.06	23.10	27.95	27.90	28.72	28.19	3.69	5.09
Lipopolysaccharide-responsive and beige-like anchor protein	LRBA	23.41	23.22	23.61	23.41	27.15	26.94	26.35	26.81	3.68	3.40
Liprin-beta-1	PPFIBP1	22.40	23.14	22.94	22.83	25.92	26.23	25.83	25.99	3.64	3.17

Protein names	Gene names	Mock (Log2 LFQ Intensity)			Mean Mock (log2 LFQ Intensity)	LITAF V144M (Log2 LFQ Intensity)			Mean LITAF V144M (log2 LFQ Intensity)	-Log (p-value)	Fold change
Protein FAM171A2	FAM171A2	22.90	23.26	22.93	23.03	24.95	24.73	24.70	24.79	3.64	1.76
182 kDa tankyrase-1-binding protein	TNKS1BP1	24.30	23.03	23.36	23.56	28.39	28.83	28.24	28.49	3.52	4.92
Niban-like protein 1	FAM129B	22.85	22.49	24.11	23.15	29.08	29.95	29.42	29.48	3.49	6.33
CD44 antigen	CD44	22.06	23.69	23.21	22.99	29.25	29.81	30.55	29.87	3.44	6.89
Dyslexia-associated protein KIAA0319-like protein	KIAA0319L	22.86	23.25	23.28	23.13	29.57	29.62	28.03	29.07	3.41	5.94
Zyxin	ZYX	23.38	24.34	23.99	23.90	27.97	28.56	27.66	28.06	3.38	4.16
Hepatocyte growth factor-regulated tyrosine kinase substrate	HGS	23.13	23.13	23.60	23.28	26.28	26.58	25.81	26.22	3.38	2.94
Drebrin-like protein	DBNL	23.16	23.13	23.24	23.18	25.90	26.77	26.96	26.54	3.30	3.37
Septin-9	Sep-09	24.08	22.69	22.57	23.12	29.13	29.30	28.33	28.92	3.28	5.80
Integrin beta-5	ITGB5	22.93	22.91	23.53	23.12	28.52	27.09	27.76	27.79	3.28	4.67
Cdc42 effector protein 1	CDC42EP1	24.10	23.18	23.05	23.44	28.03	29.32	28.32	28.56	3.24	5.11
Syntaxin-7	STX7	23.01	23.19	22.95	23.05	24.26	24.70	24.55	24.50	3.23	1.45
Dysferlin	DYSF	23.15	23.12	23.22	23.16	24.70	24.96	24.42	24.69	3.20	1.53
Multidrug resistance-associated protein 1	ABCC1	22.67	22.14	22.82	22.54	25.93	25.94	25.18	25.68	3.20	3.14
Drebrin	DBN1	23.62	22.36	23.25	23.07	26.77	26.83	27.22	26.94	3.19	3.87
Secretory carrier-associated membrane protein 1	SCAMP1	22.14	23.42	23.10	22.89	27.15	27.73	26.90	27.26	3.18	4.37
Synaptosomal-associated protein 23	SNAP23	22.87	24.29	23.62	23.59	28.48	27.94	27.74	28.05	3.18	4.46
Cytospin-B	SPECC1	23.77	23.34	23.68	23.60	26.14	26.48	25.68	26.10	3.15	2.50
Ankycorbin	RAI14	22.50	22.40	22.92	22.61	29.55	29.11	27.46	28.71	3.13	6.10
LIM and SH3 domain protein 1	LASP1	23.95	23.11	22.93	23.33	26.63	26.19	26.66	26.49	3.09	3.16
Rho GTPase-activating protein 29	ARHGAP29	23.96	24.03	23.80	23.93	27.72	28.11	26.78	27.54	3.08	3.60
cAMP-dependent protein kinase type II-alpha regulatory subunit	PRKAR2A	23.28	23.24	24.33	23.62	26.96	27.47	27.78	27.40	3.04	3.79
AP-3 complex subunit beta-1	AP3B1	22.59	22.22	21.74	22.18	24.69	25.51	25.33	25.18	2.99	2.99

Protein names	Gene names	Mock (Log2 LFQ Intensity)			Mean Mock (log2 LFQ Intensity)	LITAF V144M (Log2 LFQ Intensity)			Mean LITAF V144M (log2 LFQ Intensity)	-Log (p-value)	Fold change
Septin-7	Sep-07	23.53	23.04	22.57	23.05	26.08	25.55	25.69	25.77	2.98	2.72
Sorting nexin-3	SNX3	22.91	21.62	23.04	22.52	28.75	27.28	27.65	27.90	2.98	5.37
Perilipin-3	PLIN3	23.18	23.75	22.92	23.28	25.41	25.84	25.70	25.65	2.98	2.37
TBC1 domain family member 5	TBC1D5	23.37	23.45	22.80	23.21	26.29	27.59	26.60	26.83	2.93	3.62
Rab GTPase-activating protein 1	RABGAP1	23.05	22.93	22.91	22.96	24.53	24.30	24.96	24.60	2.93	1.64
Epidermal growth factor receptor substrate 15	EPS15	23.42	23.73	23.52	23.56	27.44	28.41	29.50	28.45	2.90	4.89
A-kinase anchor protein 12	AKAP12	24.38	23.10	22.72	23.40	27.64	28.47	28.76	28.29	2.90	4.89
Band 4.1-like protein 3	EPB41L3	23.44	24.65	23.26	23.78	30.08	29.62	28.31	29.33	2.89	5.55
Band 4.1-like protein 2	EPB41L2	22.49	23.06	22.88	22.81	30.33	29.30	27.68	29.10	2.88	6.29
Nectin-2	PVRL2	24.55	22.31	23.23	23.36	29.87	29.09	28.71	29.22	2.87	5.86
Protein bicaudal D homolog 2	BICD2	22.80	23.58	24.03	23.47	28.34	28.17	27.02	27.84	2.86	4.37
Epidermal growth factor receptor	EGFR	23.34	21.59	22.29	22.41	27.71	27.33	26.56	27.20	2.85	4.80
Golgi-associated PDZ and coiled-coil motif-containing protein	GOPC	22.96	23.72	23.40	23.36	29.83	28.40	27.66	28.63	2.84	5.27
Plasma membrane calcium-transporting ATPase 4	ATP2B4	22.41	23.97	23.69	23.35	27.83	27.43	27.09	27.45	2.83	4.10
BAG family molecular chaperone regulator 3	BAG3	23.73	23.40	23.58	23.57	28.07	26.72	26.69	27.16	2.82	3.59
Suppressor of G2 allele of SKP1 homolog	SUGT1	23.34	24.19	23.48	23.67	26.19	25.70	26.07	25.99	2.82	2.32
Arf-GAP domain and FG repeat-containing protein 1	AGFG1	23.62	22.28	23.52	23.14	26.84	27.03	26.41	26.76	2.82	3.62
Amyloid beta A4 precursor protein-binding family B member 1	APBB1	22.55	22.17	24.13	22.95	27.97	27.77	27.37	27.71	2.80	4.75
Zinc finger CCCH-type antiviral protein 1	ZC3HAV1	22.98	22.89	24.04	23.30	29.03	29.35	27.43	28.61	2.79	5.30
Vesicle-associated membrane protein 3	VAMP3	23.28	23.12	21.68	22.70	26.91	26.74	27.65	27.10	2.79	4.41
Discoidin, CUB and LCCL domain-containing protein 2	DCBLD2	23.72	22.97	22.91	23.20	27.95	27.27	29.35	28.19	2.77	4.99
PDZ and LIM domain protein 1	PDLIM1	23.89	23.34	22.48	23.24	27.50	26.55	26.83	26.96	2.76	3.72

Protein names	Gene names	Mock (Log2 LFQ Intensity)			Mean Mock (log2 LFQ Intensity)	LITAF V144M (Log2 LFQ Intensity)			Mean LITAF V144M (log2 LFQ Intensity)	-Log (p-value)	Fold change
Zinc transporter 1	SLC30A1	24.07	22.79	23.50	23.45	26.91	27.15	26.24	26.77	2.71	3.32
Neurogenic locus notch homolog protein 2	NOTCH2	22.86	23.74	22.28	22.96	27.80	27.69	26.45	27.31	2.70	4.35
Carboxypeptidase D	CPD	22.45	23.51	24.52	23.49	27.83	27.62	27.99	27.81	2.69	4.32
Extended synaptotagmin-1	ESYT1	22.89	22.25	23.07	22.73	28.36	27.93	26.29	27.53	2.67	4.79
Probable palmitoyltransferase ZDHHC20	ZDHHC20	22.74	22.84	23.31	22.96	25.31	24.94	25.97	25.41	2.67	2.45
Gap junction alpha-1 protein	GJA1	23.69	23.27	22.61	23.19	27.45	26.20	26.40	26.68	2.66	3.49
SH2 domain-containing adapter protein B	SHB	23.25	21.95	23.47	22.89	27.75	27.01	26.47	27.08	2.65	4.18
Myelin protein zero-like protein 1	MPZL1	22.74	23.09	23.25	23.02	26.39	25.93	25.11	25.81	2.63	2.79
Coiled-coil domain-containing protein 50	CCDC50	22.41	23.39	22.75	22.85	25.39	26.64	25.97	26.00	2.62	3.15
Protein FAM171B	FAM171B	22.55	23.16	23.83	23.18	25.70	25.69	25.69	25.70	2.61	2.51
Signal transducing adapter molecule 2	STAM2	22.59	22.69	23.35	22.88	25.25	26.27	26.56	26.02	2.61	3.15
TLD domain-containing protein 1	TLDC1	23.33	23.16	23.88	23.46	26.82	25.62	26.57	26.34	2.61	2.88
Raftlin	RFTN1	23.56	23.66	23.40	23.54	26.61	26.25	25.36	26.07	2.59	2.54
HLA class I histocompatibility antigen, A-3 alpha chain	HLA-A	21.81	22.35	23.51	22.55	26.78	25.91	26.12	26.27	2.56	3.71
SH3 domain-containing protein 19	SH3D19	23.77	23.65	23.21	23.54	25.69	26.03	25.11	25.61	2.55	2.07
Spectrin beta chain, non-erythrocytic 1	SPTBN1	23.74	24.42	23.78	23.98	30.06	29.06	27.58	28.90	2.55	4.92
IST1 homolog	IST1	24.33	23.41	22.51	23.41	26.77	27.23	27.65	27.21	2.54	3.80
EH domain-containing protein 1	EHD1	22.58	23.41	22.73	22.91	26.88	25.66	25.64	26.06	2.54	3.15
Spartin	SPG20	23.39	23.59	22.80	23.26	26.57	26.73	25.44	26.25	2.51	2.99
Disabled homolog 2	DAB2	22.95	23.42	24.26	23.55	27.70	27.35	26.32	27.13	2.50	3.58
Coatomer subunit beta	COPB1	23.05	23.54	23.80	23.46	24.96	25.60	25.54	25.37	2.50	1.90
Palladin	PALLD	24.95	23.82	23.19	23.99	29.88	28.56	27.97	28.80	2.49	4.81
Thioredoxin-like protein 1	TXNL1	23.18	24.57	23.34	23.70	26.82	26.78	27.75	27.12	2.48	3.42
Tight junction protein ZO-1	TJP1	23.13	23.64	22.94	23.24	30.59	29.99	27.46	29.35	2.47	6.11
Calpastatin	CAST	22.82	21.84	22.09	22.25	25.07	24.23	25.13	24.81	2.46	2.56

Protein names	Gene names	Mock (Log2 LFQ Intensity)			Mean Mock (log2 LFQ Intensity)	LITAF V144M (Log2 LFQ Intensity)			Mean LITAF V144M (log2 LFQ Intensity)	-Log (p-value)	Fold change
Band 4.1-like protein 1	EPB41L1	22.52	23.66	22.65	22.94	27.56	26.89	25.84	26.76	2.46	3.82
Fermitin family homolog 2	FERMT2	24.09	23.07	22.38	23.18	28.81	27.59	26.92	27.77	2.45	4.59
Rab11 family-interacting protein 5	RAB11FIP5	22.37	22.67	23.62	22.89	28.40	28.22	26.28	27.63	2.44	4.74
Inactive tyrosine-protein kinase 7	PTK7	22.51	22.32	22.45	22.43	27.47	26.18	25.28	26.31	2.43	3.88
Gamma-adducin	ADD3	23.35	22.50	22.16	22.67	27.52	26.97	25.62	26.70	2.43	4.03
ARF GTPase-activating protein GIT1	GIT1	24.05	22.78	22.82	23.22	26.23	26.27	25.61	26.04	2.41	2.82
ATP-dependent RNA helicase DHX29	DHX29	22.43	22.59	22.77	22.60	28.68	28.70	26.10	27.83	2.41	5.23
Protein numb homolog	NUMB	23.76	23.24	22.96	23.32	26.64	27.48	25.75	26.62	2.41	3.30
Signal transducing adapter molecule 1	STAM	22.24	24.13	23.09	23.15	26.85	26.85	28.16	27.29	2.39	4.14
Charged multivesicular body protein 4b	CHMP4B	23.72	23.21	23.17	23.37	25.42	25.91	26.86	26.06	2.39	2.70
Rho GTPase-activating protein 1	ARHGAP1	24.06	23.72	22.84	23.54	27.87	26.82	26.29	26.99	2.37	3.45
Clathrin interactor 1	CLINT1	24.37	22.30	24.52	23.73	28.31	28.63	27.68	28.21	2.36	4.48
Neuroblast differentiation-associated protein AHNAK	AHNAK	26.84	23.82	29.26	26.64	35.77	35.97	35.58	35.77	2.35	9.13
Endothelin-converting enzyme 1	ECE1	22.41	24.04	22.59	23.01	30.22	27.74	27.81	28.59	2.35	5.57
Tyrosine-protein kinase Yes	YES1	23.20	23.08	23.38	23.22	24.33	25.22	24.87	24.81	2.35	1.59
E3 ubiquitin-protein ligase NEDD4-like	NEDD4L	23.70	23.53	24.06	23.76	25.63	25.20	24.90	25.24	2.32	1.48
Girdin	CCDC88A	23.28	22.84	22.54	22.89	24.97	26.09	24.93	25.33	2.30	2.44
Transferrin receptor protein 1	TFRC	20.64	22.81	22.12	21.86	25.22	25.91	26.24	25.79	2.29	3.93
Synaptosomal-associated protein 29	SNAP29	24.03	23.90	24.17	24.03	24.99	25.76	25.71	25.49	2.28	1.45
Vacuolar protein sorting-associated protein 51 homolog	VPS51	22.85	22.47	22.33	22.55	26.56	27.04	24.92	26.17	2.27	3.62
Zinc finger protein 185	ZNF185	21.78	24.19	23.18	23.05	27.48	28.08	26.72	27.43	2.26	4.38
CD2-associated protein	CD2AP	23.64	22.37	23.00	23.01	25.42	24.87	25.37	25.22	2.26	2.22
Alpha-adducin	ADD1	23.57	22.61	24.33	23.50	27.85	27.32	26.32	27.16	2.26	3.66
Transmembrane protein 2	TMEM2	22.91	22.32	22.86	22.70	25.41	25.26	24.23	24.96	2.26	2.27
Sorting nexin-1	SNX1	22.93	23.55	23.09	23.19	28.10	27.58	25.76	27.14	2.24	3.96

Protein names	Gene names	Mock (Log2 LFQ Intensity)			Mean Mock (log2 LFQ Intensity)	LITAF V144M (Log2 LFQ Intensity)			Mean LITAF V144M (log2 LFQ Intensity)	-Log (p-value)	Fold change
NSFL1 cofactor p47	NSFL1C	23.29	24.67	23.74	23.90	26.28	26.74	27.60	26.87	2.22	2.97
4F2 cell-surface antigen heavy chain	SLC3A2	23.78	22.26	23.93	23.32	29.86	28.45	27.03	28.45	2.20	5.13
Disco-interacting protein 2 homolog B	DIP2B	23.10	22.37	23.76	23.08	25.24	26.29	25.64	25.72	2.20	2.65
WASH complex subunit strumpellin	KIAA0196	23.48	23.76	23.45	23.56	24.44	25.09	25.25	24.93	2.17	1.37
Synaptojanin-2	SYNJ2	23.28	24.07	22.93	23.43	25.34	25.89	25.18	25.47	2.15	2.04
Tyrosine-protein kinase transmembrane receptor ROR1	ROR1	22.23	23.78	22.03	22.68	26.69	26.06	25.42	26.06	2.15	3.38
Unconventional myosin-XVIIIa	MYO18A	22.96	23.37	22.61	22.98	26.30	27.70	25.45	26.48	2.15	3.51
Guanine nucleotide-binding protein G(i) subunit alpha-2	GNAI2	23.84	22.41	23.07	23.11	25.56	25.16	26.09	25.61	2.15	2.50
Sodium bicarbonate cotransporter 3	SLC4A7	22.38	24.06	23.95	23.47	27.43	28.11	26.31	27.28	2.14	3.82
Paxillin	PXN	22.77	23.98	23.93	23.56	28.60	26.51	26.90	27.34	2.13	3.78
Nectin-3	PVRL3	22.97	23.23	24.05	23.42	25.23	25.53	26.28	25.68	2.13	2.26
Talin-1	TLN1	25.28	22.35	25.36	24.33	29.98	30.24	28.86	29.70	2.12	5.37
RNA-binding motif, single-stranded-interacting protein 1	RBMS1	22.99	23.43	22.77	23.06	25.24	26.14	24.68	25.35	2.10	2.29
Protein PRRC2C	PRRC2C	22.42	22.84	22.86	22.70	25.04	27.62	26.87	26.51	2.09	3.81
26S proteasome non-ATPase regulatory subunit 4	PSMD4	23.73	21.87	23.55	23.05	26.12	25.76	26.69	26.19	2.07	3.14
Protein FAM171A1	FAM171A1	22.87	22.07	22.18	22.37	27.74	26.38	25.00	26.37	2.07	4.00
Arfaptin-2	ARFIP2	22.71	22.86	23.68	23.08	27.77	26.00	25.71	26.49	2.06	3.41
Flotillin-1	FLOT1	21.99	23.59	24.05	23.21	26.25	26.49	25.99	26.24	2.04	3.03
RNA-binding motif, single-stranded-interacting protein 2	RBMS2	22.28	24.14	21.75	22.72	25.92	27.40	26.86	26.73	2.04	4.01
Signal transducer and activator of transcription 1-alpha/beta	STAT1	22.61	24.01	22.25	22.96	25.26	25.93	25.86	25.68	2.04	2.73
Caldesmon	CALD1	26.25	23.05	23.39	24.23	30.07	28.97	28.96	29.33	2.04	5.10

Protein names	Gene names	Mock (Log2 LFQ Intensity)			Mean Mock (log2 LFQ Intensity)	LITAF V144M (Log2 LFQ Intensity)			Mean LITAF V144M (log2 LFQ Intensity)	-Log (p-value)	Fold change
Pleckstrin homology-like domain family B member 1	PHLDB1	22.56	22.83	22.39	22.59	28.05	28.93	25.48	27.49	2.03	4.89
Ras GTPase-activating protein nGAP	RASAL2	24.29	22.93	23.34	23.52	25.80	25.79	25.23	25.61	2.02	2.08
Ras-related protein Rab-23	RAB23	22.34	22.52	23.37	22.74	25.09	24.93	26.50	25.51	2.02	2.77
WD repeat-containing protein 20	WDR20	22.10	23.25	22.94	22.76	25.18	26.32	24.79	25.43	2.02	2.67
Four and a half LIM domains protein 2	FHL2	24.68	23.70	23.54	23.97	27.10	25.80	26.26	26.38	2.01	2.41
Microtubule-associated protein 2	MAP2	23.03	21.97	22.22	22.41	24.21	25.51	25.94	25.22	2.01	2.81
Merlin	NF2	25.70	22.76	22.34	23.60	30.53	29.57	28.12	29.41	1.99	5.81
Receptor tyrosine-protein kinase erbB-2	ERBB2	22.62	23.50	23.46	23.19	25.07	24.54	24.53	24.72	1.98	1.53
Protein scribble homolog	SCRIB	21.93	22.72	23.46	22.70	24.75	25.60	24.82	25.06	1.97	2.35
MAP7 domain-containing protein 3	MAP7D3	22.67	23.01	22.51	22.73	23.86	24.75	23.92	24.18	1.97	1.44
26S proteasome non-ATPase regulatory subunit 1	PSMD1	23.48	23.80	22.55	23.28	25.14	26.83	26.63	26.20	1.96	2.92
Cysteine and glycine-rich protein 1	CSRP1	22.70	24.31	23.54	23.52	25.80	25.75	26.82	26.12	1.96	2.60
Leucine-rich repeat-containing protein 59	LRRC59	23.50	22.26	23.45	23.07	24.80	24.94	25.36	25.03	1.95	1.96
Leucyl-cystinyl aminopeptidase	LNPEP	23.58	22.84	22.84	23.09	27.31	25.12	25.87	26.10	1.92	3.01
Cdc42 effector protein 3	CDC42EP3	22.31	23.27	24.05	23.21	25.40	25.18	25.71	25.43	1.87	2.22
Catenin alpha-1	CTNNA1	23.79	22.19	23.70	23.23	25.85	26.14	25.11	25.70	1.83	2.48
Mitogen-activated protein kinase kinase kinase kinase 4	MAP4K4	24.20	23.00	23.69	23.63	25.97	26.12	24.97	25.69	1.83	2.06
PDZ and LIM domain protein 4	PDLIM4	24.07	22.37	22.44	22.96	25.86	25.15	25.21	25.40	1.82	2.45
LIM and calponin homology domains-containing protein 1	LIMCH1	22.26	22.67	23.42	22.78	24.29	25.35	25.98	25.21	1.82	2.42
Transgelin	TAGLN	23.76	22.68	26.64	24.36	31.21	28.85	29.60	29.89	1.80	5.53
Ras-associated and pleckstrin homology domains-containing protein 1	RAPH1	23.78	22.65	23.03	23.15	28.75	28.89	25.56	27.73	1.80	4.58
LIM domain and actin-binding protein 1	LIMA1	22.21	23.64	24.05	23.30	25.28	26.19	26.58	26.02	1.80	2.72

Protein names	Gene names	Mock (Log2 LFQ Intensity)			Mean Mock (log2 LFQ Intensity)	LITAF V144M (Log2 LFQ Intensity)			Mean LITAF V144M (log2 LFQ Intensity)	-Log (p-value)	Fold change
Uveal autoantigen with coiled-coil domains and ankyrin repeats	UACA	22.21	23.83	23.20	23.08	26.04	25.35	24.84	25.41	1.79	2.33
Cold shock domain-containing protein E1	CSDE1	23.15	24.17	22.63	23.32	25.54	25.48	27.06	26.03	1.77	2.71
Lipoma-preferred partner	LPP	23.76	22.66	24.18	23.53	26.50	25.67	27.96	26.71	1.77	3.18
Partitioning defective 3 homolog B	PARD3B	22.82	22.83	22.55	22.73	29.07	27.52	25.14	27.24	1.77	4.51
Golgin subfamily A member 4	GOLGA4	22.63	23.70	23.58	23.30	28.35	28.29	25.37	27.34	1.75	4.04
E3 ubiquitin/ISG15 ligase TRIM25	TRIM25	23.51	23.11	22.42	23.01	24.26	25.72	25.43	25.14	1.75	2.12
WASH complex subunit FAM21A	FAM21A	22.37	23.28	22.85	22.83	26.06	26.33	24.26	25.55	1.75	2.72
Integrin-linked protein kinase	ILK	23.53	23.06	22.73	23.10	25.01	24.15	25.54	24.90	1.74	1.80
Microtubule-actin cross-linking factor 1, isoforms 1/2/3/5	MACF1	23.00	22.39	23.96	23.12	25.68	26.57	24.86	25.70	1.73	2.59
Kinesin light chain 1	KLC1	22.79	22.76	23.75	23.10	24.40	25.14	24.42	24.66	1.73	1.56
Afadin	MLLT4	22.17	23.08	23.66	22.97	29.04	29.10	25.44	27.86	1.72	4.89
Transforming growth factor beta-1-induced transcript 1 protein	TGFB1I1	22.48	23.62	22.95	23.02	25.38	24.43	26.23	25.35	1.71	2.33
Na(+)/H(+) exchange regulatory cofactor NHE-RF1	SLC9A3R1	23.09	22.44	23.78	23.10	24.59	24.65	25.49	24.91	1.70	1.81
Hematological and neurological expressed 1-like protein	HN1L	23.09	23.88	22.25	23.07	24.56	25.36	25.46	25.13	1.70	2.06
Plastin-3	PLS3	23.31	22.73	23.28	23.10	23.73	23.92	24.19	23.95	1.67	0.84
Receptor-type tyrosine-protein phosphatase eta	PTPRJ	22.42	22.26	23.24	22.64	27.64	25.06	25.12	25.94	1.67	3.30
ATP-binding cassette sub-family E member 1	ABCE1	22.24	23.26	25.60	23.70	27.28	27.13	28.42	27.61	1.66	3.91
Regulator of G-protein signaling 12	RGS12	23.13	22.90	23.69	23.24	24.52	25.41	24.30	24.74	1.66	1.50
Palmitoyltransferase ZDHHC5	ZDHHC5	23.84	23.89	22.31	23.35	27.10	27.58	25.16	26.61	1.65	3.27
PDZ and LIM domain protein 5	PDLIM5	24.77	24.34	25.62	24.91	28.70	28.06	26.37	27.71	1.62	2.80
Endophilin-A2	SH3GL1	22.53	23.30	23.59	23.14	25.57	25.58	24.19	25.12	1.61	1.97
Tumor susceptibility gene 101 protein	TSG101	23.68	22.93	22.55	23.05	24.09	25.13	25.37	24.86	1.61	1.81

Protein names	Gene names	Mock (Log2 LFQ Intensity)			Mean Mock (log2 LFQ Intensity)	LITAF V144M (Log2 LFQ Intensity)			Mean LITAF V144M (log2 LFQ Intensity)	-Log (p-value)	Fold change
Thyroid receptor-interacting protein 6	TRIP6	22.17	23.22	22.96	22.78	24.40	23.87	25.12	24.47	1.61	1.68
Ubiquitin-associated protein 2	UBAP2	23.31	23.45	22.88	23.21	25.08	27.81	25.64	26.17	1.60	2.96
Pseudopodium-enriched atypical kinase 1	PEAK1	23.04	23.96	22.56	23.18	27.44	27.33	24.79	26.52	1.60	3.33
Nuclear fragile X mental retardation-interacting protein 2	NUFIP2	22.51	22.92	22.97	22.80	24.12	26.72	25.42	25.42	1.57	2.62
Glucose-6-phosphate 1-dehydrogenase	G6PD	25.24	22.72	23.98	23.98	27.17	26.04	27.79	27.00	1.56	3.02
Ubiquitin carboxyl-terminal hydrolase 8	USP8	23.37	23.30	24.30	23.66	24.70	24.76	24.84	24.76	1.56	1.10
Tensin-1	TNS1	24.47	24.54	23.73	24.25	27.23	26.16	25.37	26.25	1.55	2.01
Pumilio homolog 1	PUM1	22.04	22.87	23.39	22.77	24.53	25.96	24.31	24.93	1.54	2.16
Plasma membrane calcium-transporting ATPase 1	ATP2B1	23.70	23.37	24.68	23.92	25.05	25.75	25.36	25.39	1.54	1.47
Testin	TES	22.67	24.08	21.97	22.91	24.79	25.02	25.82	25.21	1.53	2.30
Transmembrane protein 237	TMEM237	23.75	24.54	23.09	23.79	25.57	25.65	24.90	25.37	1.51	1.58
Sorting nexin-9	SNX9	23.46	23.61	22.78	23.28	26.97	27.27	24.49	26.24	1.50	2.96
Syntaxin-5	STX5	22.42	23.42	24.20	23.35	24.59	25.84	26.18	25.54	1.44	2.19
ADP-ribosylation factor GTPase-activating protein 3	ARFGAP3	23.25	23.53	22.70	23.16	23.74	24.49	24.28	24.17	1.42	1.01
Pleckstrin homology domain-containing family N member 1	PLEKHN1	22.83	23.48	23.48	23.26	24.14	26.43	25.45	25.34	1.39	2.08
Roundabout homolog 1	ROBO1	24.14	24.09	22.31	23.51	26.92	27.04	24.87	26.27	1.39	2.76
SH3 domain-binding protein 4	SH3BP4	23.52	22.19	23.73	23.15	25.15	24.66	24.38	24.73	1.39	1.58
Pyridoxal-dependent decarboxylase domain-containing protein 1	PDXDC1	22.44	22.43	22.98	22.61	23.51	24.51	25.73	24.58	1.38	1.97
Vigilin	HDLBP	23.50	23.50	26.43	24.48	27.93	27.09	27.21	27.41	1.35	2.93
Myosin light chain kinase, smooth muscle	MYLK	22.97	22.39	25.21	23.52	25.54	26.46	27.57	26.52	1.35	3.00
Basigin	BSG	24.30	23.68	22.73	23.57	28.33	26.04	25.24	26.54	1.35	2.97
Double-stranded RNA-binding protein Staufen homolog 2	STAU2	24.93	22.74	23.01	23.56	25.55	25.68	25.39	25.54	1.33	1.98

Protein names	Gene names	Mock (Log2 LFQ Intensity)			Mean Mock (log2 LFQ Intensity)	LITAF V144M (Log2 LFQ Intensity)			Mean LITAF V144M (log2 LFQ Intensity)	-Log (p-value)	Fold change
Synaptic vesicle membrane protein VAT-1 homolog	VAT1	24.25	23.70	23.61	23.85	24.77	24.27	25.08	24.71	1.30	0.86
Ankyrin repeat and KH domain-containing protein 1	ANKHD1	23.03	24.05	22.75	23.28	24.39	26.09	24.67	25.05	1.26	1.78
Abl interactor 1	ABI1	23.24	23.71	22.62	23.19	24.96	25.32	23.78	24.69	1.25	1.50
DnaJ homolog subfamily B member 1	DNAJB1	23.12	24.90	23.61	23.88	25.73	24.98	25.53	25.41	1.25	1.53
Synaptobrevin homolog YKT6	YKT6	23.30	24.01	23.66	23.66	27.35	25.16	24.87	25.79	1.24	2.13
Coxsackievirus and adenovirus receptor	CXADR	23.89	23.50	22.49	23.29	27.49	25.42	24.55	25.82	1.23	2.53

Table A.3. Significantly enriched proteins in the LITAF V144M condition vs. Mock. The table shows the results of label-free quantitative analysis of mass spectrometry proteomics by MaxQuant and Perseus following BioID.